Structure-property Relationships in Sterically-congested Proton-conducting Poly(phenylene)s: The Impact of Backbone Linearity

by

Nicolas Peressin

B.Sc., University of British Columbia, 2018.

Thesis Submitted in Partial Fulfillment of the
Requirements for the Degree of
Master of Science

in the
Department of Chemistry
Faculty of Science

SIMON FRASER UNIVERSITY
Spring 2020

Approval

Name:	**Nicolas Peressin**
Degree:	**Master of Science (Chemistry)**
Title:	**Structure-property Relationships in Sterically-congested Proton-conducting Poly(phenylene)s: The Impact of Backbone Linearity**
Examining Committee:	**Chair:** **Hua-Zhong Yu** Professor
	Steven Holdcroft Senior Supervisor Professor
	Jeffrey Warren Supervisor Associate Professor
	Peter Wilson Supervisor Associate Professor
	Loren Kaake Internal Examiner Assistant Professor
Date Defended/Approved:	April 9, 2020

Abstract

Decarbonatization of the World's primary energy supply is becoming increasingly more important due to a rapidly changing climate. A hydrogen-based economy offers a potential means of zero-carbon energy production through the use of fuel cells and water electrolyzers. The development of robust, thermochemically-stable hydrocarbon-based proton exchange membrane materials that resist swelling for use in these devices represent a significant hurdle in their commercial adoption.

In this thesis, the structure-property relationship of hydrocarbon-based sulfonated phenylated poly(phenylene) proton exchange membranes possessing either angled or linear backbone moieties is discussed. Polymers were synthesized using either bent (*ortho* or *meta*), or linear (*para*) biphenyl linkages and evaluated for differences in physical and electrochemical properties. Model compounds, structurally-analogous to the polymers, were prepared and characterized using spectroscopic and computational methods to elucidate structural differences and potential impacts on the properties of the respective polymers. A highly angled *ortho* biphenyl linkage resulted in a sterically hindered, rotationally-restricted molecule. When incorporated into a homo-polymer, the angled *ortho* biphenyl moiety was found to prevent membrane formation. The angled *meta* biphenyl-containing homo-polymer, while forming a membrane, exhibited a 74% increase in volumetric expansion, 31% reduction in tensile strength, and 72% reduction in the elongation at break when compared to the linear *para* biphenyl-containing analogue. The differences observed are attributed to a rotationally-restricted backbone in the angled biphenyl systems. Co-polymers containing a small fraction (≤5%) of the *ortho* or *meta* biphenyl linkage in an otherwise *para* biphenyl containing system were found to have a significantly lower degree of swelling than those containing solely *para* biphenyl linkages.

Collectively, the work presented in this thesis suggests that incorporating angled biphenyl linkages into sulfonated phenylated poly(phenylene)s leads to highly rigid, inflexible backbones that prevents chain entanglement and the formation of free-standing membranes.

Keywords: Poly(phenylene)s, linearity, structure-property, proton exchange membranes, hydrocarbon, aromatic

To my soul mate Jennifer, my parents Joanne and Leo, and my family, who through their support, have made me the person I am today.

Acknowledgements

The research presented in this thesis would not have been possible without the guidance of my senior supervisor Prof. Steven Holdcroft, who welcomed me in to his research group in January 2018. His passion and dedication to science, as well as his work-ethic have helped me stay motivated through the ups and downs of my degree. I am thankful for his support throughout the course of this work, and for the positive work environment he fosters in his research group. I would also like to thank my supervisory committee, Profs. Jeffrey Warren and Peter Wilson, for providing invaluable advice and direction during the course of this project.

I would like to thank the following people in no particular order:

To the great friends I met at SFU, who I'm sure I will be seeing more of in the future. Dr. Thomas Skalski for laying the groundwork in the area of pre-functionalized poly(phenylene)s for which this work is based. To Dr. Patrick Fortin for introducing me to and teaching me the art of home brewing, and to Thomas Holmes for patiently teaching me how to use a great deal of instrumentation.

To my past research supervisors Prof. David Perrin and Dr. Mathieu Lepage for introducing me to academic research and organic synthesis. I truly don't think I would have pursued graduate school if I hadn't had such a positive experience during my undergraduate degree.

To Prof. Barbara Frisken and Eric Schibli for helping characterize materials presented in this thesis using density functional theory calculations, and for helping me understand some complex physics concepts beyond the world of chemistry.

Dr. Eric Ye for his assistance in running and interpreting uncommon nuclear magnetic resonance spectroscopy experiments, and to Hongwen Chen for performing mass spectrometry experiments.

And finally, to Dr. Mike Adamski, who has been a great friend and mentor. Mike took me under his wing and introduced me to every bit of chemistry that would allow me to carry out my work. Our combined efforts have taken us both to Trondheim, Norway and Atlanta, USA. This project would not have been possible without his guidance.

Table of Contents

List of Tables

List of Figures

List of Schemes

List of Acronyms

°	Degree(s)
^{13}C	Carbon-13
^{1}H	Proton
AC	Alternating current
Acetone-d_6	Deuterated acetone
A_{dry}	Dry area
AEM	Anionic exchange membrane
aq.	Aqueous
A_{wet}	Wet area
A_{xs}	Cross sectional area
BTC	Bistetracyclone
C	Celsius
C_d	Double layer capacitance
CD_2Cl_2	Deuterated dichloromethane
CD_3OD	Deuterated methanol
$CDCl_3$	Deuterated chloroform
$CHCl_3$	Chloroform
$ClSO_3Si(CH_3)_3$	Trimethylsilyl Chlorosulfonate
COSY	Correlation spectroscopy
d	Doublet (NMR spectroscopy)
Đ	Dispersity
D_2O	Deuterium oxide
Da	Dalton(s)
DA	Diels-Alder
DCE	Dichloroethane
DCM	Dichloromethane
dd	Doublet of doublets (NMR spectroscopy)
DFT	Density functional theory
DI water	Deionized water
DMF	*N,N*-dimethylformamide
DMSO	Dimethylsulfoxide
DMSO-d_6	Deuterated dimethylsulfoxide

DOE	Department of Energy
DP	Degree of polymerization
DSC	Differential scanning calorimetry
EAS	Electrophilic aromatic substitution
EDG	Electron donating group(s)
EIS	Electrochemical impedance spectroscopy
eq.	Equivalent(s)
EtOAc	Ethyl acetate
EtOH	Ethanol
EWG	Electron withdrawing group(s)
EXSY	Exchange spectroscopy
F	Faraday constant
FC	Fuel cell
g	Gram(s)
GDL	Gas diffusion layer
GPC	Gel permeation chromatography (also known as SEC)
h	Hour(s)
HMBC	Heteronuclear multiple bond correlation
HOMO	Highest occupied molecular orbital
HRMS	High resolution mass spectrometry
HSQC	Heteronuclear single quantum coherence
IEC	Ion exchange capacity
IEC_{th}	Theoretical ion exchange capacity
IEC_{xp}	Experimental ion exchange capacity
kg	Kilogram(s)
kW	Kilowatt
L	Length
L	Liter(s)
LUMO	Lowest unoccupied molecular orbital
m	Mass
m	Multiplet (NMR spectroscopy)
M	Molar
m/z	Mass-to-charge ratio
***m*-BPL**	*meta*-biphenyl linker

MC-B*m*	Model compound *meta*-biphenyl
MC-B*o*	Model compound *ortho*-biphenyl
MC-B*p*	Model compound *para*-biphenyl
m_{dry}	Dry sample mass
MeOH	Methanol
meq.	Milliequivalent(s)
mg	Milligram(s)
M_{H2O}	Molar mass of water
MHz	Megahertz
min	Minutes
mL	Milliliter(s)
mm	Millimeter(s)
mmol	Millimole(s)
M_n	Number-average molecular weight
mol	Mole(s)
MPa	Megapascal(s)
mS	Millisiemen(s)
MS	Mass spectrometry
MW	Molecular weight
M_w	Weight-average molecular weight
m_{wet}	Wet sample mass
NMR	Nuclear magnetic resonance
NOE	Nuclear Overhauser effect
NOESY	Nuclear Overhauser effect spectroscopy
***o*-BPL**	*ortho*-biphenyl linker
OCV	Open circuit voltage
***p*-BPL**	*para*-biphenyl linker
PEM	Proton exchange membrane or Polymer electrolyte membrane
PFSA	Perfluorosulfonic acid
pH	Hydrogen ion concentration ($-\log_{10}[H^+]$)
Ph	Phenyl
ppm	Parts per million
PPP	Phenylated poly(phenylene)
PTFE	Poly(tetrafluoroethylene)

RH	Relative humidity
R_{ion}	Ionic resistance
ROESY	Rotating-frame Overhauser effect spectroscopy
R_{ohmic}	Resistance (ohmic)
RT	Room temperature
s	Singlet (NMR spectroscopy)
sBTC	Sulfonated bistetracyclone
SEC	Size extrusion chromatography (also known as GPC)
SPAES	Sulfonated poly(arylene ether sulfone)s
SPBI	Sulfonated poly(benzimidazole)s
SPEEK	Sulfonated poly(ether ether ketone)s
SPI	Sulfonated poly(imide)s
sPPB	Sulfonated phenylated poly(phenylene), biphenyl-linked
sPPB*m*	Sulfonated phenylated poly(phenylene), *meta*-biphenyl linked
sPPB*o*	Sulfonated phenylated poly(phenylene), *ortho*-biphenyl linked
sPPB*p*	Sulfonated phenylated poly(phenylene), *para*-biphenyl linked
SPPO	Sulfonated poly(phenylene oxide)s
sPPP	Sulfonated phenylated poly(phenylene)s
sTC	Sulfonated tetracyclone
t	Triplet (NMR spectroscopy)
T	Temperature
TC	Tetracyclone
TEA	Triethylamine
TEAsBTC	Triethylammonium salt of sulfonated bistetracyclone
TEAsTC	Triethylammonium salt of sulfonated tetracyclone
T_g	Glass transition temperature
TGA	Thermogravimetric analysis
th_{dry}	Dry thickness
THF	Tetrahydrofuran
th_{wet}	Wet thickness
TMS	Trimethylsilyl group -$Si(Me)_3$
TOCSY	Total correlated spectroscopy
TPES	Total primary energy supply
Tr-ROESY	Transverse rotating-frame Overhauser effect spectroscopy

TWh	Terawatt(s)
V_{dry}	Dry sample volume
V_{exp}	Volumetric expansion (%)
vol%	Volume percent
V_{wet}	Wet sample volume
W_{con}	Water content (by mass)
WE	Water electrolyzer(s)
wt%	Weight percent
W_{up}	Water uptake (by mass)
Z’	Impedance (real component)
Z’’	Impedance (imaginary component)
δ	Chemical shift (NMR spectroscopy)
λ	Hydration number (number of water molecules per ionic group)
μ	Micro
μ'_{H+}	Effective proton mobility
σ^{+}	Proton conductivity
ω	Frequency (angular)

Chapter 1.

Introduction

Humanity currently faces a unique dilemma. The global population of 7.6 billion (as of mid-2017) has tripled since 1950, and is continuing to rise, increasing at a rate of 1.1 percent per year or by 83 million people annually.[1] Projections estimate the global population will reach 8.6 billion by 2030, further increasing to 11.2 billion by the year 2100.[1] At the same time, rapid economic growth in the developing world has led to a 4.4 fold increase in global GDP between 1950 and 2016.[2],[3] Increasing population and goods manufacturing has led to an increasing energy demand, with the World total primary energy supply (TPES) increasing from approximately 71,000 TWh in 1973 to approximately 160,000 TWh in 2014.[4] More recently, global energy demand is continuing to grow, (by 2.9% annually in 2018), dominated by China, US, and India that together accounted for around two thirds of the growth.[5] Despite a significant shift in perception towards the use and consequences of non-renewable energy sources such as fossil fuels, 86% of the globally consumed energy in 2015 was produced from a combination of coal, oil and gas, with the remaining 14 percent coming from hydro (6.79%), nuclear (4.44%), wind (1.44%), solar (0.45%) and “other renewables” (0.89%).[6] Using 2014 energy consumption metrics, this means that nearly 138,000 TWh, equivalent to 80.6 billion barrels of oil, of non-renewable energy is supplied to the planet each year releasing 32.8 gigatons of carbon dioxide (CO_2), a potent greenhouse gas, annually.[5] While fears of fossil fuel reserve depletion in the near future exist,[7] there is a much more pertinent concern in the form of increasing surface temperatures linked to increasing atmospheric CO_2 concentrations.[8] Atmospheric CO_2 concentrations have increased drastically from a pre industrial value of 270 ppm,[9] to 407 ppm in 2019,[10] while simultaneously, average temperatures have increased by 0.85 °C (2012).[11] To further exacerbate this issue, the consequences of anthropogenic CO_2 emissions are expected to persist for many millennia due to the slow rate at which CO_2 is removed from the atmosphere.[12],[13] Moreover, a significant portion of anthropogenic CO_2 enters the ocean and increases ocean acidity which harms aquatic life and bio-diversity, presenting serious potential consequences for humanity.[14] If no effort is made to reduce greenhouse gas emissions beyond those in

place today, the planet will likely see a 3.7 – 4.8 °C increase from pre-industrial levels by the year 2100 resulting in severe and irreversible climate change.[11],[15],[16],[17]

Consequently, decarbonizing the World's primary means of energy production while simultaneously meeting the rapidly growing demand for power is perhaps the single most important challenge currently facing humanity. Renewable energy technologies, which will play a major role in achieving this goal, have seen significant adoption rates in the power sector in recent decades. For example, in 2018, the global growth in power generation was led by renewables, which grew by 14.5%, while coal and natural gas only grew by 3.0 and 3.9% respectively.[5] Unfortunately, this is not enough. In order to meet targets set by the Paris Agreement that aims to prevent global temperature from exceeding 2 °C above pre-industrial levels,[18] drastic mitigation strategies will need to be employed. To achieve this goal, it is estimated that > 50% of all energy supplied will need to come from renewable sources by 2028, and increase further to 87-94% by the year 2100.[19] Additionally, net CO_2 emissions will need to be negative by the year 2100, possible by combing renewable energy with carbon capture technology.[20] As such, it is imperative that advancements continue to be made in renewable energy technologies so that they may be a viable replacement for fossil fuel based energy.

1.1. The Hydrogen Economy

The hydrogen economy is a promising low- to zero-carbon emission means of energy production that would rely on hydrogen as a fuel source instead of fossil fuels. The hydrogen economy is based around two key technologies, water electrolyzers (WE)s that convert water to oxygen and hydrogen gas using electricity; and fuel cells (FC)s that consume oxygen and hydrogen gas to produce electricity, with water being the only by-product. Renewable energy such as nuclear, solar, hydro and wind would supply energy to WEs to produce the hydrogen and oxygen gas. In this closed loop approach, shown in Figure 1.1, energy is produced and consumed without generating harmful greenhouse gasses and could effectively replace fossil fuels as an energy source.

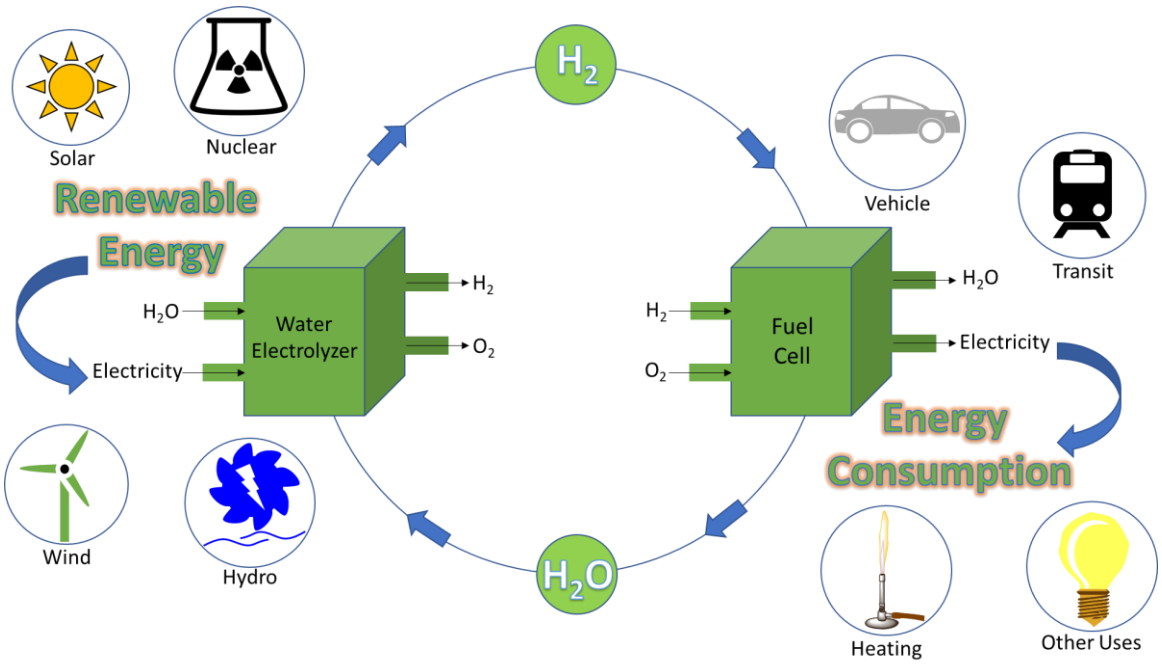

Figure 1.1: *A renewable hydrogen-based energy network based on water electrolyzers and fuel cells.*

The basic operating principles of water electrolyzers and hydrogen fuel cells are relatively simple, and were first demonstrated by lawyer and scientist William Grove in 1839.[21] As shown in Figure 1.2, both of these technologies require an anode, a cathode, and an electrolyte to function. Modern devices incorporate polymer electrolytes in place of the aqueous acid electrolyte shown in Figure 1.2, however the principle is still the same. In an electrolyzer, a potential is applied to facilitate the electrochemical splitting of H_2O to H_2 and O_2 gas, whereas in a fuel cell, H_2 and O_2 gas combine spontaneously and exothermically to H_2O. A catalyst, in this case platinum, is required for the reactions occurring to proceed at an appreciable rate.[22] The electrolyte serves to transports protons (H^+), while being impermeable to the reactant gasses (H_2 and O_2). It is also electrically insulating,[23] necessarily requiring current to travel through an external circuit, where in the case of fuel cells, is used to do useful work. In cases where the electrolyte is a polymer, it is typically referred to as a proton exchange membrane, or polymer electrolyte membrane (PEM). The standard cell potential governed by the redox processes taking place is -1.23 V for water electrolysis (non-spontaneous) and +1.23V in fuel cells (spontaneous), as shown in Equation 1.1 to Equation 1.6.

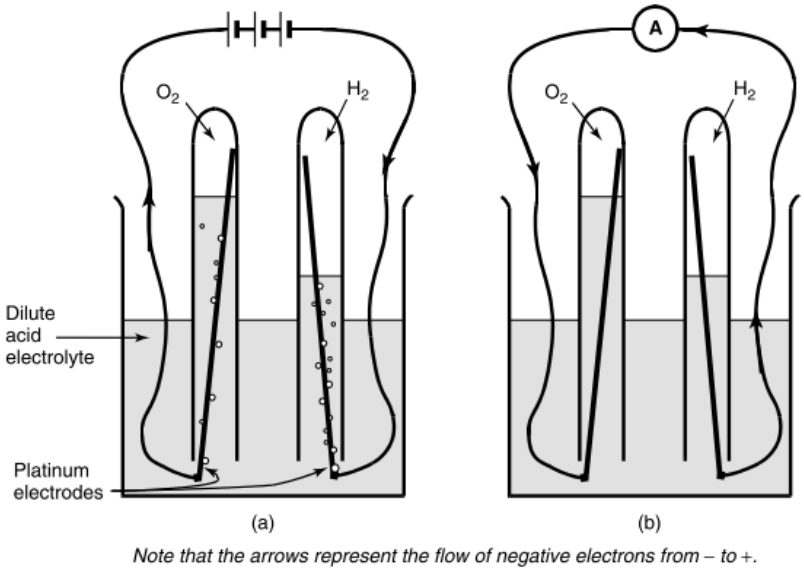

Figure 1.2: *First demonstration of a (a) water electrolyzer, and (b) fuel cell; as demonstrated by William Grove.*[21]

Electrolyzer:

Equation 1.1 Anode: $H_2O_{(l)} \rightarrow \frac{1}{2}O_{2(g)} + 2H^+ + 2e^-$

Equation 1.2 Cathode: $2H^+ + 2e^- \rightarrow H_{2(g)}$

Equation 1.3 Total Cell Reaction: $H_2O_{(l)} \rightarrow \frac{1}{2}O_{2(g)} + H_{2(g)}$ ***E° = -1.23 V***

Fuel Cell:

Equation 1.4 Anode: $H_{2(g)} \rightarrow 2H^+ + 2e^-$

Equation 1.5 Cathode: $\frac{1}{2}O_{2(g)} + 2H^+ + 2e^- \rightarrow H_2O_{(l)}$

Equation 1.6 Total Cell Reaction: $\frac{1}{2}O_{2(g)} + H_{2(g)} \rightarrow H_2O_{(l)}$ ***E° = 1.23 V***

It should be noted that it is also possible for polymer electrolytes to operate in alkaline environments, transporting hydroxide anions instead of protons. While anion exchange membranes (AEM)s have gained considerable attention in recent years,[24],[25],[26],[27] they are still a relative new topic requiring additional research and development before commercial adoption is possible.[28],[29] Proton exchange membranes

and their applications on the other hand, are more mature, better understood, and more well-established in both an academic and commercial setting.[30],[31],[32] The work described in this thesis is related to proton exchange membranes with a focus on fuel cell application, therefore, further discussion on AEMs will not be considered.

There exist significant hurdles to overcome before this hydrogen economy may be brought to fruition, however. Being a truly zero-carbon emission economy is based on the predisposition that the electricity used to produce hydrogen comes entirely from renewable sources. Currently, only 4% of commercially produced hydrogen comes from water electrolysis, while the remaining 96% is produced using fossil fuels.[33] As such, advancements to traditional renewable energy technologies must be made to increase overall efficiency and reduce costs, so that they may be a viable alternative to fossil sources. Additionally, hydrogen storage poses a significant challenge due to its very low volumetric energy density,[34] and due to hydrogen being the simplest and lightest element. Accordingly, establishing a solution to efficiently storing and transporting hydrogen is being investigated by numerous research institutions.[35],[36],[37],[38] Lastly, there remains considerable room for improvement in water electrolyzer and fuel cell technology. Cost analysis by the US Department of Energy (DOE) in 2017 found the cost to manufacture a 80 kW fuel cell system ($45/kW based on 500,000 units/year) to be well above the target of $30/kW.[39] While the cost of components such as membranes and gas diffusion layers (GDLs) can benefit from high volume production, other components such as bipolar plates and catalysts are dominated by the high commodity material costs, as illustrated in Figure 1.3.[39] As such, significant efforts have been made to reduce catalyst loadings, and eliminate the use of expensive precious metals entirely.[39],[40],[41]

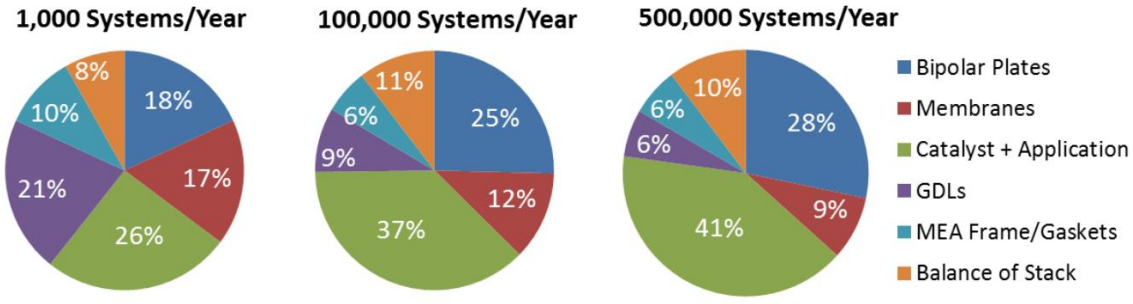

Figure 1.3: *Cost distribution of fuel cell stacks produced in low volume (1,000 units/year), medium volume (100,000 units/year), and high volume (500,000 units/year) from a US Department of Energy report.*[39]

1.2. Proton Exchange Membranes

Proton exchange membranes play a vital, central role in fuel cells and electrolyzers, facilitating proton transfer while mechanically separating two electrodes, and insulating against gas crossover and electrical current. The first commercial polymer electrolyte membranes were used to provide electricity onboard the Gemini 5 space mission in 1965, using sulfonated polystyrene as the proton exchange membrane.[42],[34] These systems exhibited a short lifetime (<200 h) however, due to poor oxidative stability of the membrane's polymer backbone,[43] and interest in them was lost with the later development of Nafion® by E.I. du Pont de Nemours & Co. in 1966.[34],[44],[45]

Perfluorosulfonic acid (PFSA) membranes such as Nafion®, which consist of a polytetrafluoroethylene (PTFE) backbone with perfluoroalkylether sulfonic acid pendant chains (Figure 1.4), represent the current commercial benchmark.[32] Nafion® exhibits a high proton conductivity of about 0.1 S cm^{-1} at room temperature when fully hydrated.[46] Furthermore, lifetimes of up to 60,000 h under fuel cell conditions have been reported,[47],[48] due to the high thermal, mechanical and chemical stability, and low swelling (33 vol% in water at room temperature) of Nafion®.[49] To put this into perspective, the US Department of Energy targets for membranes in an automotive fuel cell power system include a proton conductivity above 0.1 S cm^{-1},[50] and lifetimes exceeding 5,000 h.[51]

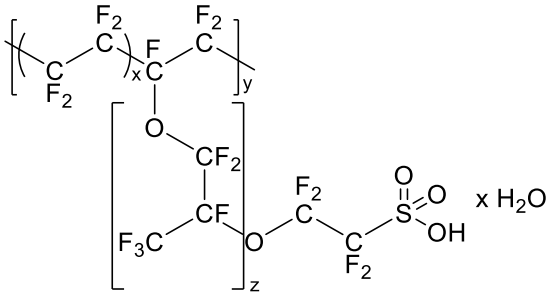

Figure 1.4: *Generic chemical structure of a perfluorosulfonic acid polymer.*

Despite its widespread commercial use and extensive evaluation as a proton exchange membrane,[23],[31] Nafion® suffers from notable drawbacks including a high material cost, and a high H_2 gas crossover resulting in gas crossover current densities of 3.8 mA cm^{-2} after 48 h of operation,[52] surpassing the DOE target of 2 mA cm^{-2}.[50]

Furthermore, there exist growing concerns over the environmental implications regarding the use and degradation of perfluorinated chemicals.[53],[34],[54],[55],[56] These drawbacks have motivated a significant amount of research in alternative, fluorine-free proton exchange membrane materials.

Hydrocarbon-based polymers have been commonplace in recent literature as potential fluorine free alternatives to Nafion®. sp^3 bonds however, such as those found in sulfonated polystyrene, were found to be particularly susceptible to attack by hydroxyl and hydroperoxyl radicals in fuel cells, formed *in-situ* as reactant gasses crossover through the membrane.[47],[57],[58] Consequently, a more attractive approach involves incorporating aromatic units into the polymer backbone due to the inherently greater thermochemical resilience of aryl-aryl and aryl-heteroatom linkages, versus that of the more labile sp^3 methylene and methine groups found in sulfonated polystyrene. Within this subset of aromatic-hydrocarbon-based PEMs exists a diverse array of synthetic strategies to obtain various chemical architectures from comparatively low-cost starting materials. Common examples includes sulfonated derivatives of poly(arylene ether sulfone)s (SPAES),[59],[60],[61],[62] poly(ether ether ketone)s (SPEEK),[31],[63] poly(phenylene oxide)s (SPPO),[64] poly(benzimidazole)s (SPBI),[65],[66],[67],[68] and poly(imide)s (SPI).[69] Examples of these chemical architectures are shown in Figure 1.5, though it should be noted these are general structures, and that many structural variants are possible.

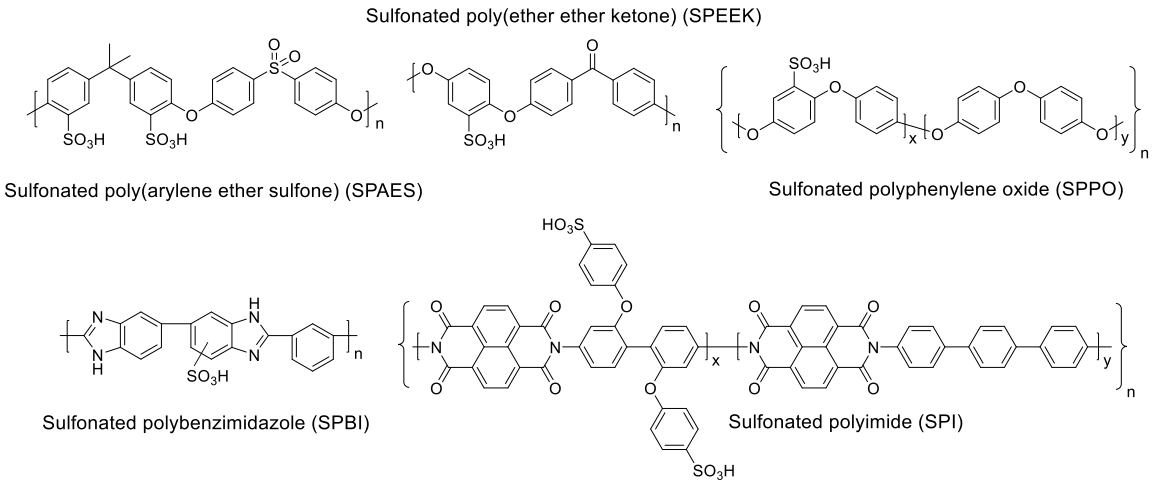

Figure 1.5: *Various aromatic-hydrocarbon-based PEMs.*

One major advantage of hydrocarbon-based PEMs is their intrinsically lower gas permeability than Nafion®,[67] limiting the *in-situ* formation of hydroxyl and hydroperoxyl radicals.[47],[58] In addition, Nafion® exhibits a glass transition (T_g) temperature (transition from a hard "glassy" state into a soft rubbery state) near 100 °C, limiting its potential operating temperature to below 100 °C. hydrocarbon-based PEMs on the other hand, exhibit significantly higher glass transition temperatures.[67] Furthermore, proton conductivity in recent PEMs is reported to have exceeded that of Nafion®.[70]

Many aromatic-hydrocarbon-based PEMs including SPAES, SPEEK, SPBI, and SPI are synthesized by simple step-growth polycondensations between commercially available substrates. In many cases, these step-growth polycondensation reactions negate the need for expensive catalysts or stringent reaction protocols such as those used in air sensitive transition metal catalyzed polymerizations. For example, poly(ether ether ketone)s are prepared through the condensation of 4,4'-difluorobenzophenone and hydroquinone disodium salt affording sodium fluoride as the condensate, as shown in Scheme 1.1. Here, a fluoride ion is easily displaced by the nucleophilic alkoxide, ultimately forming an ether bound polymer without the need for catalysis.

Scheme 1.1: *Polycondensation Reaction Between 4,4'-Difluorobenzophenone and Hydroquinone Affords Poly(ether ether ketone)*

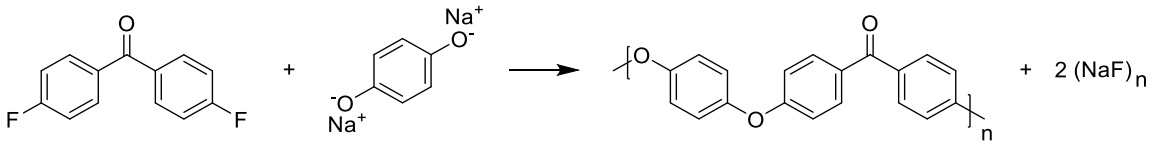

Sulfonic acid moieties are the most commonly employed acidic functional group in polymer electrolyte membranes due to their stability, simple sulfonating procedures, and their high acidity (*p*-toluenesulfonic acid pK_a = -2.8) promoting proton transport.[71] Acid functionalization provides hydrophilic sites onto an otherwise hydrophobic polymer. This combination of a hydrophobic backbone and hydrophilic acid segments is common among all classes of PEMs. Upon hydration, the hydrophobic and hydrophilic moieties segregate in to their respective domains, forming water filled ionic channels necessary for effective proton transport.[72],[73],[74] The nanoscale morphology of acid-bearing PEMs is greatly influenced by both the structure of the hydrophobic backbone, as well as the placement and quantity of hydrophilic acid moieties.[75]

Introduction of acidic functional groups has traditionally been employed post-polymerization, by subjecting the polymer substrate to a strong electrophilic sulfonating reagent such as sulfuric acid or chlorosulfonic acid.[76] Post sulfonation is simple, and can be applied on a large scale with a reasonably reproducible degree of sulfonation provided reaction conditions are carefully controlled.[70] The problem with post-sulfonation is that it leads to polymers with ill-defined structures, with little to no control over the positioning of the sulfonic acid moieties.[34],[77],[78] This can lead to polymers that are more likely to de-sulfonate at high temperatures, and to the formation of “dead end” water domains in the membrane.[70] Conversely, PEMs may be sulfonated by the pre-functionalization of monomer units prior to polymerization.[52],[76],[79],[80],[81],[82] While more challenging, this approach provides much finer control over the polymer structure, degree of sulfonation and positioning of the sulfonic acid groups.[52],[76],[79]

Despite significant efforts and progress toward solely hydrocarbon-based PEMs in recent decades, there exist common material deficiencies when compared to PFSAs. High water sorption characteristics may result in membranes with dimensional instability, poor durability and detachment of catalyst layers.[26] A low elongation at break typical of hydrocarbon-based polymers may result in the formation of brittle, inflexible membranes, especially when dry. Additionally, hydrocarbon-based polymer backbones are particularly susceptible to oxidative degradation, particularity in the presence of hydroxyl and hydroperoxyl radicals.[58],[81],[83],[84] While aromatic hydrocarbon-based PEMs are considerably more resilient than PEMs containing sp^3 linkages, the aryl-heteroatom linkages still serve as weak points. This susceptibility to oxidative degradation is emphasized in linkages containing electron donating heteroatoms such as ethers, whereby neighboring aromatic units display greater reactivity toward radical species.[58] Accordingly, development of hydrocarbon-based PEMs without these shortcomings is of significant technological importance.

1.3. Sulfonated Poly(phenylene)s

Highly sought-after polymers for PEMs are those in which the polymer backbone is comprised entirely of aryl-aryl linkages due to their inherent thermochemical stability, void of the more chemically labile heteroatomic linkages. Historically, work in this area had been limited by poor solubility in polar solvents, and the challenge of synthesizing well-defined polymer backbones comprised of rigid, sterically-encumbered aryl-aryl

linkages.[85],[86] Poly(phenylene)s comprised entirely of *para* linkages, for example, are especially insoluble in common organic solvents due to their rigid-rod nature.[87],[88],[89] Preparation of these materials commonly involve a transition-metal-catalyzed aryl-aryl coupling between difunctionalized benzene derivatives.[86] Polymer insolubility leads to precipitation out of the reaction medium containing the catalyst, which in-turn terminates the polymerization, resulting in low molecular weight polymers.[86] For example, poly(*para*-phenylene)s prepared through Yamamoto or Suzuki couplings (Scheme 1.2) afforded polymers with only 5 – 15 repeat units, where n is the number of repeat units.[86],[90],[91]

Scheme 1.2: *Poly(para-phenylene)s Prepared Through Transition-metal-catalyzed Aryl-aryl Coupling*

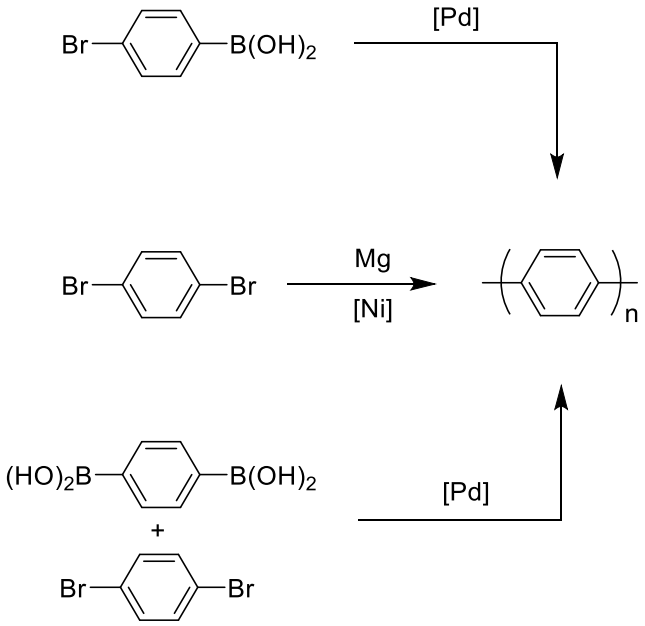

In recent decades, M. Litt *et. al.* have reported on a series of wholly aromatic sulfonated poly(*para*-phenylene)s,[92],[93] co-polymers,[46],[94] and cross-linked derivatives[95] for fuel cell and electrolyzer applications. The sulfonated polymers were prepared from pre acid-functionalized monomers through a copper-mediated Ullman reaction. Pre acid-functionalization increases solubility of the growing polymer chain in polar solvents compared their non-sulfonated analogues. The materials showed promise with their proton conductivity values greatly surpassing that of Nafion®, however, mechanical properties and dimensional stability problems limited their practical use.[46],[93],[94] The poor mechanical properties may have been due to the heterogeneous nature of the Ullman

reaction, whereby even with pre acid-functionalized monomers, the polymers were found to precipitate during polymerization,[46] limiting the molecular weight.[93]

Several approaches have been employed to mitigate the aforementioned problems ultimately leading to low molecular weights. Miyatake *et. al.* reported a series of poly(phenylene) polymers containing a mixture of *para*-phenylene, *para*-biphenylene and *meta*-biphenylene, prepared through a Yamamoto coupling of 3,3'-dichlorobiphenyl, 4,4'-dichlorobiphenyl, and 2,5-dichlorobenzenesulfonic acid as shown in Scheme 1.3. The authors found that by incorporating *meta* content into the polymer backbone, the solubility and molecular weights (up to M_w = 138,000 g mol^{-1}) of the polymers increased when compared to the strictly *para* poly(phenylene).

Scheme 1.3: *Yamamoto Coupling of 3,3'-Dichlorobiphenyl, 4,4'-Dichlorobiphenyl and 2,5'-Dichlorobenzensulfonic Acid to Afford Sulfonated Poly(phenylene)s*

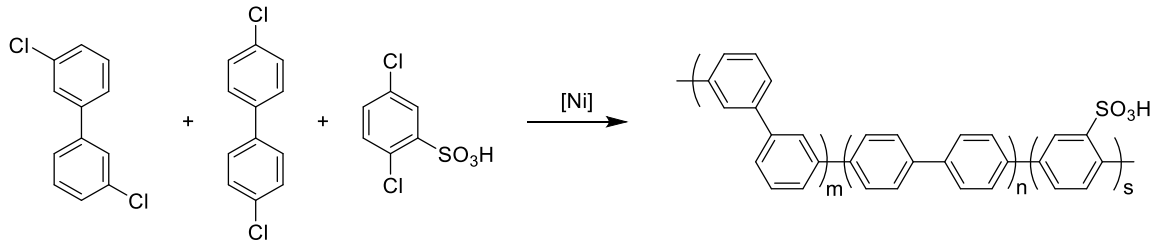

Diels-Alder poly(phenylene)s (non-sulfonated) initially reported in 1972 by Stille *et. al.*[96] using Diels-Alder step growth polymerizations have recently drawn attention due to their chemical stability and mechanical strength. In 2005 C. H. Fujimoto *et. al.*[77] reported a series of Diels-Alder poly(phenylene)s that were post-functionalized using chlorosulfonic acid to yield proton-conducting polymers known as sulfonated Diels-Alder poly(phenylenes)s, or sulfonated phenylated poly(phenylene)s (sPPP). These sPPPs exhibited high membrane tensile strength and thermochemical stability, and proton conductivity values up to 123 mS cm^{-1} at 30 °C (approx. 7% greater than a Nafion® 117 reference). When the acid content was increased beyond 2.1 sulfonic acid functional groups per repeat unit, however, the polymers were reported to have formed hydrogels upon exposure to water, limiting characterization to membranes with lower degrees of sulfonation. Furthermore, as described previously, it is generally regarded that post-sulfonation of polymers affords polymers with rather ill-defined molecular structures and reproducibility due to the multitude of functionalization positions and sequences of positions available, i.e., on multiple rings, where sulfonation could occur.

These issues were later mitigated via a pre-functionalization synthetic route to afford the acidic sPPP, that increased the number of sulfonic acid groups per repeat unit to 4, with precise control over their positioning.[79] Holmes *et al.*[58] investigated the oxidative degradation pathway of oligophenylene model compounds, and found that after subjecting the oligophenylene to H_2O_2 at 130 °C for 24 h, less than 10% had degraded, whereas sulfonated poly(arylene ether ketone) model compound degraded by 53% under identical conditions.[83] While the polymer (sPPP-H^+) remained insoluble in water at room temperature, and *in-situ* fuel cell measurements revealed up to 6 times higher proton conductivity than Nafion®, the polymer swelled excessively and eventually dissolved at elevated temperatures.

By incorporating a larger biphenyl co-monomer as shown in Scheme 1.4, however, the hydrophilicity of the polymer (sPPB-H^+), and hence swelling, was later reduced.[52] Despite possessing 4 sulfonic acid groups per repeat unit, sPPB-H^+ was completely insoluble in water at elevated temperatures (80 °C), allowing for a full suite of *in-situ* fuel cell characterization at more realistic temperatures.[52] Maximum proton conductivity values of 129 and 172 mS cm^{-1} were reported at 30 and 80 °C, respectively; slightly higher than previously reported values for sPPPs,[52] and significantly higher than values typically reported for Nafion® (approx. 100 mS cm^{-1}).[46] The polymer also displayed excellent oxidative stability, showing no chemical degradation after treatment with Fenton's reagent for 1 h at 80 °C.[52] Gas crossover, which is known to generate free radicals *in-situ*,[58] was found to be significantly lower in sPPB-H^+ than Nafion® NR-211, determined by gas crossover current densities of 0.5 vs 3.8 mA cm^{-2} respectively.[52] The chemical stability and lower gas crossover allowed sPPB-H^+ to outlive Nafion® NR-211 by a factor of 4 in an open circuit voltage (OCV) stress test, with sPPB-H^+ exhibiting an OCV of 0.71 V after 400 h, whereas Nafion® fell below 0.7 V after only 100 h.[52]

Despite significant advancements in sPPPs over recent years, this class of polymer still suffers from excessive swelling characteristics that may lead to insufficient durability and detachment of catalyst layers, limiting practical application in electrochemical devices.[26],[31],[32],[97] For example, sPPB-H^+ swells to 145 vol% of its initial volume resulting in 119 wt% water uptake.[52] While the reduction in swelling characteristics versus the initially reported sPPP-H^+ (364 vol% and 319 wt%) were significant, there is still measurable room for improvement when compared to that of Nafion® (20 vol% and 33 wt%).[79] In addition to poor mechanical properties, excessive

swelling is often met with a reduction in proton conductivity, as increased water sorption leads to a lower acid concentration within severely swollen membranes.[72],[74]

Scheme 1.4: *Synthesis of Pre-functionalized Diels-Alder Poly(phenylene)s sPPP-H$^+$ and More Hydrophobic sPPB-H$^+$*

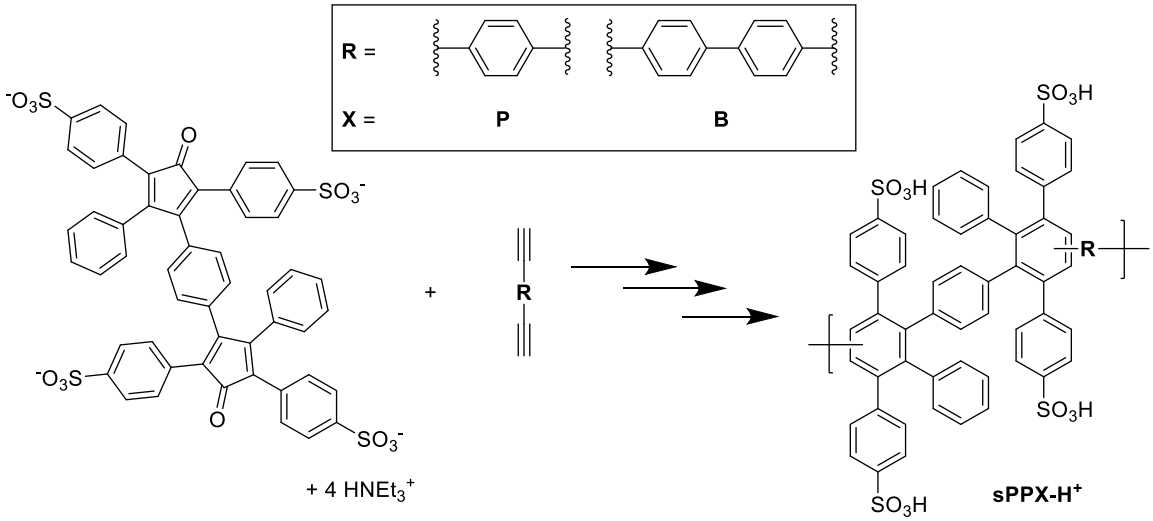

Several attractive approaches to reducing swelling in PEM materials exist. One successful strategy employed in sPPPs was to reduce the ion exchange capacity (IEC) through a copolymer-based approach, that involved introducing non-sulfonated phenylated arylene segments, and hence hydrophobicity, into the highly ionic polymer. While reducing IEC significantly reduced the swelling to 68 vol% at a 50:50 hydrophobic to hydrophilic co-monomer ratio, proton conductivity was also greatly reduced.[82] Another effective approach commonly employed in the literature to reducing swelling in PEMs has been demonstrated through cross-linking.[56],[95],[98] This approach has proven to be effective in reducing swelling, but relies on post-polymerization treatments that complicate synthesis and processing, and has typically resulted in brittle membranes.[99] Furthermore, in the case of sPPPs, cross-linking may require use of the sulfonic acid functional groups as cross-linking sites, thereby reducing the IEC and hence proton conductivity of the membranes.[95]

1.4. Angled Polymers

An interesting and potentially simple approach to reducing swelling in hydrocarbon based solid polymer electrolyte membranes was demonstrated through reducing polymer

chain linearity in sulfonated poly(imides)s,[100] as well as poly(phenylene)s.[101] It is believed that, by introducing angled moieties into polymer backbones, the resulting macroscopic structures may adopt flexible coils,[102] as opposed to rigid rods, which promote polymer chain entanglements and hence a reduction in water sorption, swelling, and elastic deformation.[29],[72],[100],[101]

Rodgers *et al.*[100] synthesized sulfonated polyimides (SPI) containing either linear (**SPI-A**) or bent (**SPI-B**) sulfones in the polymer backbone (Figure 1.6) to study various properties, including the impact on swelling, of polymers containing nonlinear units. They found that the linear **SPI-A** polymer possessed a higher water uptake over the whole IEC range measured (0.79 to 2.75 meq g^{-1}) and a large increase in water uptake between IEC = 2.15 and 2.46 meq g^{-1}, while the bent **SPI-B** polymer only showed a moderate increase in swelling over the same IEC.

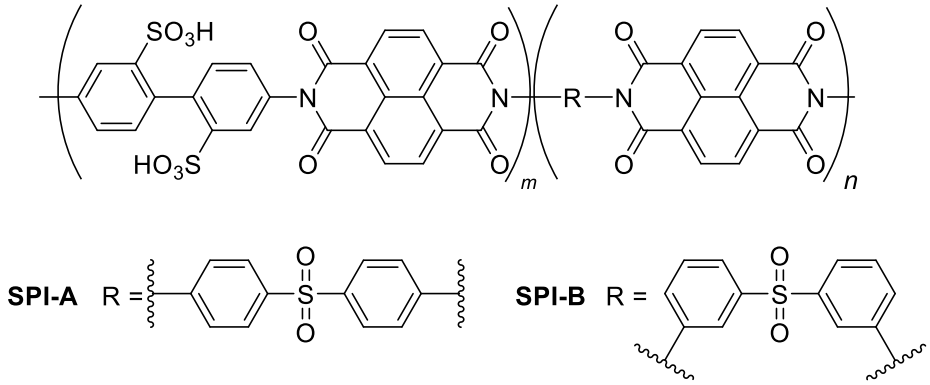

Figure 1.6: *Structure of linear (**SPI-A**) and angled (**SPI-B**) sulfonated polyimide co-polymers.*

Similarly, Miyake *et al*.[101][102] incorporated non-linear *meta*-biphenylene groups and linear *para*-biphenylene groups into the main chain of poly(phenylene)s. They found that when the ratio of *m*-phenylene/*p*-phenylene was higher that 4:1, the persistence length (which describes backbone stiffness) was similar to that of flexible polymers such as polyethylene. Membranes prepared from the *meta*-phenylene containing polymers were found to be more flexible than strictly *para*-biphenylene containing analogues. The authors argued that the improvements in membrane flexibility were due to the *m*-phenylene-rich backbone, which promoted a random coil structure and enhanced interpolymer entanglement.

This angled polymer strategy is attractive because: (1) it can be easily integrated into well-established sulfonated phenylated poly(phenylene) synthetic procedures; (2) it does not require additional post polymerization steps; and, (3) it is unlikely to cause reduction in acid content of the membrane.

1.5. Thesis Scope

Until now, sPPPs have been synthesized only using linear, *para*-functionalized co-monomers; e.g., 1,4-diethynylbenzene for sPPP-H^+ and 4,4'-diethynyl-1,1'-biphenyl for sPPB-H^+. The goal of this thesis was to study and better understand the structure-property relationship of sulfonated phenylated poly(phenylene)s possessing either angled or linear backbone moieties. This was achieved through the synthesis and characterization of sulfophenylated oligo and poly(phenylene)s containing *ortho*, *meta*, and *para* functionalized biphenyls, based on existing sPPB-H^+ architecture.[52] Poly(phenylene)s **sPPB*o*-H$^+$**, **sPPB*m*-H$^+$** and **sPPB*p*-H$^+$** containing *ortho*, *meta*, and *para* functionalized biphenyls respectively, to be discussed in this thesis, are shown in Figure 1.7.

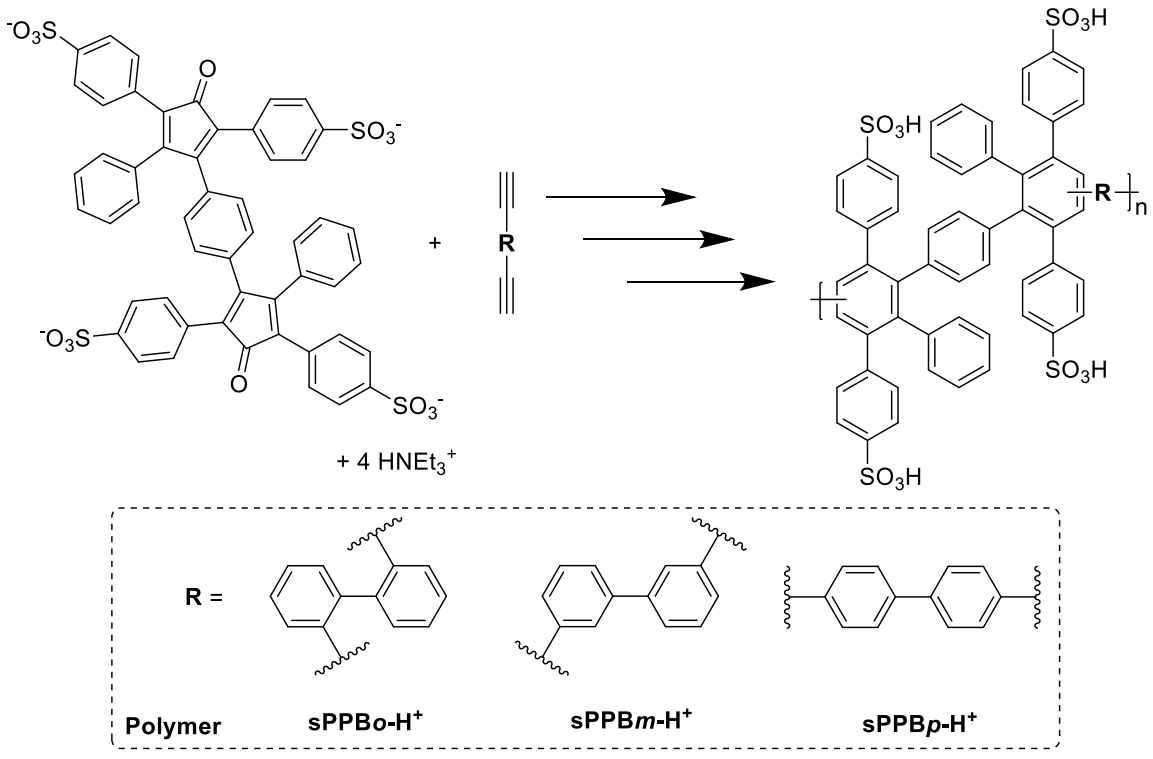

Figure 1.7: *Poly(phenylene)s **sPPBo-H$^+$**, **sPPBm-H$^+$**, and **sPPBp-H$^+$** containing ortho, meta, and para functionalized biphenyls.*

In Chapter 2, the methods utilized in the preparation and characterization of the oligo and poly(phenylene)s synthesized in this work are discussed. Many techniques were routinely used in the preparation and assessment of polymers synthesized in this thesis as proton exchange membranes. Background information, relevant theory and experimental details will be provided.

In Chapter 3, the synthesis and characterization of oligophenylene model compounds, **MC-B*o***, **MC-B*m***, **MC-B*p*** each containing an *ortho*, *meta*, or *para* functionalized biphenyl moiety respectively, is discussed. These oligophenylene model compounds were synthesized and characterized to first prove the viability of each anticipated Diels-Alder polymerization reaction. Additionally, these model compounds allowed for various characterization techniques such as mass spectrometry, and density functional theory calculations to be performed, that would otherwise be difficult to perform on polymers.

In Chapter 4, the synthesis of poly(phenylene) homo-polymers **sPPB*o*-H$^+$**, **sPPB*m*-H$^+$** and **sPPB*p*-H$^+$** is outlined. Each of these polymers contains entirely either *ortho*, *meta* or *para* biphenyls. Membranes prepared from these polymers were extensively investigated on various physico-electrochemical properties of interest to proton exchange membrane materials such as those discussed in Chapter 1.

In Chapter 5, discussions from Chapter 4 are built upon, outlining the synthesis of poly(phenylene) co-polymers containing a mixture of either *ortho* and *para,* or *meta* and *para* functionalized biphenyls. Six co-polymers were prepared in total, and as outlined in Chapter 4, membranes prepared therefrom were extensively investigated to evaluate their efficacy as proton exchange membrane materials.

Lastly, in Chapter 6, possible avenues of future work are explored, building upon conclusions drawn from this thesis. The focus on using non-linear monomeric building blocks to influence the physico-electrochemical properties in PEM materials will persist in the proposed future work.

Chapter 2.

Techniques and Methods

2.1. Introduction

The work presented in this thesis made use of several well-established literature procedures that were routinely utilized in the preparation of much of the materials. Background and relevant theory of these procedures as well as instrumentation are described in detail in this section.

2.2. Synthesis

2.2.1. Sonogashira Cross-Coupling

The Sonogashira reaction,[103] first reported in 1975, is a coupling reaction between a terminal alkyne and an aryl or vinyl halide. The reaction is performed using a palladium(0) catalyst (can be generated *in-situ*), a copper(I) co-catalyst, and an amine base under anhydrous and anaerobic conditions. Like many palladium catalyzed cross-coupling reactions, the Sonogashira reaction represents a convenient means of forming carbon-carbon bonds, and is extremely useful in preparing substituted alkynes. While many different palladium based catalysts have been used, tetrakis(triphenylphosphine) palladium, $Pd(PPh_3)_4$, and dichloro-*bis*-(triphenylphosphine)palladium, $Pd(PPh_3)_2Cl_2$, are the two most common and were both used in this work.[104],[105] The latter $Pd(PPh_3)_2Cl_2$ is especially convenient to work with due to its improved tolerance to oxygen over $Pd(PPh_3)_4$.[104],[105]

The Sonogashira cross coupling reaction follows a catalytic cycle involving first an oxidative addition of the halogenated species with the palladium catalyst, followed by *trans*-metalation with the alkyne (after activation with the copper catalyst), *cis*/*trans* isomerization and finally a reductive elimination of the coupled alkyne. The *trans*-metalation step involves a second, complimentary catalytic cycle involving a copper(I) halide, an amine base, and a terminal alkyne that is less well understood. It is thought that copper coordinates to the alkyne forming a pi-alkyne complex, increasing the acidity of the terminal proton.[106] Deprotonation of this terminal proton by the amine base results in

formation of a copper acetylide, that then undergoes *trans*-metalation with the palladium intermediate complex. The catalytic cycle for a Sonogashira cross-coupling between an aryl halide and a terminal alkyne is shown in Scheme 2.1.

Scheme 2.1: *Catalytic Cycle for a Generic Sonogashira Cross-coupling Between an Aryl Halide and a Terminal Alkyne*

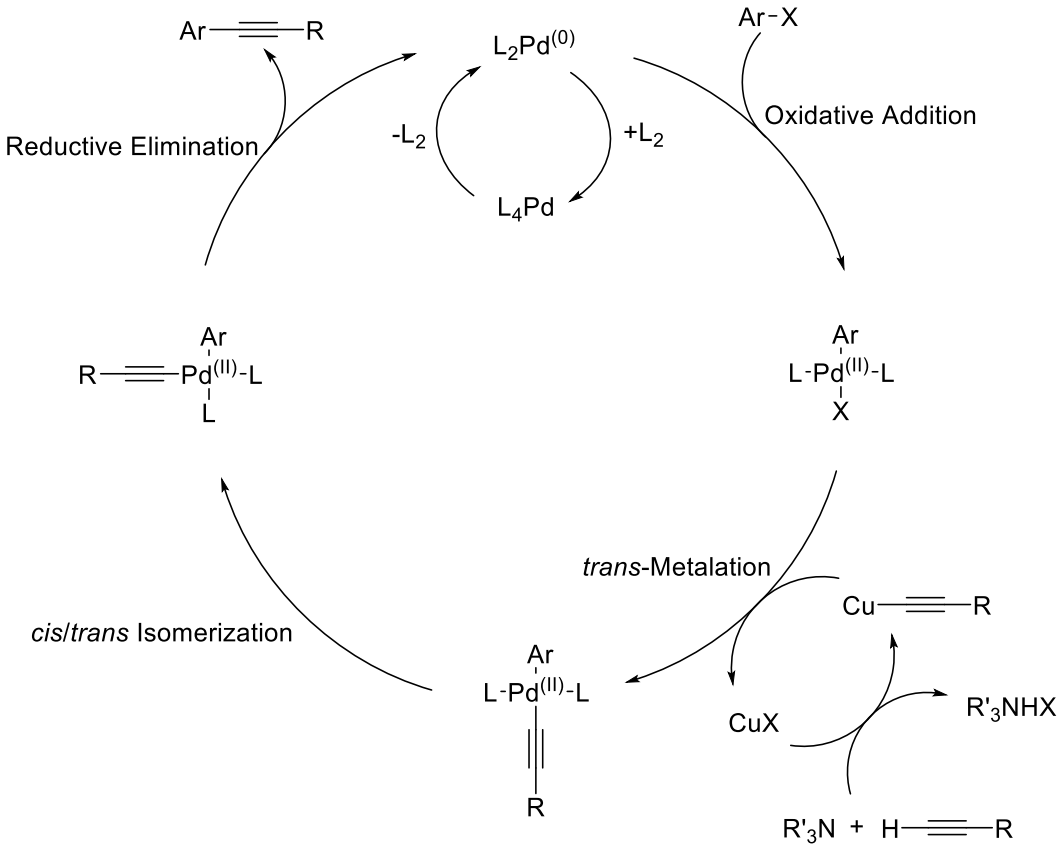

2.2.2. *n*-Butyllithium & Copper (II) Chloride Mediated Homo-Coupling

A homo-coupling reaction mediated by *n*-butyllithium (*n*-BuLi) and copper (II) chloride was utilized to afford *ortho* functionalized biphenyls. While not a well understood reaction, various authors had reported successfully coupling *ortho*-functionalized aryl moieties through its use.[107],[108],[109],[110],[111] A proposed mechanism for the homo-coupling employed in this work is shown in Scheme 2.2, based off of work published in 1966 on the coupling of lithium aryls by $CuCl_2$.[107]

Scheme 2.2: *Proposed Mechanism for the n-Butyllithium/Copper (II) Chloride Mediated Homo-coupling of ((2-Bromophenyl)ethynyl)trimethylsilane*

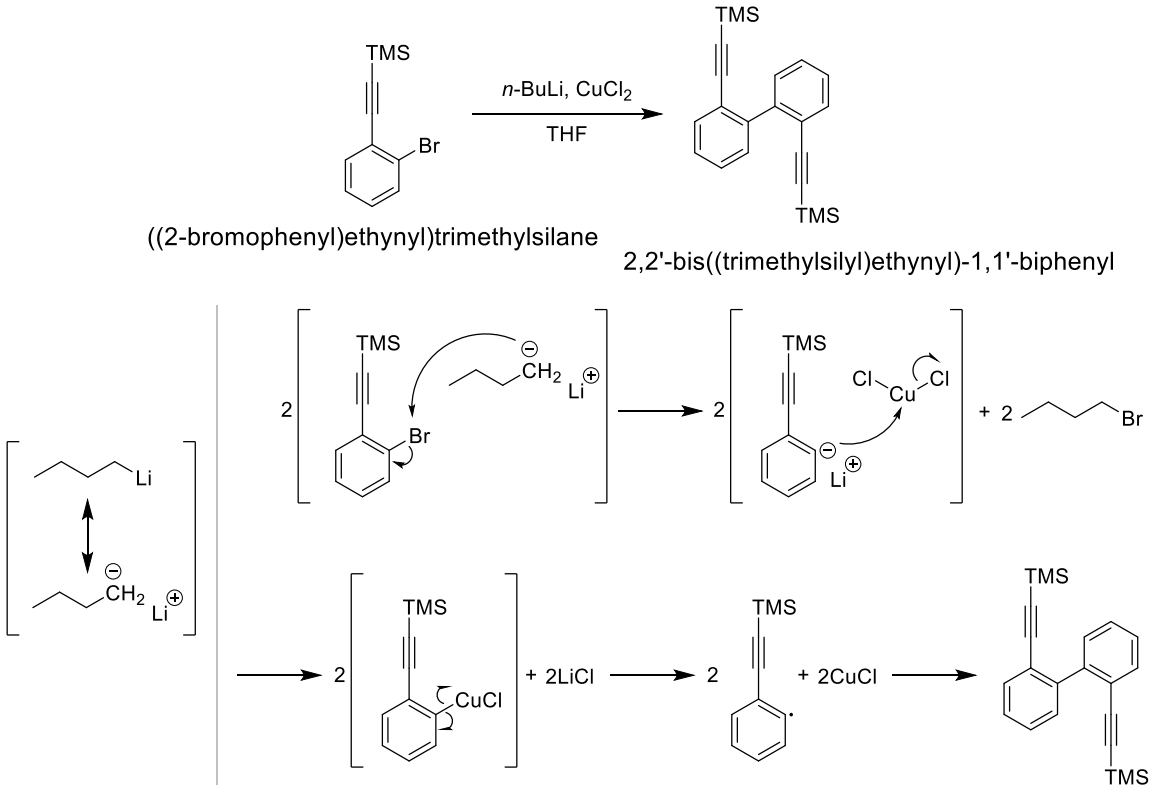

The proposed homo-coupling occurs in four steps. In the first step, nucleophilic attack by the butyl anion on bromine liberates 1-bromobutate while forming the aryl anion. Next, nucleophilic attack by the aryl anion onto $CuCl_2$ liberates LiCl while forming the aryl copper complex. Homolytic cleavage of the carbon-copper bond liberates copper (I) chloride, while forming the aryl radical species that finally couples with another aryl radical species, forming the end product 2,2'-*bis*-trimethylsilylethynyl-1,1'-biphenyl.

2.2.3. Protodesilylation of Alkynes

Protodesilylation of alkynes is an important means of generating terminal alkynes, that was used frequently in this work. Silicon-based functional groups are a diverse class of protecting group, and are necessary in the synthesis of many complex molecules such as natural products.[112] Terminal alkynes are relatively unstable over time, especially at elevated temperature and with exposure to visible and ultraviolet light due to the acidity of the proton (pK_a = approx. 25). As such, protection of the terminal alkyne functional groups

through various reactions, such as the Sonogashira reaction that was routinely employed throughout this work, and over long-time storage was necessary.

Trimethylsilyl acetylene is a relatively low cost, commercially available silyl protected analogue of acetylene. The silyl protecting group provides an added benefit in that trimethylsilyl acetylene is easy to work with as a liquid at room temperature, whereas acetylene exists as a gas. Trimethylsilyl acetylene was routinely used in Sonogashira coupling reactions to generate aromatic molecules possessing terminal alkynes that remained protected until their immediate use was required.

Protodesilylation, or silyl group deprotection, replacing the silyl functional group with a hydrogen atom may be achieved under various conditions.[113] The fundamental deprotection mechanism in all cases remains the same, involving an initial nucleophilic attack on the silicon atom. Common nucleophiles include alkoxides, hydroxide, and fluoride.[113] In this work, methoxide was used as a nucleophile, generated *in-situ* at room temperature through equilibration with the weak base potassium carbonate as shown in Scheme 2.3. Evolution of carbon dioxide helps push the equilibrium toward methoxide through Le Chatelier's principle. Nucleophilic attack of methoxide onto the silicon likely forms the pentavalent intermediate,[114] which then spontaneously decomposes into the terminal acetylide anion and methoxytrimethylsilane. The terminal acetylide anion is then protonated through nucleophilic attack on methanol yielding the desired, protonated terminal alkyne.

Importance was placed on selecting mild reaction conditions that would afford the desired product at room temperature due to the instability of terminal alkynes. In addition, workup and purification conditions were also to be performed under mild conditions. Previous reports had stated that distillation of 1,3-diethynylbezne under vacuum at temperature up to 110 °C resulted in an explosion,[115] with a similar observation being noted following a coupling reaction that resulted in an explosion injuring a lab-worker.[116] For these reasons, purification, when necessary, was performed via silica gel column chromatography.

Scheme 2.3: *Protodesilylation or Deprotection of a Trimethylsilyl Protecting Group from a Terminal Alkyne Using Potassium Carbonate and Methanol*

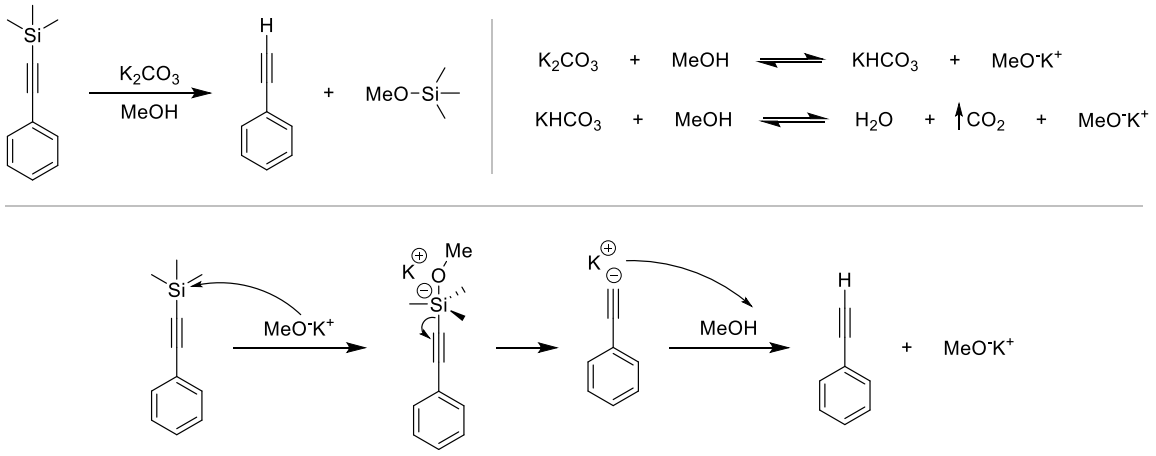

2.2.4. Oxidation of Internal Alkynes to Diketones

The selective oxidation of internal C(sp)-C(sp) bonds to diketones is a complex process that has only been successfully demonstrated using a small number of synthetic methods. Among the successful candidates, oxidations include use of catalytic copper,[117],[118] catalytic palladium in dimethyl sulfoxide (DMSO),[119],[120] sulfur trioxide in dioxane,[121] iodine in DMSO,[122] or the use of potassium permanganate.[123],[124] Metal-catalyzed reactions demand strict anhydrous reaction conditions and expensive catalytic reagents, while the use of sulfur trioxide or potassium permanganate pose safety risks involving potential thermal runaway reactions and the use of potent, toxic, oxidizing reagents. Consequently, this work utilized the iodine/DMSO promoted oxidation to convert internal alkynes to diketones.

The proposed mechanism as shown in Scheme 2.4 shares similarities with the Swern oxidation,[125],[126],[127] that uses DMSO and oxalyl chloride to convert primary or secondary alcohols to aldehydes or ketones, respectively. It is proposed that through a concerted fashion, iodine forms a cyclic iodonium, and iodide anion, analogous to the halogenation of alkenes.[128] The strained iodonium ring is attacked by DMSO relieving ring strain. Attack by a second DMSO molecule onto the electrophilic sp^2 carbon releases dimethyl sulfide forming a carbonyl. This irreversible release of dimethyl sulfide forming the first carbonyl moiety may be the driving force for this oxidation. In the last step, nucleophilic attack of iodide onto the positively charged sulfur atom forms a second carbonyl moiety, liberating iodide forming the iododimethylsulfonium iodide salt. The

generation of this sulfonium salt is supported by the appearance of a white solid material that was found to coat the condenser during the course of this reaction. In solution however, iododimethylsulfonium iodide decomposes to dimethyl sulfide and iodine, thereby regenerating iodine. As such, iodine is catalytic in this oxidation, supported by the 2 mol% relative to alkyne substrate used in the initial report.[122]

Scheme 2.4: *Proposed Mechanism for the I_2/DMSO Promoted Oxidation of an Internal Alkyne to a Diketone*

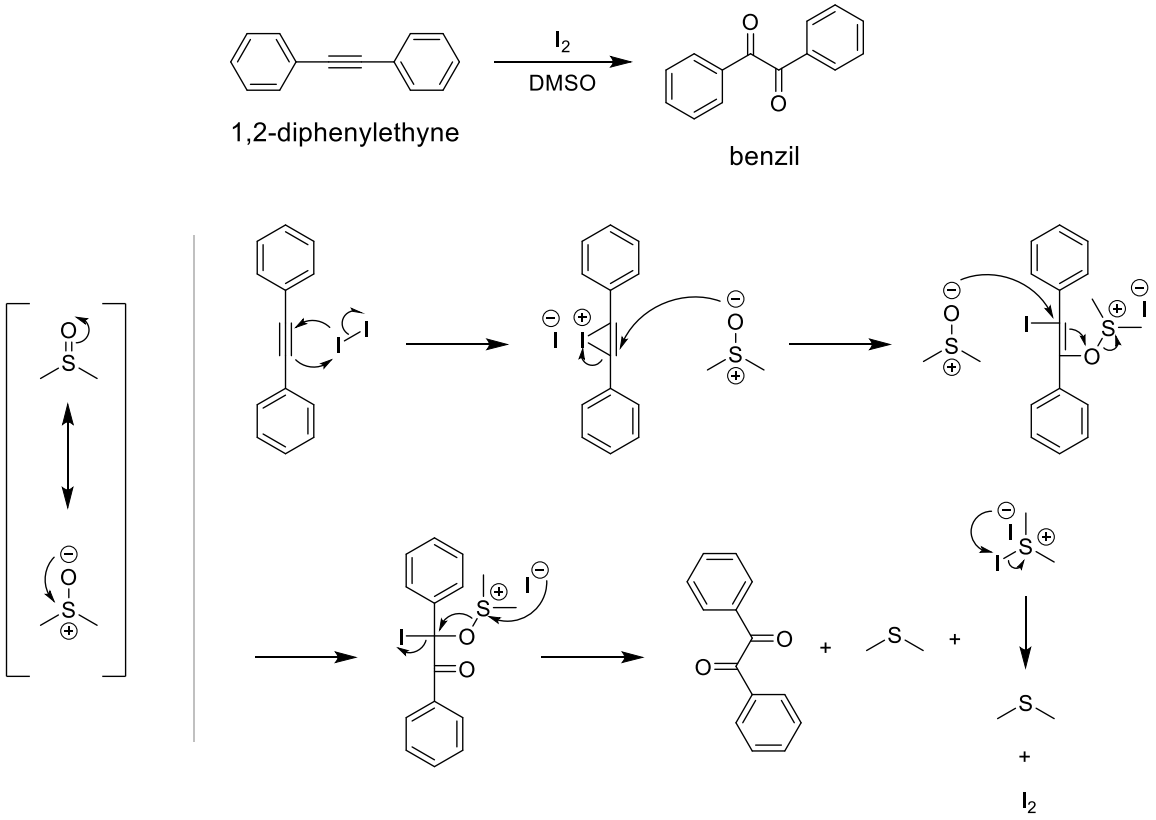

2.2.5. Knoevenagel Condensation

The Knoevenagel condensation is an aldol-like condensation reaction between an activated methylene containing species and a carbonyl containing species in the presence of a base catalyst, resulting in an α,β-unsaturated product. The mechanism of the Knoevenagel condensation is demonstrated in the coupling of benzil (carbonyl containing species) and diphenylacetone (activated methylene containing species) to afford tetracyclone in Scheme 2.5. The reaction is initiated by deprotonation of an activated α-proton on diphenylacetone resulting in the formation of a resonance stabilized enolate

displaying both oxyanion and carbanion character at the α-carbon. The α-carbon of the enolate attacks a carbonyl carbon on benzil, generating a new carbon-carbon bond. The newly generated alkoxide is protonated, generating a tertiary alcohol and regenerating the hydroxide catalyst. Deprotonation of a second α-proton on diphenylacetone results in elimination of the newly formed tertiary alcohol hydroxyl group, and the formation of a double bond. This entire process is repeated a second time, starting with deprotonation of the α-proton at the second α-carbon on diphenylacetone. The end result is tetracyclone, a highly phenylated cyclopentadienone.

Scheme 2.5: *Mechanism of the Knoevenagel Condensation Demonstrated Through the Synthesis of Tetracyclone*

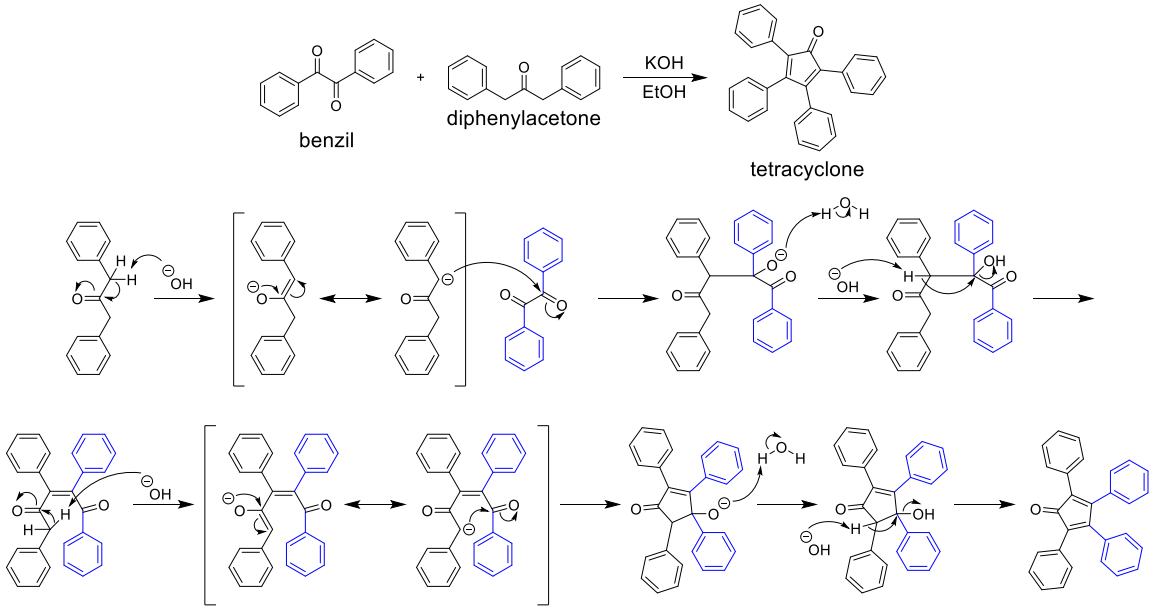

In this work, the Knoevenagel condensation reaction is employed both as shown in Scheme 2.5, and on larger substrates to afford a larger analogue of tetracyclone, bistetracyclone, as shown in Scheme 2.6.

Scheme 2.6: *Synthesis of Bistetracyclone by Knoevenagel Condensation.*

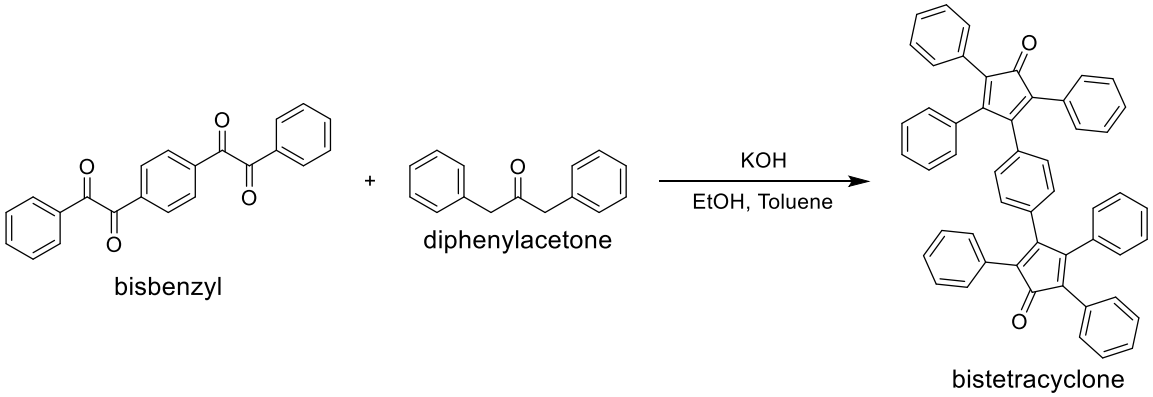

2.2.6. Electrophilic Aromatic Substitution (Sulfonation)

Electrophilic aromatic substitution (EAS) reactions are commonplace in the functionalization of aromatic substrates such as those found in poly(phenylene)s.[52],[79],[80],[81],[82] In EAS reactions, an atom attached to an aromatic ring (typically hydrogen) is replaced, or substituted, by an electrophile. Due to the electron density within aromatic rings, they are inherently nucleophilic, though aromatic stabilization reduces their reactivity. As such, electrophiles must be sufficiently electrophilic to promote nucleophilic attack and temporarily break aromaticity.

In this work, and common to most proton exchange membrane materials, sulfonation of aromatic rings is crucial, installing hydrophilic proton conducting sites onto the polymer. As discussed in Chapter 1, sulfonation of polymers has historically been employed post-polymerization by subjecting the polymer substrate to a strong electrophilic reagent such as sulfuric acid or chlorosulfonic acid. Post-sulfonation is a simple approach but ultimately leads to a number of problems as discussed in Chapter 1 stemming from the ill-defined structures produced therefrom.[34],[77],[78] Here, pre-functionalization of cyclopentadienone monomer precursor units results in a defined polymeric structure through precise positioning and quantity of sulfonation.

Scheme 2.7: *Proposed Mechanism for the Sulfonation of Tetracyclone Using Trimethylsilyl Chlorosulfonate*

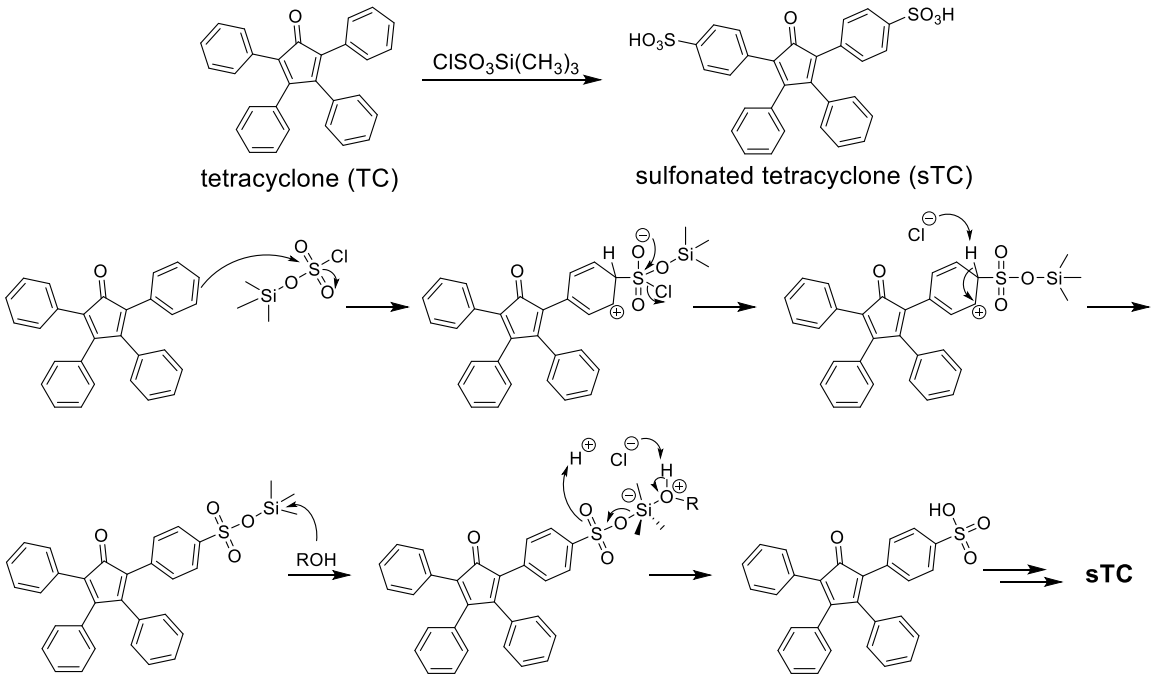

To demonstrate electrophilic aromatic substitution, a proposed reaction mechanism for the sulfonation of tetracyclone using trimethylsilyl chlorosulfonate ($ClSO_3Si(CH_3)_3$) is shown in Scheme 2.7. This sulfonating reagent has been employed in sulfonating various polymers, and is advantageous is that the sulfonate group is protected as a trimethylsilyl ester.[76] Under anhydrous conditions, the silyl ester may prevent side reactions such as crosslinking or acid catalyzed de-sulfonation at high temperatures that has been reported to occur with sulfonating reagents such as chlorosulfonic acid.[76] Nucleophilic attack from the benzene ring onto the electrophile forms a carbon-sulfur bond and eliminates a chloride ion, breaking aromaticity. A proton is abstracted from the ring by a chloride ion, restoring aromaticity. The sulfonate group protected with a trimethylsilyl ester remains protected until an alcohol (or other suitable nucleophile) is added which attacks silicon, forming a pentavalent silicon intermediate before a protodesilylation-like decomposition occurs, forming the sulfonic acid moiety. Sulfonated tetracyclone is formed after a second EAS reaction on the second benzene ring adjacent to the carbonyl occurs.

In the case of both tetracyclone and bistetracyclone, sulfonation is found to occur selectively on the benzene rings adjacent to the carbonyl, and only at the *para* positions. This can be explained by considering resonance structures of the intermediate formed

immediately following electrophilic aromatic substitution. Scheme 2.8 to Scheme 2.10 show the delocalization of positive charge through resonance stabilization in tetracyclone immediately following reaction with an electrophile (E), at the *ortho*, *meta,* or *para* positions respectively. Sulfonation at the *meta* position (Scheme 2.9) results in a reaction intermediate with only three resonance contributors regardless of whether sulfonation occurs at the phenyl ring closer or further from the carbonyl moiety. Sulfonation at the *ortho* and *para* positions (Scheme 2.8 and Scheme 2.10) result in the same degree of resonance stabilization, however, steric restriction likely disfavor EAS at the ortho positions.[77] When *para* sulfonation occurs on the upper phenyl ring closer to the carbonyl moiety, there are more resonance contributors vs when it occurs on the lower phenyl ring further from the carbonyl moiety (11 vs 7), which increases the stability of the intermediate formed, lowering the activation energy required to proceed through this pathway. Therefore, selective EAS at the *para* positions of the phenyl rings adjacent to the carbonyl moiety occurs due to a combination of steric and electronic effects as described.

Scheme 2.8: *Resonance Structures of Tetracyclone Immediately Following Reaction with Electrophile (E) at ortho Positions. δ^+ Represent a Partial Positive Charge Delocalized Through Resonance Stabilization*

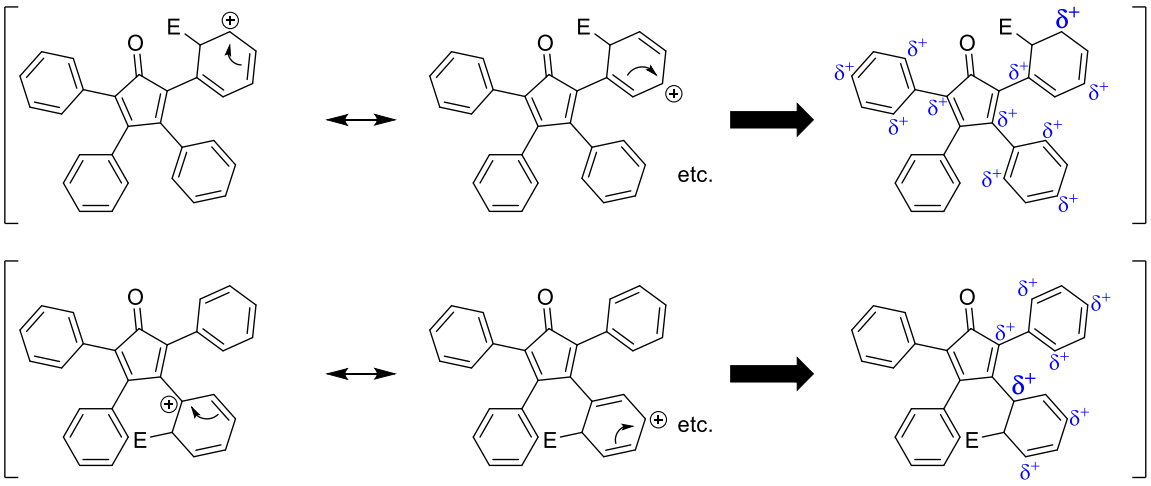

Scheme 2.9: *Resonance Structures of Tetracyclone Immediately Following Reaction with Electrophile (E) at meta Positions. δ^+ Represent a Partial Positive Charge Delocalized Through Resonance Stabilization*

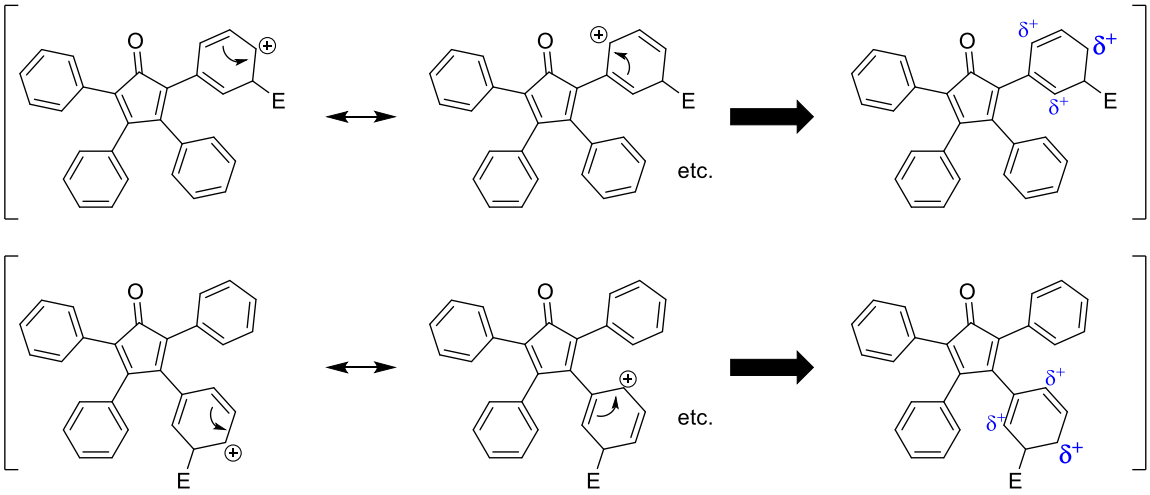

Scheme 2.10: *Resonance Structures of Tetracyclone Immediately Following Reaction with Electrophile (E) at para Positions. δ^+ Represent a Partial Positive Charge Delocalized Through Resonance Stabilization*

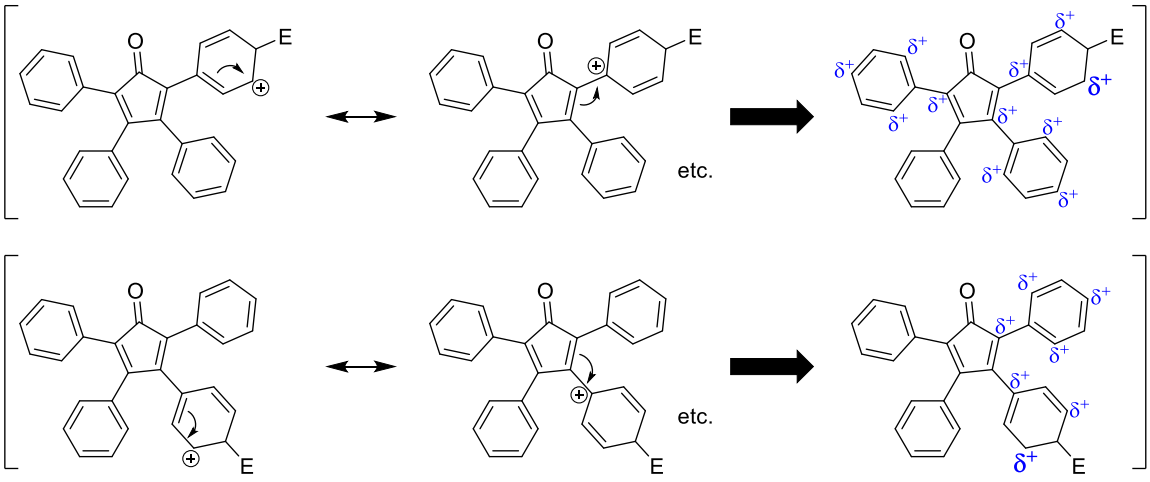

2.2.7. [4 + 2] Diels-Alder Cycloaddition

The Diels-Alder (DA) reaction, named after Otto Diels and Kurt Alder,[129] is a well-known cycloaddition between a diene and a dienophile resulting in carbon-carbon bond formation. The [4 + 2] DA reaction is thought to be a concerted process that involves the pericyclic movement of six π electrons,[130] between an appropriately substituted 1,3-

butadiene (diene) and an alkene or alkyne (dienophile). The DA reaction proceeds through a *suprafacial* (*syn*), or from the same face, interaction with respect to both the diene and dienophile to allow π-orbital overlap. As such, the diene must necessarily adopt an *s-cis* conformation to maximize π-orbital overlap. A representative DA reaction coordinate between a diene and a dienophile to form a DA cycloadduct is shown in Figure 2.1. The driving force behind a typical DA reaction is the formation of two carbon-carbon σ-bonds in place of two π-bonds, provided enough energy is supplied to overcome the activation energy (E_a) barrier.

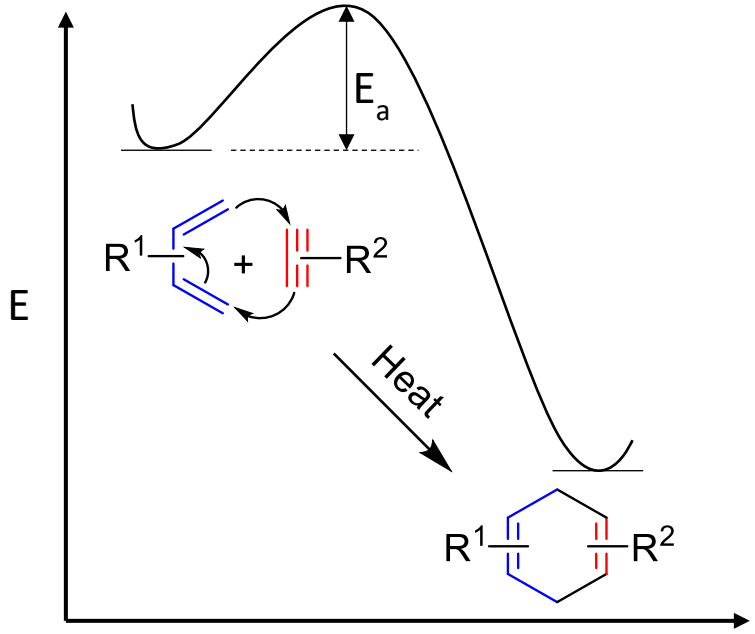

Figure 2.1: *A representative Diels-Alder reaction coordinate diagram between a substituted 1,3-butadiene (diene) and a terminal alkyne (dienophile).*

The activation energy that affects kinetics of the Diels-Alder reaction is dependent upon the energy gap between the highest occupied molecular orbital (HOMO) and lowest unoccupied molecular orbital (LUMO). In a DA reaction, electrons flow from the HOMO of the electron-rich species into the LUMO of the electron-deficient species. By convention, a regular demand DA reaction is one where electrons flow from the HOMO of an electron rich diene to the LUMO of an electron poor dienophile, whereas in an inverse demand DA reaction electrons flow from the HOMO of an electron rich dienophile to the LUMO of an electron poor diene.

The Diels-Alder reaction depicted in Figure 2.1 is a reversible process, whereby in the reverse process via a retro DA reaction, two carbon-carbon σ-bonds are broken and two π-bonds are formed. In this work however, the [4 + 2] DA cycloaddition reactions performed are irreversible. The irreversibility arises from the expulsion of a small molecule from the resulting cycloadduct, through a process known as extrusion.[131] Scheme 2.11 shows a DA and resulting extrusion of carbon monoxide following the reaction between a functionalized cyclopentadienone diene and a terminal alkyne dienophile. In this case, a strained bridged species is formed immediately following the DA reaction. The bridged intermediate spontaneously extrudes gaseous carbon monoxide, generating an aromatic center in the process. The driving force for this and similar extrusion processes is the formation of significantly lower energy products;[131] in this case carbon monoxide gas which exits the reaction medium, and an aromatic phenyl ring. DA reactions of this sort were routinely employed to afford highly phenylated oligo and poly(phenylene)s in this work.

Scheme 2.11: *Proposed Mechanism for the Diels-Alder and Extrusion Reaction Between a Functionalized Cyclopentadienone (Diene) with a Terminal Alkyne (Dienophile)*

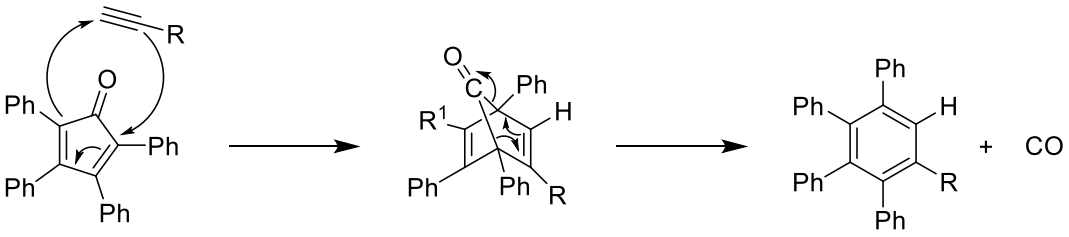

Regiochemical aspects of the Diels-Alder reaction may lead to the formation of regioisomeric products if both diene and dienophile are asymmetric. For example, if one of the cyclopentadienone phenyl rings from Scheme 2.11 is replaced with another functional group R_1, as is the case in this work, both partners in the DA reaction are asymmetric. Depending on the orientation of the dienophile with respect to the diene upon reaction, two regioisomeric products are possible; the a *meta* or *para* product, as depicted in Scheme 2.12.

Scheme 2.12: *meta and para Regioisomeric Products that Form Upon Reacting Asymmetric Cyclopentadienone and Terminal Alkyne Moieties*

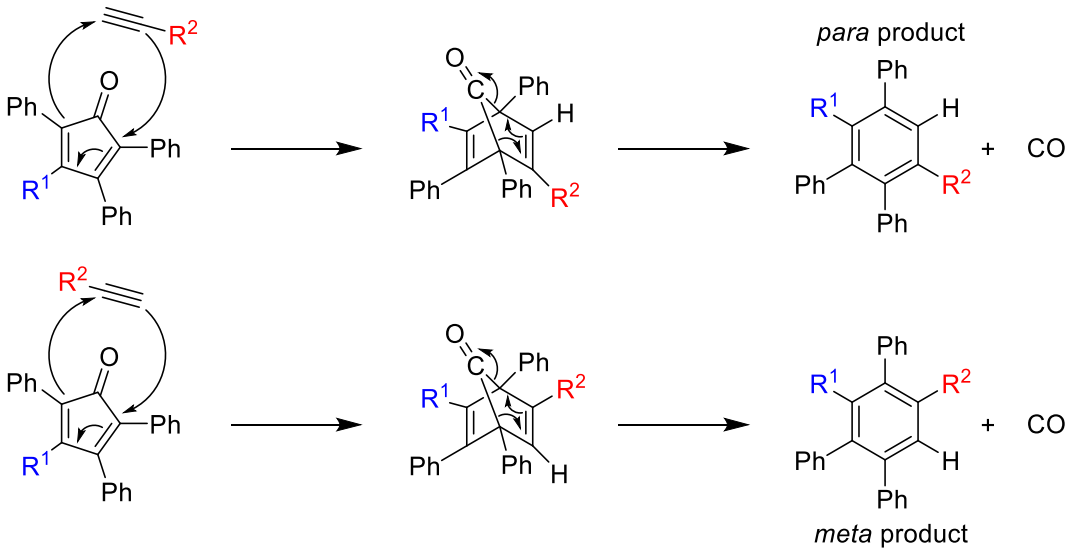

Typically, the preferred regiochemical course in a Diels-Alder reaction can be rationalized on the basis of resonance. For example, consider a regular demand DA reaction between a diene substituted with an electron donating group (EDG) and a dienophile substituted with an electron withdrawing group (EWG). The regiochemical preference may be understood by considering resonance structures, assuming that the most nucleophilic component of the diene is more likely to react with the more electrophilic component of the dienophile.[132] This is shown schematically in Scheme 2.13, where the likely major product is formed by aligning the most nucleophilic component of the diene with the most electrophilic component of the dienophile.

Scheme 2.13: *Regiochemical Aspects of Diels-Alder Reactions Rationalized Using Resonance Structures, Where the More Nucleophilic Component of the Electron Rich Species Reacts with the Most Electrophilic Component of the Electron Poor Species*

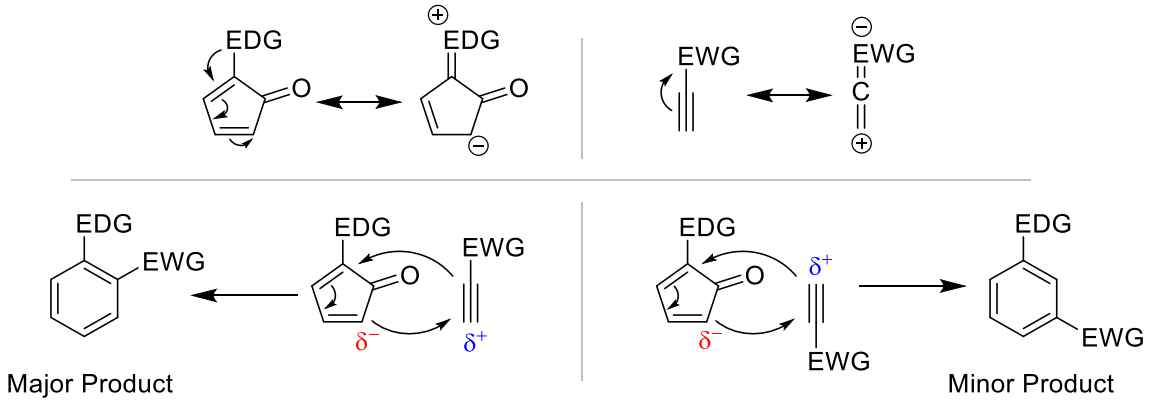

When regioselectivity is governed by EDGs and EWGs through resonance, Diels-Alder reactions follow the *ortho-para* rule. This rule states that by pairing the most electron rich component of the EDG containing substrate with the most electron poor component of the EWG containing substrate, the EDG and EWG will be either *ortho* or *para* to one another on the formed cycloadduct. It is worth noting that in this thesis, however, rationalizing regioselectivity based on EDG and EWG directed resonance is likely not possible, as the substituents on both the diene and dienophile are phenyl rings. Therefore, it is unlikely that regiochemical preference is governed by resonance. Nevertheless, the DA reactions performed in this work are indeed able to form distinct regioisomeric products, so consideration of this aspect was necessary.

2.3. Nuclear Magnetic Resonance (NMR) Spectroscopy

Nuclear magnetic resonance (NMR) spectroscopy is a crucial tool in modern day organic chemistry for the structural elucidation of molecules. NMR spectroscopy takes advantage of nuclear spin, that both ^{1}H and ^{13}C atomic nuclei possess. An NMR spectrometer places these atomic nuclei (which are essentially small bar magnets) in a large magnetic field, forcing them to align with the magnetic field. If an applied radiofrequency pulse with the right amount of energy corresponding to the unique chemical environment the nuclei is in, the nuclei can absorb this energy. In doing so, the nuclei will “flip” from being aligned with the magnetic field (lower energy state) to being aligned against the magnetic field (higher energy state). As the nuclei relax back to the lower energy state, they re-release this energy, which can be detected by the NMR spectrometer. ^{1}H, ^{13}C, ^{1}H-^{1}H COSY, ^{1}H-^{13}C HSQC and ^{1}H-^{13}C HMBC NMR spectroscopy are very common in the literature and will not be discussed. This work however, uses two lesser known NMR experiments, 2D EXSY (utilizing a NOESY pulse sequence), and 2D ROESY, both of which are described below.

2D EXSY, or exchange spectroscopy, utilizes a NOESY, or nuclear Overhauser effect spectroscopy pulse sequence. NOESY utilizes through-space magnetic interactions (dipolar coupling), as opposed to through-bond bond interaction (scalar coupling) used in more common experiments to provide information.[133] NOESY is called EXSY when it is used to identify signals (typically protons) undergoing chemical or conformational exchange within a molecule.[134],[135],[136] In a 2D EXSY experiment, cross-peaks of opposite-phase to the diagonal are due to through space NOE correlations. The phase of

cross-peaks from exchange however, is influence by the tumbling rate of the molecule. Accordingly, small molecules have exchange cross-peaks are in phase with the diagonal, while in large molecules the exchange cross-peaks are of opposite phase with the diagonal.[137]

2D ROESY, or rotating-frame Overhauser effect spectroscopy, is similar to 2D NOESY/EXSY in that it is also able to identify signals (typically protons) undergoing chemical or conformational exchange, however, it works better on large molecules. 2D ROESY is not sensitive to the tumbling rate of the molecule, and as such, cross-peaks from exchange are always in phase with the diagonal regardless of molecular size.[138] A complication in 2D ROESY experiments is TOCSY (total correlated spectroscopy) transfer that arises due to a similar spin-lock period used in both experiments.[133] The signals from TOCSY transfer can make it difficult, or impossible, to correctly identify signals arising from exchange. Transverse 2D ROESY (Tr-ROESY) however, eliminates unwelcome TOCSY transfer that standard ROESY experiments are susceptible to, by utilizing an alternating-phase spin-lock.[133],[138]

2.3.1. Experimental

Most ^{1}H NMR, ^{13}C NMR, and 2D NMR spectra were obtained on either a Bruker AVANCE III 400 MHz or Bruker AVANCE III 500 MHz instrument, both running IconNMR under TopSpin 3.6. Exchange spectroscopy experiments were performed on an Avance III 600 MHz instrument, equipped with a 5mm QCI cryoprobe running Topspin 3.6.

2.4. Mass Spectrometry (MS)

Mass spectra were recorded either on a Bruker Maxis Ultra-High-Resolution tandem time-of-flight (UHR-QTOF) mass spectrometer or with an Agilent 6210 time-of-flight LC/MS.

2.5. Density Functional Theory (DFT)

Density functional theory is a well established, commonly used computational modelling method used to investigate the ground state electronic structure of molecules. These calculations, which operate using electron density functionals (mathematic

functions of another function), may be performed in vacuum, or in explicit solvent, to approximate molecular energy, structure and properties.[139] DFT modeling is done by distributing electrons throughout atomic orbitals within a molecule, then minimizing the force interaction between nuclei by rotating bonds; this process is repeated until an energy minima is found. Becke, 3-parameter, Lee-Yang-Parr (B3LYP), used in this work, is one of the most common functionals used to represents the electron density as a function of space and time, and is the literature standard.[140] Atomic orbitals (or electronic wave functions) are represented by a basis set which is a set of basis functions, or algebraic equations, suitable for computational implementation. def2-TZVP is the basis set used in this work, and is a slightly larger and more general basis set than 6-311G(d,p).[141] DFT calculations were performed by Erich M. Schibli and Dr. Barbara J. Frisken in this work.

2.5.1. Experimental

Density functional theory calculations were performed via the Gaussian 16 Revision B01 software package,[142] using the B3LYP hybrid functional,[140] and the def2-TZVP basis set.[141] Diffuse functions were added for the oxygen atoms.[143] Calculations were performed in implicit solvent using the polarizable continuum model.[139] Relaxed dihedral energy scans were performed by iteratively rotating the dihedral of interest by 10° and optimizing the remaining geometry.

2.6. Gel Permeation Chromatography (GPC)

The molecular weight (MW) and molecular weight distribution or dispersity (Đ) of polymers are important characteristics to consider, as they govern many physical properties.[144] Gel permeation chromatography (GPC) also known as size exclusion chromatography (SEC) are standard chromatographic techniques used to determine polymer molecular weights and dispersities.[144],[145],[146] GPC is a liquid chromatography method that separates polymer molecules by their size (hydrodynamic volume), as a polymer solution passes through a column(s) packed with a porous support.[147] Smaller molecules are retained in the pores of the support to a greater degree than larger molecules, and therefore elute from the column last, while larger molecules elute first. When analyzing polymers containing ionic or polar groups, it is common to add a small amount of salt such as LiBr to prevent aggregation of polymer molecules. Using a triple

detection technique using a combination of light scattering, viscometer, and refractive index detectors, it is possible to calibrate the system using a single narrow molecular weight calibrant.[148]

The molecular weight of a polymer may be represented in a number of ways. The number average molecular weight (M_n) represents a simple arithmetic mean of molecular masses of the individual polymers. It is determined by dividing the total weight of polymer by the total number of polymers, as per Equation 2.1, where N_i is the number of polymers with weight M_i. The weight average molecular weight (M_w) is based around the fact that larger molecules contain disproportionately more of the overall mass, and will therefore have a larger contribution to polymer properties. As M_w depends not only on the number of polymers present, but also on the weight of each polymer, N_i in Equation 2.1 is replaced with N_iM_i, as shown in Equation 2.2. As M_w is biased toward higher molecular weigh polymers, M_w is always greater than M_n. The degree at which M_w is greater than M_n is representative of the molecular weight distribution, or dispersity (Đ), within a given sample of polymer as shown in Equation 2.3. As the molecular weight distribution in a given sample becomes more homogenous, the Đ decreases to a minimum of 1 ($M_w = M_n$), meaning all polymers have the same molecular weight. A representative molar mass distribution obtained through GPC can be seen in Figure 2.2.

Equation 2.1: $M_n = \frac{\sum M_i N_i}{\sum N_i}$ *Equation 2.2:* $M_w = \frac{\sum M_i^2 N_i}{\sum M_i N_i}$

Equation 2.3: $Đ = \frac{M_w}{M_n}$

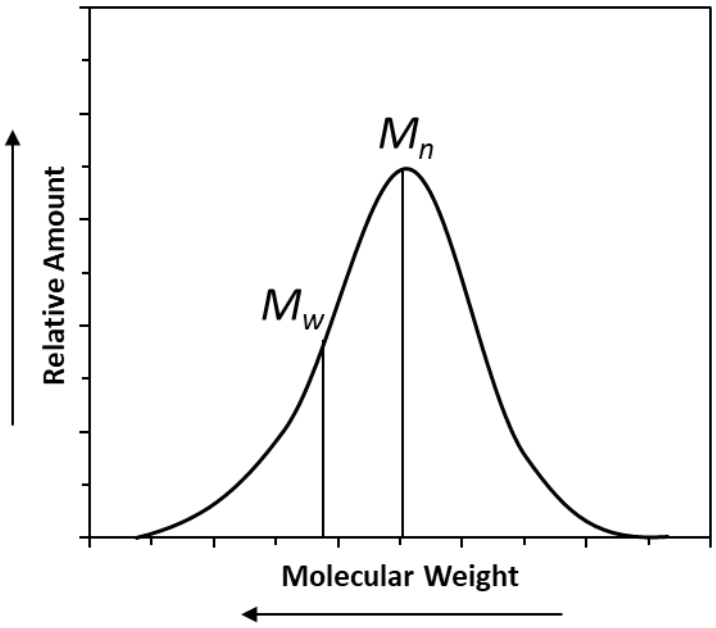

Figure 2.2: *A representative molar mass distribution of a polymer sample obtained through GPC, highlighting M_n and M_w.*

2.6.1. Experimental

Molecular weights of polymers were determined by gel permeation chromatography (GPC) using a Malvern Omnisec Resolve GPC system equipped with a Viscotek D6000M primary column and Viscotek D3000 secondary column using HPLC grade DMF (containing 0.01 M LiBr) as eluent. Measurements were collected via a triple detection technique using a combination of refractive index, right angle light scattering, and viscometer detectors. Narrow molecular weight distribution polymethyl methacrylate (PMMA; M_w = 51,092, M_n = 49,231 g mol^{-1}) standards were used to calibrate the system. Calibration was then verified by measuring a verification standard with a wider dispersity (PMMA; theoretical M_w = 95,534, M_n = 51,971 g mol^{-1}; measured M_w = 96,500, M_n = 51,200 g mol^{-1}). Polymer samples were prepared accurately to 5.0 ± 0.1 mg/mL concentrations in HPLC grade DMF (containing 0.01 M LiBr) and filtered through a 0.22 µm, 13 mm diameter CELLTREAT® PTFE filter. The injection volume was 100 µL with a flow rate of 1.0 mL min^{-1}, and the column and detector temperatures were held constant at 50 °C throughout the measurements.

2.7. Thermogravimetric Analysis (TGA)

Thermal stability of materials can be assessed using thermogravimetric analysis (TGA). A thermogravimetric analyzer incorporates a sensitive balance inside of a chamber capable reaching high temperature. In this way, the weight change as a function of time or temperature can be followed.[149] TGA may be performed under various atmospheres, such as ambient air, inert gas, or more harsh atmospheres such as those under oxidizing or reducing gasses. These measurements can be used to determine various parameters including but not limited to material decomposition temperatures and solvent retention, and can also be used to estimate compositional elements, given their decomposition temperatures are known.

2.7.1. Experimental

Polymer thermograms were obtained using a Shimadzu TGA-50 thermogravimetric analyzer. Membrane samples weighing approximately 6 mg were heated from ambient temperature to 800 °C at a heating rate of 10 °C min^{-1} under constant N_2 flow. In all cases, to normalize mass losses to a percent mass loss, the masses recorded at 220 °C were set to 100% of the sample mass. This temperature corresponded to the minima in the weight loss derivatives following loss of residual H_2O and DMSO, and is assumed to be the true dry mass of the polymer.[52],[80],[81]

2.8. Differential Scanning Calorimetry (DSC)

Differential scanning calorimetry (DSC) is a thermal analysis technique that measures the heat flow into or away from a material as a function of temperature or time.[149] This is achieved by heating or cooling both a sample and a reference at a predetermined rate. The instrument ensures that both the sample and reference maintain the same temperature throughout the heating or cooling process. In this way, if the sample undergoes any endothermic or exothermic events, the instrument heat output to the sample will have to increase or decrease respectively to maintain equivalent temperatures between sample and reference. The amount of heat required to maintain this balance is recorded, and can be plotted against temperature or time. The area under the resulting curve is a measure of the heat of transition for some endothermic or exothermic event.[149]

2.8.1. Experimental

Assessment of glass transition temperatures were measured using a Thermal Instruments Q2000 DSC under a 50 mL min^{-1} constant flow of nitrogen with a temperature ramp rate of 20 °C min^{-1}. Samples (8 ± 3 mg) were contained in aluminum Tzero® pans equipped with lids. To allow solvents to escape during heating, the pans were not sealed. Duplicate scans were performed from ambient temperature to 200 °C (2x), followed by ambient temperature up to 450 °C (2x). Duplicates (a pre-scan followed by a scan) were used to elucidate whether the endothermic events observed were reversible (e.g., glass transition), or irreversible (e.g., residual solvent evaporation; decomposition).

2.9. Membrane Preparation

2.9.1. Experimental

Polymer membranes were cast from 7.5 % w/w acid form of the polymer in DMSO solutions. Filtered polymer solutions were poured onto a glass plate and placed on a Control Coater casting table equipped with a RK PrintCoat Instrument Ltd. adjustable casting blade at a height of 650 µm used to spread and level the polymer solution. After heating at 86 ± 1 °C for a minimum of 16 h on a level surface in a dust free environment, the glass plates were removed from heat and allowed to cool at ambient temperature for a minimum of 4 h, before the membranes were removed from the glass plates. Membranes were further dried *in vacuo* at 80°C, pressed between two glass plates wrapped with lint free wipes, resulting in membranes approximately 25 µm thick.

2.10. Mechanical Strength Measurements

A tensile “pull” test may be performed to determine material mechanical properties including tensile strength, elongation at break and Young’s modulus. This is done by anchoring a material at one end and subjecting the other end to a controlled displacement (ΔL). As the pulling force (F) is increased gradually to maintain the controlled displacement, the material stretches until it eventually breaks. Material stress (σ) is defined as the force (F) a material of a given cross-sectional area (A_{xs}) experiences, typically reported in Pascals as per Equation 2.4. Material strain (ε) is a dimensionless

quantity, and represents the amount of material deformation (ΔL) with respect to its original length (L_o) as per Equation 2.5.

$$\textit{Equation 2.4: } \sigma = \frac{F}{A_{xs}} \qquad\qquad \textit{Equation 2.5: } \varepsilon = \frac{\Delta L}{L_o}$$

Pull test measurements are made by cutting a membrane into a standard wishbone shape with a known width using a cutting die.[150] The sample is then placed into the instrument, held at each end by a clamp. The top clamp (attached to a crosshead) moves at a specified speed, while the bottom clamp is held in a static position. The crosshead applies the necessary force required to move at the specified displacement speed until the material fractures. In this way, the force required to elongate a material at a constant rate until failure can be known. When the stress is plotted against the strain, a stress-strain curve such as that shown in Figure 2.3 is obtained.

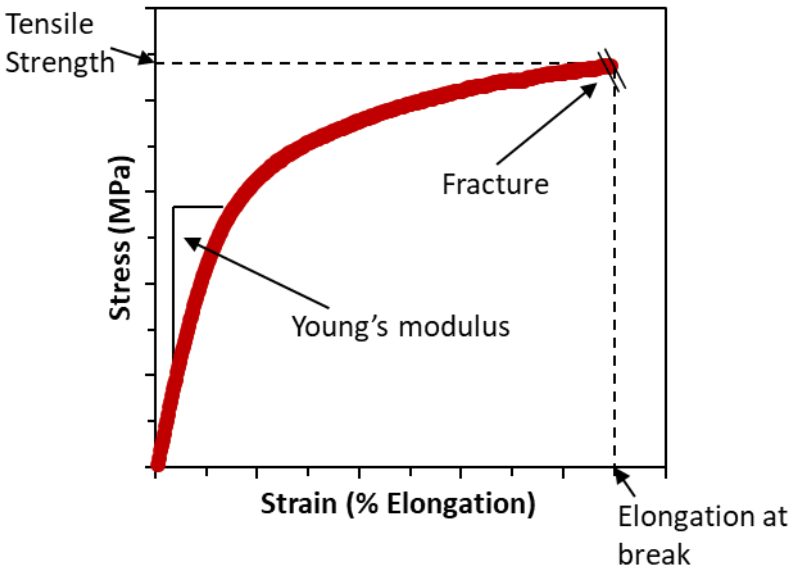

Figure 2.3: *Example of a stress-strain curve obtained through tensile pull tests.*

2.10.1. Experimental

Polymer membrane tensile strength, elongation at break and Young' moduli were assessed using an Instron 3344 Series single column system operating with a crosshead

speed of 5 mm min^{-1}. Membranes were allowed to equilibrate to ambient conditions for a minimum of 24 h, after which they were cut into a barbell-shaped samples using a standard ASTM D638 type IV specimen cutting die. The tensile strength, elongation at break, and Young's modulus reported represent the average of at least six sample measurements, with the error represented as the standard deviation.

2.11. Water Sorption Characteristics

2.11.1. Experimental

Polymer membrane water sorption characteristics were determined by measuring the mass and dimensional changes in membranes between their dry and fully hydrated states. Small membrane samples (approx. 2x3 cm) were immersed in de-ionized water for at least 24 hours before their hydrated thickness (th_{wet}), hydrated area (A_{wet}), and hydrated mass (m_{wet}) were measured. To obtain fully dried parameters, membrane samples were pressed between two glass plates wrapped with lint free wipes and dried *in vacuo* at 80°C for a minimum of 16 h, after which their dry thickness (th_{dry}), dry area (A_{dry}), and dry mass (m_{dry}) were measured. The above procedures for both hydrated and fully dried measurements were repeated in triplicate. Membrane sample areas were determined using a Canon Canoscan8400F scanner, scanning at 1600 dpi, and the resulting images were analyzed using ImageJ. Sample thicknesses were measured using a Mitutoyo Quickmike Series 293 micrometer, taking the average thickness of 5 discrete points (center and four corners). Before weighing hydrated samples, the surface of each was blotted dry to remove surface water, as described previously.[79] Sample volume (V_x, where x = wet or dry), volumetric expansion (V_{exp}), water uptake (W_{up}), and water content (W_{con}) was calculated using EquationsEquation 2.6, Equation 2.7, Equation 2.8, and Equation 2.9, respectively. The hydration number (λ), which represents the number of water molecules per sulfonic acid group within the membrane (mol H_2O/mol $-SO_3H$) was determined using Equation 2.10, where M_{H2O} is the molar mass of water (18.02 g mol^{-1}).

Equation 2.6: $V_x = A_x \times th_x$

Equation 2.7: $V_{exp} = \frac{V_{wet} - V_{dry}}{V_{dry}} \times 100\%$

Equation 2.8: $W_{up} = \frac{m_{wet} - m_{dry}}{m_{dry}} \times 100\%$

Equation 2.9: $W_{con} = \frac{m_{wet} - m_{dry}}{m_{wet}} \times 100\%$ *Equation 2.10:* $\lambda = \frac{W_{up}}{M_{H2O} \times IEC_{xp}} \times 10$

2.12. Ion Exchange Capacity (IEC)

2.12.1. Experimental

The theoretical ion exchange capacity (IEC_{th}, meq. g^{-1}) was determined using Equation 2.11, where MW is the molecular weight of one polymeric repeat unit, and n_{SO3H} is the number of moles of sulfonic acid moieties present per repeat unit. The experimental ion exchange capacity (IEC_{xp}, meq. g^{-1}) of polymer samples was measured by ion-exchange acid base titrimetric analysis in their acid form. Titrations were performed using a Metrohm 848 Titrino Plus auto titrator system. An approximately 0.01 M NaOH titrant was standardized using potassium hydrogen phthalate (KHP) as a primary standard. KHP was first dried in vacuo and a 0.01000 M KHP solution was prepared to standardize the NaOH, after which three KHP solutions were titrated to their endpoint to accurately determine the concentration of the NaOH solution. Membrane samples of known mass were submerged in 1 M H_2SO_4 over a period of 3 days, replacing with fresh acid every 24 hours to ensure all acid sites were protonated. The membranes were then soaked in deionized water over a period of 3 days, replacing with fresh deionized water daily to remove residual acid. The membranes were then submerged in 20 mL of 1 M aqueous NaCl for 24 hours to displace the acidic protons into solution before the membranes were removed and rinsed and the resulting acidic solutions were titrated. This process was repeated at least three times, with at least three membranes, providing at minimum nine measurements. IEC_{xp} was calculated according to Equation 2.12, where V_t is the volume and C_t is the concentration of standardized titrant required to reach the endpoint.

Equation 2.11: $IEC_{th} = \frac{n_{SO3H}}{MW} \times 1000$ *Equation 2.12:* $IEC_{xp} = \frac{V_t \times C_t}{m_{dry}}$

2.13. Electrochemical Impedance Spectroscopy (EIS)

Electrochemical impedance spectroscopy is a non-destructive technique that sweeps an alternating potential from high to low frequency (ω) across the leads of an electrochemical cell and measures the current response. Assuming the excitation potential is sinusoidal, the current response will also be sinusoidal, at the same frequency. Any capacitive elements in the electrochemical cell will result in a phase shift of the measured current response. This technique allows for the construction of a Nyquist Plot of the "imaginary" (Z'') component of impedance versus the "real" (Z') component of impedance.

A Nyquist plot is created by plotting the endpoint of the vector created from the magnitude impedance (|Z|) and the phase shift (θ) over a range of frequencies. Figure 2.4 shows an example of a Nyquist plot representative of a proton exchange membrane conductivity cell, that can be represented by a simple Randles circuit consisting of a resistor and a capacitor in parallel, with a resistor in series. In this cell, R_{ohmic} corresponds to the cells contact resistance (equal to the impedance at the high frequency x-axis intercept), R_{ion} corresponds to the ionic resistance of the membrane, and C_d is the double layer (electrode/electrolyte) capacitance. In this thesis, R_{ion} is of primary interest as it is used to calculate proton conductivity (σ_{H^+}).

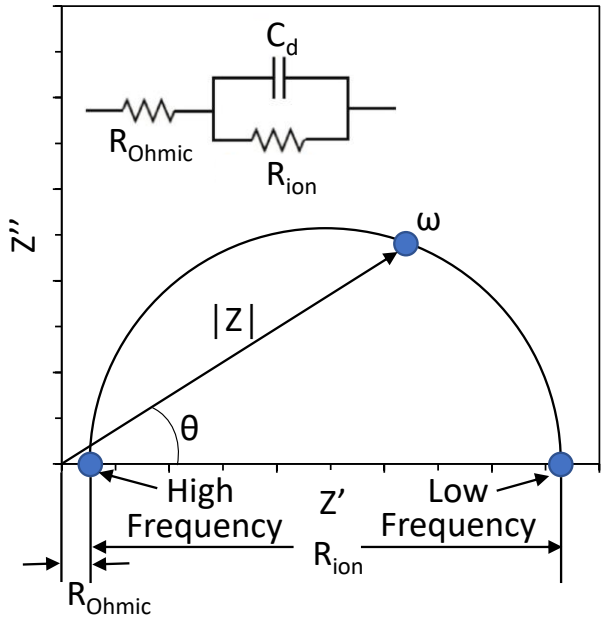

Figure 2.4: *Nyquist plot representative of a proton exchange membrane conductivity cell, modeled using a simple Randles circuit.*

2.13.1. Experimental

Ex-situ proton conductivity of polymer membranes was measured using alternating current (AC) impedance spectroscopy. Hydrated membranes were cut into 5 x 15 mm samples and soaked in 1 M H_2SO_4 for a period of three days, replacing the acid solution daily to ensure all acid sites were protonated. This was followed by soaking the membrane samples in DI H_2O for a period of three days, replacing the DI H_2O daily to rinse away any residual acid. Following pre-treatment, membrane samples were loaded into a total of six conductivity cells, each in a two-electrode configuration as described previously.[151] Cells were placed in an Espec model SH-241 humidity chamber to control temperature and relative humidity (RH), and connected to a Solartron 1260 frequency response analyzer. Measurements were performed by applying a 10 mV sinusoidal AC potential over a frequency range of 10 MHz – 100 Hz.[52] Membranes were measured at 30, 40, 50, 60, 70, 80, 90, and 95% RH, at both 30 and 80 °C. Samples were equilibrated for a minimum of 1 h after changing measurement conditions. During this period, measurements were taken every 15 min to confirm the system had reached equilibrium. The ionic resistance (R_{ion}) in ohms of each sample was determined by fitting the Nyquist plot to a simple Randles equivalent circuit. Proton conductivity (σ_{H^+}) in S cm^{-1} was calculated using Equation 2.13, where L is the distance between electrodes (cm) and A_{xs} is the cross-sectional area of the membrane (cm^2). From the proton conductivity the effective proton mobility (μ'_{H+}) was calculated for a given set of conditions (e.g., 30 °C, 95% RH) using Equation 2.14, where F is the Faraday constant (96,485 C mol^{-1}) and [-SO_3H] is the analytical acid concentration of the hydrated polymer membrane (mmol SO_3H cm^{-3}). [-SO_3H] was calculated using the moles of SO_3H (determined via titration) and the volume of a hydrated membrane sample (V_{wet}) as shown in Equation 2.15.

Equation 2.13: $\sigma_{H^+} = \frac{L}{R_{ion} \times A_{xs}}$ *Equation 2.14*: $\mu'_{H+} = \frac{\sigma_{H^+}}{F \times [-SO_3H]}$

Equation 2.15: $[SO_3H] = \frac{moles\ of\ SO_3H}{V_{wet}}$

Chapter 3.

Sulfonated Oligophenylene Model Compounds

This chapter was reproduced in part with permission from: N. Peressin, M. Adamski, E. M. Schibli, E. Ye, B. J. Frisken, S. Holdcroft, *Macromolecules* **2020**, DOI 10.1021/acs.macromol.0c00310. Copyright 2020 American Chemical Society.

My contributions to this collaborative effort included the synthesis and characterization of all organic molecules and polymers, aside from the following. Dr. Michael Adamski synthesized and provided the following compounds: 4,4'-*bis*-trimethylsilylethynyl-1,1'-biphenyl, 4,4'-diethynyl-1,1'-biphenyl (*para* biphenyl linker, ***p*-BPL**) and 4,4'-biphenyl model compound (**MC-B*p***). Dr. Eric Ye performed the exchange NMR experiments, and Eric Schibli performed the DFT experiments.

This work was financially supported by the Natural Sciences and Engineering Research Council of Canada (NSERC), DuPont, and the British Columbia Automobile Association (BCAA).

3.1. Introduction

As discussed in Chapter 1, thermochemically robust hydrocarbon-based proton exchange membranes as alternatives to PFSA-based membranes are highly sought after. In 2015, S. Holdcroft *et. al.*[79] reported the synthesis of a well-defined, pre-sulfonated phenylated poly(phenylene) homo-polymer (sPPP-H^+). Despite possessing high proton conductivity and *ex-situ* oxidative stability, the membranes swelled excessively and eventually dissolved at elevated temperatures. More recently, a larger biphenyl co-monomer was incorporated into the poly(phenylene) backbone, reducing the polymer's (sPPB-H^+) hydrophilicity.[52] While this did significantly reduced the degree of swelling (from 364 vol.% to 145 vol%), there is still much room for improvement when compared to Nafion®, that swells only by 20% volumetrically.

In both sPPP-H^+ and sPPB-H^+, the dienophile co-monomer (a functionalized phenyl, or biphenyl moiety respectively) is linear. Various research groups have suggested that incorporating non-linear units into a polymer backbone may be advantageous in obtaining robust, flexible, low swelling membranes.[100],[101],[102] The argument is that by introducing angled moieties into polymer backbones, the resulting macroscopic structures may adopt flexible coils,[102] as opposed to rigid rods, which promote polymer chain entanglements and hence a reduction in water sorption, swelling, and elastic deformation.[29],[72],[100],[101]

In this work, non-linear biphenyl units are incorporated into the backbone of sulfonated phenylated poly(phenylene) polymers. In this chapter specifically, the viability of the Diels-Alder reaction between each of an *ortho*, *meta*, and *para* functionalized biphenyl dienophile linker (designated ***o*-BPL**, ***m*-BPL**, and ***p*-BPL**, respectively), and a diene will be assessed. This will be achieved through the synthesis and subsequent characterization of oligophenylene model compounds, **MC-B*o***, **MC-B*m***, **MC-B*p*** each containing an *ortho*, *meta*, or *para* functionalized biphenyl moiety respectively as shown in Figure 3.1. Each of these oligophenylene model compounds are structurally analogous to their corresponding polymers, but because they are small molecules, they are easily characterized by NMR and mass spectrometry unlike their polymeric counterparts. Furthermore, density functional theory calculations which will be considered in this chapter are much less computationally expensive when performed on small molecules than on polymeric systems.

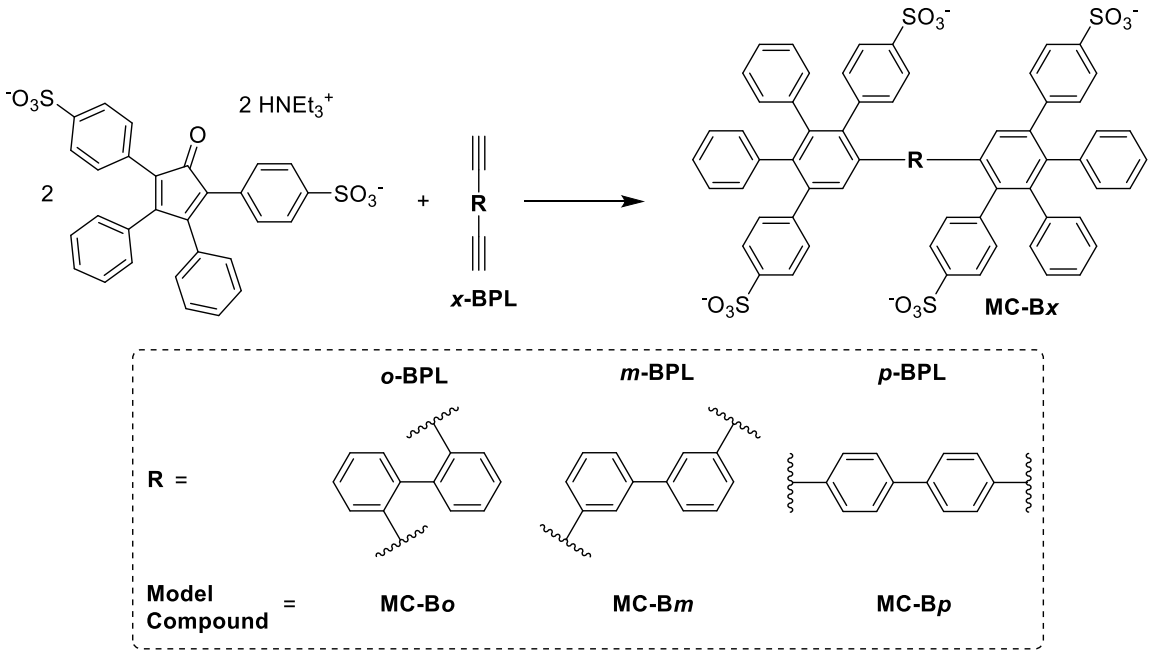

Figure 3.1: *Synthesis of oligophenylene model compounds* ***MC-Bo****,* ***MC-Bm****, and* ***MC-Bp****.*

3.2. Experimental

3.2.1. Materials

All chemicals were purchased from the specified vendors and used as received unless otherwise stated. Dimethylsulfoxide (DMSO, spectrograde), iodine (I_2, resublimed), potassium carbonate (K_2CO_3, ACS grade), sodium hydroxide (NaOH, ACS grade), sodium thiosulfate ($Na_2S_2O_3$, reagent grade, 100%), and sodium chloride (NaCl, >99%) were purchased from ACP Chemicals Inc. Activated carbon (G-60), hydrochloric acid (HCl, ACS reagent, 36.5-38%), and triethylamine (NEt_3, 99%) were purchased from Anachemia Science. Hexanes (reagent grade), *n*-butyl alcohol (*n*-BuOH, reagent grade), pentane (reagent grade) potassium hydroxide (KOH, reagent grade, min 85%), sulfuric acid (H_2SO_4, reagent grade, 95-98%), and tetrahydrofuran (THF, ACS grade) were purchased from Caledon Laboratory Chemicals. 1,3-(diphenyl)propan-2-one (1,3-diphenylacetone, 98%), 1,4-diiodobenzene (98%), 1-bromo-2-iodobenzene (2-bromoiodobenzene, 98%), 3,3'-dibromobiphenyl (95%), and phenylacetylene (98%) were purchased from Combi-Blocks Inc. Ethanol (anhydrous, 99%) was purchased from

Commercial Alcohols. Acetone (certified ACS), Celite® (545 filter aid, not acid-washed powder), dichloromethane (DCM, CH_2Cl_2, certified ACS stabilized), diethyl ether (Et_2O, certified ACS), ethyl acetate (certified ACS), methanol (MeOH reagent grade), *n*-butyl lithium (*n*-BuLi, 2.5 M in hexanes), silica gel (S825-1, 230-400 mesh, grade 60), and toluene (certified ACS) were purchased from Fischer Scientific. Potassium hydrogen phthalate (KHP, 99.95%) was purchased from MCB Manufacturing Chemists, Inc. Dichloroethane was purchased from MilliporeSigma EMD Millipore Corp. 4,4'-diiodobiphenyl, benzil (98%), copper iodide (CuI, 99.5%), diethylamine (>99.5%), dimethylformamide (DMF, Chromatosolv® HPLC grade), lithium bromide (LiBr, ReagentPlus®, >99%), nitrobenzene ($PhNO_2$, 98%, ReagentPlus®), and trimethylsilyl chlorosulfonate ($TMSSO_3Cl$, 99%) were purchased from MilliporeSigma Sigma-Aldrich Canada Co. Trimethylsilylacetylene was purchased from Oakwood Chemicals. Argon (PP 4.8) was purchased from Praxair. *bis*-(Triphenylphosphine)palladium(II) dichloride ($Pd(PPh)_3)_2Cl_2$, 97%) was purchased from Strem Chemicals. Deionized water (DI H_2O, resistivity >18.2 MΩ cm) was obtained from a Millipore Milli-Q water purification system.

3.2.2. Synthesis

Tetraphenylcyclopentadienone (Tetracyclone, TC)

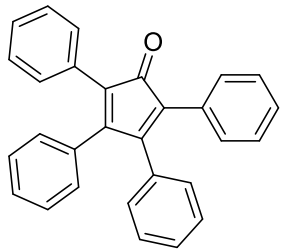

This compound was synthesized using previously reported methodologies.[79] To a two-necked round bottom flask equipped with a stir bar was added anhydrous ethanol (125 mL), benzil (13.3 g, 63.3 mmol, 1.0 eq.) and 1,3-(diphenyl)propan-2-one (13.3 g, 63.3 mmol, 1.0 eq.). The flask was equipped with condenser and a capped addition funnel and stirred under reflux for 30 min allowing for complete dissolution. KOH (3.46 g, 61.7 mmol, 0.97 eq. dissolved in 18 mL anhydrous ethanol) was added drop-wise to the two-necked round bottom flask containing the reaction mixture. The resulting black solution was stirred at reflux for an additional 30 min, then cooled to 0 °C in an ice bath. The mixture was filtered and the precipitate was washed with cold water (2 x 75 mL) and cold ethanol (4 x 75 mL) and dried under airflow for 20 min before being dried *in vacuo* at 50 °C for 16 h. The product was collected as a glossy black crystalline powder (20.4 g, 53.0 mmol, 84% yield). ^{1}H NMR (400 MHz, $CDCl_3$) δ (ppm): 7.25 – 7.21 (m, 12H), 7.17 (t, *J* = 7.4 Hz, 4H), 6.93 (d, *J* = 7.0 Hz, 4H). ^{13}C NMR (101 MHz, $CDCl_3$) δ (ppm): 200.48, 154.67, 133.31, 130.96, 130.32, 129.49, 128.63,

128.17, 128.14, 127.61, 125.52. All spectral data were in good agreement with those reported in the literature.[52],[79]

Sulfonated Tetracyclone (sTC)

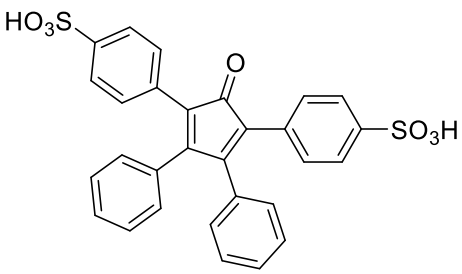

This compound was synthesized using previously reported methodologies.[79] To a 500 mL two-necked round bottom flask containing a stir bar was added dichloroethane (375 mL). The flask was equipped with a septum and a sealed drop funnel and the system was degassed with argon. Tetraphenylcyclopentadienone (4.98 g, 13.0 mol, 1.00 eq.) was added to the dichloroethane and the mixture was stirred and degassed with argon for 15 min. Trimethylsilyl chlorosulfonate (13.0 mL, 15.9 g, 84.4 mmol, 6.5 eq) was diluted in argon-degassed dichloroethane (15 mL), injected into the drop funnel, and added dropwise to the flask while stirring. The mixture was stirred for 19 h, then ethanol (3.5 mL) was added, followed by additional stirring for 2 h. The volatile solvents were partially evaporated until the mixture was a thick paste, then diethyl ether was added to the flask. The product was isolated filtration, washed with diethyl ether and dried *in vacuo* at 80 °C for 16 h to afford the product as a bright purple powder (5.60 g, 10.28 mmol, 79 % yield). ^{1}H NMR (400 MHz, DMSO-d_6) δ 7.46 (d, J = 8.4 Hz, 4H), 7.31 – 7.21 (m, 6H), 7.12 (d, J = 8.3 Hz, 4H), 6.97 (d, J = 6.5 Hz, 4H), 9.95 (s, H_2O/H_3O^+). All spectral data were in good agreement with those reported in the literature.[79]

Triethylammonium Salt of Sulfonated Tetracyclone (TEAsTC)

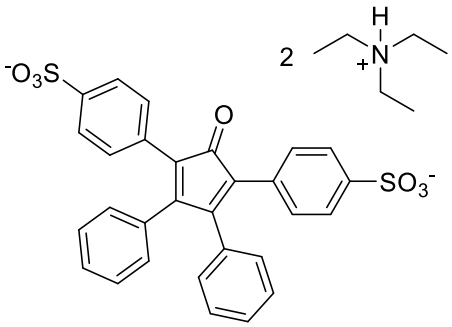

This compound was synthesized using previously reported methodologies.[79] To a 500 mL round bottom flask containing a stir bar was added *n*-butyl alcohol (310 mL) and 4,4'-(2-oxo-4,5 diphenylcyclopenta-3,5-diene-1,3-diyl)dibenzenesulfonic acid (5.60 g, 10.28 mmol, 1.0 eq.). The flask was equipped with a drop funnel containing triethylamine (14.3 mL, 103 mmol, 10.0 eq.) that was added dropwise to the mixture under stirring. The reaction was stirred at room temperature for 16 h, filtered, and

the precipitate was washed with diethyl ether. The precipitate was dried *in vacuo* at 80 °C for 16 h to afford the product as a bright purple powder (6.85 g, 9.17 mmol, 89% yield). ^{1}H NMR (400 MHz, DMSO-d_6) δ 8.84 (s, 2H), 7.46 (d, J = 8.4 Hz, 4H), 7.31 – 7.21 (m, 6H), 7.11 (d, J = 8.4 Hz, 4H), 6.97 (d, J = 6.4 Hz, 4H), 3.09 (q, J = 7.3 Hz, 12H), 1.17 (t, J = 7.3 Hz, 18H). All spectral data were in good agreement with those reported in the literature.[79]

4,4'-*bis*-Trimethylsilylethynyl-1,1'-biphenyl

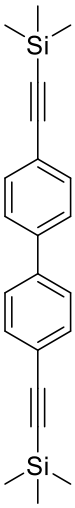

This compound was synthesized using previously reported methodologies.[152] To a 500 mL argon filled 3-necked round-bottom flask equipped with a stir bar was added 4,4'-diiodopiphenyl (10.09 g, 24.85 mmol), and diethylamine (320 mL). Catalytic amounts of $Pd(PPh_3)_2Cl_2$ (174 mg, 0.249 mmol) and CuI (47 mg, 0.25 mmol) were added, the flask was sealed with a septum and stirring was initiated. Trimethylsilylacetylene (7.4 mL, 52 mmol) was injected through the septum, and the resulting mixture was left to stir at 51 °C for 36 h. The reaction was cooled to room temperature and the resulting white precipitate was removed by filtration. The filtrate was collected and the solvent mixture was evaporated *in vacuo*. The resulting dark brown residue was purified via silica gel column chromatography using hexanes as an eluent to afford the pure product as a white crystalline solid (6.06 g, 17.5 mmol, 70 % yield). ^{1}H NMR (500 MHz, Acetone-d_6) δ 7.71 (d, J = 8.4 Hz, 4H), 7.56 (d, J = 8.3 Hz, 4H), 0.25 (s, 18H). ^{13}C NMR (126 MHz, acetone-D_6) δ 140.90, 133.22, 127.73, 123.39, 105.66, 95.60, -0.02. All spectral data were in good agreement with those reported in the literature.[52]

4,4'-Diethynyl-1,1'-biphenyl (*para* Biphenyl Linker, *p*-BPL)

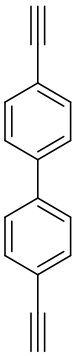

This compound was synthesized using previously reported methodologies.[152] To a 50 mL round-bottom flask equipped with a stir bar was dissolved 4,4'-*bis*-trimethylsilylethynyl-1,1'-biphenyl (1.80 g, 5.19 mmol) in a diethyl ether/methanol solvent mixture (1:1, 30 mL). K_2CO_3 (7.18 g, 51.9 mmol) was added slowly under vigorous stirring, and the reaction was stirred for an additional 6 h at room temperature. The reaction mixture was poured into water (250 mL), and the aqueous layer extracted with DCM (3 x 125 mL). The organic extracts were combined, dried over $MgSO_4$, and the solvent mixture was evaporated *in vacuo* to afford the pure product as a light beige crystalline solid (1.04 g, 5.14 mmol, 99 % yield).

^{1}H NMR (500 MHz, Acetone-D_6) δ (ppm): 7.72 (d, *J* = 8.4 Hz, 1H), 7.60 (d, *J* = 8.3 Hz, 1H), 3.74 (s, 1H). ^{13}C NMR (126 MHz, acetone-d_6) δ (ppm): 141.10, 133.39, 127.83, 122.67, 83.90, 80.14. All spectral data were in good agreement with those reported in the literature.[52]

3,3'-*bis*-Trimethylsilylethynyl-1,1'-biphenyl

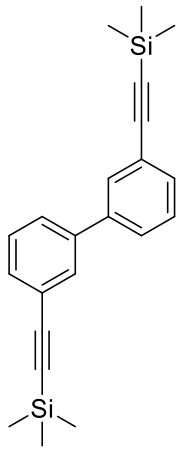

To an argon-degassed 250 mL Schlenk flask was added 3,3'-dibromobiphenyl (4.99 g, 15.99 mmol, 1.0 eq.), degassed triethylamine (54 mL), and degassed toluene (71 mL). The mixture was heated to 80 °C until starting materials were fully dissolved, then catalytic amounts of CuI (94 mg, 0.49 mmol, 0.031 eq.) and $Pd(PPh_3)_4$ (504 mg, 0.436 mmol, 0.027 eq.) were added to flask and stirred for 1 h. Argon-degassed trimethylsilylacetylene (12.0 mL, 8.28 g, 84.3 mmol, 5.3 eq.) was injected into the flask, and the mixture was stirred for 16 h at 80 °C. The mixture was cooled to room temperature and the solids were filtered out, collecting the filtrate before removing the volatile solvents by evaporation *in vacuo*. The resulting solid was suspended in hexanes and filtered through a silica plug via hexanes (750 mL) before removing the hexanes by evaporation *in vacuo*. The crude product was purified by silica gel column chromatography using 80 g silica gel and hexanes as an eluent. The product was isolated as an orange oil that crystallized as white crystalline product with a small amount of orange liquid following 16 h at 7 °C. The orange liquid was discarded, and the product was recrystallized in a minimum volume of methanol. The product was collected as a white crystalline solid (4.27 g, 12.3 mmol, 77 % yield). ^{1}H NMR (500 MHz, $CDCl_3$) δ (ppm): 7.69 (dd, *J* = 1.7, 1.7 Hz, 1H), 7.52 (ddd, *J* = 7.8, 2.0, 1.2 Hz, 1H), 7.45 (ddd, *J* = 7.7, 1.4, 1.4 Hz, 1H), 7.37 (dd, *J* = 7.7, 7.7 Hz, 1H), 0.27 (s, 9H). HRMS (M = $C_{22}H_{30}NSi_2$): $[M+NH_4]^+$ Measured 364.1896, Calculated 364.1911

3,3'-Diethynyl-1,1'-biphenyl (*meta* Biphenyl Linker, *m*-BPL)

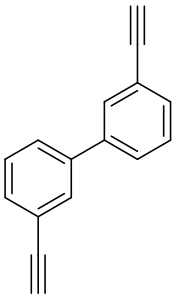

To a solution of methanol (11 mL) and THF (11mL) was added 3,3'-*bis*-trimethylsilylethynyl-1,1'-biphenyl (1.01 g, 2.91 mmol, 1.0 eq.) and a stir bar. K_2CO_3 (4.23 g, 30.6 mmol, 10.5 eq.) was added to the mixture and was stirred vigorously for 16 h at room temperature. The volatile solvents were evaporated and the remaining solids were dissolved in a minimum volume of dichloromethane and passed through a short silica gel column, washing with dichloromethane. The product was further purified via silica gel column chromatography using hexanes/dichloromethane as an eluent. The product was collected as a light beige crystalline solid (0.59 g, 2.91 mmol, 100% yield). ^{1}H NMR (400 MHz, $CDCl_3$) δ (ppm): 7.71 (dd, *J* = 1.8, 1.8 Hz, 2H), 7.56 (ddd, *J* = 7.8, 1.5, 1.5 Hz, 2H), 7.49 (ddd, *J* = 7.7, 1.4, 1.4 Hz, 2H), 7.40 (dd, *J* = 7.7, 7.7 Hz, 1H), 3.11 (s, 2H). ^{13}C NMR (101 MHz, $CDCl_3$) δ (ppm): 140.59, 131.41, 130.98, 129.03, 127.71, 122.93, 83.59, 77.61.

2,2'-Diiodo-1,1'-biphenyl

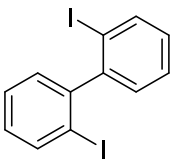

To a dry 50 mL round bottom flask was added 2,2'-dibromo-1,1'-biphenyl (0.498 g, 1.59 mmol) and diethyl ether (2.4 mL). The mixture was stirred under argon flow until the starting material was dissolved. The contents were cooled to -78 °C in a dry ice/acetone bath. *N*-butyllithium (1.9 mL, 2.5 M, 4.7 mmol) was added dropwise by syringe and the resulting slurry was stirred overnight while warming to room temperature. The mixture was cooled to 0 °C in an ice bath and a solution of iodine (0.96 g, 3.78 mmol) in diethyl ether (5 mL) was added dropwise by syringe. The mixture was stirred for 2.5 h while it warmed to room temperature. The reaction was quenched by addition of an aqueous solution of sodium thiosulfate in water (0.26 g in 15 mL water). The ether phase was collected and the aqueous phase was extracted five times with diethyl ether (5 mL each). The combined ethereal phases were dried over $MgSO_4$, filtered and the solvent was evaporated under reduced pressure to give the product as a yellow solid (0.494 g, 1.22 mmol, 76%). ^{1}H NMR (400 MHz, acetone-d_6) δ (ppm): 7.99 (dd, *J* = 8.0, 1.2 Hz, 1H), 7.51 (td, *J* = 7.5, 1.2 Hz, 1H), 7.23 (dd, *J* = 7.6, 1.7 Hz, 1H), 7.17 (ddd, *J* = 8.0, 7.4, 1.7 Hz, 1H). ^{13}C NMR (101 MHz, Acetone-d6) δ 150.01,139.86, 130.90, 130.47, 129.16, 99.99.

((2-Bromophenyl)ethynyl)trimethylsilane

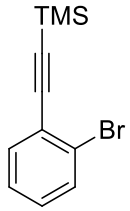

To a round bottom flask was added degassed THF (230 mL), degassed triethylamine (84 mL), and 2-iodobromobenzene (15.0 mL, 33.4g, 117 mmol, 1.0 eq) and the mixture was stirred under flow of argon. $Pd(Ph_3)_2Cl_2$ (2.08 g, 2.97 mmol, 0.025 eq.) and CuI (0.58 g, 3.02 mmol, 0.026 eq.) were added to the reaction mixture, the flask was sealed and again degassed with argon. Trimethylsilylacetylene (19.1 mL, 13.2 g, 134 mmol, 1.15 eq.) was injected into the flask by syringe and the mixture was stirred at room temperature for 1 h. The reaction mixture was diluted with diethyl ether (1.5 L) and solids were removed by filtration through Celite®. The filtrate was collected and concentration *in vacuo* and the resulting orange liquid was purified by column chromatography on silica gel (200 g) using hexanes as an eluent to afford the product as a yellow oil (30.09 g, 118.8 mmol, quant.). ^{1}H NMR (500 MHz, CD_2Cl_2) δ (ppm): 7.59 (dd, *J* = 8.0, 1.3 Hz, 1H), 7.49 (dd, *J* = 7.7, 1.8 Hz, 1H), 7.27 (td, *J* = 7.6, 1.3 Hz, 1H), 7.19 (td, *J* = 7.9, 1.7 Hz, 1H), 0.27 (s, 9H). ^{13}C NMR (126 MHz, CD_2Cl_2) δ (ppm): 134.15, 132.95, 130.29, 127.64, 126.02, 125.72, 103.44, 100.18, 0.05.

2,2'-*bis*-Trimethylsilylethynyl-1,1'-biphenyl

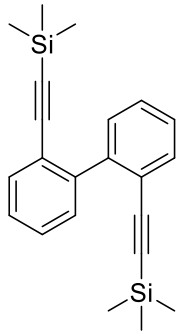

To a dry 500 mL round bottom flask containing a stir bar was added freshly distilled THF (250 mL), ((2-bromophenyl)ethynyl)trimethylsilane (5.00 g, 19.75 mmol, 1.00 eq.), and cooled to -78 °C in dry ice/acetone under an argon atmosphere. To the flask was added *n*-butyllithium in hexanes (2.5 M, 8.8 mL, 22.0 mmol, 1.1 eq.) dropwise by syringe. The reaction mixture was stirred at -78 °C for 45 min, after which $CuCl_2$ (8.25 g, 61.36 mmol, 3.11 eq.) was added to the reaction mixture. The reaction was allowed to warm up to ambient temperature over 90 min, and the solids were removed by filtration through alumina using hexanes (1.5 L) as an eluent. The filtrate was collected, concentrated *in vacuo*, and the residue was purified by column chromatography on silica gel (190 g) using hexanes as an eluent to afford 2,2'-*bis*-trimethylsilylethynyl-1,1'-biphenyl as a pale-yellow oil (0.960 g, 2.769 mmol, 28% yield). ^{1}H NMR (400 MHz, CD_2Cl_2) δ (ppm): 7.54 (ddd, *J* = 7.4, 1.6, 0.6 Hz, 1H), 7.44 (ddd, *J* = 7.6, 1.6, 0.6 Hz, 1H), 7.37 (td, *J* = 7.6, 1.6 Hz, 1H), 7.31 (td, *J* = 7.5, 1.6 Hz, 1H), 0.06 (s, 9H).^{13}C NMR (101 MHz, CD_2Cl_2) δ (ppm): 144.04, 132.72, 130.78, 128.45, 127.87, 123.20, 105.02, 98.08, -0.03. HRMS (M = $C_{22}H_{27}Si_2$): $[M+H]^+$ Measured 347.1686, Calculated 347.1646.

2,2'-Diethynyl-1,1'-biphenyl (*ortho* Biphenyl Linker, *o*-BPL)

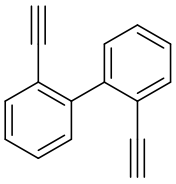

To an argon-degassed 250 mL round bottom flask containing a stir bar was added methanol (89.0 mL) and 2,2'-*bis*-trimethylsilylethynyl-1,1'-biphenyl (4.32 g, 12.5 mmol, 1.00 eq.) and the mixture was stirred vigorously. K_2CO_3 (7.05 g, 51.0 mmol, 4.09 eq.) was added to the flask and the mixture was stirred vigorously for 16 h. The volatile solvents were removed by evaporation *in vacuo* and the residue was dissolved in a minimum volume of dichloromethane (32 mL) and filtered through a short silica gel column using dichloromethane (300 mL) as an eluent to afford the product as a beige/orange solid (2.45 g, 12.1 mmol, 97% yield). The product was further purified by recrystallization in ethanol to obtain a white crystalline solid. ^{1}H NMR (400 MHz, DMSO-d_6) δ (ppm): 7.59 (dd, J = 7.4, 1.4 Hz, 1H), 7.46 (ddd, J = 7.5, 7.5, 1.5 Hz, 1H), 7.40 (ddd, J = 7.5, 7.5, 1.5 Hz, 1H), 7.36 (dd, J = 7.3, 1.5 Hz, 1H), 3.98 (s, 1H). ^{13}C NMR (101 MHz, DMSO-D_6) δ (ppm): 142.66, 132.57, 129.90, 128.36, 127.71, 121.09, 83.34, 82.39. HRMS (M = $C_{16}H_{11}$): $[M+H]^+$ Measured 203.0860, Calculated 203.0855.

4,4'-Biphenyl Model Compound (MC-B*p*)

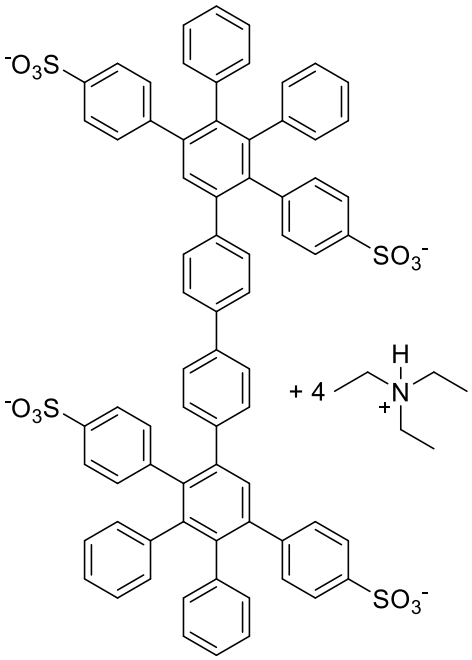

To a dry and argon-degassed 25 mL Schlenk flask equipped with a stir bar was added 4,4'-diethynyl-1,1'-biphenyl (0.165 g, 0.817 mmol, 1.0 eq.), TEAsTC (1.251 g, 1.675 mmol, 2.05 eq.), and degassed nitrobenzene (13.0 mL). The flask was sealed with a septum, and three freeze-pump-thaw cycles were performed using liquid nitrogen. The mixture was stirred vigorously for 10 min, then left to react at 215° C with medium stirring for 48 h. The reaction was cooled to room temperature. Ethyl acetate (2 mL) was added to facilitate precipitation, and the reaction was poured into ethyl acetate (200 mL) and refluxed for 4 h, filtrated, and precipitate washed twice with boiling ethyl acetate and once with diethyl ether. The compound was dried under vacuum overnight at 80 °C to yield pure product as a faint gray solid (1.227 g, 0.748 mmol, 92%).

^{1}H NMR (600 MHz, CD_3OD) δ (ppm): 7.66 (d, J = 8.0 Hz, 4H), 7.51 (s, 2H), 7.45 (t, J = 7.2 Hz, 8H), 7.28 (d, J = 8.0 Hz, 4H), 7.25 (d, J = 8.0 Hz, 4H), 7.06 (d, J = 8.1 Hz, 4H), 6.98 – 6.83 (m, 20H), 3.17 and 2.99 (two q, J = 7.3 Hz, 24H), 1.27 (two overlapping t, J = 7.1 Hz, 36H). ^{13}C NMR (150 MHz, CD_3OD) δ (ppm): 145.18, 144.35, 143.80, 143.74, 143.46, 141.89, 141.87, 141.66, 141.25, 141.05, 140.99, 140.12, 139.76, 132.64, 132.64, 132.62, 132.54, 132.10, 131.53, 130.91, 128.12, 127.86, 127.17, 126.94, 126.74, 126.36, 125.72, 47.92 and 43.55, 11.57 and 9.24. HRMS (M = $C_{72}H_{50}O_{12}S_4$): $[M-H]^-$ wasn't observed, Calculated 1233.6401; $[M-2H]^{2-}$ Measured 616.4654, Calculated 616.1020; $[M-3H]^{3-}$ Measured 410.6887, Calculated 410.3989; $[M-4H]^{4-}$ Measured 307.7937, Calculated 307.5474. $[M+H]^+$ ($C_6H_{16}N$): Measured 102.1297, Calculated 102.1277. All spectral data were in good agreement with those reported in the literature.[52]

3,3'-Biphenyl Model Compound (MC-B*m*)

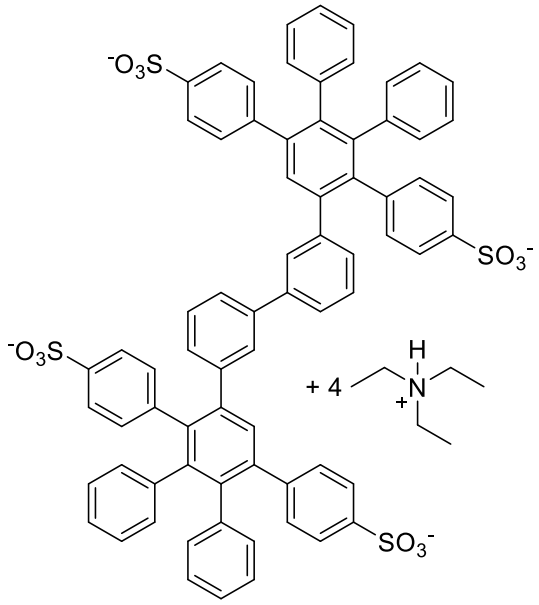

To a dry and argon-degassed pressure vessel equipped with a stir bar was added 3,3'-diethynyl-1,1'-biphenyl (0.142 g, 0.702 mmol, 1.0 eq.), TEAsTC (1.075 g, 1.439 mmol, 2.05 eq.), and degassed nitrobenzene (19.0 mL). The mixture was stirred vigorously for 30 min under a flow of argon obtain complete dissolution. The pressure vessel was sealed with a Teflon lid and the reaction was heated to 170 °C with medium stirring for 94 h. The reaction was cooled to room temperature and precipitated into ethyl acetate (200 mL), filtered, washing the precipitate twice with ethyl acetate and once with diethyl ether. The solids were dissolved into methanol (10 mL) and precipitated into diethyl ether (300 mL) before filtering, washing with diethyl ether and air drying for 1 h. The product was collected as an off-white powder (1.065 g, 0.6494 mmol, 93% yield). ^{1}H NMR (400 MHz, CD_3OD) δ (ppm): 7.65 (d, *J* = 8.4 Hz, 4H), 7.51 (s, 2H), 7.49 (d, *J* = 8.3 Hz, 4H), 7.32 – 7.23 (m, 8H), 7.19 (s, 2H), 7.08 (d, *J* = 8.3 Hz, 4H), 6.97 – 6.83 (m, 22H), 3.16 (q, *J* = 7.3 Hz, 24H), 1.26 (t, *J* = 7.3 Hz, 36H). ^{13}C NMR (101 MHz, CD_3OD) δ (ppm): 145.18, 144.44, 144.00, 143.89, 143.49, 142.97, 142.06, 141.93, 141.65, 141.29, 141.09, 141.02, 140.21, 132.71, 132.63, 132.56, 132.05, 130.91, 130.18, 129.78, 129.67, 128.07, 127.83, 126.90, 126.72, 126.35,

125.78, 48.01, 9.27. HRMS (M = $C_{72}H_{50}O_{12}S_4$): $[M-H]^-$ Measured 1233.228, Calculated 1233.2112; $[M-2H]^{2-}$ Measured 616.113, Calculated 616.1020; $[M-3H]^{3-}$ Measured 410.410, Calculated 410.3989; $[M-4H]^{4-}$ Measured 307.555, Calculated 307.5474

2,2'-Biphenyl Model Compound (MC-B*o*)

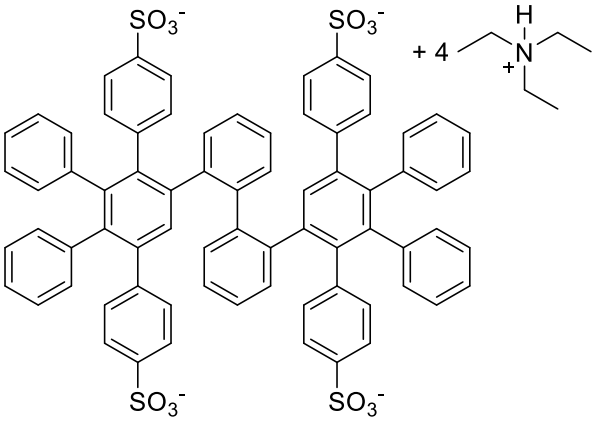

To a dry and argon-degassed pressure vessel equipped with a stir bar was added 2,2'-diethynyl-1,1'-biphenyl (0.149 g, 0.738 mmol, 1.0 eq.), TEAsTC (1.130 g, 1.513 mmol, 2.05 eq.), and degassed nitrobenzene (19.0 mL). The mixture was stirred vigorously for 1 h under a flow of argon obtain complete dissolution. The pressure vessel was sealed with a Teflon lid and the reaction was heated to 170 °C with medium stirring for 94 h. The reaction was cooled to room temperature and precipitated into ethyl acetate (200 mL), filtered, washing the precipitate twice with ethyl acetate and once with diethyl ether. The solids were dissolved into methanol (20 mL) and precipitated into diethyl ether (300 mL) before filtering, washing with diethyl ether and air drying for 1 h and drying at 80 °C *in vacuo* for 16 h. The product was collected as an off-white powder (0.902 g, 0.550 mmol, 75% yield). ^{1}H NMR (500 MHz, CD_3OD) δ (ppm) 7.86 – 5.80 (m, 46H), 3.16 (q, *J* = 7.3 Hz, 24H), 1.26 (t, *J* = 7.3 Hz, 36H). ^{1}H NMR (500 MHz, DMSO-d_6) δ (ppm): 8.91 (s, 4H), 7.61 – 5.61 (m, 46H), 3.06 (q, *J* = 7.3 Hz, 24H), 1.13 (t, *J* = 7.3 Hz, 36H). ^{13}C NMR (130 °C, 101 MHz, DMSO-d_6) δ (ppm): 145.81, 145.42, 141.45, 140.39, 139.53, 139.01, 138.80, 138.35, 138.16, 131.70, 130.61, 130.44, 129.78, 127.90, 125.92, 125.54, 125.18, 124.79, 124.61, 123.89, 123.47, 46.04, 7.97. HRMS (M = $C_{72}H_{50}O_{12}S_4$): $[M-H]^-$ Measured 1233.6401, Calculated 1233.2112; $[M-2H]^{2-}$ Measured 616.1305, Calculated 616.1020; $[M-3H]^{3-}$ Measured 410.5702, Calculated 410.3989; $[M-4H]^{4-}$ Measured 307.7595, Calculated 307.5474

3.3. Results and Discussion

3.3.1. Monomer and Precursor Synthesis

The pre acid-functionalized diene precursor **TEAsTC** was prepared using previous literature procedure,[79] described in greater detail in the Chapter 2. The *meta* and *para* biphenyl monomers ***m*-BPL** and ***p*-BPL** were prepared in two facile steps from a di-halogenated biphenyl through a Sonogashira cross-coupling and subsequent protodesilylation, using modified literature procedures, as shown in Scheme 3.1a and b respectively.[153] The *ortho* biphenyl monomer ***o*-BPL** was prepared using a different approach, because the Sonogashira cross coupling attempted between 2,2'-dibromobiphenyl and trimethylsilylacetylene did not proceed, potentially due to steric limitations. Instead, a three-step synthetic pathway utilizing 2-iodobromobenzene was followed, involving a Sonogashira cross coupling, an *n*-butyllithium-mediated homo-coupling of the ((2-bromophenyl)ethynyl)trimethylsilane intermediate species, and a protodesilylation, as shown in Scheme 3.1c.

The overall yields for ***o*-BPL**, ***m*-BPL**, and ***p*-BPL** were 27%, 77%, and 84% respectively. The low yield for ***o*-BPL** was due to the *n*-butyllithium-mediated homo-coupling step, that resulted in 28% yield after purification via silica gel column chromatography. Purification following this homo-coupling was likely unnecessary, as the final product following protodesilylation was purified via silica gel column chromatography as well. Consequently, forgoing purification until after the protodesilylation would likely lead to a higher yield.

Scheme 3.1: *Synthesis of Biphenyl Co-monomers (a)* ***o-BPL****, (b)* ***m-BPL****, and (c)* ***p-BPL***

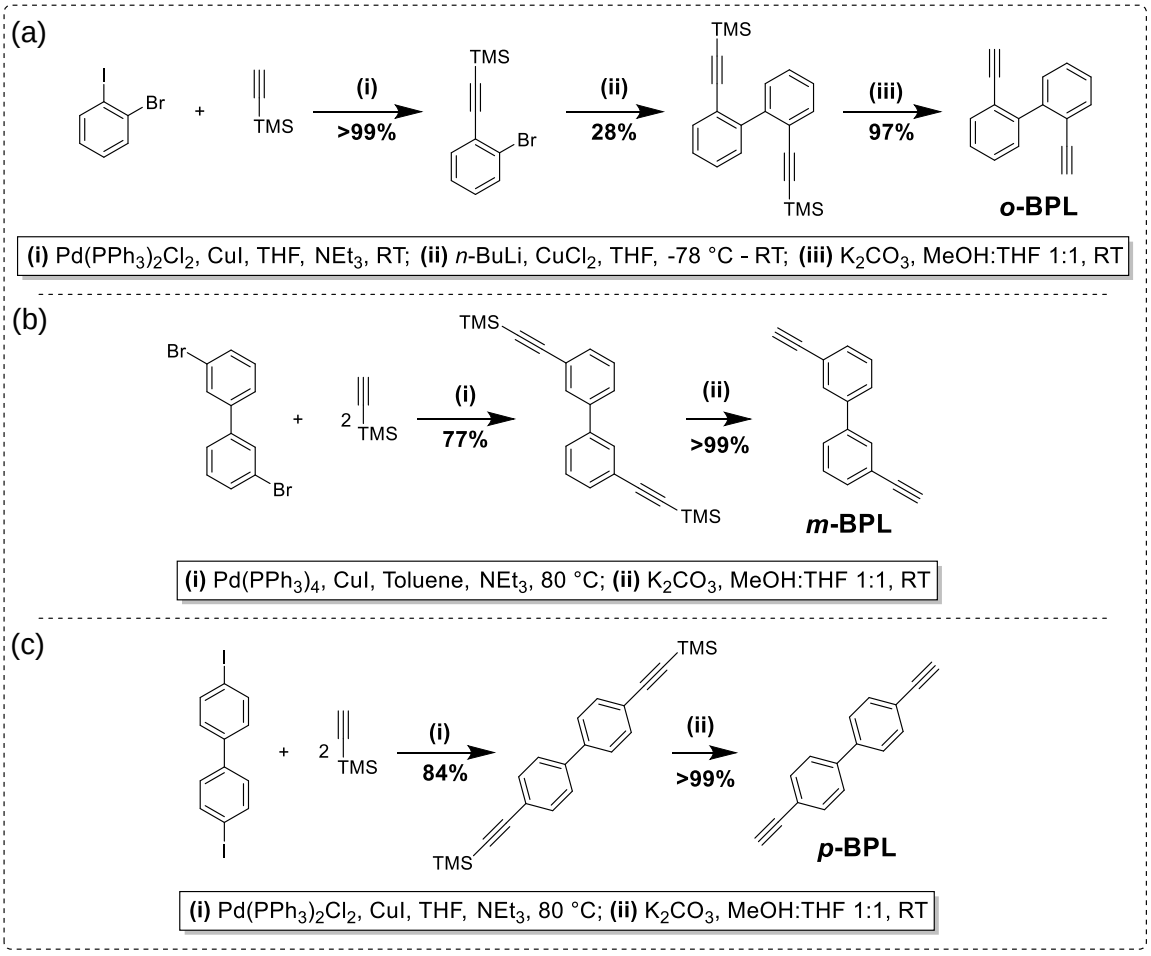

Due to the low ***o*-BPL** yield**,** an additional reaction pathway was investigated in an attempt to increase the yield. The reaction pathway involves a Sonogashira coupling similar to how ***m*-BPL** and ***p*-BPL** are prepared, but using a diiodo biphenyl as opposed to a dibromo biphenyl. Since iodine is a better leaving group than bromine, oxidative addition with palladium in the Sonogashira coupling using an iodinated species should be more favorable than with the brominated species. 2,2'-diiodobiphenyl was obtained in 76% yield by converting 2,2'-dibromobiphenyl by a lithium-halogen exchange using *n*-butyllithium and iodine following literature procedures.[154] Unfortunately, the Sonogashira coupling between 2,2'-diiodobiphenyl and trimethylsilyl acetylene proved to be unsuccessful as was the case when using 2,2'-dibromobiphenyl, potentially due to steric limitations.

3.3.2. Model Compound Synthesis

Oligophenylene model compounds **MC-B*o***, **MC-B*m***, and **MC-B*p*** were prepared as a means of investigating the viability of a Diels-Alder reaction between the *ortho*, *meta*, and *para* biphenyl linkers (***o*-BPL**, ***m*-BPL**, and ***p*-BPL**, respectively), with **TEAsTC**, a mono-functional analogue of the bi-functional **TEAsBTC** monomer to be used in polymerization. Oligophenylene model compound syntheses were also used to probe reaction conditions prior to polymerization, employing conditions identical to those of the intended polymerization conditions. In this way, the stability of the respective dienophiles at the temperatures and reaction times necessary to facilitate the DA cycloaddition could be probed.

Scheme 3.2: *Synthesis of Oligophenylene Model Compounds **MC-Bo**, **MC-Bm**, and **MC-Bp***

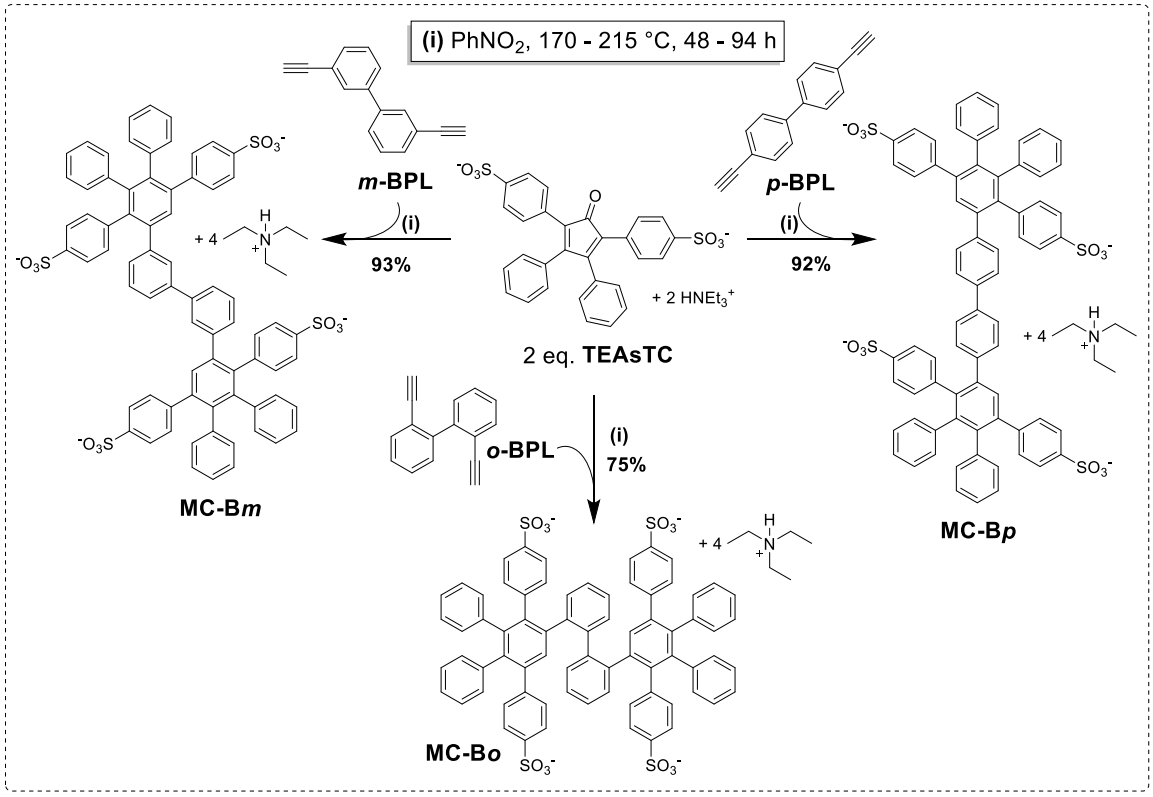

Model compounds **MC-B*o***, **MC-B*m***, and **MC-B*p*** were obtained through a [4 + 2] Diels-Alder cycloaddition between two equivalents of **TEAsTC** diene, and dienophile monomers ***o*-BPL**, ***m*-BPL**, or ***p*-BPL** respectively, as shown in Scheme 3.2. Good yields of 75%, 93% and 92% were achieved for ***o*-BPL**, ***m*-BPL**, and ***p*-BPL** respectively.

3.3.3. Model Compound Characterization

Characterization of each model compound via NMR spectroscopy and mass spectrometry showed exclusive formation of the desired products, verifying the stability of each respective biphenyl dienophile precursor under the reaction conditions utilized. The four triethylammonium counter ions present served effectively as internal probes during ^{1}H NMR characterizations,[52],[79],[81] where 36 methyl and 24 methylene protons were observed relative to the 46 aromatic protons found on each model compound. Analysis of mass spectra revealed four distinct molecular ion peaks with expected isotope spacing corresponding to the mono, di, tri, and tetra-anionic species $[M-H]^{-}$, $[M-2H]^{2-}$, $[M-3H]^{3-}$, and $[M-4H]^{4-}$, respectively. All obtained spectra for these model compounds are shown in Appendix A – Supporting Information for Chapter 3.

During NMR characterization, it was found that the *ortho* biphenyl-containing **MC-B*o*** displayed signs of atropisomerism, a form of stereoisomerism arising from hindered rotation about a chemical bond. This was investigated further using variable temperature and exchange spectroscopy (EXSY) NMR analysis. At room temperature, both ^{1}H and ^{13}C NMR spectra (see Appendix A Figures A 41, A 42, A 45, and A 46) contained more signals than would be expected for the symmetrical molecule **MC-B*o***, despite possessing correct relative proton integrations in the aromatic region. As the experiment temperatures were increased, the diastereotopic proton signals broadened until they eventually merged at the coalescence temperature at which free rotation was achieved, as shown in Figure 3.2.[155] Similarly, the number of peaks in the ^{13}C NMR spectrum was reduced to the expected number when measured at 130 °C, compared to 21 °C, as shown in Appendix A Figures A 44 vs A 42, respectively. This behavior is commonly observed in compounds that are locked in multiple meta-stable configurations, i.e. atropisomers.[156]

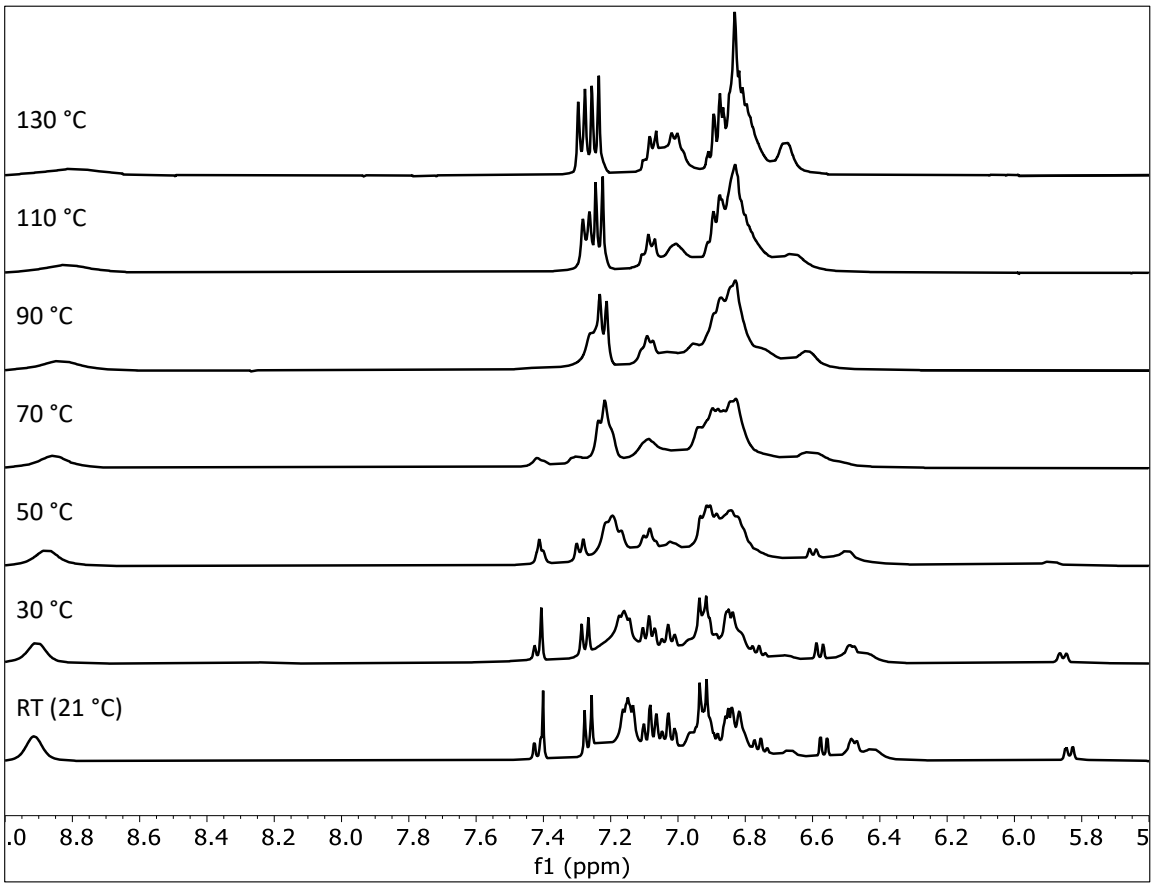

Figure 3.2: *Variable temperature ^{1}H NMR of **MC-Bo** in DMSO-d_6; free rotation appears to be achieved above approx. 70 °C.*

Exchange spectroscopy (EXSY) is a technique utilizing a NOESY (nuclear Overhauser effect spectroscopy) pulse sequence that can provide information about conformational interconversion taking place within a molecule.[134],[135],[136] A NOESY NMR experiment was initially performed with mixing times that overlapped with the timescale of the interconversion process, resulting in formation of cross-peaks in-phase with the diagonal that represent either NOE (through space correlations) or interconverting proton signals.[137],[157] In small molecules, cross-peaks corresponding to exchange can be distinguished from NOE correlations, that are of opposite phase to the diagonal, and are typically weaker than exchange signals.[137] The NOESY spectrum of **MC-B*o*** (Figure 3.3a) possessed multiple cross-peaks in-phase with the diagonal, and no signals with opposite phase to the diagonal. The NOESY spectrum suggests either that through-space NOE signals were being buried by the stronger EXSY signals, or more likely, that the molecule

is large enough that the NOE signals were in fact also in-phase with the diagonal, indistinguishable from the EXSY signals.[137]

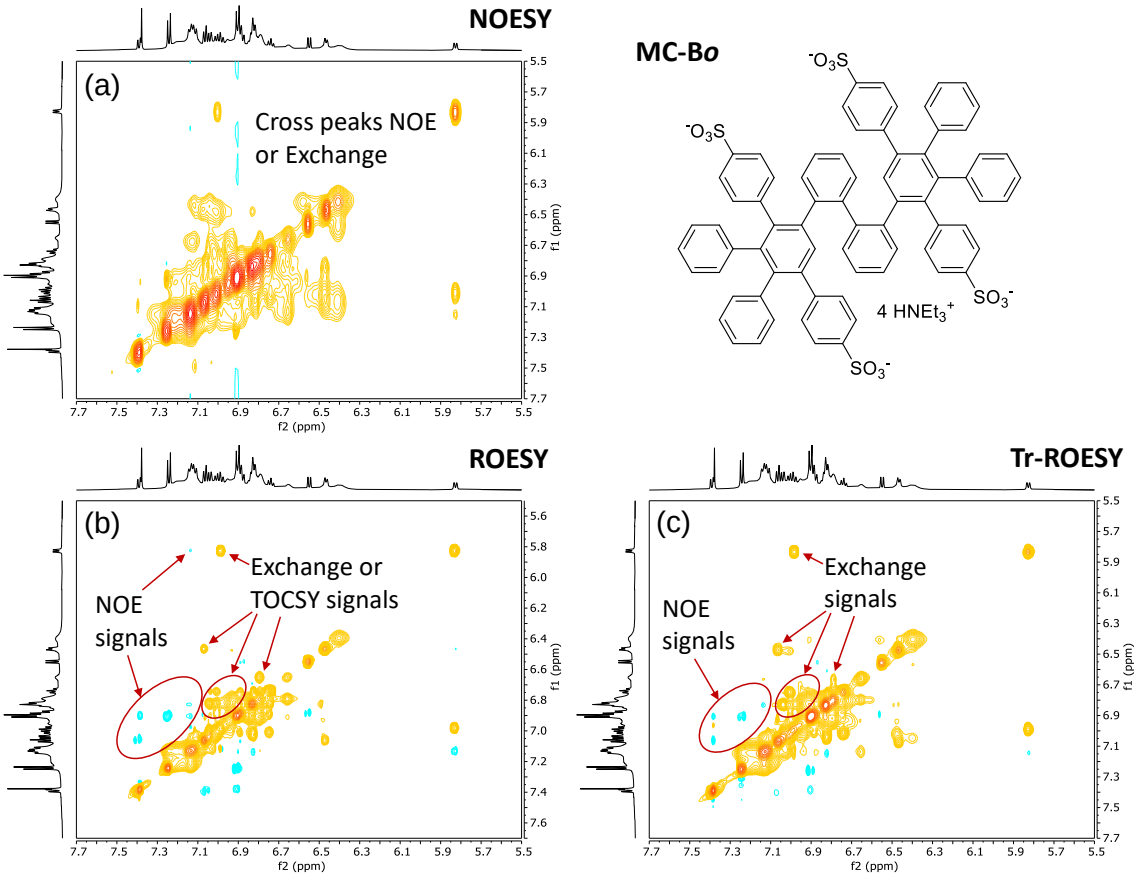

Figure 3.3: ***MC-Bo*** *exchange spectroscopy experiments utilizing (a) NOESY, (b) ROESY, and (c) Tr-ROESY pulse sequences. Cross peaks represent conformational exchange, NOE, or TOCSY transfer as highlighted.*

An experiment utilizing a ROESY (rotating-frame Overhauser effect spectroscopy) pulse sequence (Figure 3.3b) was performed to differentiate between NOE and exchange correlations that were indistinguishable in the NOESY experiment. In ROESY, cross-peaks due to conformational exchange will have opposite phase to those due to NOE regardless of molecular size, unlike in NOESY, and will be in phase with the diagonal.[138] Therefore, exchange correlations can be distinguished from NOE correlations using ROESY,[138] however, effects from TOCSY, that have the same phase as the exchange correlations, may also be present in a ROESY spectrum.[138] Shown in Figure 3.3b, there exist multiple peaks of opposite phase (cyan) to the diagonal that correspond to NOE

transfer, as well as multiple peaks in-phase with the diagonal (orange) that could correspond to exchange or TOCSY transfer. To confirm these signals were in fact due to exchange and not due to TOCSY transfer, a transverse ROESY (Tr-ROESY) experiment was performed. Tr-ROESY utilizes alternating-phase spin-lock, and is highly efficient at suppressing TOCSY transfer.[133],[138] Consequently, all cross-peaks in-phase with the diagonal in Figure 3.3c correspond to exchanging protons, and not NOE or TOCSY transfer. That is, based on the data provided in Figure 3.3, it appears as though **MC-B*o*** exists as rotationally strained atropisomers, rotating slowly on the NMR timescale between multiple meta-stable configurations.

3.3.4. Density Functional Theory

The model compounds were examined computationally via density functional theory (DFT) calculations to better understand their conformations and energy barriers to rotation (and hence polymer flexibility). Given that **MC-B*o*** exhibited signs of atropisomerism by NMR, a significantly higher rotational energy barrier about the central biphenyl moiety was expected versus that of **MC-B*m*** and **MC-B*p***. The optimal geometries and corresponding electron density isosurfaces (mapped with electrostatic potential) of **MC-B*o***, **MC-B*m*** and **MC-B*p*** in implicit water are shown in Figure 3.4. It is immediately apparent that the *ortho* biphenyl-containing **MC-B*o*** is highly sterically encumbered, much more-so than model compounds containing a *meta* (**MC-B*m***) or *para* biphenyl (**MC-B*p***), that likely significantly restricts molecular rotation.

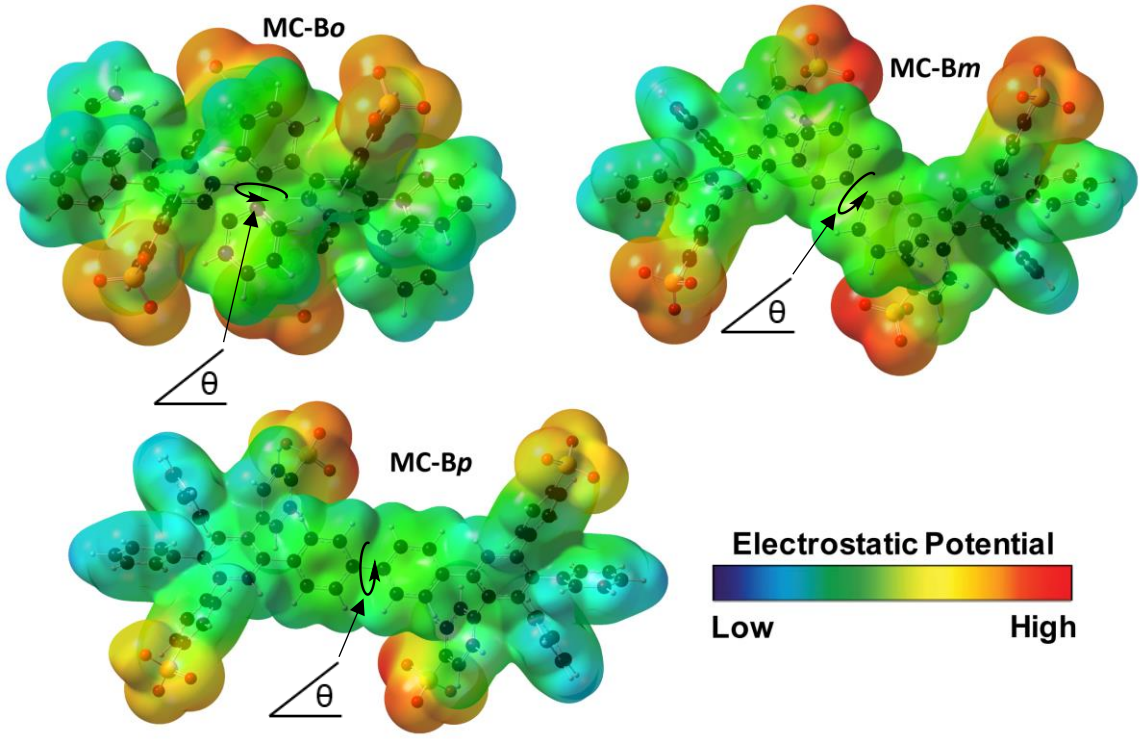

Figure 3.4: *Optimized nuclei geometry and electron density isosurfaces of model compounds mapped with electrostatic potential in water via DFT.*

The calculated optimal biphenyl dihedral angle of the central biphenyl moieties in each model compound (indicated in Figure 3.4) are given in Table 3.1. It should be noted that both **MC-B*o*** and **MC-B*m*** appear to adopt an optimal geometry in which the substituents bound to the central biphenyl are facing in opposite directions (i.e., the substituents are *trans* with respect to the central biphenyl). A zero-degree dihedral angle is defined as when the phenyls are in plane and the substituents are in the *trans* configuration. The dihedral angle of the central biphenyl moiety in **MC-B*o*** was found to be nearly 18° larger than in either **MC-B*m*** or **MC-B*p***. This increase is consistent with the notion that a sterically encumbered structure such as **MC-B*o*** would likely display molecular distortions in order to accommodate the bulky phenyl and sulfo-phenyl pendant groups. Furthermore, the molecular energy of **MC-B*o*** in its optimized geometry was significantly greater (11.6 kcal·mol^{-1}), that likewise suggested that the molecule is strained.

Table 3.1: *Optimal Dihedral Angle (Degrees) and Energy Difference Relative to* ***MC-Bp*** *in its Optimal Geometry (kcal mol^{-1}) of Model Compounds in their Optimal Geometry*

	Optimal Biphenyl Dihedral Angle	**Energy Difference Relative to MC-B*p* (kcal mol^{-1})**
MC-B*o*	53.84°	11.6
MC-B*m*	36.88°	0.5
MC-B*p*	36.22°	0

To examine rotational energy barriers, a relaxed dihedral scan was performed in 10° increments, beginning at each respective optimized geometry. The energy difference between the incremental configurations versus optimal geometries were calculated. In this way, the energy barrier to molecular rotation was estimated for **MC-B*o***, **MC-B*m***, and **MC-B*p***, as shown in Figure 3.5. Therefore, a higher rotational energy barrier represents a system that is less able to rotate. It should be noted that for each model compound in various configurations with varying biphenyl dihedral angles, the energy difference was determined relative to the energy of that same model compounds in its optimal geometry. As such, the energy barriers of each model compound depicted in Figure 3.5 are relative to the energy of that same model compound in its optimal geometry, and are not absolute. While both **MC-B*m*** and **MC-B*p*** share very similar rotational energy barriers, **MC-B*o*** displays a drastic increase in energy as the central biphenyl dihedral angle is rotated. Moreover, the presence of two distinct local energy minima at dihedral angles of 53.84° and 263.84° are observed, suggesting that the molecule may be locked in one of two conformations. This finding agrees with the experimental NMR findings that suggested atropisomerism in the *ortho* biphenyl-containing model compound **MC-B*o***.

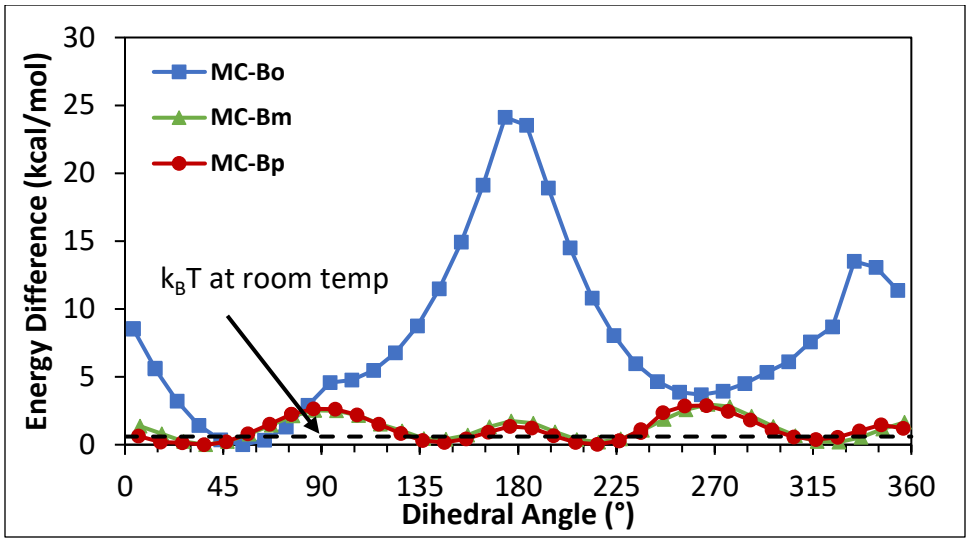

Figure 3.5: *Rotational energy barriers about central biphenyl in model compounds via DFT. Y-axis represents energy difference from optimal geometry for the corresponding model compound.*

3.4. Conclusions

Three model compounds **MC-B*o***, **MC-B*m***, and **MC-B*p*** were successfully prepared from *ortho*, *meta*, and *para*-substituted biphenyl constituents, respectively, as structural analogues to the respective polymers **sPPB*o*-H$^+$**, **sPPB*m*-H$^+$**, and **sPPB*p*-H$^+$**. These molecular models served as effective probes to assessing biphenyl monomer reactivity prior to polymerization, and were simpler to characterize. NMR spectroscopy suggested atropisomerism in the *ortho* biphenyl-containing **MC-B*o***, that caused restriction of rotation about the central biphenyl moiety. DFT calculations of **MC-B*o***, **MC-B*m***, and **MC-B*p*** supported these findings, and highlighted a particularly large energy barrier of rotation in the case of **MC-B*o***.

Chapter 4.

Angled and Linear Sulfonated Phenylated Poly(phenylene) Homo-polymers

This chapter was reproduced in part with permission from: N. Peressin, M. Adamski, E. M. Schibli, E. Ye, B. J. Frisken, S. Holdcroft, *Macromolecules* **2020**, DOI 10.1021/acs.macromol.0c00310. Copyright 2020 American Chemical Society.

My contributions included the entirety of the synthesis, characterization, and testing of polymer and membrane properties.

This work was financially supported by the Natural Sciences and Engineering Research Council of Canada (NSERC), DuPont, and the British Columbia Automobile Association (BCAA).

4.1. Introduction

The work described in Chapter 3 had successfully demonstrated that each of the three biphenyl dienophile co-monomers ***o*-BPL**, ***m*-BPL**, and ***p*-BPL** would undergo a Diels-Alder reaction with a functionalized cyclopentadienone diene. In this chapter, ***o*-BPL**, ***m*-BPL**, and ***p*-BPL** were used to prepare phenylated poly(phenylene)s **sPPB*o*-H$^+$**, **sPPB*m*-H$^+$**, and **sPPB*p*-H$^+$** respectively, as shown in Figure 4.1. As discussed in Chapter 1, hydrocarbon-based proton exchange membranes, particularly sulfonated phenylated poly(phenylene)s, are a promising class of PEMs due to their inherent thermochemical stability. Current iterations of these materials however, swell considerably when introduced to water, and are brittle in the dry state, potentially due to their rigid-rod like nature. Various literature sources have suggested that by incorporating non-linear units into the polymer backbone, the polymeric structure might adopt flexible coils,[102] promoting chain entanglement while simultaneously reducing water sorption, swelling, and elastic deformation.[29],[72],[100],[101]

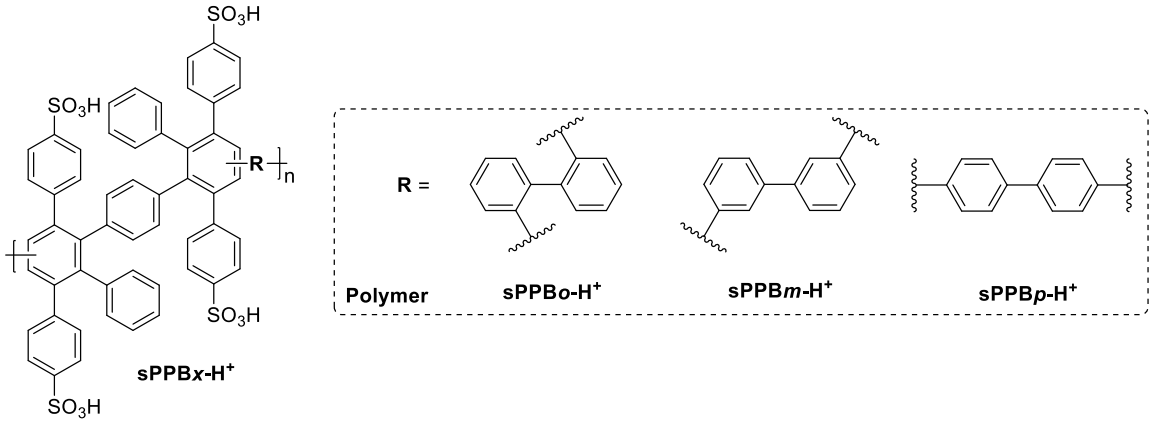

Figure 4.1: *Structure of **sPPBo-H$^+$**, **sPPBm-H$^+$**, and **sPPBp-H$^+$** incorporating linear and non-linear biphenyls.*

As such, three polymers possessing linear (*para*), and non-linear (*ortho* and *meta*) functionalized biphenyls incorporated into the poly(phenylene) backbone (Figure 4.1) were investigated. The polymers, and membranes prepared therefrom, were extensively investigated to assess their efficacy as proton exchange membrane materials, and to better understand the impact of incorporating non-linear biphenyl moieties into the polymer backbone. Polymer stereochemistry and solubility characteristics were assessed by NMR

spectroscopy, and molecular weights estimated via gel permeation chromatography. Thermal degradation profiles of the polymers were obtained via thermogravimetric analysis (TGA), and glass transition temperature (T_g) analysis was performed via differential scanning calorimetry (DSC). Mechanical properties of membranes cast from the polymers were assessed via tensile stress tests. Finally, water sorption, acid content, and proton conductivity were assessed through mass/dimensional analysis, acid-base titrations, and electrochemical impedance spectroscopy (EIS), respectively. All of the techniques, and relevant parameters used are described in detail in Chapter 2.

4.2. Experimental

4.2.1. Materials

The materials used in this chapter were the same as those outlined in Chapter 3.

4.2.2. Synthesis

1,4-*bis*-Phenylethynylbenzene

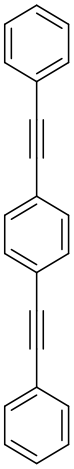

To a 2 L round bottom flask containing an inert atmosphere of argon was added THF (330 mL) and triethylamine (53 mL) and the mixture was degassed with argon under high stirring. To the flask was added 1,4-diiodobenzene (50.0 g, 151.6 mmol, 1.00 eq.) and phenylacetylene (34.0 mL, 31.7 g, 310 mmol, 2.05 eq.) and the mixture was again degassed with argon under high stirring. To the flask was added $Pd(PPh_3)_2Cl_2$ (70 mg, 0.010 mmol, 0.0005 eq.) and CuI (19 mg, 0.010 mmol, 0.0005 eq.), after which the flask was sealed and heated to 50 °C for 16 h. The reaction was cooled to room temperature, transferred to a smaller 500 mL round bottom flask, and the solvent was evaporated under vacuum until approx. 125 mL remained. The product was precipitated by pouring the concentrated mixture into 1 L distilled H_2O. The light brown precipitate was filtered and collected via a Buchner funnel and filter paper, rinsing with distilled H_2O (100 mL x 5). Upon drying *in vacuo* at 80 °C the product was collected as a beige powder. ^{1}H NMR (400 MHz, $CDCl_3$) δ 7.54 (dd, *J* = 6.4, 2.8 Hz, 4H), 7.51 (s, 4H), 7.39 – 7.33 (m, 6H). All spectral data were in good agreement with those reported in the literature.[80]

2,2'-(1,4-Phenylene)-*bis*-1-phenylethane-1,2-dione (bisbenzyl)

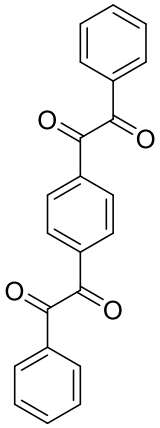

To a 500 mL round bottom flask was added a stir bar, 1,4-*bis*-phenylethynylbenzene (10.0 g, 35.9 mmol, 1 eq.), DMSO (300 g), and elemental iodine (4.60 g, 18.1 mmol, 0.50 eq.). The round bottom flask was equipped with a condenser and heated to reflux at 155 °C, and the reaction was monitored by TLC and ^{1}H NMR, reaching full conversion after 16 h. The yellow product was precipitated while simultaneously quenching leftover iodine by pouring the reaction mixture into a solution of sodium thiosulfate (2.5 wt%, 62.5 g, 418 mmol) in H_2O (2.5 L) under high stirring. This mixture was stirred for 30 min before the precipitate was filtered, collected and air dried via a medium frit sintered glass Buchner funnel. The dry crude product was dissolved in a minimum volume of dichloromethane (400 mL) in a 1.5 L beaker under stirring. Sodium thiosulfate (5.0 g, 32 mmol) and $MgSO_4$ (5.0 g, 42 mmol) were added to the beaker and the mixture was stirred for 10 min. The mixture was poured through medium frit sintered glass Buchner funnel containing 2 cm silica gel, 1.5 cm activated charcoal and 1.5 cm packed Celite® all separated by filter paper, and rinsed with dichloromethane (600 mL) to obtain a bright orange solution. The solvent was removed by evaporation *in vacuo*, and the product was purified affording a yellow crystalline solid by recrystallization in ethanol (5.3 g, 15.5 mmol, 43% yield). ^{1}H NMR (400 MHz, CD_2Cl_2) δ (ppm): 8.11 (s, 4H), 7.97 (dd, *J* = 8.4, 1.3 Hz, 4H), 7.71 (t, *J* = 7.5 Hz, 2H), 7.55 (t, *J* = 7.9 Hz, 4H). All spectral data were in good agreement with those reported in the literature.[80]

4,4'-(1,4-Phenylene)-*bis*-2,3,5-triphenylcyclopenta-2,4-dien-1-one (Bistetracyclone, BTC)

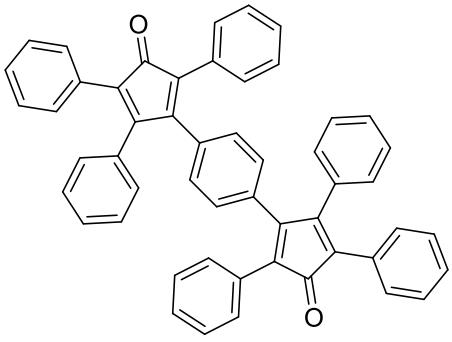

To a two-necked round bottom flask with a stir bar was added bisbenzyl (5.3 g, 15.5 mmol, 1.0 eq.), 1,3-(diphenyl)propan-2-one (6.67 g, 31.1 mmol, 2.05 eq.), ethanol (53 mL), and toluene (5.3 mL). The round bottom flask was equipped with a condenser and heated to 80 °C in an oil bath until starting material was fully dissolved. Upon complete dissolution, the oil bath temperature was raised to 130 °C. In a separate vial was added

KOH (1.09 g, 19.4 mmol, 1.25 eq.) and methanol (5.3 mL) and the vial was placed in an ultrasonication bath until the KOH was fully dissolved. The KOH solution was added to the two-neck flask dropwise after which the reaction was allowed to reflux for 60 min. The reaction mixture was cooled to room temperature, and placed in a fridge at 7 °C for 16 h to precipitate the product. The precipitate was filtered and washed with cold ethanol before being dried *in vacuo* at 60 °C for 16 h to obtain bistetracyclone (8.13 g, 11.8 mmol, 76% yield). ^{1}H NMR (400 MHz, CD_2Cl_2) δ (ppm): 7.30 – 7.17 (m, 26H), 6.93 (d, *J* = 7.0 Hz, 4H), 6.78 (s, 4H). ^{13}C NMR (101 MHz, CD_2Cl_2) δ (ppm): 200.65, 155.01, 154.75, 134.22, 133.62, 131.50, 131.35, 130.71, 130.65, 129.83, 129.57, 129.09, 128.58, 128.17, 128.12. All spectral data were in good agreement with those reported in the literature.[79]

Tetra(*para*-Sulfonated) Bistetracyclone (sBTC)

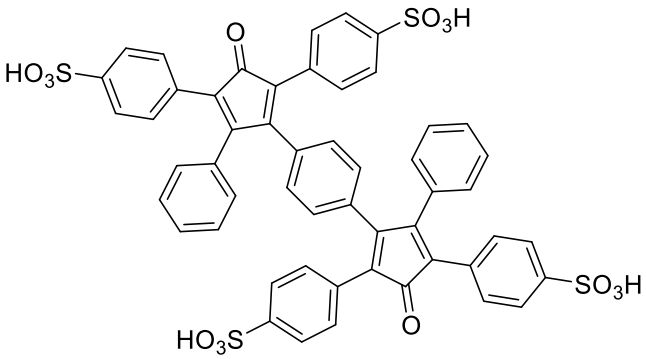

To a 3 L three-necked round bottom flask with a stir bar was added dichloroethane (700 mL). The flask was equipped with a sealed drop funnel containing argon-degassed dichloroethane (37 mL), sealed with rubber septa, and the system was degassed under a flow of argon for 2 h. Bistetracyclone (8.12 g, 11.8 mmol, 1.0 eq.) was added to the flask, and the mixture was stirred and degassed with argon for 60 min. Trimethylsilyl chlorosulfonate (37.0 mL, 45.3 g, 240 mmol, 20.4 eq.) was injected into the drop funnel by syringe, after which the contents of the drop funnel was added dropwise to the flask under high stirring. The reaction was stirred for 16 h, after which ethanol (74 mL) was added to quench the remaining trimethylsilyl chlorosulfonate. The flask was then filled to the neck with diethyl ether, and poured into a mixture of diethyl ether (3.0 L) and pentane (1.0 L) under high stirring. The resulting precipitate was filtered via a sintered glass Buchner funnel and washed with pentane and cold diethyl ether. Drying *in vacuo* at 60 °C for 16 h afforded tetra(para-sulfonated) bistetracyclone as a purple powder (10.80 g, 10.68 mmol, 91 % yield). ^{1}H NMR (400 MHz, DMSO-d_6) δ (ppm): 7.50 (d, *J* = 8.4 Hz, 4H), 7.46 (d, *J* = 8.3 Hz, 4H), 7.33 (t, *J* = 7.3 Hz, 2H), 7.25 (t, *J* = 7.5 Hz, 4H), 7.13 (d, *J* = 8.3 Hz, 4H), 7.07 (d, *J* = 8.4 Hz, 4H), 6.92 (d, *J* = 7.2 Hz, 4H), 6.85 (s, 4H). All spectral data were in good agreement with those reported in the literature.[79]

Tetra(*para*-sulfonated) Bistetracyclone Triethylammonium Salt (TEAsBTC)

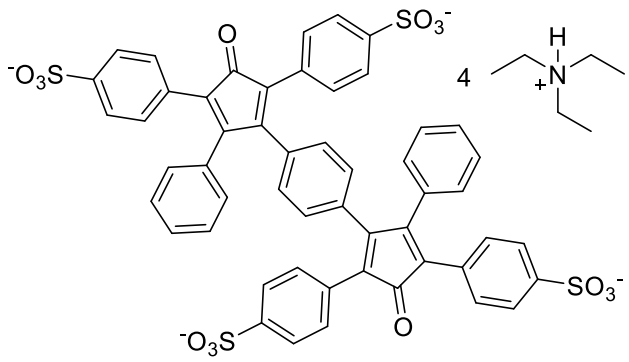

To a 2 L round bottom flask containing a stir bar was added tetra(para-sulfonated) bistetracyclone (sBTC) (10.80 g, 10.68 mmol, 1.0 eq.) and *n*-butyl alcohol (600 mL) and was stirred vigorously for 2 h. To the round bottom flask was added triethylamine (89 mL, 65 g, 640 mmol, 60 eq.) dropwise under vigorous stirring for 16 h. To the round bottom flask was added diethyl ether (200 mL) and the mixture was stirred for 30 min before the precipitate was filtered and washed with diethyl ether (2 x 80 mL). Drying *in vacuo* at 80 °C afforded the product as a bright purple powder (14.24 g, 10.68 mmol, 94 % yield). ^{1}H NMR (400 MHz, DMSO-d_6) δ (ppm): 8.85 (s, 4H), 7.50 (d, *J* = 8.4 Hz, 4H), 7.46 (d, *J* = 8.4 Hz, 4H), 7.33 (t, *J* = 7.4 Hz, 2H), 7.25 (t, *J* = 7.5 Hz, 4H), 7.13 (d, *J* = 8.4 Hz, 4H), 7.07 (d, *J* = 8.4 Hz, 4H), 6.92 (d, *J* = 7.1 Hz, 4H), 6.85 (s, 4H), 3.10 (q (two overlapped) *J* = 7.2 Hz, 24H), 1.17 (t, *J* = 7.3 Hz, 36H). All spectral data were in good agreement with those reported in the literature.[79]

Sulfonated Polyphenylene *ortho*-Biphenyl Triethylammonium Salt (sPPB*o*-HNEt3$^+$)

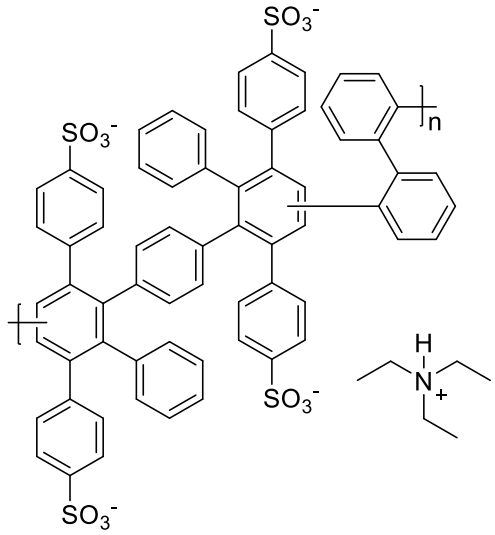

To a clean and dry 150 mL pressure vessel degassed with argon and equipped with a stir bar was added 2,2'-diethynyl-1,1'-biphenyl (0.291 g, 1.44 mmol, 1.015 eq.), tetra(para-sulfonated) bistetracyclone triethylammonium salt (2.010 g, 1.420 mmol, 1.00 eq.), and degassed nitrobenzene (40 mL) and the mixture was stirred under argon flow for 1 h. The pressure vessel was sealed with a Teflon lid and the mixture was heated to 185 °C for 72 h under high stirring. The nitrobenzene was decanted from the polymer film inside the flask, to which was added DMSO (30 mL) and the mixture was stirred at 80 °C for 16 h. The resulting solution was poured into ethyl acetate (600 mL) under stirring, let stir for 1 h, and the brown precipitate was filtered and washed with ethyl acetate. Drying

in vacuo at 80 °C for 16 h afforded the product as a dark brown solid (2.024 g, 91% yield). ^{1}H NMR (400 MHz, DMSO-d_6) δ (ppm): 8.89 (s, 4H), 7.79 – 5.64 (m, 40H), 3.03 (s, 24H), 1.09 (s, 36H). GPC analysis: M_n = 261,800 g mol^{-1}, M_w = 408,400 g mol^{-1}, Đ = 1.56.

Sulfonated Polyphenylene *ortho*-Biphenyl (sPPB*o*-H$^+$)

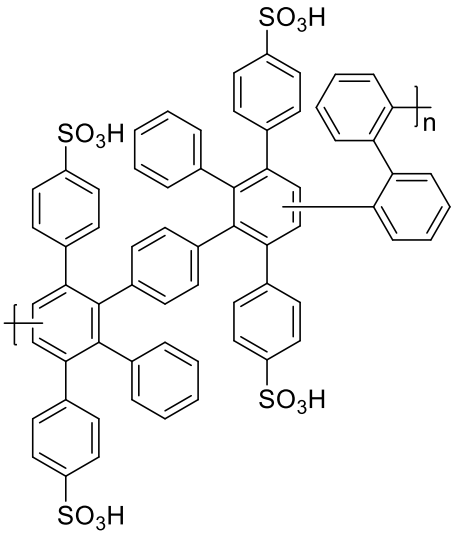

To a 500 mL round bottom flask equipped with a stir bar was added sPPB*o*-HNEt$_3^+$ (1.997 g) and methanol (102 mL) and the mixture was stirred to complete dissolution. A methanolic solution of sodium hydroxide (33.2 mL, 2M NaOH in methanol) was added dropwise to the mixture under high stirring, and the mixture was stirred at room temperature for 16 h. The solvents were removed *in vacuo* until the mixture resembled a thick paste, after which deionized H_2O (approx. 200 mL) was added to the flask and the solvents were immediately removed *in vacuo* until the mixture resembled a thick paste. Deionized H_2O (200 mL) was added and removed *in vacuo* once more. To the flask was added HCl (1M, approx. 100mL) until the pH of the mixture was 0 and the mixture was stirred for 16 h. The polymer was filtered, washed with HCl (1M) and deionized H_2O and dried *in vacuo* at 80 °C for 16 h before collecting the product as a brown solid (1.323 g, 89% yield). ^{1}H NMR (400 MHz, DMSO-d_6) δ (ppm): 7.79 – 5.64 (m, 40H), 3.71 (s, H_2O/H_3O^+). GPC analysis: M_n = 240,000 g mol^{-1}, M_w = 289,500 g mol^{-1}, Đ = 1.21.

Sulfonated Polyphenylene *meta*-Biphenyl Triethylammonium Salt (sPPB*m*-HNEt3$^+$)

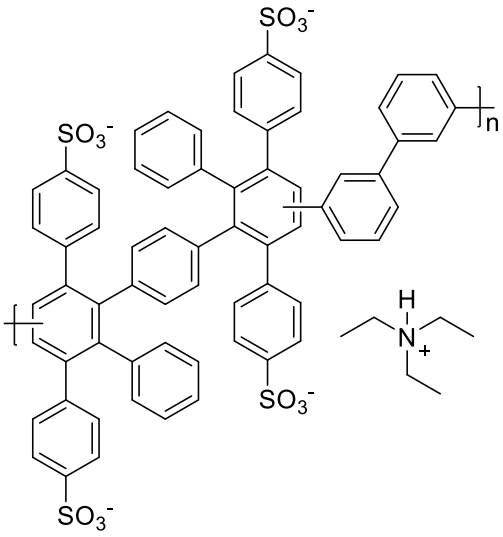

To a clean and dry 150 mL pressure vessel degassed with argon and equipped with a stir bar was added 3,3'-diethynyl-1,1'-biphenyl (0.250 g, 1.24 mmol, 1.015 eq.), tetra(*para*-sulfonated) bistetracyclone triethylammonium salt (1.724 g, 1.218 mmol, 1.00 eq.), and degassed nitrobenzene (35 mL) and the mixture was stirred under argon flow for 1 h. The pressure vessel was sealed with a Teflon lid and the mixture was heated to 180 °C for 96 h, followed by 195 °C for 16 h under high stirring. The nitrobenzene was decanted from the polymer film inside the flask, to which was added DMSO (35 mL) and the mixture was stirred at 135 °C for 16 h. The resulting solution was poured into ethyl acetate (600 mL) under stirring, let stir for 1 h, and the brown precipitate was filtered and washed with ethyl acetate. Drying *in vacuo* at 80 °C for 16 h afforded the product as a dark brown solid (1.659 g, 87% yield). ^{1}H NMR (400 MHz, DMSO-d_6) δ (ppm): 8.90 (s, 4H), 7.70 – 6.01 (m, 40H), 3.05 (q (two overlapped), J = 7.2 Hz, 24H), 1.12 (t, J = 7.3 Hz, 36H). GPC analysis: M_n = 689,900 g mol^{-1}, M_w = 1,209,000 g mol^{-1}, Đ = 1.75.

Sulfonated Polyphenylene *meta*-Biphenyl (sPPB*m*-H$^+$)

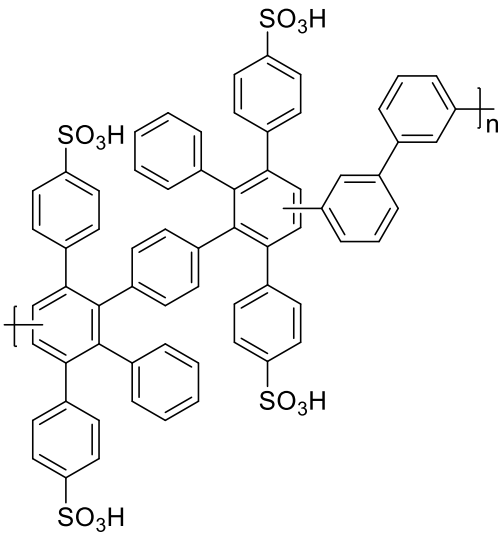

To a 500 mL round bottom flask equipped with a stir bar was added sPPB*m*-HNEt$_3^+$ (0.893 g) and methanol (200 mL) and the mixture was stirred to complete dissolution. A methanolic solution of sodium hydroxide (40 mL, 2M NaOH in methanol) was added dropwise to the mixture under high stirring, and the mixture was stirred at room temperature for 16 h. The solvents were removed *in vacuo* until the mixture resembled a thick paste, after which deionized H_2O (approx. 150 mL) was added to the flask and the solvents were immediately removed *in vacuo* until the mixture was a thick paste. Deionized H_2O

(150 mL) was added and removed *in vacuo* once more. To the flask was added HCl (1M, approx. 150mL) until the pH of the mixture was 0 and the mixture was stirred for 16 h. The polymer was filtered, washed with HCl (1M) and deionized H_2O and dried *in vacuo* at 80 °C for 16 h before collecting the product as a brown solid (0.622 g, 93% yield). ^{1}H NMR (400 MHz, DMSO-d_6) δ (ppm): 7.70 – 6.01 (m, 40H), 3.77 (s, H_2O/H_3O^+). GPC analysis: M_n = 655,600 g mol^{-1}, M_w = 1,158,000 g mol^{-1}, Đ = 1.77.

Sulfonated Polyphenylene *para*-Biphenyl Triethylammonium Salt (sPPB*p*-HNEt3$^+$)

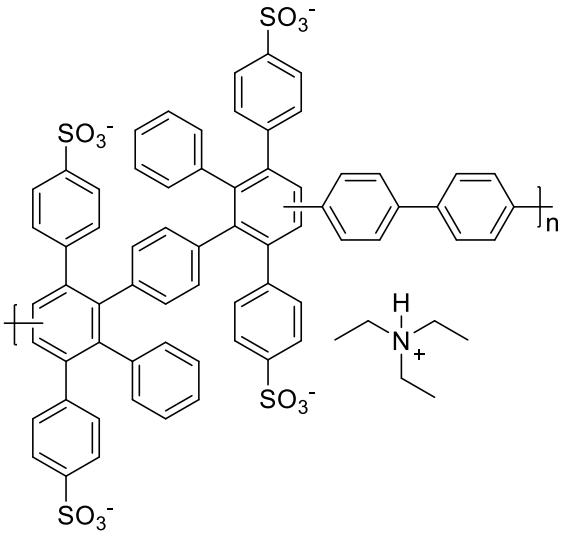

To a clean and dry 150 mL pressure vessel degassed with argon and equipped with a stir bar was added 4,4'-diethynyl-1,1'-biphenyl (0.290 g, 1.434 mmol, 1.015 eq.), tetra(para-sulfonated) bistetracyclone triethylammonium salt (2.000 g, 1.413 mmol, 1.00 eq.), and degassed nitrobenzene (40 mL) and the mixture was stirred under argon flow for 1 h. The pressure vessel was sealed with a Teflon lid and the mixture was heated to 170 °C for 96 h under high stirring. The nitrobenzene was decanted from the polymer film inside the flask, to which was added DMSO (50 mL) and the mixture was stirred at 80 °C for 16 h. The resulting solution was poured into ethyl acetate (600 mL) under stirring, let stir for 1 h, and the brown precipitate was filtered and washed with ethyl acetate. Drying *in vacuo* at 80 °C for 16 h afforded the product as a light brown solid (1.882 g, 85% yield). ^{1}H NMR (400 MHz, DMSO-d_6) δ (ppm): 8.89 (s, 4H), 8.20 – 5.92 (m, 40H), 3.05 (q (two overlapped), J = 7.3 Hz, 24H), 1.12 (t, J = 7.3 Hz, 36H).

Sulfonated polyphenylene *para*-biphenyl (sPPB*p*-H$^+$)

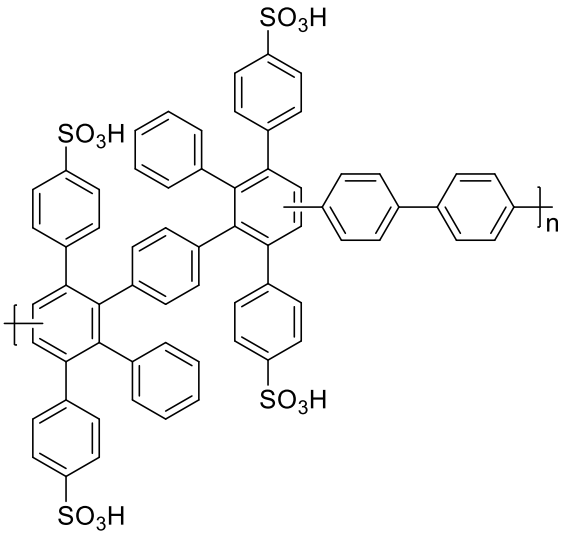

To a 500 mL round bottom flask equipped with a stir bar was added sPPB*p*-HNEt$_3^+$ (1.8128 g) and methanol (93 mL) and the mixture was stirred to complete dissolution. NaOH (30 mL, 2M in methanol) was added dropwise to the mixture under high stirring, and the mixture was stirred at room temperature for 16 h. The solvents were removed *in vacuo* until the mixture resembled a thick paste, after which deionized H_2O (approx. 150 mL) was added to the flask and the solvents were immediately removed *in vacuo* until the mixture was a thick paste. Deionized H_2O (150 mL) was added and removed *in vacuo* once more. To the flask was added HCl (1M, approx. 150mL) until the pH of the mixture was 0 and the mixture was stirred for 16 h. The polymer was filtered, washed with HCl (1M) and deionized H_2O and dried *in vacuo* at 80 °C for 16 h before collecting the product as a light brown solid (1.273 g, 95% yield). ^{1}H NMR (400 MHz, DMSO-d_6) δ (ppm): 8.20 – 5.92 (m, 40H), 4.06 (s, H_2O/H_3O^+). GPC analysis: M_n = 82,500 g mol^{-1}, M_w = 164,300 g mol^{-1}, Đ = 1.99.

4.3. Results and Discussion

4.3.1. Polymer Synthesis and Characterization

Syntheses of the *ortho*, *meta*, and *para* biphenyl-containing polymers **sPPBo-H$^+$**, **sPPBm-H$^+$**, and **sPPBp-H$^+$**, respectively, were achieved in three steps from **TEAsBTC** and either ***o*-BPL**, ***m*-BPL**, or ***p*-BPL**, respectively (Scheme 4.1). **TEAsBTC** was prepared in five steps starting from 1,4-diiodobenzene and phenylacetylene according to previously reported methodologies,[79] as described in the Chapter 2. Diels-Alder polycondensations were carried out initially using the reaction conditions employed during model compound synthesis. A stoichiometric ratio of 1.015 equivalents of the biphenyl (***x*-BPL**) to 1.000 equivalents of **TEAsBTC** was used, yielding alkyne-terminated, triethylammonium-functionalized **sPPB*x*-HNEt$_3^+$**, where ***x*** corresponds to ***o*** (*ortho*), ***m*** (*meta*), or ***p*** (*para*). Conversion to acidic form **sPPB*x*-H$^+$** was achieved by: (1) treatment with NaOH in

methanol to liberate the triethylammonium counter ions, effectively exchanging to sodium counter ions ($–SO_3^-HNEt_3^+ \rightarrow –SO_3^-Na^+$); and (2), treatment with aqueous hydrochloric acid to exchange the sodium counter ions for acidic protons ($–SO_3^-Na^+ \rightarrow –SO_3^-H^+$).

Scheme 4.1: *Synthesis of Polymers* ***sPPBo-H⁺****,* ***sPPBm-H⁺****, and* ***sPPBp-H⁺***

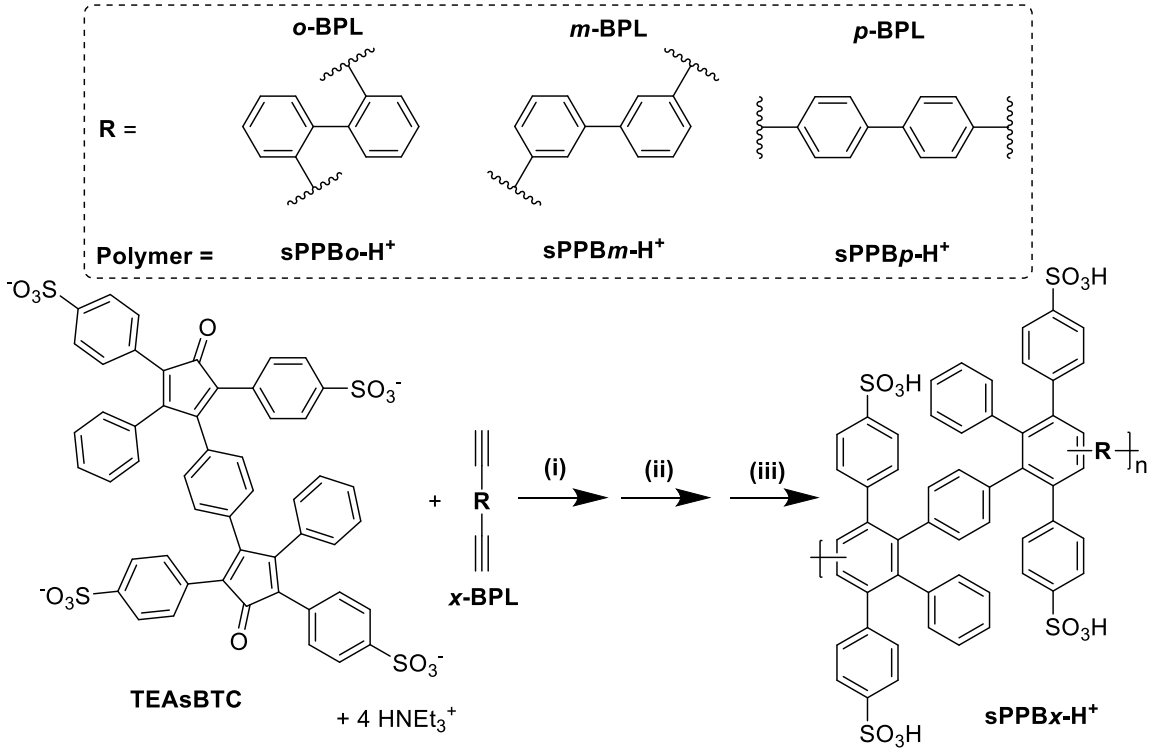

The initial, triethylammonium-containing polymers **sPPB*x*-HNEt$_3^+$** were obtained in excess of 85% yield. Each polymer was characterized using ^{1}H NMR spectroscopy in DMSO-d_6 to confirm successful polymerization. Analogous to model compound characterizations, the triethylammonium counter-ions present in the polymers served as internal probes, allowing for verification that polymers possessing the expected repeat units were obtained following polymerization (Figure 4.2). 36 methyl, 24 methylene, and 4 acidic (Et_3NH^+) were observed relative to the 40 aromatic protons in each of **sPPB*o*-HNEt$_3^+$**, **sPPB*m*-HNEt$_3^+$**, and **sPPB*p*-HNEt$_3^+$**. This was expected, given that each of the three materials are regioisomers and possess the same chemical formula. The ^{1}H NMR signals were significantly broader in **sPPB*o*-HNEt$_3^+$** and **sPPB*m*-HNEt$_3^+$** compared to that of **sPPB*p*-HNEt$_3^+$**, being especially broad in **sPPB*o*-HNEt$_3^+$**. This behavior is typical in polymer systems with restricted rotation, as the chemical environment of otherwise

equivalent protons within each repeat unit is different.[158],[159],[160] This observation agrees with the atropisomerism of **MC-B*o***. Although **MC-B*m*** did not exhibit this characteristic, when extended to a polymeric system as in **sPPB*m*-HNEt$_3^+$**, there may exist some degree of rotational restriction.

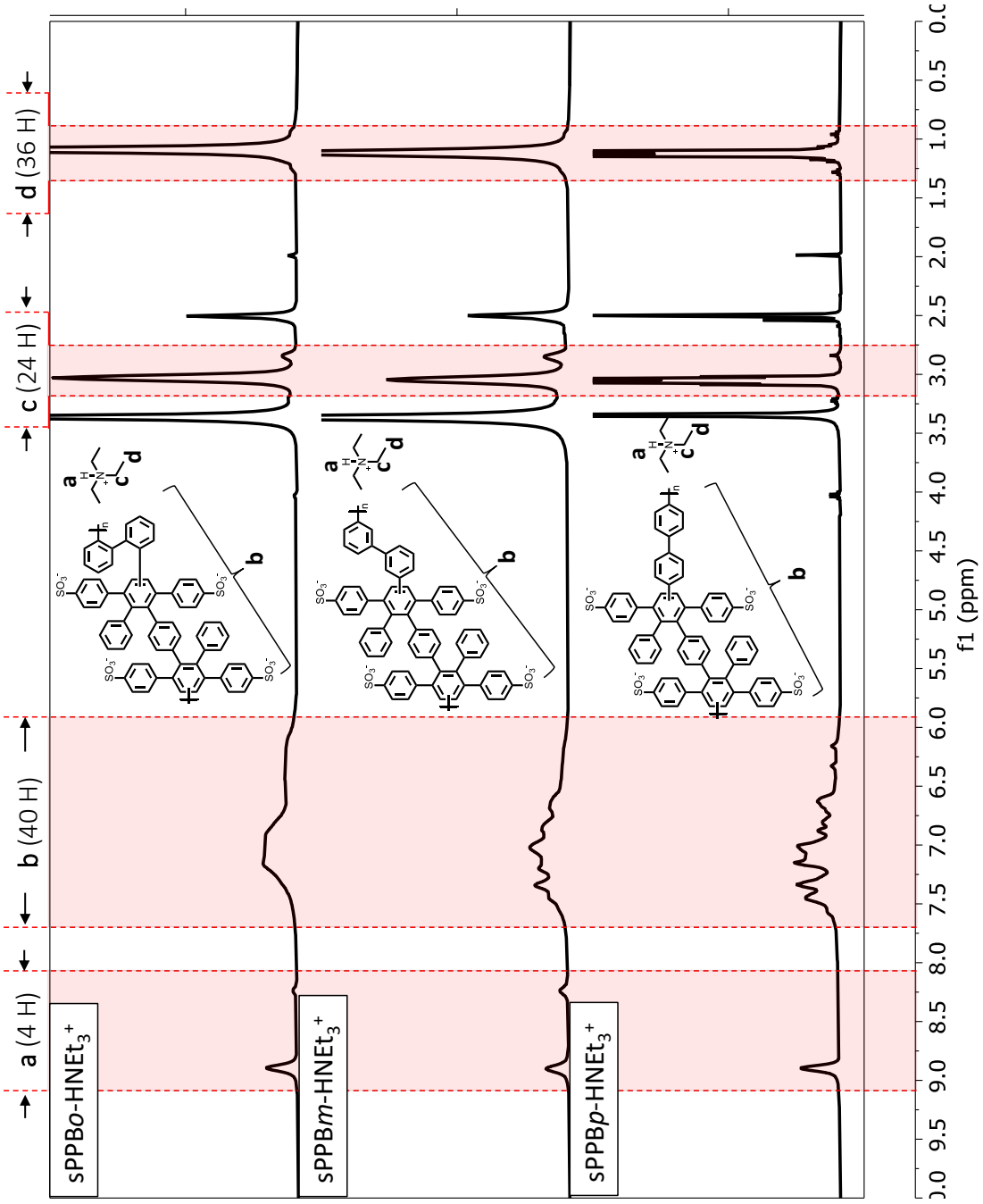

Figure 4.2: *^{1}H NMR of **sPPBo-HNEt$_3^+$**, **sPPBm-HNEt$_3^+$**, and **sPPBp-HNEt$_3^+$**. Integration confirms 40 aromatic protons relative to triethylammonium internal probes in each case.*

Conversion of the polymers from triethylammonium form (**sPPB*x*-HNEt$_3^+$**) to acid form (**sPPB*x*-H$^+$**) was achieved successfully in yields between 89-95%. The resulting polymers were characterized by ^{1}H NMR spectroscopy, displaying an absence of the triethylammonium methyl, methylene, and acidic (Et_3NH^+) proton peaks, as expected (see Appendix B, Figures B 8, B 10 and B 12). Despite possessing the same overall degree of hydrophilicity (4 sulfonic acid groups per repeat unit), **sPPB*o*-H$^+$** was unexpectedly water-soluble. Gel permeation chromatography (GPC) characterization of polymers after acid conversion revealed estimated number-average molecular weights (M_n) of 78,300 and 240,000 g mol^{-1} for **sPPB*o*-H$^+$**; 68,800 and 655,600 g mol^{-1} for **sPPB*m*-H$^+$**; and 82,500 g mol^{-1} for **sPPB*p*-H$^+$**, with dispersity values (Đ) ranging between 1.16 and 1.99, as shown in Table 4.1. Dispersity values for both **sPPB*o*-H$^+$** and **sPPB*m*-H$^+$** were notably lower than those typically reported for polymers prepared by Diels-Alder polycondensation (Đ ≥ 2).[77],[79],[52],[82] The measured dispersity values appear to increase from **sPPB*o*-H$^+$** to **sPPB*m*-H$^+$**, and again to **sPPB*p*-H$^+$** as the polymer backbone becomes less rotationally hindered. It is possible that this is a limitation of the GPC, whereby as the polymer becomes less flexible-coil like and more rigid-rod like, the size exclusion column is unable to efficiently separate polymers of differing molecular weights causing an apparent reduction in dispersity values.

Table 4.1: *Number Average Molecular Weight (M_n), Weight Average Molecular Weight (M_w), and Dispersity (Đ) for Assessed **sPPBx-H$^+$** Polymers*

Polymer	M_n (g mol^{-1})	M_w (g mol^{-1})	Đ
sPPB*o*-H$^+$	78,300	91,100	1.16
	240,000	298,500	1.21
sPPB*m*-H$^+$	68,800	89,600	1.30
	655,600	1,158,000	1.77
sPPB*p*-H$^+$	82,500	164,300	1.99

Polymer molecular weights were controlled by varying the polymerization temperature and reaction time. Higher molecular weight polymers were typically obtained with higher temperatures, and longer reaction times. As many polymer properties are dependent upon molecular weight,[149] polymers with similar molecular weights (M_n = 78,300, 68,800 and 82,500 g mol^{-1} for **sPPB*o*-H$^+$**, **sPPB*m*-H$^+$**, and **sPPB*p*-H$^+$** respectively) were initially prepared for comparative evaluation. However, at these

molecular weights, **sPPB*o*-H$^+$** and **sPPB*m*-H$^+$** were unable to form robust, free standing-membranes. Obtaining higher molecular weight polymers allowed **sPPB*m*-H$^+$** (M_n = 655,600) to form a robust free-standing membrane, while **sPPB*o*-H$^+$** (M_n = 240,000) was still unable to form a membrane. Synthesis of higher molecular weight **sPPB*p*-H$^+$** was unsuccessful, presumably due to its inherent low solubility in polar solvents that may have caused it to precipitate out of the reaction medium at lower molecular weights. Consequently, analysis of some of the membrane's properties were conducted using polymers with differing molecular weights, and is indicated appropriately.

4.3.2. NMR Analysis – Solubility and Regiochemistry

A simple visual solubility test involving immersion of a membrane sample in DI H_2O for 1 and 150 h was initially employed to assess polymer solubility (Figure 4.3a and b). While it was evident that **sPPB*o*-H$^+$** had fully dissolved and that **sPPB*m*-H$^+$** began showing signs of mechanical deterioration and dissolution over time, **sPPB*p*-H$^+$** remained intact. To complement these qualitative findings, ^{1}H NMR spectroscopy in deuterium oxide (D_2O) was used to probe sample solubility. Samples (25.3 mg) of each **sPPB*o*-H$^+$** (M_n = 78,300 g mol^{-1}), **sPPB*m*-H$^+$** (M_n = 68,800 g mol^{-1}), and **sPPB*p*-H$^+$** (M_n = 82,500 g mol^{-1}) were immersed in 2.0 mL D_2O and stirred vigorously for 72 h. Following filtration, ^{1}H NMR spectra were collected and normalized to the residual solvent peak at 4.790 ppm, as shown in Figure 4.3c. The aromatic proton signals of **sPPB*o*-H$^+$** were easily observable in the spectrum, indicating an appreciable fraction of the sample had dissolved. The aromatic proton signals of **sPPB*m*-H$^+$** were marginally visible, suggesting partial water solubility, whereas the **sPPB*p*-H$^+$** spectrum contained no visible proton signals.

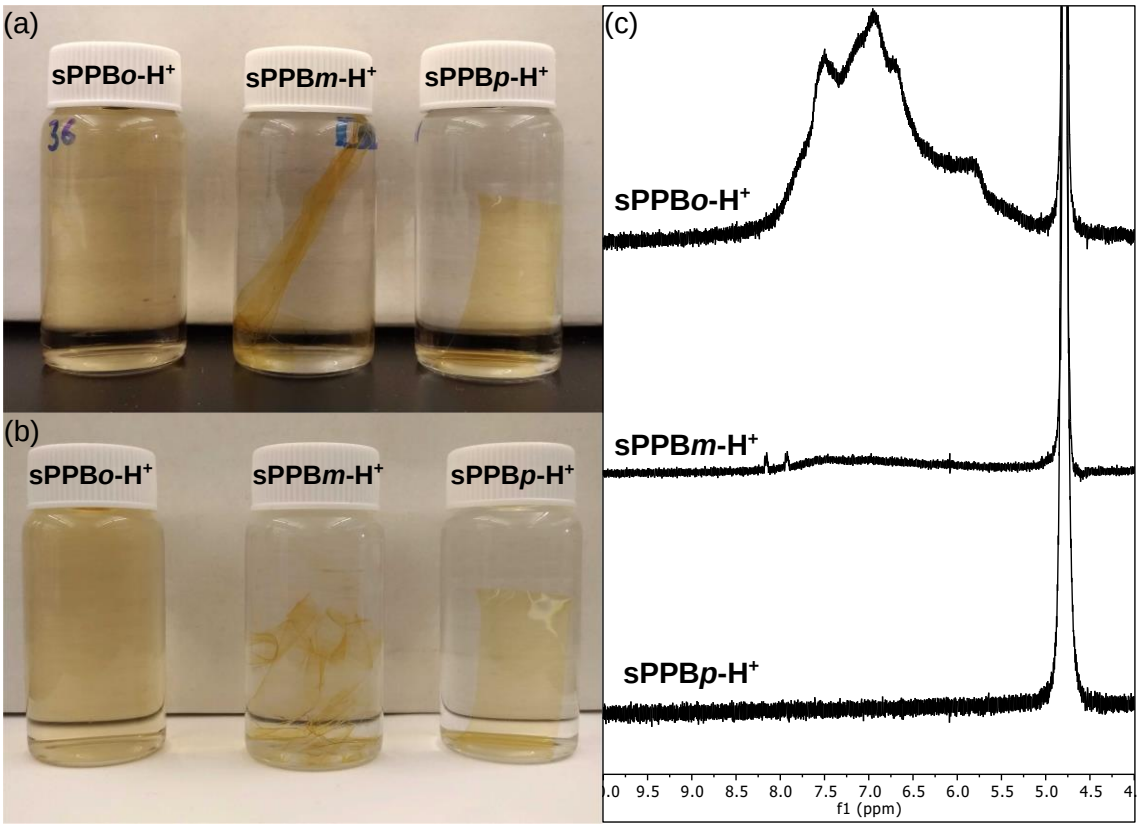

Figure 4.3: *Polymers after immersion in water for (a) 1 h, and (b) 150 h; and (c) ^{1}H NMR in D_2O after stirring 25.3 mg of each polymer in 2.0 mL D_2O for 72 h.*

As discussed in Chapter 2, regiochemical aspects of the Diels-Alder reaction may lead to the formation of regioisomeric products. In general, the most nucleophilic component of the electron rich species is more likely to react with the more electrophilic component of the electron poor species in a Diels-Alder cycloaddition. In the case of reacting **TEAsBTC** with either ***o*-BPL**, ***m*-BPL**, or ***p*-BPL** however, it is not immediately clear which carbon atoms possess the greatest degree of nucleophilicity and electrophilicity. Nevertheless, a representative sPPP Diels-Alder condensation showing both possible DA addition products, *meta* and *para*, is shown in Scheme 4.2.

Scheme 4.2: *Representation of Regiochemical Implications of the Diels-Alder Reaction Leading to meta and para Regioisomeric Products*

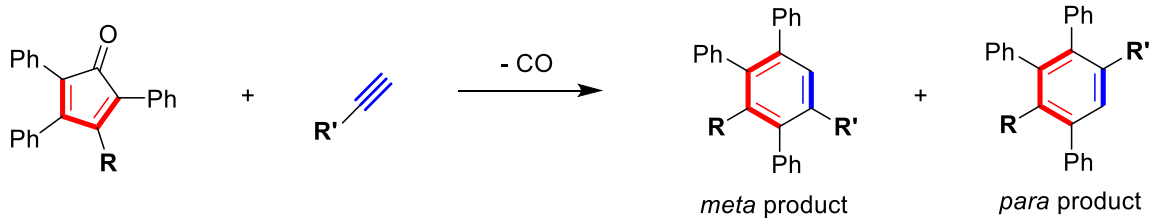

meta product *para* product

It has been well documented that Diels-Alder polycondensations afford a mix of structural isomers due to formation of both *meta* and *para* backbone linkages, as a consequence of the two possible orientations the alkyne dienophile may occupy with respect to the cyclopentadienone diene during reaction.[86],[87],[79],[80],[161],[162] The Diels-Alder *meta-meta*, *para-para*, and *meta-para* (DA *m-m*, DA *p-p*, DA *m-p*) adducts that may form in sPPPs as a consequence of the Diels-Alder reaction are shown in Figure 4.4. Previous reports have detailed the use of ^{1}H NMR spectroscopy to obtain a relative ratio between these adducts formed, initially by using small molecule model compounds,[161] and later polymeric structures.[79],[80] Three distinct ^{1}H NMR signals observed between 6.52 – 6.42 ppm, 6.37 – 6.28 ppm, and 6.20 – 6.10 ppm were attributed to the aromatic “core” protons (Figure 4.4) within the unique chemical environments of the DA *p-p*, DA *m-m*, or DA *m-p* adducts, respectively.[79]

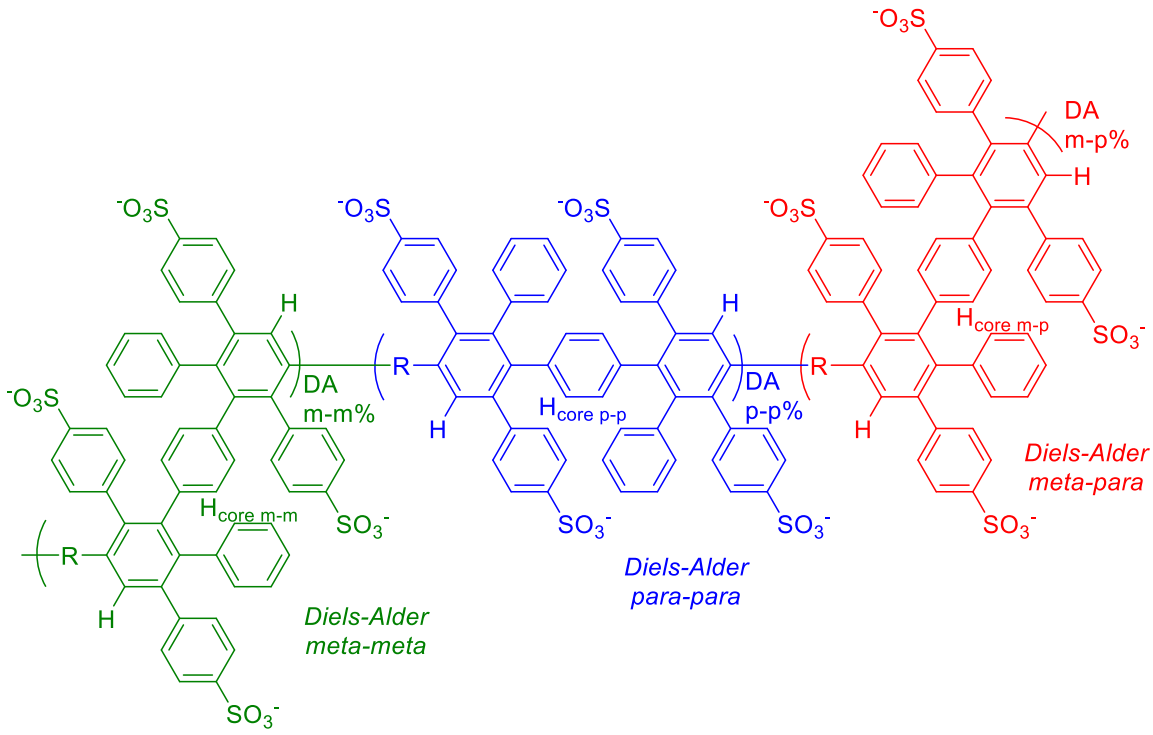

Figure 4.4: *Diels-Alder meta-meta, para-para, and meta-para adducts that can form in sPPPs.*

It was possible to perform this analysis on both **sPPB*m*-H⁺** (Figure 4.5), and **sPPB*p*-H⁺** (Figure 4.6), where the NMR spectra contained broad peaks corresponding to the DA *p*-*p*, DA *m*-*m*, or DA *m*-*p* adducts. Due to the broadness of the peaks however, the results presented here are considered best estimates, as there is likely a significant degree of error associated with the NMR integration. The ^{1}H NMR signals in **sPPB*o*-H⁺** were far too broad to identify the core aromatic protons, and it was therefore not possible to perform a regioisomeric analysis on this polymer. The ratio of DA *m*-*m* : DA *p*-*p* : DA *m*-*p* adducts in **sPPB*m*-H⁺** was found to be 48:32:20, that gave an overall Diels-Alder *meta:para* linkage ratio of 58:42. The ratio of DA *m*-*m* : DA *p*-*p* : DA *m*-*p* adducts in **sPPB*p*-H⁺** were 37:30:33, that gave an overall Diels-Alder *meta:para* linkage ratio of 53:47. These results suggest that both ***m*-BPL** and ***p*-BPL** prefer *meta* addition; however, the effect is pronounced with ***m*-BPL**.

sPPB*m*-HNEt$_3^+$							Overall Ratio	
para-para		*meta-meta*		*meta-para*			*meta*	*para*
6.47 ppm		6.35 ppm		6.20 ppm			**58%**	**42%**
Integration	%	Integration	%	Integration	%			
1.00	**32%**	1.47	**48%**	0.60	**20%**			

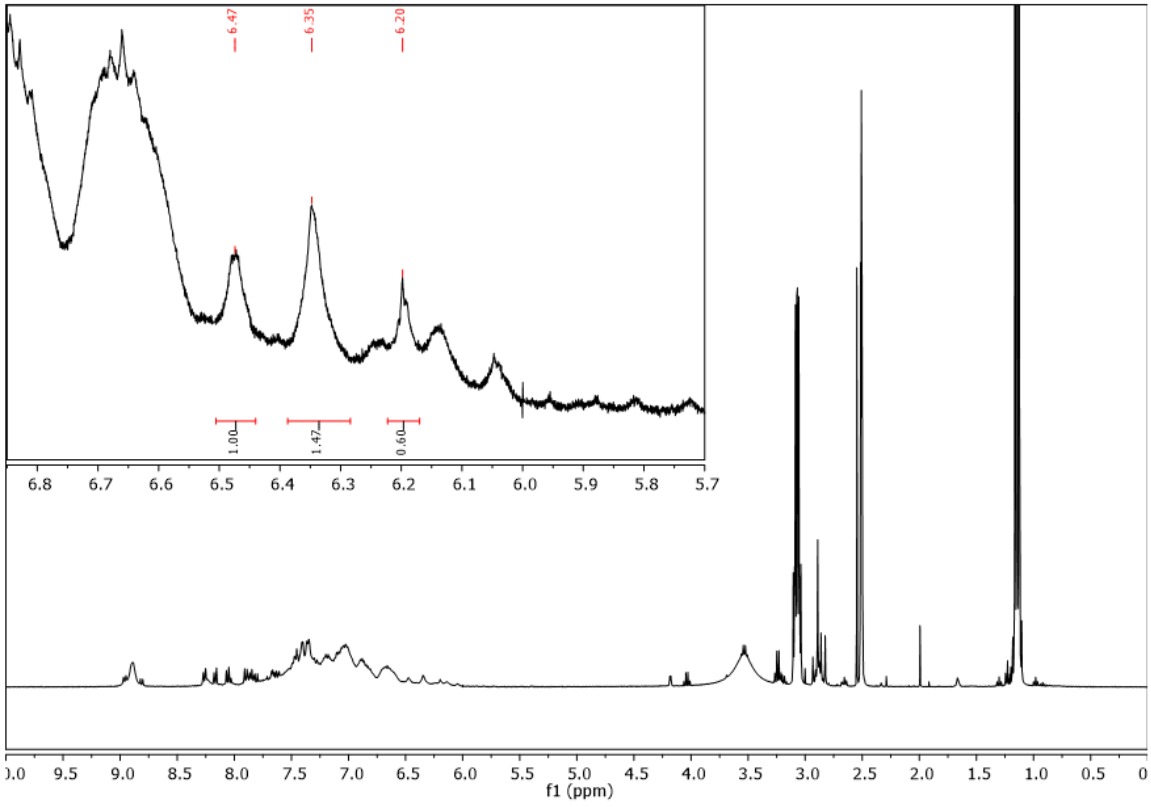

Figure 4.5: *Regiochemical analysis of* ***sPPBm-HNEt$_3^+$****; peaks at 6.47 ppm, 6.35 ppm and 6.20 ppm represent para-para, meta-meta and meta-para adducts respectively.*

sPPB*p*-HNEt$_3^+$							Overall Ratio	
para-para		*meta-meta*		*meta-para*			*meta*	*para*
6.47 ppm		6.32 ppm		6.15 ppm			**53%**	**47%**
Integration	%	Integration	%	Integration	%			
1.00	**30%**	1.21	**37%**	1.08	**33%**			

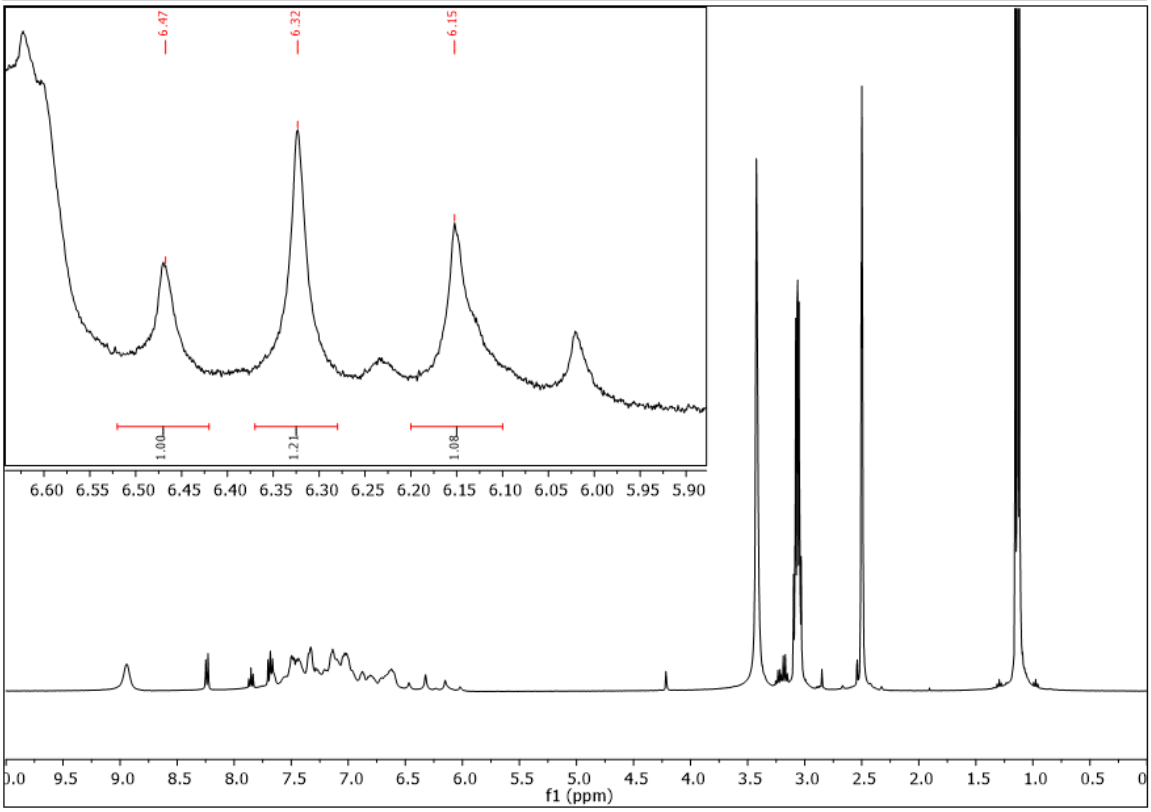

Figure 4.6: *Regiochemical analysis of* ***sPPBp-HNEt$_3^+$****; peaks at 6.47 ppm, 6.32 ppm and 6.15 ppm represent para-para, meta-meta and meta-para adducts respectively.*

4.3.3. Thermal Properties

Thermal stability of the three polymers **sPPB*o*-H$^+$** (M_n = 78,300 g mol^{-1}), **sPPB*m*-H$^+$** (M_n = 68,800 g mol^{-1}), and **sPPB*p*-H$^+$** (M_n = 82,500 g mol^{-1}) was examined using thermogravimetric analysis. All three polymers exhibited a four-step weight loss profile upon heating, as shown in Figure 4.7. The two initial weight loss events occurring under 100 °C and 180 °C can be attributed to evaporation of water and residual DMSO. It should be noted that because **sPPB*o*-H$^+$** did not form a substantial membrane, its drying was less efficient, and it hence contained a greater amount of residual DMSO than the other two polymers. At 220 °C and above, two distinct weight loss events were observed corresponding to thermal degradation of the polymer itself. Gradual thermolysis of the pendent -SO_3H moieties was found to occur between 220 °C and 450 °C. This weight loss corresponded to 27%, 27%, and 29% of the overall polymer mass for **sPPB*o*-H$^+$**, **sPPB*m*-H$^+$**, and **sPPB*p*-H$^+$**, respectively. This agreed well with the theoretical mass percent of sulfonic acid groups present – 28%. Beyond 450 °C there was a sharp decrease in sample mass attributed to total decomposition of the phenylated poly(phenylene) backbone, accounting for 73%, 73%, and 71% of the overall polymer mass for **sPPB*o*-H$^+$**, **sPPB*m*-H$^+$**, and **sPPB*p*-H$^+$**, respectively. The theoretical mass percent of the poly(phenylene) backbone with respect to the overall polymer is 72%. While the thermograms of the three polymers were similar, it appeared as though the **sPPB*o*-H$^+$** poly(phenylene) backbone had fully decomposed at a lower temperature than **sPPB*m*-H$^+$** and **sPPB*p*-H$^+$** (516 °C vs. 563 °C and 551 °C, respectively), suggesting instability of the polymer structure that may be due to steric strain. Collectively, the thermograms help confirm that the three polymers share a common chemical composition, as well as correct (expected) acid contents.

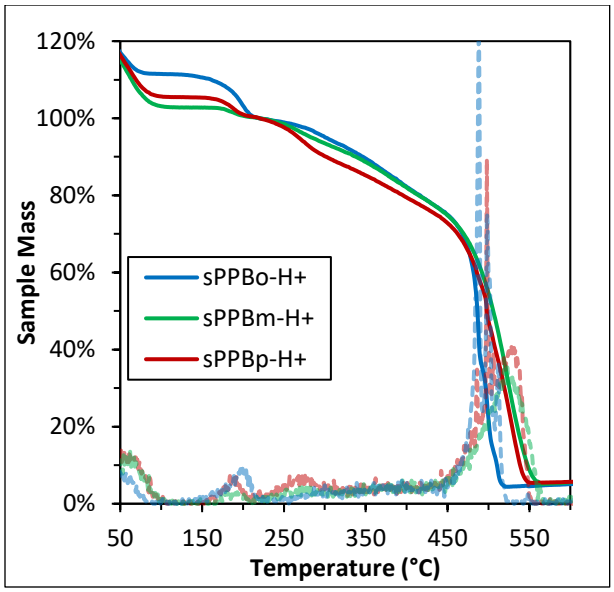

Figure 4.7: *Thermograms (solid curves) and thermogram derivatives (dashed curves) for* ***sPPBo-H+****,* ***sPPBm-H+****, and* ***sPPBp-H+*** *polymers normalized to respective sample massed measured at 220 °C.*

Differential scanning calorimetry was used to investigate the glass transition temperature (T_g) in the same three polymer systems **sPPB*o*-H⁺**, **sPPB*m*-H⁺**, and **sPPB*p*-H⁺**, and as a complimentary tool to TGA. The glass transition temperature is typically higher in polymers with stiff backbones and bulky side groups.[163],[164] Therefore, changes in polymer T_g may provide insight into the flexibility or rigidity of the polymer backbone due to altering the linearity of the incorporated biphenyl moiety.

Each DSC scan was run in duplicate to elucidate whether the endothermic events observed were glass transitions, or due to residual solvent evaporating and/or decomposition events taking place. DSC curves are shown in Figure 4.8. In each case, the dashed curves represent an initial pre-scan, and the solid curves represent a second scan immediately following. Scans 1 and 2 (red) were performed from room temperature to 200 °C and back, whereas scans 3 and 4 (blue) were performed from room temperature to 450 °C and back. For all polymer systems, endothermic transitions were observed in both pre-scans (dashed curves) upon heating, but were not observed upon cooling, suggesting an irreversible process had occurred. Immediately following the pre-scans, duplicate scans were performed (solid curves) in which no thermal events were observed. This again suggested that the endothermic transitions observed in the pre-scans were due

to irreversible processes. The endothermic events occurring in scan 1 were attributed to loss of residual H_2O and DMSO, while the endothermic events in scan 3 were attributed to thermolysis of the pendant -SO_3H moieties. These observations agreed well with the TGA findings, in which mass losses occurred within very similar temperature ranges (< 180 °C and 220-450 °C). The thermolysis of pendent -SO_3H moieties in **sPPB*m*-H$^+$** appeared to occur in two distinct events, while in **sPPB*o*-H$^+$** and **sPPB*p*-H$^+$**, only one peak was observed; it's not evidently clear why two peaks were observed in **sPPB*m*-H$^+$**, however.

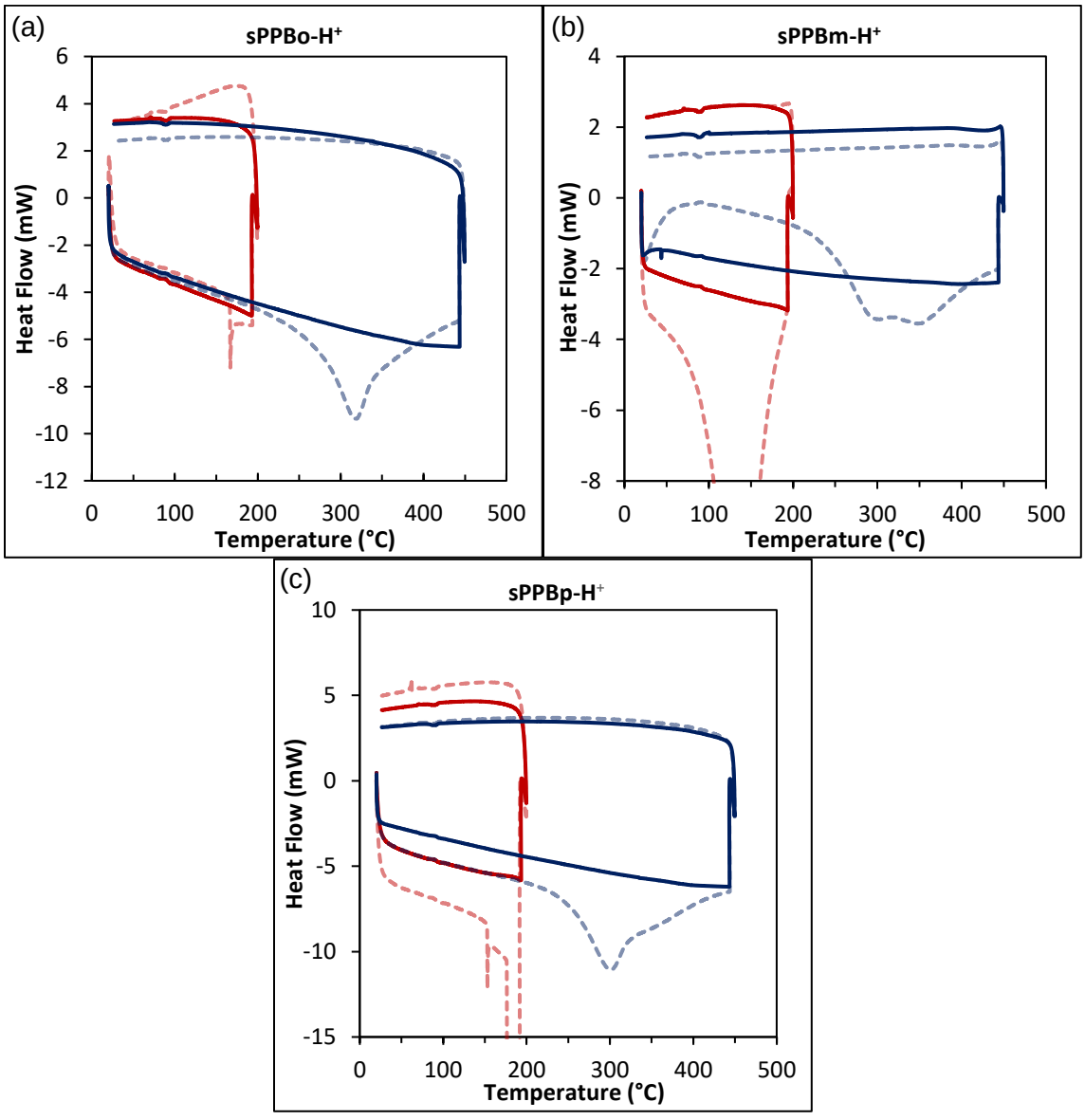

Figure 4.8: *DSC scans for (a) **sPPBo-H$^+$**, (b) **sPPBm-H$^+$**, and (c) **sPPBp-H$^+$**. Red curves are scan 1 and 2, blue curves are scan 3 and 4, dashed curves are pre-scans.*

4.3.4. Mechanical Properties

To further probe the polymers prepared, each was cast into a thin membrane. **sPPB*o*-H$^+$** was completely unable to form a robust membrane despite possessing high molecular weights, up to M_n = 240,000.[52],[77],[79] Upon removal from the glass casting plate, the cast **sPPB*o*-H$^+$** polymer fractured into small pieces. The brittleness of this polymer may be explained by the atropisomerism observed in the corresponding model compound, **MC-B*o***. This moiety, when integrated into a polymer backbone, may significantly hinder backbone rotation and overall mobility, and hence polymer chain entanglement, that is integral to formation of robust membranes.[72] Although **sPPB*m*-H$^+$** did form membranes that were readily handled without evidence of mechanical deterioration, samples began to show signs of damage when immersed in water beyond 150 h in samples possessing M_n < 154,700 g mol^{-1}. Again, the poor membrane integrity observed might be attributed to the inflexible polymer backbone. For this reason, a high molecular weight polymer (M_n = 655,600 g mol^{-1}) was used for subsequent membrane characterization, as it remained intact upon immersion in water. In contrast, **sPPB*p*-H$^+$** (M_n = 82,500) formed a durable membrane that remained intact following immersion in water.

Following membrane casting and drying, the mechanical properties of membranes **sPPB*m*-H$^+$** (M_n = 68,800 and 655,600 g mol^{-1}) and **sPPB*p*-H$^+$** (M_n = 82,500 g mol^{-1}) were assessed at ambient temperature and relative humidity. The *ortho* biphenyl-containing **sPPB*o*-H$^+$** was not measured because the polymer was not able to form a substantial membrane. The elongation at break, tensile strength and Young's modulus of the measured materials are given in Table 4.2

Table 4.2: *Mechanical Properties of **sPPBm-H$^+$** and **sPPBp-H$^+$** Measured Via Tensile Stress Test Under Ambient Conditions*

Polymer	M_n (g mol^{-1})	Elongation at Break (%)	Tensile Strength (MPa)	Young's Modulus (MPa)
sPPB*o*-H$^+$	-	-	-	-
sPPB*m*-H$^+$	68,800	4.7 ± 1.3	28.9 ± 5.4	857 ± 72
sPPB*m*-H$^+$	655,600	8.1 ± 0.9	29.2 ± 3.5	905 ± 84
sPPB*p*-H$^+$	82,500	16.8 ± 2.3	41.9 ± 2.1	1218 ± 94
Nafion NR-211	N/A	270 ± 4	20 ± 0.2	154 ± 28

The mechanical properties of **sPPB*m*-H$^+$** were assessed twice, using membranes possessing largely differing estimated number average molecular weights. The higher molecular weight polymer (M_n = 655,600 g mol^{-1}) possessed a number average molecular weight nearly 10 times higher than that of the lower molecular weight membrane (M_n = 68,800 g mol^{-1}). While the two **sPPB*m*-H$^+$** membranes were found to have comparable tensile strength and Young's moduli, the elongation at break was reduced by 42% in the lower molecular weight sample. **sPPB*m*-H$^+$** was found to exhibit a significantly lower elongation at break, tensile strength, and Young's modulus than **sPPB*p*-H$^+$**, by 52, 30 and 26% respectively, despite possessing a significantly higher molecular weight (M_n = 655,600 g mol^{-1} vs 82,500 g mol^{-1}). More significantly due to the similar molecular weights, **sPPB*m*-H$^+$** (M_n = 68,800 g mol^{-1}) possessed a 72, 31, and 30% reduced elongation at break, tensile strength, and Young's modulus, respectively, versus that of **sPPB*p*-H$^+$** (M_n = 82,500 g mol^{-1}).

The reduced mechanical properties may be due to the inherent inflexibility of the hindered, highly phenylated **sPPB*m*-H$^+$** polymer backbone. Many polymer properties are determined by backbone stiffness, and literature has shown that the incorporation of angled moieties into polymer backbones can reduce backbone stiffness and is desirable in forming tough, flexible membranes through enhanced chain entanglement.[101] However, this is under the assumption that the polymer backbone is able to rotate freely; if rotation is hindered, such as in the case of both **sPPB*o*-H$^+$** and **sPPB*m*-H$^+$**, the backbone will be even more rigid than the linear biphenyl containing analogue **sPPB*p*-H$^+$**, as shown schematically in Figure 4.9. It is also believed that chain entanglement is decreased in polymers containing bulky functional groups,[29] such as the highly phenylated systems presented herein. Consequently, one must consider the overall flexibility of the polymer backbone, as it is not always the case that the incorporation of non-linear moieties will increase flexibility.

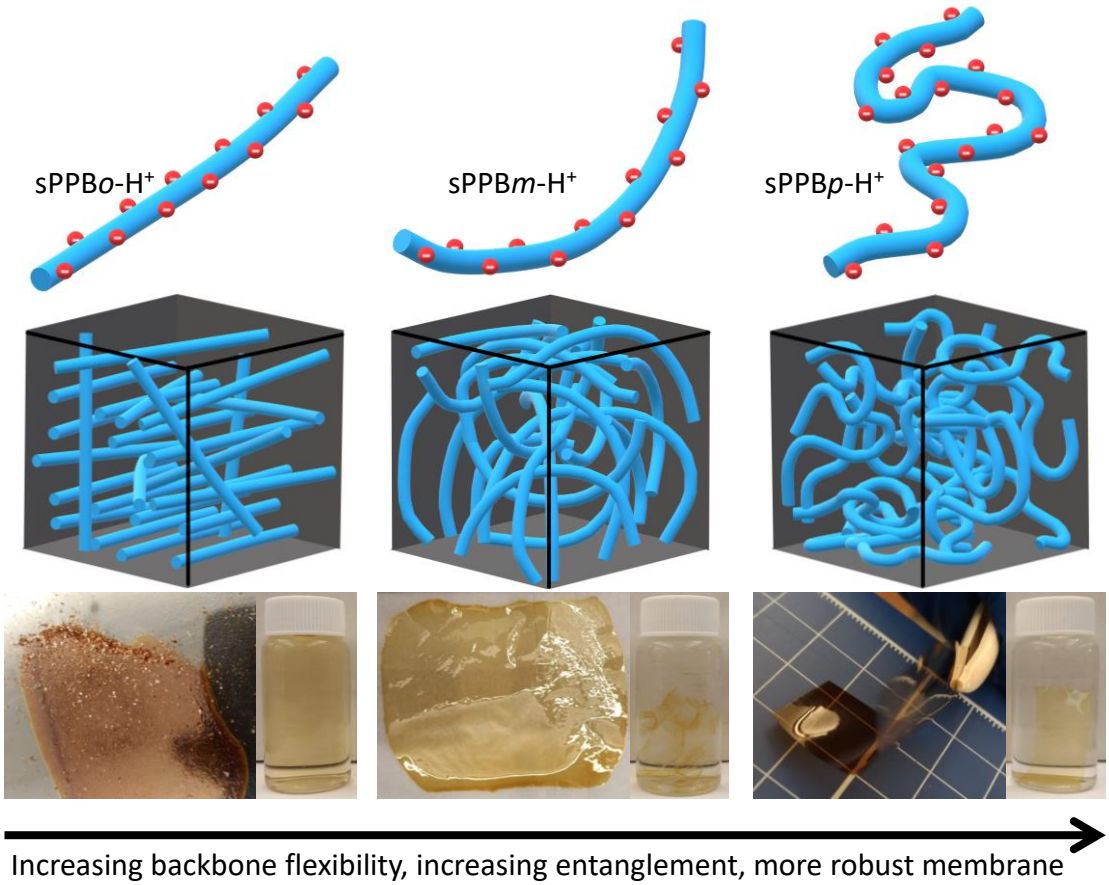

Figure 4.9: *Schematic illustration of backbone stiffness impacting molecular entanglement in* ***sPPBo-H+****,* ***sPPBm-H+****, and* ***sPPBp-H+****.*

4.3.5. Water Sorption, Ion Exchange Capacity and Proton Conductivity

Water sorption and ion exchange capacity are directly related to the spatial proximity between -SO_3H groups within a membrane, and hence the proton conductivity, through Equation 2.14,[72],[74] where σ_{H+} is the proton conductivity, F is Faraday's constant, [SO_3H] is the analytical acid concentration within a swollen membrane (Equation 2.15), and μ'_{H+} is the effective proton mobility. The effective proton mobility is derived from proton conductivity measurements, and incorporates terms relating to acid dissociation, tortuosity of the aqueous domains through the membrane, and the spatial proximity of neighboring acid groups.[72],[74] It can be seen then, that acid and water content have a strong influence on proton conductivity.

Table 4.3 lists the volumetric expansion (change in membrane volume) and water uptake (change in membrane weight) between fully dried and fully hydrated membranes, as well as the water content and hydration number in hydrated **sPPB*m*-H$^+$**, **sPPB*p*-H$^+$**, and Nafion® NR-211. There was an obvious and drastic increase in the water sorption characteristics of **sPPB*m*-H$^+$** (M_n = 655,600 g mol^{-1}) compared to **sPPB*p*-H$^+$** (M_n = 82,500 g mol^{-1}). It should be noted that water uptake measurements on lower molecular weight **sPPB*m*-H$^+$** were not possible due to the membrane fragmentation upon immersion in H_2O. Consequently, the water sorption characteristics of **sPPB*m*-H$^+$** are likely being underestimated, as longer polymer chains (higher molecular weight) would increase molecular entanglement and reduce swelling.[165]

The *meta* biphenyl-containing polymer **sPPB*m*-H$^+$** displayed a nearly two-fold increase in water uptake versus the *para* biphenyl-containing polymer **sPPB*p*-H$^+$** (257 vs. 130 wt%). This was corroborated by a measurable increase in volumetric expansion (259 vs. 149 vol%). Similarly, membrane water content increased by 30% in **sPPB*m*-H$^+$** compared to **sPPB*p*-H$^+$**. Overall, this equates to **sPPB*m*-H$^+$** possessing approximately twice the number of water molecules per sulfonic acid moiety (hydration number, λ) when compared to **sPPB*p*-H$^+$** in a fully hydrated state, with λ = 50 ± 4 vs. 24 ± 1 mol H_2O·mol^{-1} SO_3H, respectively. The differences observed in polymer water sorption further complement the notion that a sterically-hindered backbone incapable of unrestricted rotation, such as in **sPPB*o*-H$^+$** and potentially **sPPB*m*-H$^+$**, reduces polymer chain entanglement. In the context of acid-functionalized polymers, such as polymer electrolyte membranes, this results in weakened intermolecular forces and increased polymer-H_2O interactions when hydrated, yielding significant, disadvantageous increases to membrane swelling upon hydration.

Table 4.3: *Polymer Membrane Water Sorption Properties at Ambient Temperature: Volume Expansion (%), Water Uptake (%), Water Content (%), and Hydration Number (mol H_2O/mol -SO_3H)*

Polymer	M_n (g mol^{-1})	V_{exp} (%)	W_{up} (%)	W_{con} (%)	λ (mol H_2O/-SO_3H)
sPPB*o*-H$^+$	240,000	Dissolved	Dissolved	Dissolved	Dissolved
sPPB*m*-H$^+$	655,600	259 ± 8	257 ± 19	73 ± 2	50 ± 4
sPPB*p*-H$^+$	82,500	149 ± 10	130 ± 5	56 ± 1	24 ± 1
Nafion NR-211	N/A	33 ± 2[a]	20 ± 1[a]	17 ± 1[a]	12 ± 2[a,b]

[a] Data from Peron *et al*.[49] [b] Data from Luo *et al*.[166]

The analytical ion exchange capacity, measured by titration, has historically been marginally (~15%) lower than the theoretical ion exchange capacity in sPPPs, suggesting that some of the sulfonic acid moieties are not exchanging during the titration experiments.[52],[79],[81],[82] The measured ion exchange capacity, as well as the analytical acid concentration, proton conductivity at 30 and 80 °C (95% RH), and effective proton mobility at 30 and 80 °C (95% RH) of polymer membranes are listed in Table 4.4. **sPPB*o*-H$^+$** is excluded from the data because it was water soluble, and hence the measurements were not possible. The ion exchange capacity of **sPPB*m*-H$^+$** (M_n = 655,600 g mol^{-1}) was found to be slightly lower than that of **sPPB*p*-H$^+$** (M_n = 82,500 g mol^{-1}) outside of experimental error. In both cases, the theoretical IEC was 3.46 meq g^{-1}. A significant difference in the analytical acid concentration was observed between the two membranes. This was due to the higher swelling in **sPPB*m*-H$^+$** compared to **sPPB*p*-H$^+$**, that effectively caused dilution of the acid moieties present in the former.

Table 4.4: *Polymer Membrane Water Sorption, Acid Content, and Electrochemical Properties: IEC_{exp}, $[SO_3H]$, Proton Conductivity at 95% RH, and Proton Mobility at 95% RH*

Polymer	IEC_{exp} (meq. g^{-1})	$[SO_3H]$ (mmol cm^{-3})	σ_{H+} (30 °C, 95% RH) (mS cm^{-1})	σ_{H+} (80 °C, 95% RH) (mS cm^{-1})	μ'_{H+} (30 °C, 95% RH) (10^{-3} cm^2 V^{-1} s^{-1})	μ'_{H+} (80 °C, 95% RH) (10^{-3} cm^2 V^{-1} s^{-1})
sPPB*o*-H$^+$	-	-	-	-	-	-
sPPB*m*-H$^+$	2.87 ± 0.08	0.81 ± 0.04	136 ± 6	273 ± 19	1.74 ± 0.12	3.49 ± 0.30
sPPB*p*-H$^+$	3.03 ± 0.06	1.42 ± 0.04	169 ± 14	263 ± 35	1.23 ± 0.11	1.92 ± 0.26

The proton conductivity, measured over a range of relative humidity values at both 30 and 80 °C for **sPPB*m*-H$^+$** (M_n = 655,600 g mol^{-1}), **sPPB*p*-H$^+$** (M_n = 82,500 g mol^{-1}), and Nafion® NR-211 as a reference, is shown in Figure 4.10. At 30 °C, **sPPB*p*-H$^+$** exhibited the highest proton conductivity with a maximum proton conductivity value of 169 ± 14 mS cm^{-1} (95% RH). **sPPB*m*-H$^+$** exhibited lower proton conductivity values over the entire relative humidity range. This is likely due to reduced acid concentration measured in **sPPB*m*-H$^+$**, which is a considerable predictor of proton conductivity,[72] as per Equation 2.14. Both membranes possessed higher proton conductivity values than Nafion® NR-211 over the entire range of relative humidity values. At 80 °C, there were insignificant differences between the proton conductivity measured for **sPPB*m*-H$^+$** and **sPPB*p*-H$^+$**.

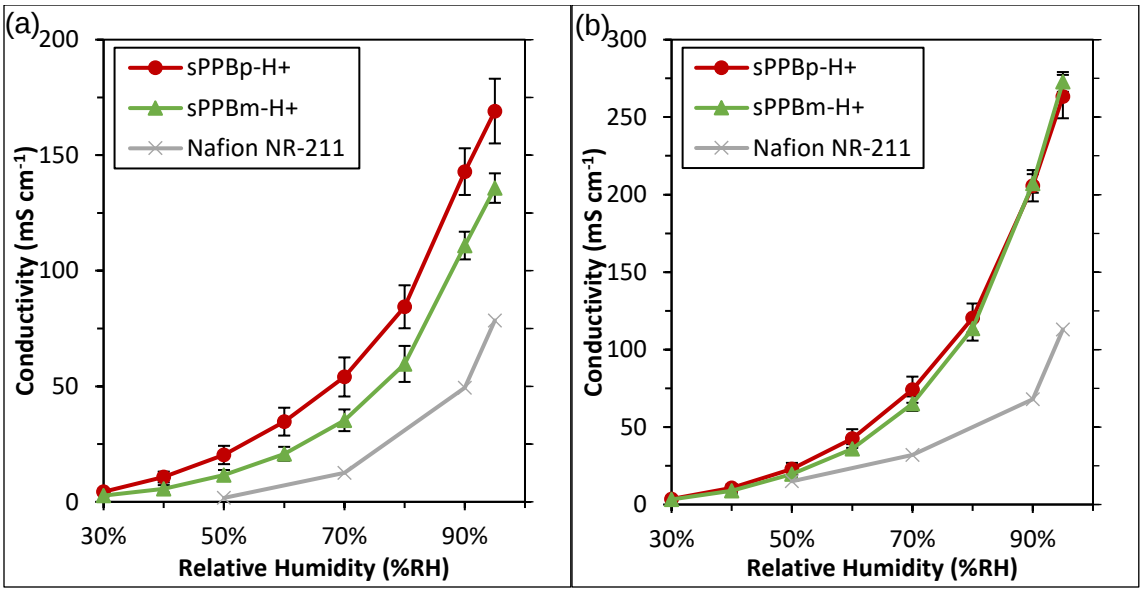

Figure 4.10: *Proton conductivity of **sPPBp-H⁺**, **sPPBm-H⁺**, and Nafion NR-211 as a function of relative humidity at (a) 30 °C, and (b) 80 °C.*

4.4. Conclusions

Polymers **sPPB*o*-H⁺**, **sPPB*m*-H⁺**, and **sPPB*p*-H⁺** were synthesized in good yield possessing number average molecular weights between 68,800 and 655,600 g mol^{-1}. TGA and DSC measurements revealed the three polymers shared similar thermal degradation profiles through thermolysis of pendent sulfonic acid moieties (approx. 28% by mass) followed by thermolysis of the polymer backbone, and that no polymer possessed a glass transition temperature below 450 °C. **sPPB*o*-H⁺** was unable to form membranes (M_n < 240,000 g mol^{-1}) and was water soluble, whereas **sPPB*m*-H⁺** formed membranes with poor mechanical integrity below a M_n threshold (154,700 g mol^{-1}). In contrast, **sPPB*p*-H⁺** was robust and completely insoluble at modest M_n (82,500 g mol^{-1}). The poor membrane forming capability of the former two polymers was attributed to the rotationally hindered backbones in **sPPB*m*-H⁺**, and especially in **sPPB*o*-H⁺**, that would promote rigid macroscopic structures lacking appreciable chain entanglement.

Physical and electrochemical properties of the membranes prepared from the polymers **sPPB*m*-H⁺** and **sPPB*p*-H⁺** were evaluated to further elucidate the impact of the non-linear biphenyl moieties. Despite possessing a significantly higher molecular weight,

sPPB*m*-H$^+$ displayed a 74% increase in volumetric expansion, 30% reduction in tensile strength, 52% reduction in the elongation at break, and 26% reduction in Young's moduli when compared to **sPPB*p*-H$^+$**. Electrochemically, **sPPB*m*-H$^+$** was found to have lower proton conductivity at 30 °C, and similar proton conductivity at 80 °C versus **sPPB*p*-H$^+$**. The lower conductivity values were attributed to excessive membrane swelling, that resulted in reduction of acid concentration within the membrane. Therefore, in the case of sulfonated phenylated poly(phenylene)s, a more rigid polymer backbone appears to have a detrimental impact on membrane mechanical strength and water sorption characteristics. These properties, in-turn, appear to impact electrochemical properties as well. The results presented herein cumulatively stress the importance of polymer backbone flexibility and macroscopic chain entanglement in advanced functional polymeric materials, such as selective ion-conducting membranes. While angled moieties appear to provide enhanced backbone flexibility in other polymeric systems,[29],[72],[100],[101],[102] they were found to produce sterically-encumbered, rotationally restricted systems when incorporated into sulfonated phenylated poly(phenylenes)s due to their highly phenylated structure. These rotationally restricted polymers resulted in membranes with poor physical and electrochemical properties, or were unable to form membranes at all, likely due to the lack of macroscopic chain entanglement caused therefrom.

Chapter 5.

Angled and Linear Sulfonated Phenylated Poly(phenylene) Co-polymers

My contributions included the entirety of the synthesis, characterization, and testing of membrane properties.

This work was financially supported by the Natural Sciences and Engineering Research Council of Canada (NSERC), DuPont, and the British Columbia Automobile Association (BCAA).

5.1. Introduction

In chapter 4, it was described that the introduction of non-linear *ortho* and *meta* functionalized biphenyl moieties into sulfonated phenylated poly(phenylene)s had a negative impact on the membrane forming capabilities, mechanical strength, and water sorption characteristics. The effect was so pronounced, that **sPPB*o*-H$^+$** was completely unable to form a membrane even at appreciable molecular weights. I argued that incorporation of non-linear biphenyl moieties caused sterically-encumbered, rotationally restricted systems when incorporated into sulfonated phenylated poly(phenylenes)s due to their highly phenylated structure. Due to this, assessment of **sPPB*o*-H$^+$** membrane was not possible, limiting the scope of this study.

To overcome this problem, a series of co-polymers possessing various small amounts of either *ortho*, or *meta* biphenyl in an otherwise *para* biphenyl containing system were prepared. In this way, the impact of progressively increasing the non-linear biphenyl content could be assessed. In total, six co-polymers were prepared; three *ortho*/*para* biphenyl containing polymers **sPPB*po*H$^+$-x%**, and three *meta*/*para* biphenyl containing polymers **sPPB*pm*H$^+$-x%**, where **x** is the percent of *ortho* or *meta* biphenyl incorporation with respect to the overall amount of biphenyl. For example, **sPPB*po*H$^+$-5%** contained 5% *ortho* biphenyl, and 95% *para* biphenyl, as shown in Scheme 5.1. In the case where **x** = 0, the polymer **sPPB*p*-H$^+$**, which is the same as the homo-polymer discussed in Chapter 4, contains only *para* biphenyl.

From these polymers, membranes were cast and various physico-electrochemical properties were assessed as in Chapter 4. Mechanical properties of membranes were assessed via tensile stress tests. Water sorption properties were assessed via mass and dimensional analysis of membranes in their dry and hydrated states. Acid content was assessed via acid-base titrations, and proton conductivity was assessed via electrochemical impedance spectroscopy (EIS). All of these techniques and the accompanying parameters used are described in detail in Chapter 2.

Scheme 5.1: *Structures of* ***sPPBpo-H$^+$*** *and* ***sPPBpm-H$^+$***

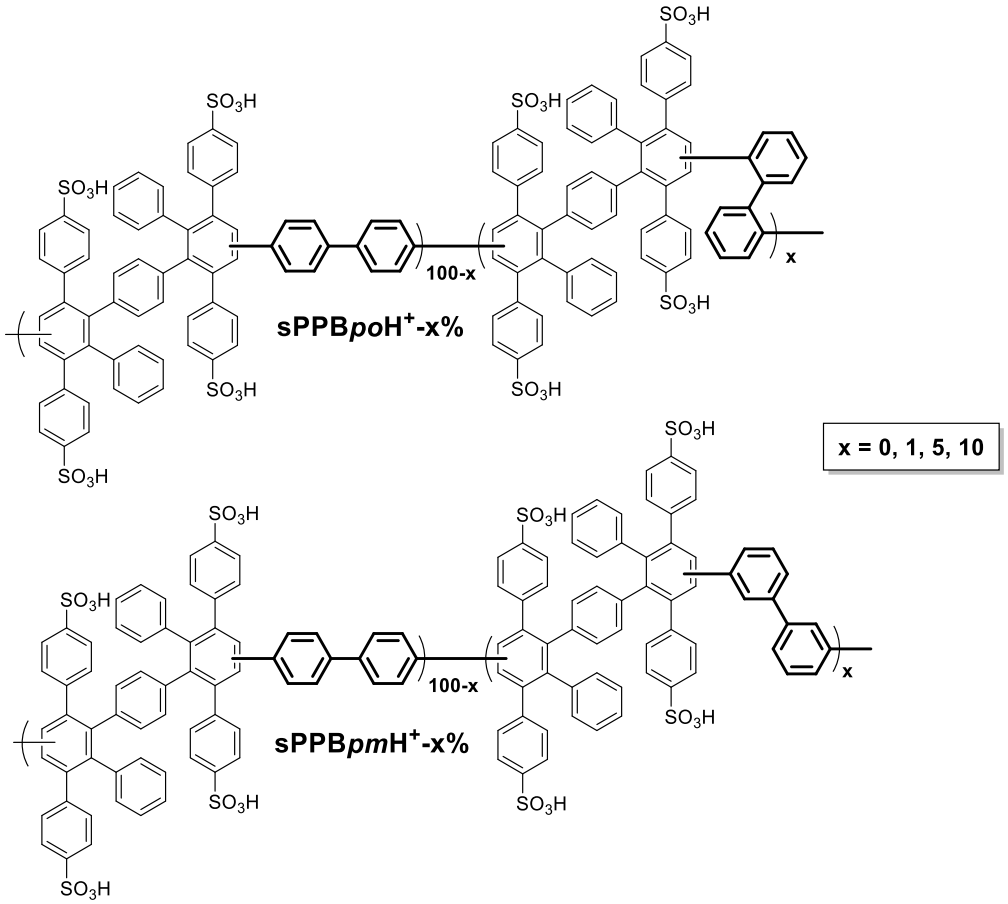

5.2. Experimental

5.2.1. Materials

The materials used in this chapter were the same as those outlined in Chapter 3.

5.2.2. Synthesis

Sulfonated Poly(phenylene) *para*-Biphenyl Triethylammonium Salt (sPPB*p*-HNEt3$^+$)

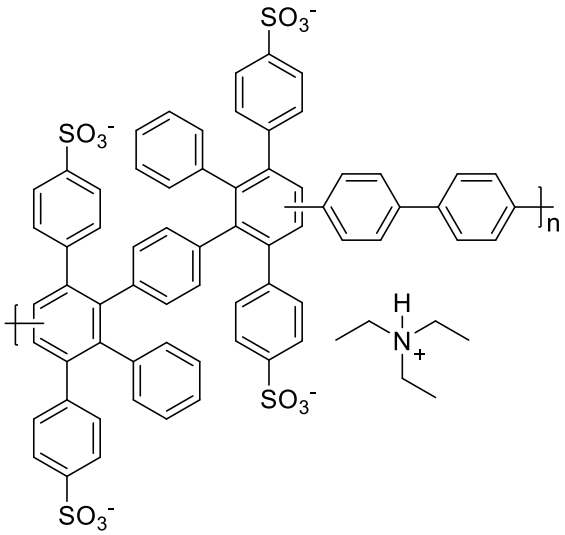

To a clean and dry 150 mL pressure vessel degassed with argon and equipped with a stir bar was added 4,4'-diethynyl-1,1'-biphenyl (0.290 g, 1.43 mmol, 1.015 eq.), tetra(*para*-sulfonated) bistetracyclone triethylammonium salt (2.000 g, 1.413 mmol, 1.00 eq.), and degassed nitrobenzene (40 mL) and the mixture was stirred under argon flow for 1 h. The pressure vessel was sealed with a Teflon lid and the mixture was heated to 170 °C for 96 h under high stirring. The nitrobenzene was decanted from the polymer film inside the flask, to which was added DMSO (50 mL) and the mixture was stirred at 80 °C for 16 h. The resulting solution was poured into ethyl acetate (600 mL) under stirring, let stir for 1 h, and the brown precipitate was filtered and washed with ethyl acetate. Drying *in vacuo* at 80 °C for 16 h afforded the product as a light brown solid (1.882 g, 85% yield). ^{1}H NMR (400 MHz, DMSO-d_6) δ 8.89 (s, 4H), 8.20 – 5.92 (m, 40H), 3.05 (q (two overlapped), J = 7.3 Hz, 24H), 1.12 (t, J = 7.3 Hz, 36H).

Sulfonated Poly(phenylene) *para*-Biphenyl (sPPB*p*-H^+)

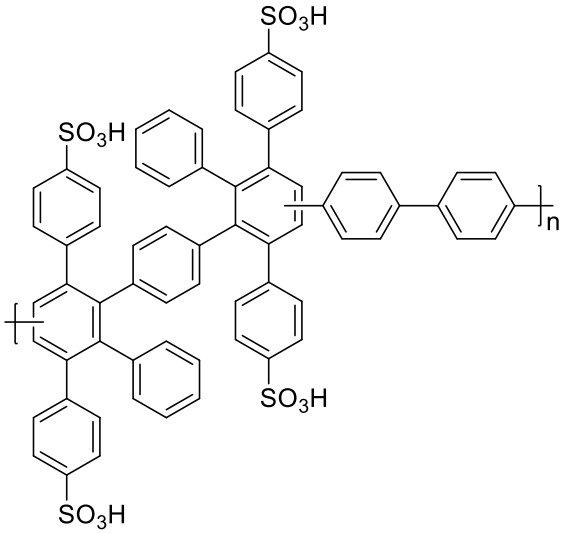

To a 500 mL round bottom flask equipped with a stir bar was added sPPB*p*-$HNEt_3^+$ (1.813 g) and methanol (93 mL) and the mixture was stirred to complete dissolution. A methanolic solution of sodium hydroxide (30 mL, 2M NaOH in methanol) was added dropwise to the mixture under high stirring, and the mixture was stirred at room temperature for 16 h. The solvents were removed *in vacuo* until the mixture resembled a thick paste, after which approx. deionized H_2O (150 mL) was added to the flask and the solvents were immediately removed *in vacuo* until the mixture was a thick paste. Deionized H_2O (150 mL) was added and removed *in vacuo* once more. To the flask was added HCl (1M, approx. 150mL) until the pH of the mixture was 0 and the mixture was stirred for 16 h. The polymer was filtered, washed with HCl (1M) and deionized H_2O and dried *in vacuo* at 80 °C for 16 h before collecting the product as a light brown solid (1.273 g, 95% yield). ^{1}H NMR (400 MHz, DMSO-d_6) δ (ppm): 8.20 – 5.92 (m, 40H), 4.06 (s, H_2O/H_3O^+). GPC analysis: M_n = 82,500 g mol^{-1}, M_w = 164,300 g mol^{-1}, Đ = 1.99.

Sulfonated Poly(phenylene) *para-ortho*-1%-Biphenyl Triethylammonium Salt (sPPB*po*$HNEt_3^+$-1%)

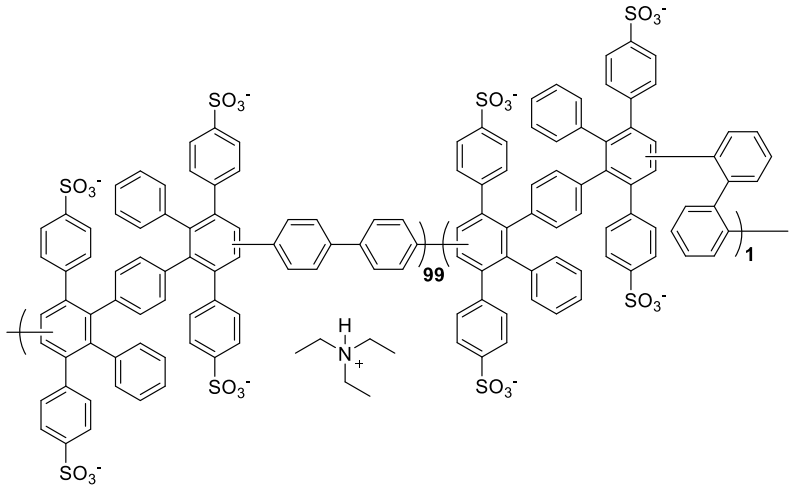

To a clean and dry 150 mL pressure vessel degassed with argon and equipped with a stir bar was added 2,2'-diethynyl-1,1'-biphenyl (0.0030 g, 0.015 mmol, 0.010 eq.), 4,4'-diethynyl-1,1'-biphenyl (0.287 g, 1.42 mmol, 1.004 eq.),

tetra(*para*-sulfonated) bistetracyclone triethylammonium salt (2.001 g, 1.413 mmol, 1.000 eq.), and degassed nitrobenzene (40 mL) and the mixture was stirred under argon flow for 1 h. The pressure vessel was sealed with a Teflon lid and the mixture was heated to 170 °C for 96 h under high stirring. The nitrobenzene was decanted from the polymer film inside the flask, to which was added DMSO (50 mL) and the mixture was stirred at 80 °C for 16 h. The resulting solution was poured into ethyl acetate (600 mL) under stirring, let stir for 1 h, and the brown precipitate was filtered and washed with ethyl acetate. Drying *in vacuo* at 80 °C for 16 h afforded the product as a light brown solid (1.929 g, 87% yield). ^{1}H NMR (400 MHz, DMSO-d_6) δ 8.90 (s, 4H), 8.03 – 5.95 (m, 40H), 3.05 (q (two overlapped), J = 7.3 Hz, 24H), 1.12 (t, J = 7.3 Hz, 36H).

Sulfonated Poly(phenylene) *para-ortho*-1%-Biphenyl (sPPB*po*H$^+$-1%)

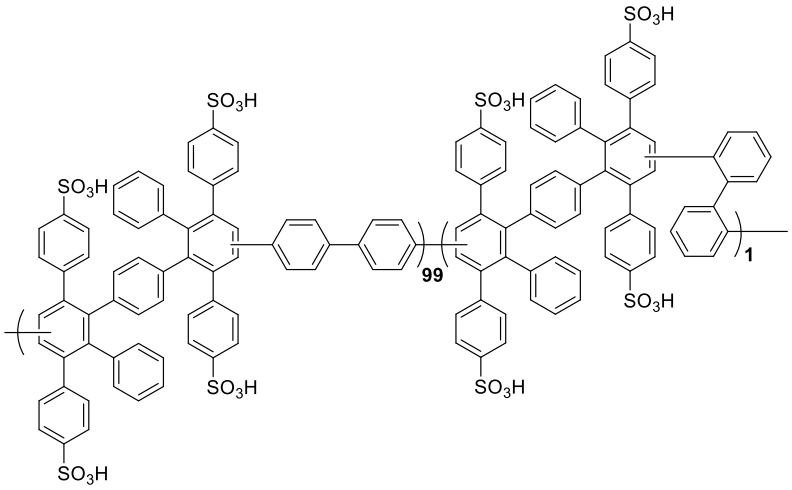

To a 500 mL round bottom flask equipped with a stir bar was added sPPB*po*HNEt$_3^+$-1% (1.876 g) and methanol (96 mL) and the mixture was stirred to complete dissolution. A methanolic solution of sodium hydroxide (31 mL, 2M NaOH in methanol) was added dropwise to the mixture under high stirring, and the mixture was stirred at room temperature for 16 h. The solvents were removed *in vacuo* until the mixture resembled a thick paste, after which ca. deionized H_2O (150 mL) was added to the flask and the solvents were immediately removed *in vacuo* until the mixture was a thick paste. Deionized H_2O (150 mL) was added and removed *in vacuo* once more. To the flask was added HCl (1M, ca. 150mL) until the pH of the mixture was 0 and the mixture was stirred for 16 h. The polymer was filtered, washed with HCl (1M) and deionized H_2O and dried *in vacuo* at 80 °C for 16 h before collecting the product as a light brown solid (1.296 g, 93% yield). ^{1}H NMR (400 MHz, DMSO-d_6) δ 8.03 – 5.95 (m, 40H), 3.90 (s, H_2O/H_3O^+). GPC analysis: M_n = 94,210 g mol^{-1}, M_w = 134,100 g mol^{-1}, Đ = 1.42.

Sulfonated Poly(phenylene) *para-ortho*-5%-Biphenyl Triethylammonium Salt (sPPB*po*HNEt$_3^+$-5%)

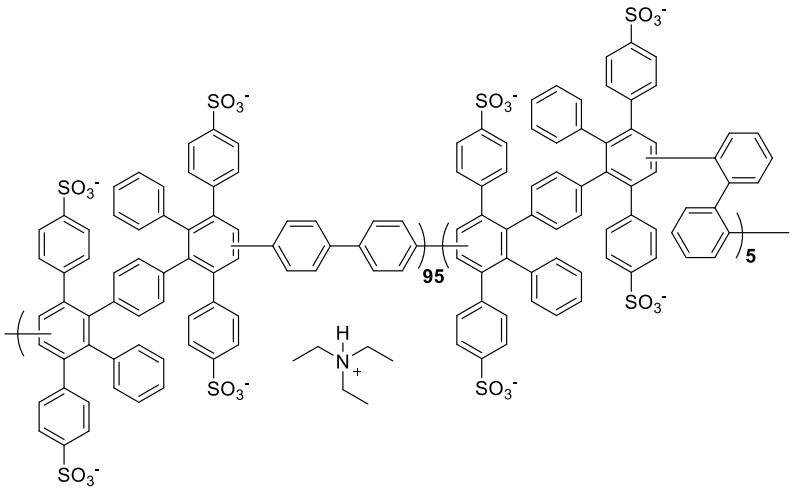

To a clean and dry 150 mL pressure vessel degassed with argon and equipped with a stir bar was added 2,2'-diethynyl-1,1'-biphenyl (0.015 g, 0.072 mmol, 0.051 eq.), 4,4'-diethynyl-1,1'-biphenyl (0.276 g, 1.36 mmol, 0.965 eq.), tetra(*para*-sulfonated) bistetracyclone triethylammonium salt (2.000 g, 1.413 mmol, 1.000 eq.), and degassed nitrobenzene (40 mL) and the mixture was stirred under argon flow for 1 h. The pressure vessel was sealed with a Teflon lid and the mixture was heated to 180 °C for 72 h under high stirring. The nitrobenzene was decanted from the polymer film inside the flask, to which was added DMSO (50 mL) and the mixture was stirred at 80 °C for 16 h. The resulting solution was poured into ethyl acetate (600 mL) under stirring, let stir for 1 h, and the brown precipitate was filtered and washed with ethyl acetate. Drying *in vacuo* at 80 °C for 16 h afforded the product as a light brown solid (1.898 g, 86% yield). ^{1}H NMR (400 MHz, DMSO-d_6) δ 8.90 (s, 4H), 7.77 – 5.95 (m, 40H), 3.05 (q (two overlapped), J = 7.3 Hz, 24H), 1.12 (t, J = 7.3 Hz, 36H).

Sulfonated Poly(phenylene) *para-ortho*-5%-Biphenyl (sPPB*po*H$^+$-5%)

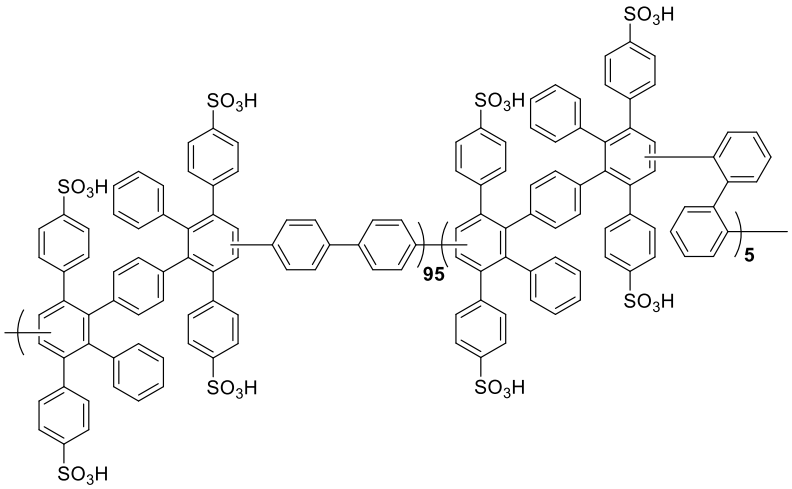

To a 500 mL round bottom flask equipped with a stir bar was added sPPB*po*HNEt$_3^+$-5% (1.835 g) and methanol (94 mL) and the mixture was stirred to complete dissolution. A methanolic solution of sodium hydroxide (31 mL, 2M NaOH in methanol) was added dropwise to the mixture under high stirring, and the mixture was stirred at room temperature for 16 h. The solvents were removed *in vacuo* until the mixture resembled a thick paste, after which ca. deionized H_2O (150 mL) was added to the flask and the solvents were immediately removed *in vacuo* until the mixture was a thick paste. Deionized H_2O (150 mL) was added and removed *in vacuo* once more. To the flask was added HCl (1M, ca. 150mL) until the pH of the mixture was 0 and the mixture was stirred for 16 h. The polymer was filtered, washed with HCl (1M) and deionized H_2O and dried *in vacuo* at 80 °C for 16 h before collecting the product as a light brown solid (1.292 g, 95% yield). ^{1}H NMR (400 MHz, DMSO-d_6) δ 7.77 – 5.95 (m, 40H), 3.91 (s, H_2O/H_3O^+). GPC analysis: M_n = 102,400 g mol^{-1}, M_w = 183,200 g mol^{-1}, Đ = 1.79.

Sulfonated Poly(phenylene) *para-ortho*-10%-Biphenyl Triethylammonium Salt (sPPB*po*HNEt$_3^+$-10%)

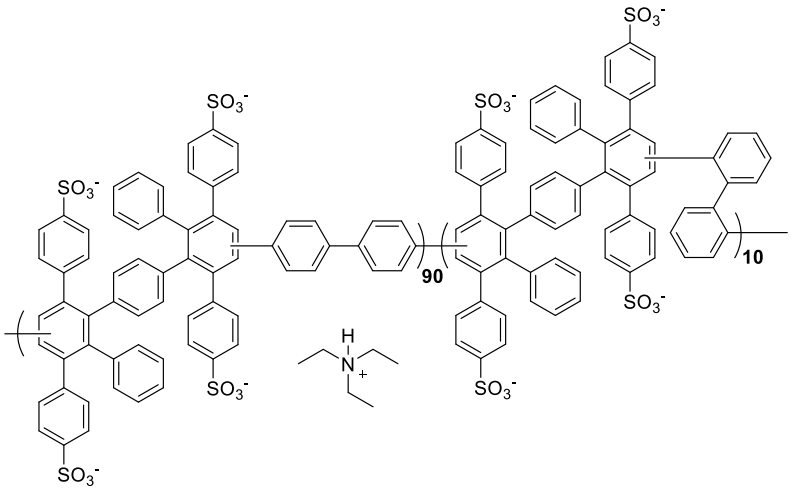

To a clean and dry 150 mL pressure vessel degassed with argon and equipped with a stir bar was added 2,2'-diethynyl-1,1'-biphenyl (0.029 g, 0.14 mmol, 0.102eq.), 4,4'-diethynyl-1,1'-biphenyl (0.261 g, 1.29

mmol, 0.914 eq.), tetra(*para*-sulfonated) bistetracyclone triethylammonium salt (2.000 g, 1.413 mmol, 1.000 eq.), and degassed nitrobenzene (40 mL) and the mixture was stirred under argon flow for 1 h. The pressure vessel was sealed with a Teflon lid and the mixture was heated to 180 °C for 72 h under high stirring. The nitrobenzene was decanted from the polymer film inside the flask, to which was added DMSO (50 mL) and the mixture was stirred at 80 °C for 16 h. The resulting solution was poured into ethyl acetate (600 mL) under stirring, let stir for 1 h, and the brown precipitate was filtered and washed with ethyl acetate. Drying *in vacuo* at 80 °C for 16 h afforded the product as a light brown solid (2.021 g, 92% yield). ^{1}H NMR (400 MHz, DMSO-d_6) δ 8.90 (s, 4H), 8.04 – 5.90 (m, 40H), 3.05 (m, 24H), 1.12 (t, J = 7.3 Hz, 36H).

Sulfonated Poly(phenylene) *para-ortho*-10%-Biphenyl (sPPB*po*H$^+$-10%)

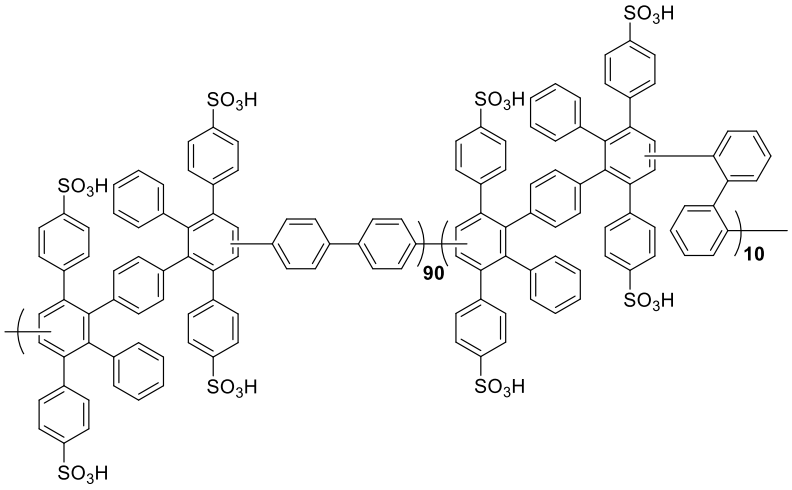

To a 500 mL round bottom flask equipped with a stir bar was added sPPB*po*HNEt$_3^+$-10% (1.971 g) and methanol (101 mL) and the mixture was stirred to complete dissolution. A methanolic solution of sodium hydroxide (33 mL, 2M NaOH in methanol) was added dropwise to the mixture under high stirring, and the mixture was stirred at room temperature for 16 h. The solvents were removed *in vacuo* until the mixture resembled a thick paste, after which ca. deionized H_2O (150 mL) was added to the flask and the solvents were immediately removed *in vacuo* until the mixture was a thick paste. Deionized H_2O (150 mL) was added and removed *in vacuo* once more. To the flask was added HCl (1M, ca. 150mL) until the pH of the mixture was 0 and the mixture was stirred for 16 h. The polymer was filtered, washed with HCl (1M) and deionized H_2O and dried *in vacuo* at 80 °C for 16 h before collecting the product as a light brown solid (1.325 g, 91% yield). ^{1}H NMR (400 MHz, DMSO-d_6) δ 8.04 – 5.90 (m, 40H), 3.97 (s, H_2O/H_3O^+). GPC analysis: M_n = 109,900 g mol^{-1}, M_w = 146,000 g mol^{-1}, Đ = 1.33.

Sulfonated Poly(phenylene) *para-ortho*-50%-Biphenyl Triethylammonium Salt (sPPB*po*HNEt$_3^+$-50%)

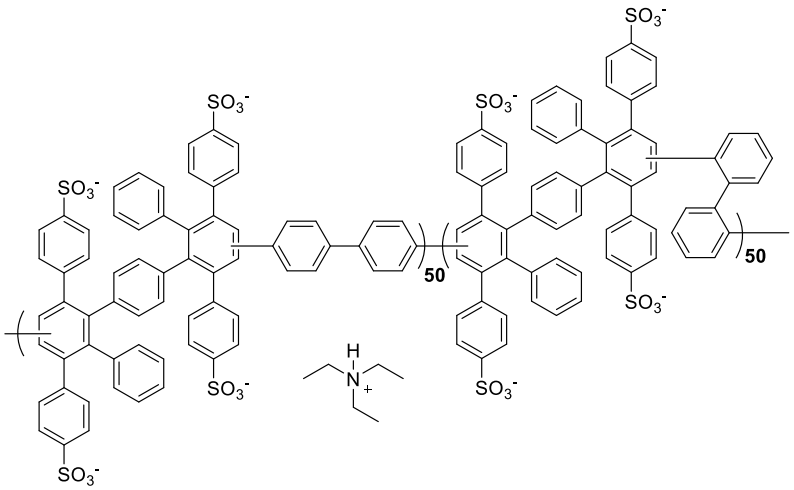

To a clean and dry 150 mL pressure vessel degassed with argon and equipped with a stir bar was added 2,2'-diethynyl-1,1'-biphenyl (0.145 g, 0.717 mmol, 0.508 eq.), 4,4'-diethynyl-1,1'-biphenyl (0.145 g, 0.717 mmol, 0.508 eq.), tetra(*para*-sulfonated) bistetracyclone triethylammonium salt (2.000 g, 1.413 mmol, 1.000 eq.), and degassed nitrobenzene (40 mL) and the mixture was stirred under argon flow for 1 h. The pressure vessel was sealed with a Teflon lid and the mixture was heated to 180 °C for 72 h under high stirring. The nitrobenzene was decanted from the polymer film inside the flask, to which was added DMSO (40 mL) and the mixture was stirred at 80 °C for 16 h, then at 120 °C for 30 min. The resulting solution was poured into ethyl acetate (600 mL) under stirring, let stir for 1 h, and the brown precipitate was filtered and washed with ethyl acetate. Drying *in vacuo* at 80 °C for 16 h afforded the product as a light brown solid (2.038 g, 92% yield). ^{1}H NMR (400 MHz, DMSO-d_6) δ 8.90 (s, 4H), 8.05 – 5.90 (m, 40H), 3.04 (q (two overlapped), J = 6.9 Hz, 24H), 1.11 (t, J = 7.2 Hz, 36H). GPC analysis: M_n = 261,900 g mol^{-1}, M_w = 494,700 g mol^{-1}, Đ = 1.89

Sulfonated Poly(phenylene) *para-ortho*-50%-Biphenyl (sPPB*po*H$^+$-50%)

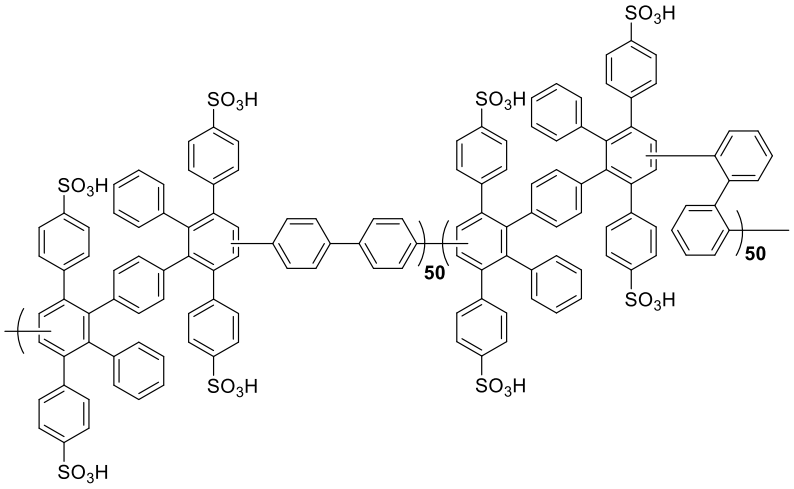

To a 500 mL round bottom flask equipped with a stir bar was added sPPB*po*HNEt$_3^+$-50% (1.986 g) and methanol (102 mL) and the mixture was stirred to complete dissolution. A methanolic solution of sodium hydroxide (33 mL, 2M NaOH in methanol) was added dropwise to the mixture under high stirring, and the mixture was stirred at room temperature for 16 h. The solvents were removed *in vacuo* until the mixture resembled a thick paste, after which ca. deionized H_2O (150 mL) was added to the flask and the solvents were immediately removed *in vacuo* until the mixture was a thick paste. Deionized H_2O (150 mL) was added and removed *in vacuo* once more. To the flask was added HCl (1M, ca. 150mL) until the pH of the mixture was 0 and the mixture was stirred for 16 h. The polymer was filtered, washed with HCl (1M) and deionized H_2O and dried *in vacuo* at 80 °C for 16 h before collecting the product as a light brown solid (1.354 g, 92% yield). ^{1}H NMR (400 MHz, DMSO-d_6) δ 8.05 – 5.90 (m, 40H), 3.77 (s, H_2O/H_3O^+). GPC analysis: M_n = 149,900 g mol^{-1}, M_w = 234,800 g mol^{-1}, Đ = 1.57.

Sulfonated Poly(phenylene) *para-meta*-1%-Biphenyl Triethylammonium Salt (sPPB*pm*HNEt$_3^+$-1%)

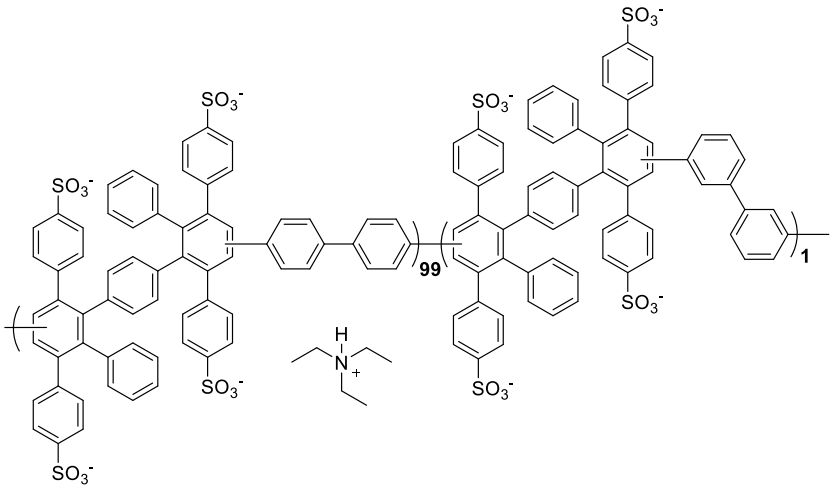

To a clean and dry 150 mL pressure vessel degassed with argon and equipped with a stir bar was added 3,3'-diethynyl-1,1'-biphenyl (0.0030 g, 0.015 mmol, 0.010 eq.), 4,4'-diethynyl-

1,1'-biphenyl (0.287 g, 1.42 mmol, 1.005 eq.), tetra(*para*-sulfonated) bistetracyclone triethylammonium salt (2.000 g, 1.413 mmol, 1.000 eq.), and degassed nitrobenzene (40 mL) and the mixture was stirred under argon flow for 1 h. The pressure vessel was sealed with a Teflon lid and the mixture was heated to 170 °C for 96 h under high stirring. The nitrobenzene was decanted from the polymer film inside the flask, to which was added DMSO (50 mL) and the mixture was stirred at 80 °C for 16 h. The resulting solution was poured into ethyl acetate (600 mL) under stirring, let stir for 1 h, and the brown precipitate was filtered and washed with ethyl acetate. Drying *in vacuo* at 80 °C for 16 h afforded the product as a light brown solid (1.762 g, 80% yield). ^{1}H NMR (400 MHz, DMSO-d_6) δ 8.90 (s, 4H), 7.86 – 5.93 (m, 40H), 3.05 (q (two overlapped), J = 7.3 Hz, 24H), 1.12 (t, J = 7.3 Hz, 36H).

Sulfonated Poly(phenylene) *para-meta*-1%-Biphenyl (sPPB*pm*H$^+$-1%)

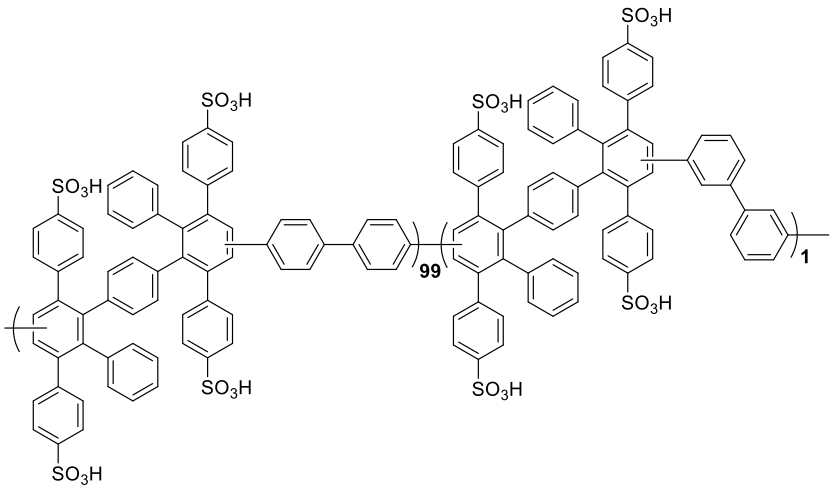

To a 500 mL round bottom flask equipped with a stir bar was added sPPB*pm*HNEt$_3^+$-1% (1.703 g) and methanol (90 mL) and the mixture was stirred to complete dissolution. A methanolic solution of sodium hydroxide (30 mL, 2M NaOH in methanol) was added dropwise to the mixture under high stirring, and the mixture was stirred at room temperature for 16 h. The solvents were removed *in vacuo* until the mixture resembled a thick paste, after which ca. deionized H_2O (150 mL) was added to the flask and the solvents were immediately removed *in vacuo* until the mixture was a thick paste. Deionized H_2O (150 mL) was added and removed *in vacuo* once more. To the flask was added HCl (1M, ca. 150mL) until the pH of the mixture was 0 and the mixture was stirred for 16 h. The polymer was filtered, washed with HCl (1M) and deionized H_2O and dried *in vacuo* at 80 °C for 16 h before collecting the product as a light brown solid (1.229 g, 97% yield). ^{1}H NMR (400 MHz, DMSO-d_6) δ 7.86 – 5.93 (m, 40H), 4.09 (s, H_2O/H_3O^+). GPC analysis: M_n = 65,030 g mol^{-1}, M_w = 91,890 g mol^{-1}, Đ = 1.41.

Sulfonated Poly(phenylene) *para-meta*-5%-Biphenyl Triethylammonium Salt (sPPB*pm*HNEt$_3^+$-5%)

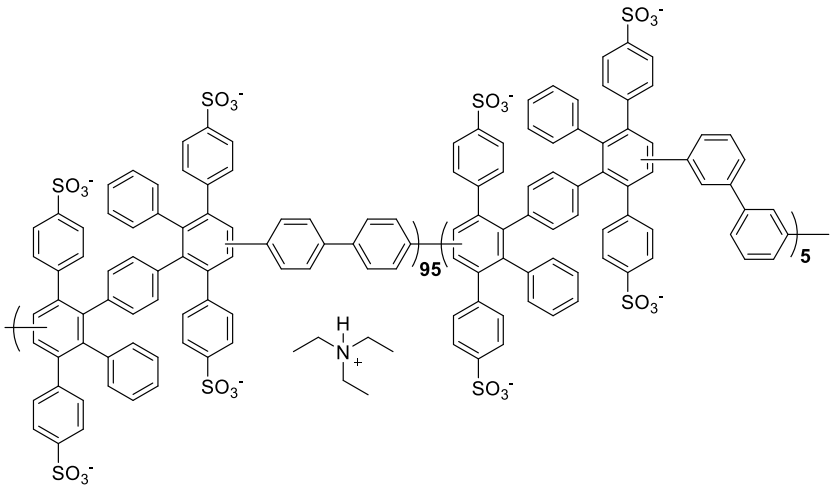

To a clean and dry 150 mL pressure vessel degassed with argon and equipped with a stir bar was added 3,3'-diethynyl-1,1'-biphenyl (0.015 g, 0.072 mmol, 0.051 eq.), 4,4'-diethynyl-1,1'-biphenyl (0.276 g, 1.36 mmol, 0.964 eq.), tetra(*para*-sulfonated) bistetracyclone triethylammonium salt (2.000 g, 1.413 mmol, 1.000 eq.), and degassed nitrobenzene (40 mL) and the mixture was stirred under argon flow for 1 h. The pressure vessel was sealed with a Teflon lid and the mixture was heated to 170 °C for 96 h under high stirring. The nitrobenzene was decanted from the polymer film inside the flask, to which was added DMSO (50 mL) and the mixture was stirred at 80 °C for 16 h. The resulting solution was poured into ethyl acetate (600 mL) under stirring, let stir for 1 h, and the brown precipitate was filtered and washed with ethyl acetate. Drying *in vacuo* at 80 °C for 16 h afforded the product as a light brown solid (1.763 g, 80% yield). ^{1}H NMR (400 MHz, DMSO-d_6) δ 8.89 (s, 4H), 7.73 – 5.92 (m, 40H), 3.05 (q (two overlapped), J = 7.2 Hz, 24H), 1.12 (t, J = 7.3 Hz, 36H).

Sulfonated Poly(phenylene) *para-meta*-5%-Biphenyl (sPPB*pm*H$^+$-5%)

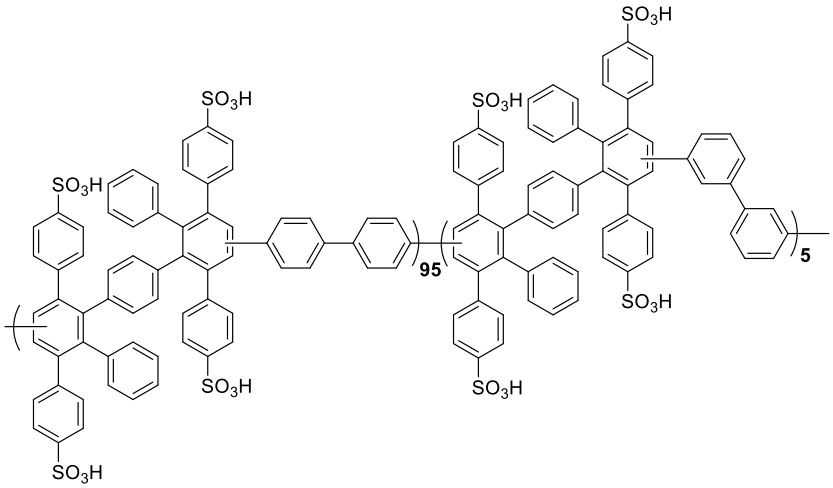

To a 500 mL round bottom flask equipped with a stir bar was added sPPB*pm*HNEt$_3^+$-5% (1.712 g) and methanol (87 mL) and the mixture was stirred to complete dissolution. A methanolic solution of sodium hydroxide (29 mL, 2M NaOH in methanol) was added dropwise to the mixture under high stirring, and the mixture was stirred at room temperature for 16 h. The solvents were removed *in vacuo* until the mixture resembled a thick paste, after which ca. deionized H_2O (150 mL) was added to the flask and the solvents were immediately removed *in vacuo* until the mixture was a thick paste. Deionized H_2O (150 mL) was added and removed *in vacuo* once more. To the flask was added HCl (1M, ca. 150mL) until the pH of the mixture was 0 and the mixture was stirred for 16 h. The polymer was filtered, washed with HCl (1M) and deionized H_2O and dried *in vacuo* at 80 °C for 16 h before collecting the product as a light brown solid (1.219 g, 96% yield). ^{1}H NMR (400 MHz, DMSO-d_6) δ 7.73 – 5.92 (m, 40H), 4.37 (s, H_2O/H_3O^+). GPC analysis: M_n = 95,770 g mol^{-1}, M_w = 127,800 g mol^{-1}, Đ = 1.33.

Sulfonated Poly(phenylene) *para-meta*-10%-Biphenyl Triethylammonium Salt (sPPB*pm*HNEt$_3^+$-10%)

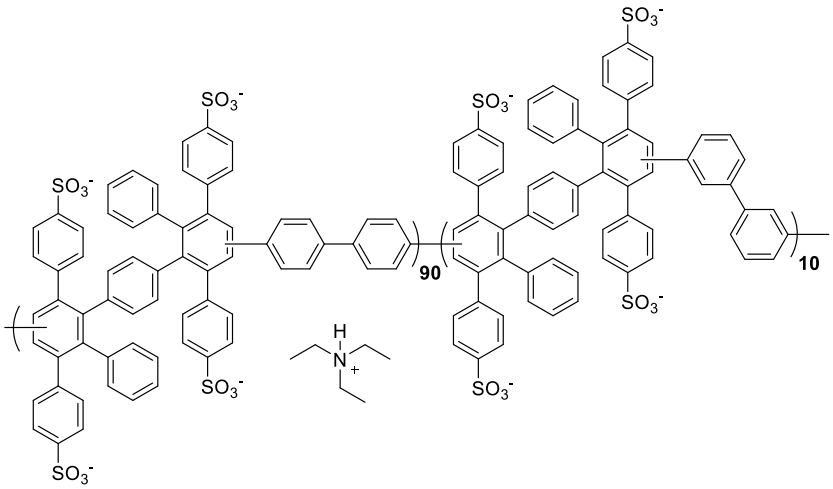

To a clean and dry 150 mL pressure vessel degassed with argon and equipped with a stir bar was added 3,3'-diethynyl-1,1'-biphenyl (0.029 g, 0.14

mmol, 0.101 eq.), 4,4'-diethynyl-1,1'-biphenyl (0.261 g, 1.29 mmol, 0.914 eq.), tetra(*para*-sulfonated) bistetracyclone triethylammonium salt (2.000 g, 1.413 mmol, 1.000 eq.), and degassed nitrobenzene (40 mL) and the mixture was stirred under argon flow for 1 h. The pressure vessel was sealed with a Teflon lid and the mixture was heated to 170 °C for 96 h under high stirring. The nitrobenzene was decanted from the polymer film inside the flask, to which was added DMSO (50 mL) and the mixture was stirred at 80 °C for 16 h. The resulting solution was poured into ethyl acetate (600 mL) under stirring, let stir for 1 h, and the brown precipitate was filtered and washed with ethyl acetate. Drying *in vacuo* at 80 °C for 16 h afforded the product as a light brown solid (1.813 g, 82% yield). ^{1}H NMR (400 MHz, DMSO-d_6) δ 8.90 (s, 4H), 7.75 – 5.90 (m, 40H), 3.05 (q (two overlapped), J = 7.3 Hz, 24H), 1.12 (t, J = 7.3 Hz, 36H).

Sulfonated Poly(phenylene) *para-meta*-10%-Biphenyl (sPPB*pm*H$^+$-10%)

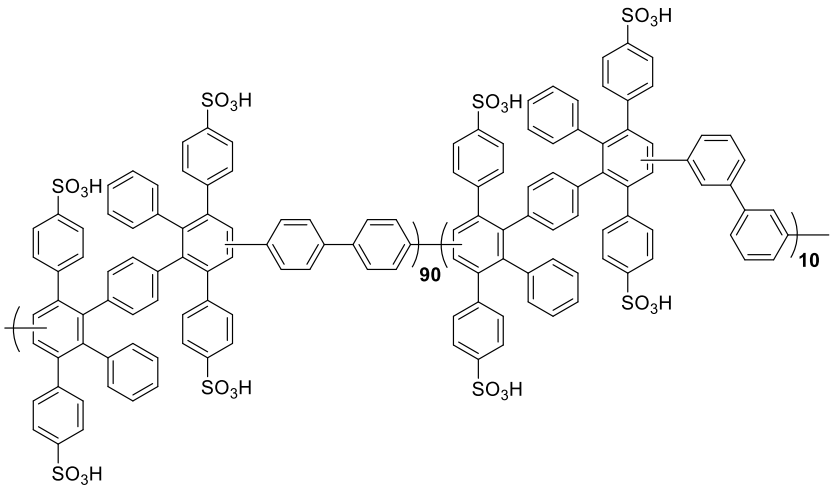

To a 500 mL round bottom flask equipped with a stir bar was added sPPB*pm*HNEt$_3^+$-10% (1.759 g) and methanol (90 mL) and the mixture was stirred to complete dissolution. A methanolic solution of sodium hydroxide (29 mL, 2M NaOH in methanol) was added dropwise to the mixture under high stirring, and the mixture was stirred at room temperature for 16 h. The solvents were removed *in vacuo* until the mixture resembled a thick paste, after which ca. deionized H_2O (150 mL) was added to the flask and the solvents were immediately removed *in vacuo* until the mixture was a thick paste. Deionized H_2O (150 mL) was added and removed *in vacuo* once more. To the flask was added HCl (1M, ca. 150mL) until the pH of the mixture was 0 and the mixture was stirred for 16 h. The polymer was filtered, washed with HCl (1M) and deionized H_2O and dried *in vacuo* at 80 °C for 16 h before collecting the product as a light brown solid (1.273 g, 98% yield). ^{1}H NMR (400 MHz, DMSO-d_6) δ 7.75 – 5.90 (m, 40H), 4.38 (s, H_2O/H_3O^+). GPC analysis: M_n = 95,580 g mol^{-1}, M_w = 125,900 g mol^{-1}, Đ = 1.32.

5.3. Results and Discussion

5.3.1. Polymer Synthesis and Characterization

Polymers were synthesized in three steps from co-monomers **TEAsBTC** and ***p*-BPL**, with small amounts (0 – 10 mol%) of either ***o*-BPL**, or ***m*-BPL**, as shown in Scheme 5.2. The overall monomeric ratio in each polymer was 1.015 equivalents biphenyl dienophile to 1.000 equivalents diene monomer **TEAsBTC**. **sPPB*p*-H$^+$** was synthesized using only ***p*-BPL** as the dienophile. **sPPB*po*H$^+$-X%** was synthesized using a combination of ***p*-BPL** and ***o*-BPL** dienophiles with varied ratios. Similarly, **sPPB*pm*H$^+$-X%** was synthesized using a combination of ***p*-BPL** and ***m*-BPL** dienophiles with varied ratios. Of the 1.015 equivalents biphenyl dienophile used during polymerization reactions, 1, 5, or 10 mol% was ***o*-BPL** or ***m*-BPL** as indicated by the "**X%**" in **sPPB*po*H$^+$-X%** or **sPPB*pm*H$^+$-X%** respectively. Therefore, all polymers consisted primarily of *para* biphenyl dienophile. A universal reference polymer **sPPB*p*-H$^+$** was prepared that contained no ***o*-BPL** or ***m*-BPL** (x = 0%). Following Diels-Alder polycondensation reactions in nitrobenzene, triethylammonium-functionalized polymers were obtained, indicated by "$HNEt_3^+$" in the polymer name (e.g., **sPPB*p*-HNEt$_3^+$**). Polymers were acid functionalized by consecutive treatment with sodium hydroxide in methanol to liberate and remove the triethylamine counter ions, followed by treatment with aqueous hydrochloric acid to exchange the sodium counter ions with acidic protons.

It should also be noted that a polymer containing 50 mol% ***o*-BPL** and 50 mol% ***p*-BPL** was initially prepared with relatively high molecular weight (M_n = 149,900 g mol^{-1}, M_w = 234,800 g mol^{-1}). A membrane cast from the resulting polymer **sPPB*po*H$^+$-50%** even retained its structural integrity upon removal from the casting plate, which was not the case for **sPPB*o*-H$^+$** from Chapter 4, and initially looked promising. However, upon drying the membrane using the standard drying protocol described in Chapter 2, the membrane, broke apart into many small pieces. Due to the poor membrane integrity at high loadings of the *ortho* biphenyl (≥ 50%), a low degree of incorporation for ***o*-BPL** and ***m*-BPL** of 1, 5, and 10 mol% was chosen.

Scheme 5.2: *Synthetic Pathway Toward Co-polymers* ***sPPBpoH⁺-X%*** *and* ***sPPBpmH⁺-X%***

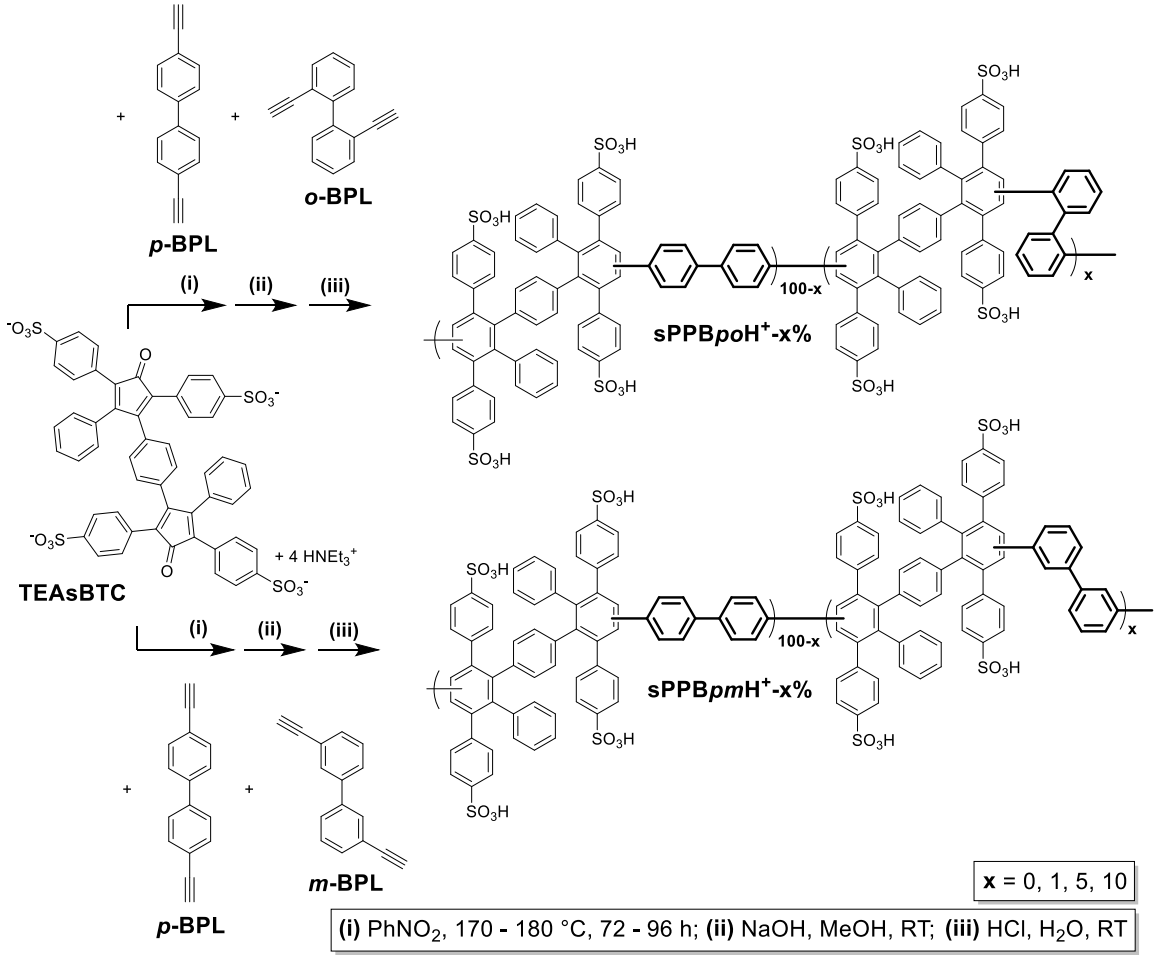

Following polycondensation reactions, triethylammonium functionalized polymers were obtained in yields between 80 and 92%. Each triethylammonium functionalized polymer was characterized by ^{1}H NMR spectroscopy in DMSO-d_6 to confirm successful polymerization. Here, the triethylammonium counter ions acted as NMR markers for integration, allowing confirmation that the sulfonic acid moieties were retained following polymerization. In each case, 36 methyl, 24 methylene, and 4 acidic (Et_3NH^+) were observed relative to the 40 aromatic protons. All spectra can be seen in Appendix C – Supporting Information for Chapter 5.

Conversion of the polymers from their triethylammonium form to their acid form was achieved in yields between 93 and 97%. The reaction temperature, time, and yields following polymerization (yield 1) and following conversion to acid form (yield 2) for each co-polymer is shown in Table 5.1. In all cases, the reaction temperature used varied

between 170 and 180 °C, for a length of 72 – 96 h. After converting the polymers to their acid from, they were again characterized by ^{1}H NMR spectroscopy. In this way, successful conversion could be confirmed by the observed disappearance of triethylammonium methyl, methylene, and acidic (Et_3NH^+) at 1.12, 3.05, and 8.90 ppm respectively, and the appearance of an H_2O/H_3O^+ peak (3.9 – 4.4 ppm). All spectra can be found in Appendix C – Supporting Information for Chapter 5. Gel permeation chromatography (GPC) was used to obtain an estimated number and weight average molecular weight (M_n and M_w), degree of polymerization based on the number average molecular weight (DP), and dispersity (Đ) for all polymers, as shown in Table 5.2. Dispersity values (omitting **sPPB*po*H$^+$-5%**) were found to decrease with increasing *ortho* or *meta* biphenyl incorporation. These findings are consistent with dispersity values reported in Chapter 4, that found sPPBs containing *ortho* or *meta* biphenyl moieties to have lower dispersity. It is unclear whether these results are real, or an artifact of the GPC measurements caused by a more rigid polymer backbone; it's likely that the size exclusion column is unable to efficiently separate rigid-rod polymers of different molecular weights, leading to lower than expected dispersity values.

Table 5.1: *Reaction Time, Reaction Temperature and Yields for Co-polymers. Yield 1 Corresponds to the Yield of Triethylammonium Functionalized Polymer Following Polymerization; Yield 2 Corresponds to Acid Conversion*

Polymer	Temp (°C)	Time (h)	Yield 1	Yield 2
sPPB*p*-H$^+$	170	96	85%	95%
sPPB*po*H$^+$-1%	170	96	87%	93%
sPPB*po*H$^+$-5%	180	72	86%	95%
sPPB*po*H$^+$-10%	180	72	92%	91%
sPPB*pm*H$^+$-1%	170	96	80%	97%
sPPB*pm*H$^+$-5%	170	96	80%	96%
sPPB*pm*H$^+$-10%	170	96	82%	98%

Table 5.2: *Number Average Molecular Weight (M_n), Weight Average Molecular Weight (M_w), Degree of Polymerization Using M_n (DP), and Dispersity (Đ) of Co-polymers*

Polymer	M_n (g mol^{-1})	M_w (g mol^{-1})	DP (M_n)	Đ
sPPB*p*-H$^+$	82,500	164,300	72	1.99
sPPB*po*H$^+$-1%	94,210	134,100	82	1.42
sPPB*po*H$^+$-5%	102,400	183,200	89	1.78
sPPB*po*H$^+$-10%	109,900	146,000	95	1.32
sPPB*pm*H$^+$-1%	65,030	91,890	56	1.41
sPPB*pm*H$^+$-5%	95,770	127,800	83	1.33
sPPB*pm*H$^+$-10%	95,580	125,900	83	1.31

Polymers were cast into membranes in their acid forms as described in Chapter 2. After drying, membranes with areas of approximately 250 cm^2 and thicknesses of 25 µm were obtained in each case, as shown in Figure 5.1. All membranes were easy to handle at ambient conditions and were insoluble in water at room temperature. When swollen in water however, co-polymers were notably fragile and difficult to handle without tearing.

Figure 5.1: *Free-standing co-polymer membranes **sPPBpoH$^+$-X%** and **sPPBpmH$^+$-X%** following casting and drying.*

5.3.2. Mechanical Properties

Mechanical properties including elongation at break, tensile strength, and Young's modulus are important parameters to consider in proton exchange membrane materials. When incorporated into a device, a membrane must be able to withstand mechanical stresses such as those imposed by gas pressure and seals. Mechanical properties of the polymer membranes were assessed using an Instron 3344 series single column system at ambient temperature and relative humidity, as described in the Chapter 2.

Representative stress vs strain curves of each polymer membrane can be seen in Figure 5.2. The mechanical properties of sPPB co-polymers containing non-linear *ortho* and *meta* biphenyl moieties were significantly reduced, even at a low 1 mol% incorporation.

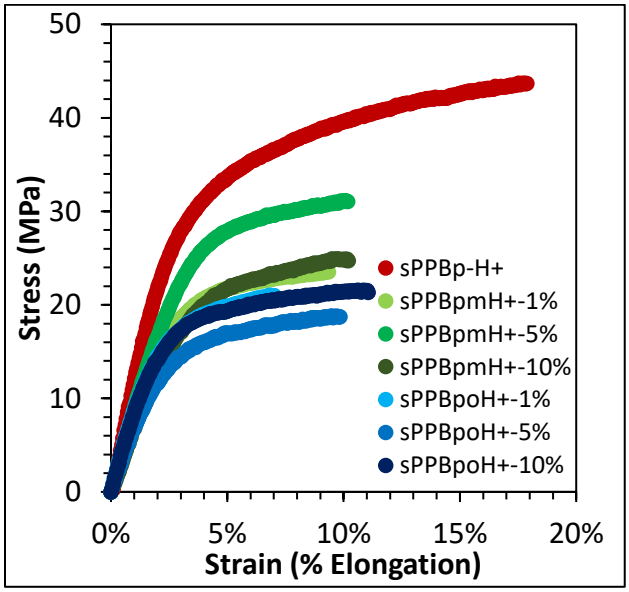

Figure 5.2: *Representative stress vs strain curves of polymer membranes at ambient conditions.*

To quantify the stress vs strain curves, Table 5.3 lists the average elongation at break, tensile strength, and Young's modulus of each polymer membrane. It can be seen that each of these parameters is significantly reduced in the co-polymers, compared to the strictly linear biphenyl moiety containing **sPPB*p*-H$^+$**. Interestingly, elongation at break was nearly identical in all co-polymers, regardless of whether the *ortho* or *meta* biphenyl moiety was incorporated, or the degree (mol %) of which it was incorporated. Tensile strength in the *meta* biphenyl containing co-polymers appeared to be slightly higher than the *ortho* biphenyl containing co-polymers. This may be a reflection of the increased rigidity that the *ortho* biphenyl moiety imparts over the *meta* biphenyl moiety, but no trends were noted with the degree of incorporation. Evidently, incorporating non-linear biphenyl moieties that likely restrict the flexibility of the sPPB backbone, even in small amounts, has a negative impact on polymer mechanical properties.

Table 5.3: *Measured Elongation at Break, Tensile Strength, and Young's Modulus of Co-polymer Membranes*

	Elongation at Break (%)	Tensile Strength (MPa)	Young's Modulus (MPa)
sPPB*p*-H$^+$	16.8 ± 2.3	41.9 ± 2.1	1218 ± 94
sPPB*po*H$^+$-1%	6.5 ± 1.4	21.3 ± 1.8	852 ± 50
sPPB*po*H$^+$-5%	9.6 ± 1.2	19.6 ± 1.6	678 ± 58
sPPB*po*H$^+$-10%	11.0 ± 1.4	21.9 ± 1.3	860 ± 58
sPPB*pm*H$^+$-1%	9.5 ± 0.3	23.3 ± 0.5	804 ± 18
sPPB*pm*H$^+$-5%	9.9 ± 1.1	31.1 ± 0.8	899 ± 32
sPPB*pm*H$^+$-10%	10.4 ± 1.6	25.0 ± 2.0	724 ± 65

5.3.3. Water Sorption, Ion Exchange Capacity and Proton Conductivity

As discussed in Chapter 4, water sorption and ion exchange capacity play a role in proton conductivity as they directly impact the spatial proximity between -SO_3H groups within the proton exchange membrane. The spatial proximity between -SO_3H groups, as well as acid dissociation and tortuosity of the aqueous domains through the membrane impact the effective proton mobility, and in turn, conductivity, through the membrane.[72],[74] The relevant relationships were described in Chapter 4, in Equation 2.13 to Equation 2.15.

The volumetric expansion of polymer membranes after being hydrated from a fully dry state can be seen in Figure 5.3a and b. Interestingly, a reduction in swelling was observed when the non-linear biphenyl moieties were incorporated in small amounts. For example, in **sPPB*po*H$^+$-X%**, swelling was decreased from 149 vol% at 0 mol% incorporation (**sPPB*p*-H$^+$**), to 126 vol% at 1 mol% and further to 114 vol% at 5 mol% non-linear biphenyl. In **sPPB*pm*H$^+$-X%**, swelling was reduced from 149 vol% at 0 mol% to 121 vol% at 1 mol% non-linear biphenyl. At higher contents of non-linear biphenyls, however, swelling began to increase. This is consistent with findings from Chapter 4 that found swelling to have increased to 259% in a polymer containing only *meta* biphenyl linkages (i.e., 100 mol% incorporation). There appears to be a fine balance between a flexible backbone that promotes molecular entanglement, and rigid “kinks” that prevent these entanglements from coming apart. If too many inflexible “kinks” are incorporated, for

example in **sPPB*pm*H$^+$-10%**, the polymer backbone becomes too rigid and unable to efficiently entangle, resulting in increased swelling.

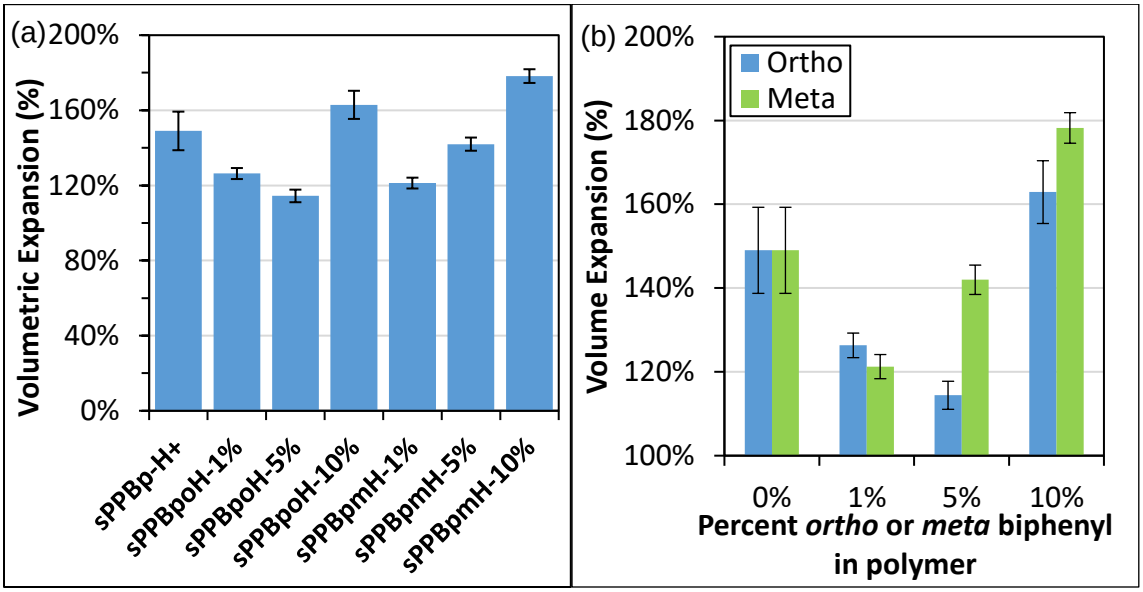

Figure 5.3: *Measured (a) volumetric expansion (swelling) of co-polymer membranes, and (b) swelling of co-polymer membranes as a function of non-linear biphenyl incorporation.*

Table 5.4 lists the volumetric expansion, water uptake, water content, hydration number, experimental IEC, and analytical acid concentration within **sPPB*p*-H$^+$** and co-polymers **sPPB*po*H$^+$-X%** and **sPPB*pm*H$^+$-X%**. While volumetric expansion was reduced significantly at low percent incorporation of non-linear biphenyl moieties, water uptake, water content, and hydration number were not, aside from **sPPBpoH$^+$-5%**, that had significantly lower values. Ion exchange capacity in all membranes was found to be the same within error aside from **sPPBpoH$^+$-5%** that had a significantly lower IEC. Analytical acid concentration values, which were calculated using the measured IEC and the volume of the hydrated membrane at ambient temperature as in Equation 2.15, were found to be similar to one another within error. Significant deviations in acid concentration versus the reference polymer **sPPB*p*-H$^+$** (1.42 ± 0.04 mmol cm^{-3}) were only noted in **sPPB*po*H$^+$-10%** and **sPPB*pm*H$^+$-10%**, that unsurprisingly also contained the two highest volumetric expansion values. In these cases, the reduction in analytical acid concentration was due to increased water uptake effectively diluting the acid concentration within the membrane.

Table 5.4: *Volumetric Expansion (V_{exp}), Water Uptake (W_{up}), Water Content (W_{con}), Hydration Number (λ), Experimental Ion Exchange Capacity (IEC_{exp}), and Analytical Acid Content ($[SO_3H]$) in Co-polymers*

Polymer	V_{exp} (%)	W_{up} (%)	W_{con} (%)	λ (mol H_2O/-SO_3H	IEC_{exp} (meq. g^{-1})	$[SO_3H]$ (mmol cm^{-3})
sPPB*p*-H$^+$	149 ± 10	130 ± 5	56 ± 1	23.7 ± 1.0	3.03 ± 0.06	1.42 ± 0.04
sPPB*po*H$^+$-1%	126 ± 3	128 ± 8	56 ± 2	24.3 ± 2.5	2.92 ± 0.24	1.39 ± 0.12
sPPB*po*H$^+$-5%	114 ± 3	86 ± 4	46 ± 1	19.7 ± 1.5	2.42 ± 0.15	1.33 ± 0.10
sPPB*po*H$^+$-10%	163 ± 7	153 ± 10	60 ± 2	27.8 ± 2.3	3.06 ± 0.16	1.28 ± 0.09
sPPB*pm*H$^+$-1%	121 ± 3	126 ± 3	56 ± 1	23.2 ± 1.9	3.01 ± 0.23	1.50 ± 0.12
sPPB*pm*H$^+$-5%	142 ± 4	137 ± 6	58 ± 1	23.4 ± 1.5	3.24 ± 0.15	1.45 ± 0.07
sPPB*pm*H$^+$-10%	178 ± 4	159 ± 2	61 ± 1	28.2 ± 2.2	3.13 ± 0.24	1.22 ± 0.11

Proton conductivity was measured at numerous relative humidity (RH) steps, between 30 and 95% at both 30 and 80 °C, as shown in Figure 5.4a and b respectively. At 30 °C, all co-polymers except for **sPPB*po*H$^+$-1%** possessed lower proton conductivity than **sPPB*p*-H$^+$**. At 80 °C, **sPPB*po*H$^+$-5%** and **sPPB*pm*H$^+$-5%** exhibited measurably reduced proton conductivity versus the other co-polymers, that approached values within error of **sPPB*p*-H$^+$**. In general, the data suggests that proton conductivity decreases with the following molar ratio of angled biphenyl incorporation: 0 > 1 > 10 > 5 mol%. This suggests that the mobility of protons within **sPPB*po*H$^+$-5%** and **sPPB*pm*H$^+$-5%** is poorest, which may relate to morphological differences caused by the angled biphenyl moieties.

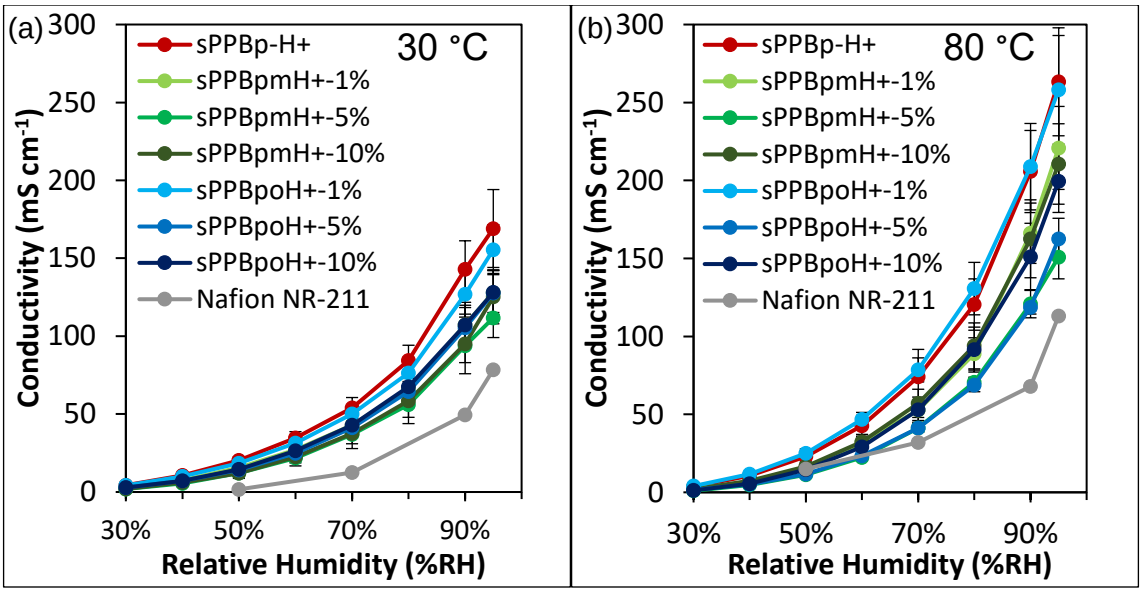

Figure 5.4: *Proton conductivity of co-polymer membranes between 30 and 95% RH at (a) 30 °C and (b) 80 °C.*

To further probe the differences observed via proton conductivity measurements, membrane analytical acid concentration (Equation 2.15) and proton mobility (Equation 2.14) were calculated. Data are provided in Table 5.5, including values for proton conductivity (95% RH) at 30 and 80 °C. Under both sets of conditions, the calculated proton mobility was lowest in polymers containing 5 mol% of angled biphenyl linkages (i.e., **sPPB*po*H$^+$-5%** and **sPPB*pm*H$^+$-5%**). These data reflect the aforementioned trends observed in membrane proton conductivity with respect to angled biphenyl content: 0 > 1 > 10 > 5 mol%. The analytical acid concentration [SO_3H] decreased with increasing angled biphenyl content, regardless of stereochemistry (*ortho* versus *meta*). However, the differences were moderate (overall range 1.22 – 1.50 mmol cm^{-3}). Based on these data, proton mobility appears to more strongly dictate overall membrane proton conductivity in sulfonated, phenylated poly(phenylene) copolymers, but, both parameters predict the observed decreases in membrane proton conductivity. Hence, the design of a stiffer polymer backbone, such as one containing inflexible, angled biphenyls, yields a polymer membrane with reduced analytical acid concentration and effective proton mobility, and therefore, reduced proton conductivity.

Table 5.5: *Proton Conductivity and Proton Mobility Values for Co-polymer Membranes*

Polymer	$[SO_3H]$ (mmol cm^{-3})	σ_{H+} (30 °C, 95% RH) (mS cm^{-1})	σ_{H+} (80 °C, 95% RH) (mS cm^{-1})	μ'_{H+} (30 °C, 95% RH) (10^{-3} cm^2 V^{-1} s^{-1})	μ'_{H+} (80 °C, 95% RH) (10^{-3} cm^2 V^{-1} s^{-1})
sPPBp-H$^+$	1.42 ± 0.04	169 ± 14	263 ± 35	1.23 ± 0.11	1.92 ± 0.26
sPPBpoH$^+$-1%	1.39 ± 0.12	156 ± 16	258 ± 35	1.16 ± 0.16	1.92 ± 0.31
sPPBpoH$^+$-5%	1.33 ± 0.10	128 ± 13	162 ± 13	0.99 ± 0.13	1.26 ± 0.14
sPPBpoH$^+$-10%	1.28 ± 0.09	128 ± 14	200 ± 20	1.03 ± 0.13	1.61 ± 0.20
sPPBpmH$^+$-1%	1.50 ± 0.12	128 ± 14	221 ± 27	0.88 ± 0.12	1.52 ± 0.22
sPPBpmH$^+$-5%	1.45 ± 0.07	112 ± 13	151 ± 14	0.80 ± 0.10	1.08 ± 0.11
sPPBpmH$^+$-10%	1.22 ± 0.11	125 ± 17	211 ± 26	1.06 ± 0.17	1.79 ± 0.30

5.4. Conclusions

Co-polymer analogues of **sPPB-H$^+$** containing a mixture of *ortho* and *para* (**sPPB*po*H$^+$-X%**), or *meta* and *para*-(**sPPB*pm*H$^+$-X%**) biphenyl moieties in the polymer backbone were synthesized to better understand the impact of a progressively stiffened polymer backbone. These were compared to a reference polymer **sPPB*p*-H$^+$**, that contained solely *para* biphenyl moieties. In each case, the mol % of *ortho* or *meta* biphenyl versus overall biphenyl content (sum of 100%) was varied between 0 and 10%. Polymers with comparable molecular weights were synthesized in yields exceeding 80%, and showed full retention of pre-functionalized sulfonic-acid moieties via ^{1}H NMR spectroscopy using triethylammonium counter ions as internal markers.

Conversion of polymers to their acidic form was achieved in excellent yield, affording membranes with an approximate thickness of 25 µm. Mechanical properties of the sPPB membranes containing non-linear *ortho* and *meta* biphenyl moieties were measurably reduced (up to 61% elongation at break and 53% tensile strength), however, no explicit trends were observed with respect to the molar ratio of *ortho* or *meta* biphenyls incorporated. On average, **sPPB*pm*H$^+$-X%** displayed slightly higher tensile strength values than **sPPB*po*H$^+$-X%**, but both co-polymers yielded membranes with greater fragility compared to **sPPB*p*-H$^+$**.

Water sorption measurements revealed that sPPB co-polymers possessing lesser quantities (1-5 mol%) of *ortho* or *meta* biphenyl moieties displayed noteworthy reductions in volumetric swelling upon hydration of up to 35 vol%. This was also corroborated by reductions in water uptake of up to 44 wt%, but only in polymers containing *ortho* biphenyls. When assessed as proton-conducting membranes, both series of membranes showed generally decreasing proton conductivity with angled biphenyl content in the order of 0 > 1 > 10 > 5 mol%. Both analytical acid concentration and effective proton mobility of the membranes decreased upon addition of angled biphenyl co-monomers, with a greater change noted in the latter. The reduction in proton conductivity appears to be primarily due to the reduced proton mobility, that appears to be a consequence of the stiff, inflexible polymer backbones that result from incorporating non-linear, rotationally restricted biphenyl moieties.

Collectively, incorporation of inflexible, angled biphenyl “kinks” into a polymer backbone appears to diminish chain entanglement within membranes, that in turn decreases both physical and electrochemical properties. The work discussed in this chapter reinforces the importance of considering chain flexibility and entanglement during polymeric design aimed at improving such parameters.

Chapter 6.

Conclusions and Future Work

6.1. Conclusions

The work presented in this thesis pertained to the synthesis and characterization of a series of oligo(phenylene) small molecules and poly(phenylene) homo-polymers and co-polymers, each of which incorporated linear (*para*) or non-linear (*ortho* or *meta*) biphenyl moieties. In Chapter 3, the successful preparation and characterization of three small molecule model compounds **MC-B*o***, **MC-B*m***, and **MC-B*p*** was discussed, thus proving the viability of the Diels-Alder reaction between each of the *ortho*, *meta*, and *para* functionalized biphenyl dienophile linkers with a diene, that would be necessary for polymerization. Both NMR spectroscopy and DFT calculations suggested atropisomerism in the *ortho* biphenyl-containing **MC-B*o***, caused by a sterically congested structurer, restricting rotation about the central biphenyl moiety. The restricted rotation found to exist in **MC-B*o*** was found to have a detrimental impact on the corresponding polymer **sPPB*o*-H$^+$** and even on the *meta* biphenyl containing **sPPB*m*-H$^+$** membrane properties that were explored in Chapter 4.

In Chapter 4, the preparation of homo-polymers containing strictly either the *ortho*, *meta*, or *para* biphenyl, along with an extensive investigation of these polymers to assess their properties pertinent to proton exchange membrane materials was discussed. Polymers were synthesized in good yields, and NMR spectroscopy, thermogravimetric analysis, and differential scanning calorimetry suggested that the three polymers shared a common chemical composition. However, **sPPB*o*-H$^+$** was water soluble and was unable to form a free-standing membrane despite possessing appreciable molecular weights, and **sPPB*m*-H$^+$** formed membranes with poor mechanical integrity below a M_n threshold (154,700 g mol^{-1}). In contrast, **sPPB*p*-H$^+$** was robust and completely insoluble at modest M_n (82,500 g mol^{-1}). The poor membrane forming capability of the former two polymers was attributed to the rotationally hindered backbones in **sPPB*m*-H$^+$**, and especially in **sPPB*o*-H$^+$**, that would promote rigid macroscopic structures lacking appreciable chain entanglement. Ultimately, this would lead to **sPPB*m*-H$^+$** displaying a 74% increase in volumetric expansion, 30% reduction in tensile strength, 52% reduction in elongation at

break, and 26% reduction in Young's moduli, as well as a lower proton conductivity at 30 °C attributed to the excessive swelling when compared to **sPPB*p*-H⁺**.

In Chapter 5, a series of co-polymers that were prepared by incorporating lesser amounts of either *ortho*, or *meta* biphenyl in an otherwise *para* biphenyl containing system was discussed. This would allow for the preparation of free-standing membranes containing the *ortho* biphenyl moiety, that was not possible in the homo-polymer. This would also allow assessment of incrementally increasing the non-linear biphenyl content. A total of 7 polymer membranes (six co-polymers and one homo-polymer) were prepared in good yields exceeding 80 %, with all having similar molecular weights, where the *ortho* or *meta* biphenyl composition in relation to the overall biphenyl content was varied between 0 and 10%. All co-polymers were found to exhibit considerably worse mechanical properties than **sPPB*p*-H⁺**. Interestingly, co-polymers possessing a small amount of *ortho* or *meta* biphenyl moieties were found to swell less than the strictly *para* biphenyl containing **sPPB*p*-H⁺**. It was rationalized that a small number of inflexible kinks may help polymer chains from coming apart when immersed in water, without impacting the ability for the chains to entangle by making them too rigid.

Ultimately, the results presented in this thesis cumulatively stress the importance of polymer backbone flexibility and macroscopic chain entanglement in advanced functional polymeric materials, such as proton exchange membranes. While angled moieties appear to provide enhanced backbone flexibility in other polymeric systems,[29],[72],[100],[101],[102] they were found to produce sterically-encumbered, rotationally restricted systems when incorporated into sulfonated phenylated poly(phenylenes)s due to their highly phenylated structure. These rotationally restricted polymers resulted in membranes with poor physical and electrochemical properties, or were unable to form membranes at all, likely due to the lack of macroscopic chain entanglement caused therefrom.

6.2. Future Work

The work presented in this thesis has provided evidence that the poor physico-electrochemical properties in **sPPB*o*-H⁺** and **sPPB*m*-H⁺** stem from rotational restriction about the angled biphenyl, leading to rigid, inflexible polymer backbones. As discussed in Chapter 1, incorporating non-linear units into a polymer backbone has been shown to be

beneficial in preparing flexible, low swelling membranes.[29],[72],[100],[101],[102] It would appear that this is the case so long as the backbone is free to rotate, which is not true in the case of sulfonated phenylated poly(phenylene)s such as those presented in this thesis, as they are inherently sterically-encumbered systems.

Consequently, future work in this area should aim to incorporate non-linear units, while simultaneously reduce the degree of steric hinderance. In this way, the backbone lacking steric congestion may be able to rotate freely about the non-linear moieties, thereby forming flexible coils as was initially intended in this thesis. This may be achieved by increasing the length of the dienophile co-monomer. Miyake *et. al.*[101],[102] have recently incorporated a penta-phenylene monomer (QP monomer) containing *meta* and *para* functionalized phenylene groups where the *meta*/*para* ratio is 4:1 as shown in Scheme 6.1. The polymer SPP-QP formed therefrom was found to have unexpectedly high membrane flexibility that the authors argued was due to interpolymer entanglement caused by the random coil structure caused by the combination of *meta* and *para* phenylene groups.

Scheme 6.1: *Large Penta-phenylene Monomer Used by Miyake et. al. to Prepare Polymer SPP-QP*

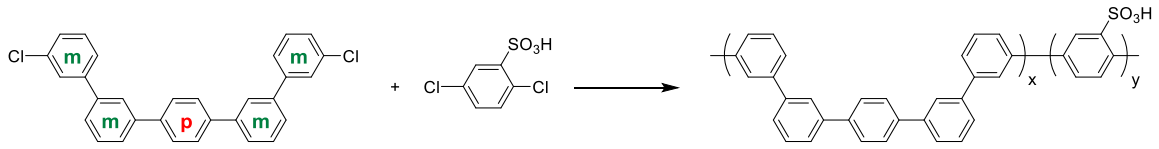

QP **SPP-QP**

It would be possible to take a similar approach with sulfonated phenylated poly(phenylene) systems as well. Instead of using a small biphenyl co-monomer, such as those used in this thesis, a larger penta-phenylene analogue similar to the QP monomer used by Miyake *et. al.*[101],[102] could be used. Scheme 6.2 overviews a potential synthetic pathway towards a penta-phenylene dienophile co-monomer that could be used in Diels-Alder polymerization to prepare sulfonated phenylated poly(phenylene)s. Steps **(i)** and **(ii)** have been successfully carried out by Miyake *et. al.*[101] in good yields to prepare QP. Steps **(iii)** and **(iv)** would involve a Sonogashira cross-coupling to install the silyl protected alkynes, followed by a protodesilylation to expose the bare terminal alkynes. The latter steps employ reactions that have been performed routinely throughout this thesis.

Scheme 6.2: *Synthesis of Larger Penta-phenylene Dienophile Co-monomer*

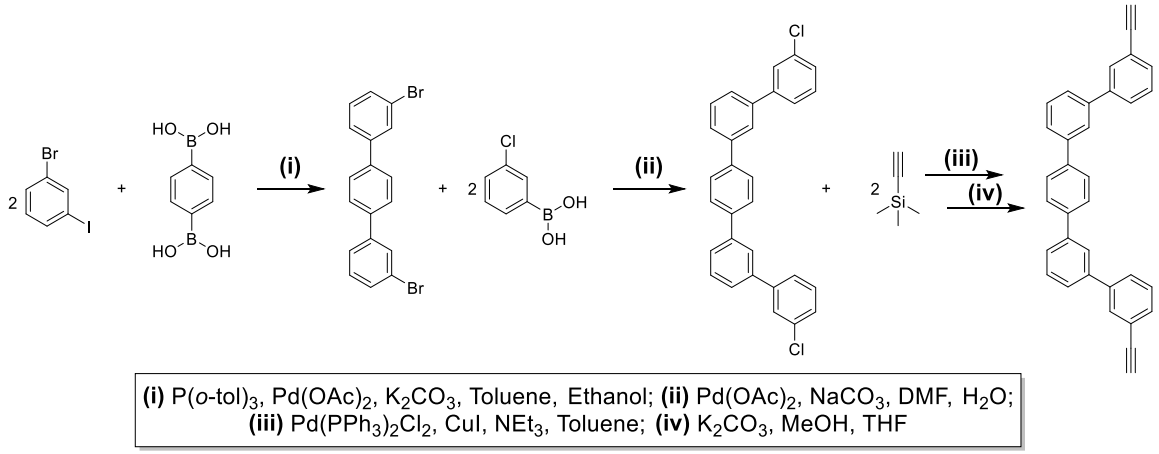

(i) P(*o*-tol)$_3$, Pd(OAc)$_2$, K_2CO_3, Toluene, Ethanol; **(ii)** Pd(OAc)$_2$, $NaCO_3$, DMF, H_2O; **(iii)** Pd(PPh_3)$_2Cl_2$, CuI, NEt_3, Toluene; **(iv)** K_2CO_3, MeOH, THF

Polymers prepared in this way may circumvent the rigid backbone issues observed in **sPPB*o*-H$^+$** and **sPPB*m*-H$^+$**. The penta-phenylene monomer would provide sufficient space between the highly phenylated, sulfonated components, allowing room for rotation. Of course, the ion exchange capacity of the polymer would be considerably lower that any **sPPB** analogue (2.88 vs 3.46 meq. g^{-1}, respectively) due to the additional hydrophobic content. This would likely reduce the proton conductivity, but the potential enhancements to mechanical strength and water sorption properties may be enough to make up for the loss in conductivity. To make a direct comparison between linear and non-linear polymers, a completely linear penta-phenylene monomer could also be synthesized, as in Scheme 6.3. In this way, two polymers with the same chemical composition and ion exchange capacity, only differing in the linearity, could be directly compared.

From these two penta-phenylene co-monomers, sulfonated phenylated poly(phenylene) polymers could be prepared. Scheme 6.4 shows a Diels-Alder polymerization reaction between **TEAsBTC** and each of the two newly proposed penta-phenylene dienophile co-monomers. One potential issue with this work is solubility of the large hydrophobic monomers. With that said however, QP monomer was found to be soluble in a variety of solvents such as DMF, and a mixture of DMF, toluene and H_2O.

Scheme 6.3: *Synthesis of Completely Linear Penta-phenylene Dienophile Co-monomer*

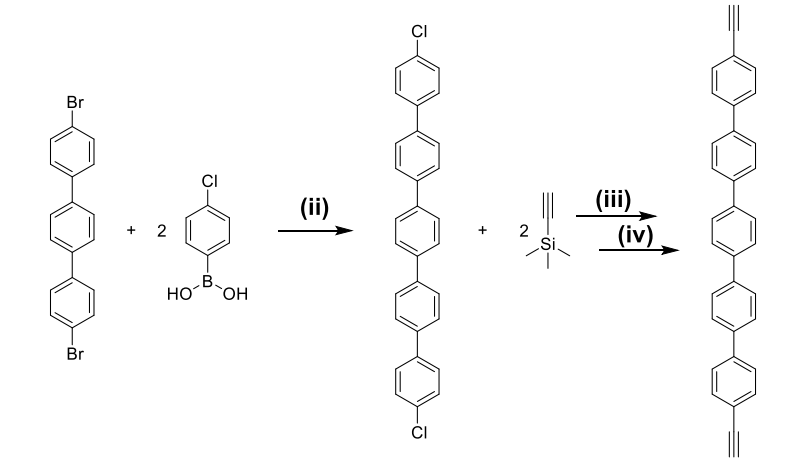

(i) $Pd(OAc)_2$, $NaCO_3$, DMF, H_2O; **(ii)** $Pd(PPh_3)_2Cl_2$, CuI, NEt_3, Toluene; **(iii)** K_2CO_3, MeOH, THF

Scheme 6.4: *Synthesis of Sulfonated Phenylated Poly(phenylene) Containing a Large Spacer Unit, Allowing Room for Rotation*

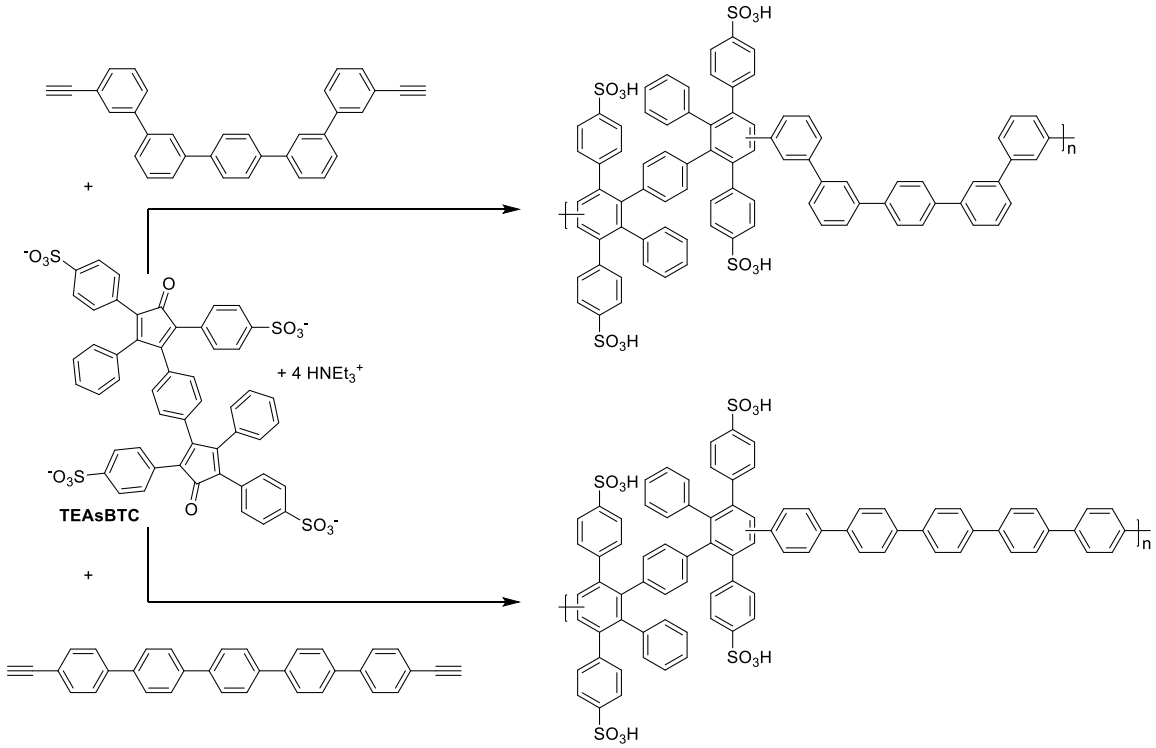

If either the solubility, or the reduced IEC are found to be an issue, sulfonation of the penta-phenylene co-monomers could be considered. This would effectively increase solubility of the monomers in polar solvents by increasing hydrophilic content, while simultaneously increasing the IEC of the respective polymers. As we have seen in Chapter 2, pre-sulfonation of monomers is a complex process that would bring additional challenges to reaction design, that are beyond the scope of this thesis. Challenges would include controlling the positioning and extent of sulfonation in a way that would not restrict rotation of the polymer backbone, and complications in performing transition metal catalyzed cross-coupling reactions between sulfonic acid moiety containing aromatic substituents. It may be possible to circumvent complications due to the latter point by converting the acid groups to their neutralized salt forms, such as their sodium or triethylammonium counterpart. Ultimately, if these penta-phenylene monomers could be sulfonated to their mono-sulfonated analogue, as shown in Scheme 6.5, the IEC of the resulting polymer would be 3.60 meq. g^{-1}, similar to that of **sPPB-H$^+$** at 3.46 meq. g^{-1}. Placing the sulfonic acid group on the central phenyl ring as shown in Scheme 6.5, furthest from the highly phenylated component, might reduce steric effects that could potentially restrict rotation.

Scheme 6.5: *Synthesis of Sulfonated Phenylated Poly(phenylene) Containing a Pre-sulfonated Penta-phenylene Spacer Unit*

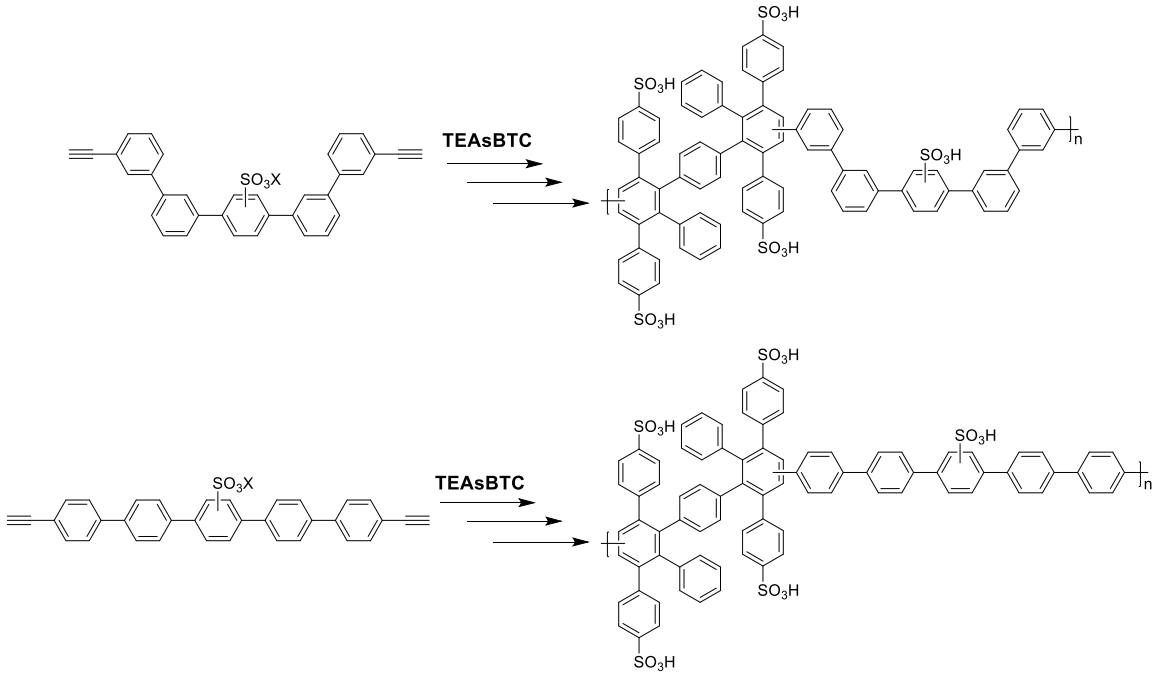

References

[1] *World Population Prospects: Key Findings and Advance Tables*, United Nations, Department Of Economic And Social Affairs, New York, **2017**.

[2] M. Roser, “Economic Growth” https://ourworldindata.org/economic-growth (accessed Nov. 26, 2019).

[3] J. Bolt, R. Inklaar, H. de Jong, J. L. van Zanden, H. de Jong, J. L. van Zanden, *Rebasing ‘Maddison’: New Income Comparisons and the Shape of Long-Run Economic Development*, **2018**.

[4] *Key World Energy Statistics*, International Energy Agency, Paris, **2016**.

[5] *BP Statistical Review of World Energy*, Beyond Petroleum, London, **2019**.

[6] *World Energy Resources 2016*, World Energy Council, Wales, **2016**.

[7] S. Shafiee, E. Topal, *Energy Policy* **2009**, *37*, 181–189. https://doi.org/10.1016/j.enpol.2008.08.016.

[8] J. T. Houghton, L. G. Meira Filho, B. A. Callander, N. Harris, A. Kattenberg, K. Maskell, *Climate Change 1995: The Science of Climate Change*, Cambridge University Press, Cambridge, **1996**.

[9] T. M. L. Wigley, *Clim. Change* **1983**, *5*, 315–320. https://doi.org/10.1007/BF02423528.

[10] P. Tans, “Trends in Atmospheric Carbon Dioxide” https://www.esrl.noaa.gov/gmd/ccgg/trends/global.html (accessed Nov. 11, 2019).

[11] R. K. Pachauri, L. Meyer, Eds. , *Climate Change 2014: Synthesis Report*, Intergovernmental Panel On Climate Change, Geneva, **2014**.

[12] A. E. Dessler, *Introduction to Modern Climate Change*, Cambridge University Press, New York, **2012**. https://doi.org/10.1017/CBO9781107415324.004.

[13] D. Archer, M. Eby, V. Brovkin, A. Ridgwell, L. Cao, U. Mikolajewicz, K. Caldeira, K. Matsumoto, G. Munhoven, A. Montenegro, et al., *Annu. Rev. Earth Planet. Sci.* **2009**, *37*, 117–134. https://doi.org/10.1146/annurev.earth.031208.100206.

[14] O. Hoegh-Guldberg, P. J. Mumby, A. J. Hooten, R. S. Steneck, P. Greenfield, E. Gomez, C. D. Harvell, P. F. Sale, A. J. Edwards, K. Caldeira, et al., *Science* **2007**, *318*, 1737–1743. https://doi.org/10.1126/science.1152509.

[15] P. J. Sellers, D. S. Schimel, B. Moore, J. Liu, A. Eldering, *Proc. Natl. Acad. Sci. U. S. A.* **2018**, *115*, 7860–7868. https://doi.org/10.1073/pnas.1716613115.

[16] C. D. Thomas, A. Cameron, R. E. Green, M. Bakkenes, L. J. Beaumont, Y. C. Collingham, B. F. N. Erasmus, M. Ferreira De Siqueira, A. Grainger, L. Hannah, et al., *Nature* **2004**, *427*, 145–148. https://doi.org/10.1038/nature02121.

[17] M. C. Urban, *Science* **2015**, *348*, 571–573. https://doi.org/10.1126/science.aaa4984.

[18] J. Rogelj, M. Den Elzen, N. Höhne, T. Fransen, H. Fekete, H. Winkler, R. Schaeffer, F. Sha, K. Riahi, M. Meinshausen, *Nature* **2016**, *534*, 631–639. https://doi.org/10.1038/nature18307.

[19] G. A. Jones, K. J. Warner, *Energy Policy* **2016**, *93*, 206–212. https://doi.org/10.1016/j.enpol.2016.02.044.

[20] D. P. van Vuuren, E. Stehfest, M. G. J. den Elzen, T. Kram, J. van Vliet, S. Deetman, M. Isaac, K. K. Goldewijk, A. Hof, A. M. Beltran, et al., *Clim. Change* **2011**, *109*, 95–116. https://doi.org/10.1007/s10584-011-0152-3.

[21] J. Larminie, A. Dicks, *Fuel Cell Systems Explained*, John Wiley & Sons Ltd, West Sussex, **2003**. https://doi.org/10.1002/9781118878330.

[22] A. L. Dicks, D. A. J. Rand, *Fuel Cell Systems Explained*, John Wiley & Sons Ltd, Hoboken, NJ, USA, **2018**. https://doi.org/10.1002/9781118706992.

[23] C. Sequeira, D. Santos, Eds. , *Polymer Electrolytes Fundamentals and Applications*, Woodhead Publishing, Cambridge, UK, **2010**.

[24] J. Ran, L. Wu, Y. He, Z. Yang, Y. Wang, C. Jiang, L. Ge, E. Bakangura, T. Xu, *J. Memb. Sci.* **2017**, *522*, 267–291. https://doi.org/10.1016/j.memsci.2016.09.033.

[25] K. D. Kreuer, *Chem. Mater.* **2014**, *26*, 361–380. https://doi.org/10.1021/cm402742u.

[26] X. Zhang, T. Higashihara, M. Ueda, L. Wang, *Polym. Chem.* **2014**, *5*, 6121–6141. https://doi.org/10.1039/C4PY00898G.

[27] D. R. Dekel, *J. Power Sources* **2018**, *375*, 158–169. https://doi.org/10.1016/j.jpowsour.2017.07.117.

[28] M. R. Hibbs, C. H. Fujimoto, C. J. Cornelius, *Macromolecules* **2009**, *42*, 8316–8321. https://doi.org/10.1021/ma901538c.

[29] D. W. Shin, M. D. Guiver, Y. M. Lee, *Chem. Rev.* **2017**, *117*, 4759–4805. https://doi.org/10.1021/acs.chemrev.6b00586.

[30] K. A. Mauritz, R. B. Moore, *Chem. Rev.* **2004**, *104*, 4535–4585. https://doi.org/10.1021/cr0207123.

[31] M. A. Hickner, H. Ghassemi, Y. S. Kim, B. R. Einsla, J. E. McGrath, *Chem. Rev.* **2004**, *104*, 4587–4611. https://doi.org/10.1021/cr020711a.

[32] H. Zhang, P. K. Shen, *Chem. Rev.* **2012**, *112*, 2780–2832. https://doi.org/10.1021/cr200035s.

[33] K. S. V. Santhanam, R. J. Press, M. J. Miri, A. V. Bailey, G. A. Takacs, *Introduction to Hydrogen Technology*, John Wiley & Sons, Hoboken, NJ, USA, **2017**.

[34] A. Kraytsberg, Y. Ein-Eli, *Energy and Fuels* **2014**, *28*, 7303–7330. https://doi.org/10.1021/ef501977k.

[35] L. Schlapbach, L. Schlapbach, A. Züttel, *Nature* **2001**, *414*, 265–358. https://doi.org/10.1038/35104634.

[36] N. L. Rosi, J. Eckert, M. Eddaoudi, D. T. Vodak, J. Kim, M. O'Keeffe, O. M. Yaghi, *Science* **2003**, *300*, 1127–1129. https://doi.org/10.1126/science.1083440.

[37] A. C. Dillon, K. M. Jones, T. A. Bekkedahl, C. H. Kiang, D. S. Bethune, M. J. Heben, *Nature* **1997**, *386*, 377–379. https://doi.org/10.1038/386377a0.

[38] G. Mulder, J. Hetland, G. Lenaers, *Int. J. Hydrogen Energy* **2007**, *32*, 1324–1331. https://doi.org/10.1016/j.ijhydene.2006.10.012.

[39] A. Wilson, G. Kleen, D. Papageorgopoulos, *Fuel Cell System Cost - 2017; DOE Hydrogen and Fuel Cells Program Record*, **2017**. https://doi.org/10.1115/1.4036738.

[40] S. Martin, B. Martinez-Vazquez, P. L. Garcia-Ybarra, J. L. Castillo, *J. Power Sources* **2013**, *229*, 179–184. https://doi.org/10.1016/j.jpowsour.2012.12.029.

[41] F. Jaouen, E. Proietti, M. Lefèvre, R. Chenitz, J. P. Dodelet, G. Wu, H. T. Chung, C. M. Johnston, P. Zelenay, *Energy Environ. Sci.* **2011**, *4*, 114–130. https://doi.org/10.1039/c0ee00011f.

[42] W. Grubb, L. Niedrach, *J. Electrochem. Soc.* **1960**, *107*, 131–135.

[43] C. H. Park, C. H. Lee, M. D. Guiver, Y. M. Lee, *Prog. Polym. Sci.* **2011**, *36*, 1443–1498. https://doi.org/10.1016/j.progpolymsci.2011.06.001.

[44] N. H. Behling, *Fuel Cells: Current Technology Challenges and Future Research Needs*, Elsevier B.V, Amsterdam, Netherlands, **2013**. https://doi.org/10.1016/C2011-0-04424-1.

[45] Y. Tanaka, *Ion Exchange Membranes Fundamentals and Applications*, Elsevier, Amsterdam, Netherlands, **2015**.

[46] K. Si, D. Dong, R. Wycisk, M. Litt, *J. Mater. Chem.* **2012**, *22*, 20907–20917. https://doi.org/10.1039/c2jm33066k.

[47] H. Hou, M. L. Di Vona, P. Knauth, *ChemSusChem* **2011**, *4*, 1526–1536. https://doi.org/10.1002/cssc.201000415.

[48] Q. Li, R. He, J. O. Jensen, N. J. Bjerrum, *Chem. Mater.* **2003**, *15*, 4896–4915. https://doi.org/10.1021/cm0310519.

[49] J. Peron, A. Mani, X. Zhao, D. Edwards, M. Adachi, T. Soboleva, Z. Shi, Z. Xie, T. Navessin, S. Holdcroft, *J. Memb. Sci.* **2010**, *356*, 44–51. https://doi.org/10.1016/j.memsci.2010.03.025.

[50] C. Houchins, G. J. Kleen, J. S. Spendelow, J. Kopasz, D. Peterson, N. L. Garland, D. L. Ho, J. Marcinkoski, K. E. Martin, R. Tyler, et al., *Membranes* **2012**, *2*, 855–878. https://doi.org/10.3390/membranes2040855.

[51] N. L. Garland, T. G. Benjamin, J. P. Kopasz, *ECS Trans.* **2007**, *11*, 923–931. https://doi.org/10.1149/1.2781004.

[52] M. Adamski, T. J. G. Skalski, B. Britton, T. J. Peckham, L. Metzler, S. Holdcroft, *Angew. Chemie - Int. Ed.* **2017**, *56*, 9058–9061. https://doi.org/10.1002/anie.201703916.

[53] K. Sopian, W. R. Wan Daud, *Renew. Energy* **2006**, *31*, 719–727. https://doi.org/10.1016/j.renene.2005.09.003.

[54] A. Daryaei, G. C. Miller, J. Willey, S. R. Choudhury, B. Vondrasek, D. Kazerooni, M. R. Burtner, C. Mittelsteadt, J. J. Lesko, J. S. Riffle, et al., *ACS Appl. Mater. Interfaces* **2017**, *9*, 20067–20075. https://doi.org/10.1021/acsami.7b02401.

[55] M. Feng, R. Qu, Z. Wei, L. Wang, P. Sun, Z. Wang, *Sci. Rep.* **2015**, *5*, 9859, 1–8. https://doi.org/10.1038/srep09859.

[56] H. Hou, M. L. Di Vona, P. Knauth, *J. Memb. Sci.* **2012**, *423–424*, 113–127. https://doi.org/10.1016/j.memsci.2012.07.038.

[57] M. Mench, E. C. Kumbur, T. N. Veziroglu, *Polymer Electrolyte Fuel Cell Degradation*, Academic Press, New York and London, **2011**. https://doi.org/10.1016/C2010-0-67819-9.

[58] T. Holmes, T. J. G. Skalski, M. Adamski, S. Holdcroft, *Chem. Mater.* **2019**, *31*, 1441–1449. https://doi.org/10.1021/acs.chemmater.8b05302.

[59] B. Bae, K. Miyatake, M. Watanabe, *Macromolecules* **2009**, *42*, 1873–1880. https://doi.org/10.1021/ma8026518.

[60] Y. S. Kim, M. A. Hickner, L. Dong, B. S. Pivovar, J. E. McGrath, *J. Memb. Sci.* **2004**, *243*, 317–326. https://doi.org/10.1016/j.memsci.2004.06.035.

[61] Y. Chang, G. F. Brunello, J. Fuller, M. L. Disabb-Miller, M. E. Hawley, Y. S. Kim, M. A. Hickner, S. S. Jang, C. Bae, *Polym. Chem.* **2013**, *4*, 272–281. https://doi.org/10.1039/c2py20666h.

[62] E. K. Pefkianakis, V. Deimede, M. K. Daletou, N. Gourdoupi, J. K. Kallitsis, *Macromol. Rapid Commun.* **2005**, *26*, 1724–1728. https://doi.org/10.1002/marc.200500540.

[63] P. Xing, G. P. Robertson, M. D. Guiver, S. D. Mikhailenko, K. Wang, S. Kaliaguine, *J. Memb. Sci.* **2004**, *229*, 95–106. https://doi.org/10.1016/j.memsci.2003.09.019.

[64] A. A. Argun, J. N. Ashcraft, P. T. Hammond, *Adv. Mater.* **2008**, *20*, 1539–1543. https://doi.org/10.1002/adma.200703205.

[65] D. J. Jones, J. Rozière, *J. Memb. Sci.* **2001**, *185*, 41–58. https://doi.org/10.1016/S0376-7388(00)00633-5.

[66] S. Qing, W. Huang, D. Yan, *J. Polym. Sci. Part A Polym. Chem.* **2005**, *43*, 4363–4372. https://doi.org/10.1002/pola.20842.

[67] L. Gubler, T. Nauser, F. D. Coms, Y. H. Lai, C. S. Gittleman, *J. Electrochem. Soc.* **2018**, *165*, 3100–3103. https://doi.org/10.1149/2.0131806jes.

[68] S. Y. Lee, N. R. Kang, D. W. Shin, C. H. Lee, K.-S. Lee, M. D. Guiver, N. Li, Y. M. Lee, *Energy Environ. Sci.* **2012**, *5*, 9795. https://doi.org/10.1039/c2ee21992a.

[69] N. Li, J. Liu, Z. Cui, S. Zhang, W. Xing, *Polymer* **2009**, *50*, 4505–4511. https://doi.org/10.1016/j.polymer.2009.07.039.

[70] I. Manke, N. Kardjilov, C. Hartnig, *Polymer Electrolyte Membrane and Direct Methanol Fuel Cell Technology*, Woodhead Publishing, Cambridge, UK, **2012**. https://doi.org/10.1016/B978-1-84569-774-7.50009-8.

[71] G. G. Scherer, Ed. , *Fuel Cells II. Advances in Polymer Science*, Springer, Berlin, Heidelberg, **2008**. https://doi.org/10.1038/216619a0.

[72] T. J. Peckham, S. Holdcroft, *Adv. Mater.* **2010**, *22*, 4667–4690. https://doi.org/10.1002/adma.201001164.

[73] K. D. Kreuer, *J. Memb. Sci.* **2001**, *185*, 29–39. https://doi.org/10.1016/S0376-7388(00)00632-3.

[74] T. J. Peckham, J. Schmeisser, M. Rodgers, S. Holdcroft, *J. Mater. Chem.* **2007**, *17*, 3255–3268. https://doi.org/10.1039/b702339a.

[75] Y. Yang, A. Siu, T. J. Peckham, S. Holdcroft, in *Fuel Cells II. Adv. Polym. Sci.* (Ed.: G.G. Scherer), Springer, Berlin, Heidelberg, **2008**, pp. 55–126.

[76] G. Maier, J. Meier-Haack, in *Fuel Cells II. Adv. Polym. Sci.* (Ed.: G.G. Scherer), Springer, Berlin, Heidelberg, **2008**, pp. 1–62.

[77] C. H. Fujimoto, M. A. Hickner, C. J. Cornelius, D. A. Loy, *Macromolecules* **2005**, *38*, 5010–5016. https://doi.org/10.1021/ma0482720.

[78] E. M. W. Tsang, Z. Zhang, A. C. C. Yang, Z. Shi, T. J. Peckham, R. Narimani, B. J. Frisken, S. Holdcroft, *Macromolecules* **2009**, *42*, 9467–9480. https://doi.org/10.1021/ma901740f.

[79] T. J. G. Skalski, B. Britton, T. J. Peckham, S. Holdcroft, *J. Am. Chem. Soc.* **2015**, *137*, 12223–12226. https://doi.org/10.1021/jacs.5b07865.

[80] M. Adamski, T. J. G. Skalski, S. Xu, M. Killer, E. M. Schibli, B. J. Frisken, S. Holdcroft, *Polym. Chem.* **2019**, *10*, 1668–1685. https://doi.org/10.1039/c8py01804a.

[81] M. Adamski, T. Skalski, E. M. Schibli, M. Killer, W. Yang, N. Peressin, B. J. Frisken, S. Holdcroft, *J. Memb. Sci.* **2020**, *595*, 117539. https://doi.org/10.1016/j.memsci.2019.117539.

[82] T. J. G. Skalski, M. Adamski, B. Britton, E. M. Schibli, T. J. Peckham, T. Weissbach, T. Moshisuki, S. Lyonnard, B. J. Frisken, S. Holdcroft, *ChemSusChem* **2018**, *11*, 4033–4043. https://doi.org/10.1002/cssc.201801965.

[83] C. Perrot, L. Gonon, M. Bardet, C. Marestin, A. Pierre-Bayle, G. Gebel, *Polymer* **2009**, *50*, 1671–1681. https://doi.org/10.1016/j.polymer.2008.12.051.

[84] L. Gonon, A. Morin, C. Perrot, G. Gebel, C. Marestin, *J. Power Sources* **2009**, *195*, 493–502. https://doi.org/10.1016/j.jpowsour.2009.08.001.

[85] J. K. Kallitsis, H. Naarmann, *Synth. Met.* **1991**, *44*, 247–257. https://doi.org/10.1016/0379-6779(91)91813-P.

[86] A. J. Berresheim, M. Müller, K. Müllen, *Chem. Rev.* **1999**, *99*, 1747–1785. https://doi.org/10.1021/cr970073+.

[87] J. K. Stille, G. K. Noren, *Macromolecules* **1972**, *5*, 49–55. https://doi.org/10.1021/ma60025a013.

[88] M. Remmers, B. Müller, K. Martin, H. J. Räder, W. Köhler, *Macromolecules* **1999**, *32*, 1073–1079. https://doi.org/10.1021/ma981260s.

[89] A. Abdulkarim, F. Hinkel, D. Jänsch, J. Freudenberg, F. E. Golling, K. Müllen, *J. Am. Chem. Soc.* **2016**, *138*, 16208–16211. https://doi.org/10.1021/jacs.6b10254.

[90] T. Yamamoto, Y. Hayashi, A. Yamamoto, *Bull. Chem. Soc. Jpn.* **1978**, *51*, 2091–2097. https://doi.org/10.1246/bcsj.51.2091.

[91] A. D. Schlüter, G. Wegner, *Acta Polym.* **1993**, *44*, 59–69. https://doi.org/10.1002/actp.1993.010440201.

[92] H. Kim, M. H. Litt, *Macromolecules* **2003**, *11*, 458–466. https://doi.org/10.1007/BF03218976.

[93] M. Litt, S. Granados-Focil, J. Kang, K. Si, R. Wycisk, *ECS Trans.* **2010**, *33*, 695–710. https://doi.org/10.1149/1.3484565.

[94] S. Granados-focil, M. Litt, *Prepr. Pap.-Am. Chem. Soc., Div. Fuel Chem.* **2004**, *49*, 528–529.

[95] K. Si, R. Wycisk, D. Dong, K. Cooper, M. Rodgers, P. Brooker, D. Slattery, M. Litt, *Macromolecules* **2013**, *46*, 422–433. https://doi.org/10.1021/ma301875n.

[96] J. K. Stille, F. W. Harris, R. O. Rakutis, H. Mukamal, *Polym. Lett.* **1966**, *4*, 791–793.

[97] K. Goto, I. Rozhansk, Y. Yamakawa, T. Otsuki, Y. Naito, *Polym. J.* **2009**, *41*, 95–104. https://doi.org/10.1295/polymj.PJ2008220.

[98] M. Li, G. Zhang, S. Xu, C. Zhao, M. Han, L. Zhang, H. Jiang, Z. Liu, H. Na, *J. Power Sources* **2014**, *255*, 101–107. https://doi.org/10.1016/j.jpowsour.2013.12.116.

[99] D. Plackett, A. Siu, Q. Li, C. Pan, J. O. Jensen, S. F. Nielsen, A. A. Permyakova, N. J. Bjerrum, *J. Memb. Sci.* **2011**, *383*, 78–87. https://doi.org/10.1016/j.memsci.2011.08.038.

[100] M. Rodgers, Y. Yang, S. Holdcroft, *Eur. Polym. J.* **2006**, *42*, 1075–1085. https://doi.org/10.1016/j.eurpolymj.2005.11.011.

[101] J. Miyake, R. Taki, T. Mochizuki, R. Shimizu, R. Akiyama, M. Uchida, K. Miyatake, *Sci. Adv.* **2017**, *3*, eaao0476, 1–8. https://doi.org/10.1126/sciadv.aao0476.

[102] K. Shiino, J. Miyake, K. Miyatake, *Chem. Commun.* **2019**, *55*, 7073–7076. https://doi.org/10.1039/c9cc02475a.

[103] K. Sonogashira, Y. Tohda, N. Hagihara, *Tetrahedron Lett.* **1975**, *16*, 4467–4470.

[104] R. Chinchilla, C. Nájera, *Chem. Rev.* **2007**, *107*, 874–922. https://doi.org/10.1021/cr050992x.

[105] R. Chinchilla, C. Nájera, *Chem. Soc. Rev.* **2011**, *40*, 5084–5121. https://doi.org/10.1039/c1cs15071e.

[106] P. Bertus, F. Fécourt, C. Bauder, P. Pale, *New J. Chem.* **2004**, *28*, 12–14. https://doi.org/10.1039/b309094a.

[107] V. W. Heitz, R. Ullrich, *Die Makromol. Chemie* **1966**, *98*, 29–41.

[108] N. Sakai, K. C. Brennan, L. A. Weiss, S. Matile, *J. Am. Chem. Soc.* **1997**, *119*, 8726–8727. https://doi.org/10.1021/ja971513h.

[109] J. Hassan, M. Sévignon, C. Gozzi, E. Schulz, M. Lemaire, *Chem. Rev.* **2002**, *102*, 1359–1469. https://doi.org/10.1021/cr000664r.

[110] T. Kawase, A. Konishi, Y. Hirao, K. Matsumoto, H. Kurata, T. Kubo, *Chem. - A Eur. J.* **2009**, *15*, 2653–2661. https://doi.org/10.1002/chem.200802471.

[111] T. Matsuda, K. Kato, T. Goya, S. Shimada, M. Murakami, *Chem. - A Eur. J.* **2016**, *22*, 1941–1943. https://doi.org/10.1002/chem.201504937.

[112] P. G. M. Wuts, T. W. Greene, in *Greene's Prot. Groups Org. Synth.*, John Wiley & Sons, Hoboken, NJ, USA, **2006**.

[113] P. G. M. Wuts, in *Greene's Prot. Groups Org. Synth.*, John Wiley & Sons, Hoboken, NJ, USA, **2014**, pp. 1194–1223.

[114] P. E. Dietze, *J. Org. Chem.* **1993**, *58*, 5653–5662. https://doi.org/10.1021/jo00073a025.

[115] T. X. Neenan, G. M. Whitesides, *J. Org. Chem.* **1988**, *53*, 2489–2496. https://doi.org/10.1021/jo00246a018.

[116] D. F. Perepichka, S. Jeeva, *Chem. Engineering News* **2010**, *88*, 1–2.

[117] H. Min, T. Palani, K. Park, J. Hwang, S. Lee, *J. Org. Chem.* **2014**, *79*, 6279–6285. https://doi.org/10.1021/jo501089k.

[118] W. Zhang, J. Zhang, Y. Liu, Z. Xu, *Synlett* **2013**, *24*, 2709–2714. https://doi.org/10.1055/s-0033-1338983.

[119] K. W. Chi, M. S. Yusubov, V. D. Filimonov, *Synth. Commun.* **1994**, *24*, 2119–2122. https://doi.org/10.1080/00397919408010224.

[120] J. Yang, H. Zhu, Y. Huang, W. Huang, W. Wang, *RSC Adv.* **2016**, *6*, 100067–100071. https://doi.org/10.1039/c6ra22677a.

[121] V. Rogatchov, V. Filimonov, M. Yusubov, *Synthesis* **2004**, *2001*, 1001–1003. https://doi.org/10.1055/s-2001-14558.

[122] M. S. Yusubov, V. D. Filimonov, *Synthesis* **1991**, 131–132.

[123] S. Baskaran, J. Das, S. Chandrasekaran, *J. Org. Chem.* **1989**, *54*, 5182–5184. https://doi.org/10.1021/jo00282a042.

[124] X. Yu, N. Guttenberger, E. Fuchs, M. Peters, H. Weber, R. Breinbauer, *ACS Comb. Sci.* **2015**, *17*, 682–690. https://doi.org/10.1021/acscombsci.5b00107.

[125] K. Omura, D. Swern, *Tetrahedron* **1978**, *34*, 1651–1660. https://doi.org/10.1016/0040-4020(78)80197-5.

[126] A. J. Mancuso, S. L. Huang, D. Swern, *J. Org. Chem.* **1978**, *43*, 2480–2482. https://doi.org/10.1021/jo00406a041.

[127] A. J. Mancuso, D. S. Brownfain, D. Swern, *J. Org. Chem.* **1979**, *44*, 4148–4150. https://doi.org/10.1021/jo01337a028.

[128] W. H. Brown, B. L. Iverson, E. V. Anslyn, C. S. Foote, in *Org. Chem.*, Mary Finch, Belmonth, CA, **2014**.

[129] O. Diels, K. Alder, *Justus Liebigs Ann. Chem.* **1928**, *460*, 98–122.

[130] W. H. Brown, B. L. Iverson, E. V. Anslyn, C. S. Foote, *Organic Chemistry*, Mary Finch, Belmonth, CA, **2014**.

[131] B. P. Stark, A. J. Duke, *Extrusion Reactions*, Pergamon Press, Oxford, **1967**. https://doi.org/10.1055/sos-sd-010-00834.

[132] F. A. Carey, R. J. Sundberg, *Advanced Organic Chemistry Part A: Structure and Mechanisms*, Springer, Berlin, Heidelberg, **2007**. https://doi.org/10.1021/ed065pA139.2.

[133] T. D. W. Clardige, *High-Resolution NMR Techniques in Organic Chemistry*, Elsevier Ltd, Oxford, **2009**. https://doi.org/10.1021/ja004717y.

[134] C. Zhao, C. Anklin, N. L. Greenbaum, in *Methods Enzymol.* (Ed.: D.H. Burke-Aguero), Academic Press, **2014**, pp. 267–285. https://doi.org/10.1016/B978-0-12-801122-5.00012-X.

[135] K. Kloiber, R. Spitzer, M. Tollinger, R. Konrat, C. Kreutz, *Nucleic Acids Res.* **2011**, *39*, 4340–4351. https://doi.org/10.1093/nar/gkq1361.

[136] M. P. Latham, G. R. Zimmermann, A. Pardi, *J. Am. Chem. Soc.* **2009**, *131*, 5052–5053. https://doi.org/10.1021/ja900695m.

[137] H. C. Gaede, in *Mod. NMR Spectrosc. Educ.* (Eds.: D. Rovnyak, R. Stockland Jr), American Chemical Society, Washington, DC, **2007**, pp. 176–189. https://doi.org/10.1021/bk-2007-0969.ch013.

[138] C. Karunakaran, P. Santharaman, M. Balamurugan, in *Spin Reson. Spectrosc. - Princ. Appl.*, Elsevier Inc., Amsterdam, Netherlands, **2018**, pp. 49–110. https://doi.org/10.1016/B978-0-12-813608-9.00002-2.

[139] G. Scalmani, M. J. Frisch, *J. Chem. Phys.* **2010**, *132*, 114110. https://doi.org/10.1063/1.3359469.

[140] P. J. Stephens, F. J. Devlin, C. F. Chabalowski, M. J. Frisch, *J. Phys. Chem.* **1994**, *98*, 11623–11627. https://doi.org/10.1021/j100096a001.

[141] F. Weigend, R. Ahlrichs, *Phys. Chem. Chem. Phys.* **2005**, *7*, 3297–3305. https://doi.org/10.1039/b508541a.

[142] M. J. Frisch, G. W. Trucks, H. B. Schlegel, G. E. Scuseria, M. A. Robb, J. R. Cheeseman, G. Scalmani, V. Barone, G. A. Petersson, H. Nakatsuji, et al., **2016**.

[143] D. Rappoport, F. Furche, *J. Chem. Phys.* **2010**, *133*, 134015. https://doi.org/10.1063/1.3484283.

[144] S. Mori, H. G. Barth, *Size Exclusion Chromatography*, Springer, Berlin, Heidelberg, **2003**. https://doi.org/10.1007/978-3-540-46382-5.

[145] R. J. Young, P. A. Lovell, *Introduction to Polymers*, Chapman & Hall, London, **1991**.

[146] T. Williams, *J. Mater. Sci.* **1970**, *5*, 811–820. https://doi.org/10.1016/0160-9327(84)90124-8.

[147] C. Y. Kuo, T. Provder, in *Detect. Data Anal. Size Exclusion Chromatogr.*, American Chemical Society, Washington, DC, **1987**, pp. 2–28. https://doi.org/10.1021/bk-1987-0352.ch001.

[148] Malvern Instruments, *Principles of Triple Detection GPC / SEC*, **2015**.

[149] C. E. Carraher, *Polymer Chemistry*, Marcel Kekker, Inc., New York, **2003**. https://doi.org/10.1080/0020739X.2017.1409367.

[150] D. Roylance, *Mechanical Properties of Materials*, MIT, Cambridge, MA, **2008**. https://doi.org/10.1109/ICT.2007.4569446.

[151] Z. Xie, C. Song, B. Andreaus, T. Navessin, Z. Shi, J. Zhang, S. Holdcroft, *J. Electrochem. Soc.* **2006**, *153*, E173–E178. https://doi.org/10.1149/1.2258091.

[152] L. Liu, Z. Liu, W. Xu, H. Xu, D. Zhang, D. Zhu, *Tetrahedron* **2005**, *61*, 3813–3817. https://doi.org/10.1016/j.tet.2005.01.133.

[153] T. D. Schafer, Laurel L. and Nitschke, Jonathan R. and Mao, Shane S. H. and Liu, Feng-Q. and Harder, Gabriele and Haufe, Markus and Tilley, *Electrochemistry* **2002**, *8*, 74–83. https://doi.org/10.1002/1521-3765(20020104)8:1<74::AID-CHEM74>3.0.CO;2-P.

[154] C. Röben, J. A. Souto, E. C. Escudero-Adán, K. Muñiz, *Org. Lett.* **2013**, *15*, 1008–1011. https://doi.org/10.1021/ol3034884.

[155] J. G. Schantl, in *Adv. Heterocycl. Chem.* (Ed.: A.R. Katritzky), Academic Press, **2010**, pp. 185–207. https://doi.org/10.1016/S0065-2725(10)09906-X.

[156] D. Casarini, E. Foresti, F. Gasparrini, L. Lunazzi, D. Macciantelli, D. Misiti, C. Villani, *J. Org. Chem.* **1993**, *58*, 5674–5682. https://doi.org/10.1021/jo00073a028.

[157] J. Jeener, B. H. Meier, P. Bachmann, R. R. Ernst, *J. Chem. Phys.* **1979**, *71*, 4546–4553. https://doi.org/10.1063/1.438208.

[158] H. N. Cheng, T. Asakura, A. D. English, Eds. , *NMR Spectroscopy of Polymers: Innovative Strategies for Complex Macromolecules*, American Chemical Society, Washington, **2011**.

[159] F. A. Bovey, *High Resolution NMR of Macromolecules*, Academic Press, New York and London, **1972**.

[160] J. C. Randall, *NMR and Macromolecules: Sequence, Dynamic, and Domain Structure*, American Chemical Society, Washington, **1983**.

[161] Z. B. Shifrina, M. S. Averina, A. L. Rusanov, M. Wagner, K. Müllen, *Macromolecules* **2000**, *33*, 3525–3529. https://doi.org/10.1021/ma991369f.

[162] J. K. Stille, R. O. Rakutis, H. Mukamal, F. W. Harris, *Macromolecules* **1968**, *1*, 431–436. https://doi.org/10.1021/ma60005a012.

[163] K. Kunal, C. G. Robertson, S. Pawlus, S. F. Hahn, A. P. Sokolov, *Macromolecules* **2008**, *41*, 7232–7238. https://doi.org/10.1021/ma801155c.

[164] C. A. P. Joziasse, H. Veenstra, D. W. Grijpma, A. J. Pennings, *Macromol. Chem. Phys.* **1996**, *197*, 2219–2229. https://doi.org/10.1002/macp.1996.021970713.

[165] I. M. Ward, J. Sweeney, *Mechanical Properties of Solid and Liquid Polymers*, John Wiley & Sons, Hoboken, NJ, USA, **2013**. https://doi.org/10.1016/0025-5416(67)90014-6.

[166] X. Luo, A. Wright, T. Weissbach, S. Holdcroft, *J. Power Sources* **2018**, *375*, 442–451. https://doi.org/10.1016/j.jpowsour.2017.05.030.

Appendix A.

Supporting Information for Chapter 3

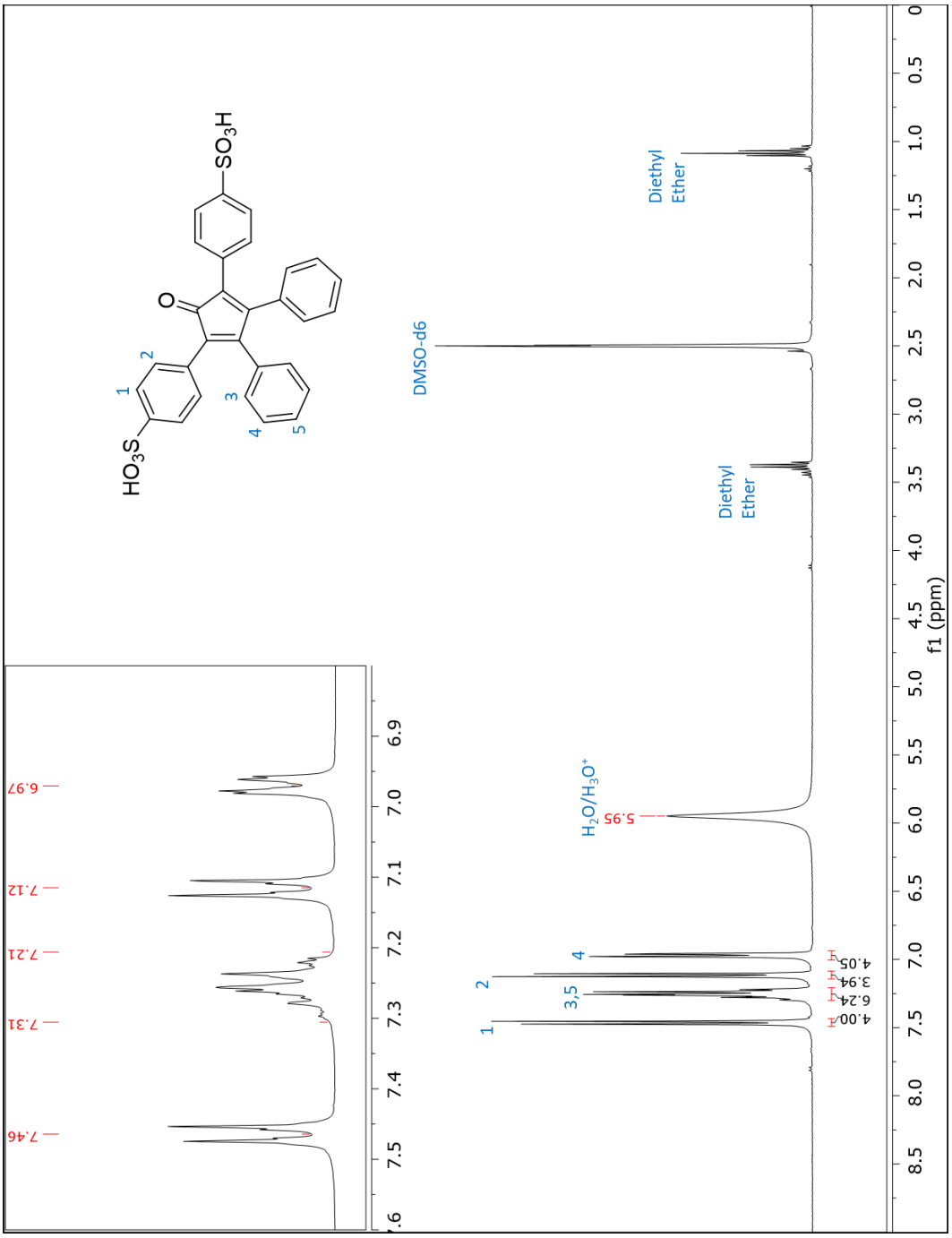

Figure A 1: *^{1}H NMR spectrum of 4,4'-(2-oxo-4,5-diphenylcyclopenta-3,5-diene-1,3-diyl)dibenzenesulfonic acid (sTC).*

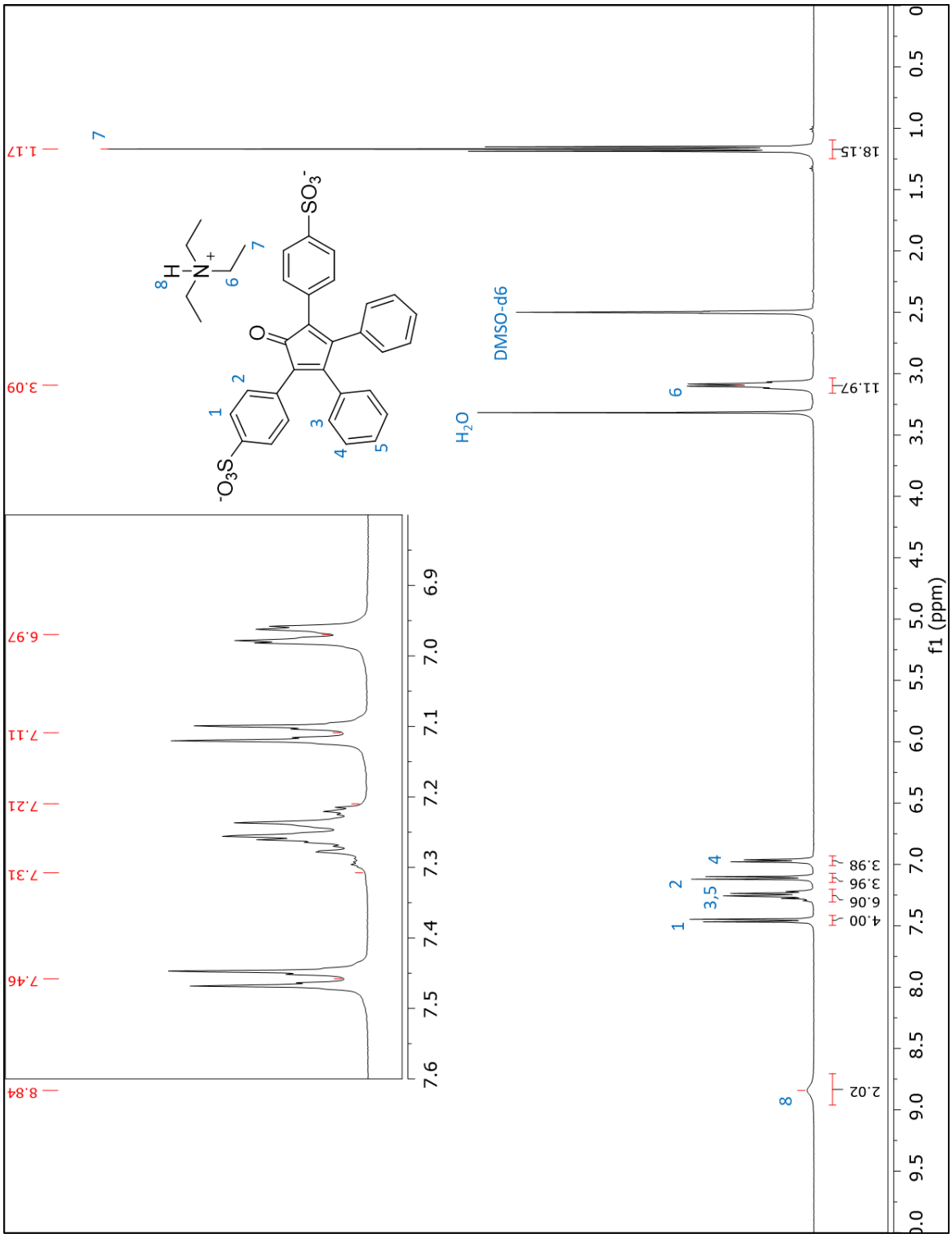

Figure A 2: *^{1}H NMR spectrum of 4,4'-(2-oxo-4,5-diphenylcyclopenta-3,5-diene-1,3-diyl)dibenzenesulfonate-triethylammonium salt (TEAsTC).*

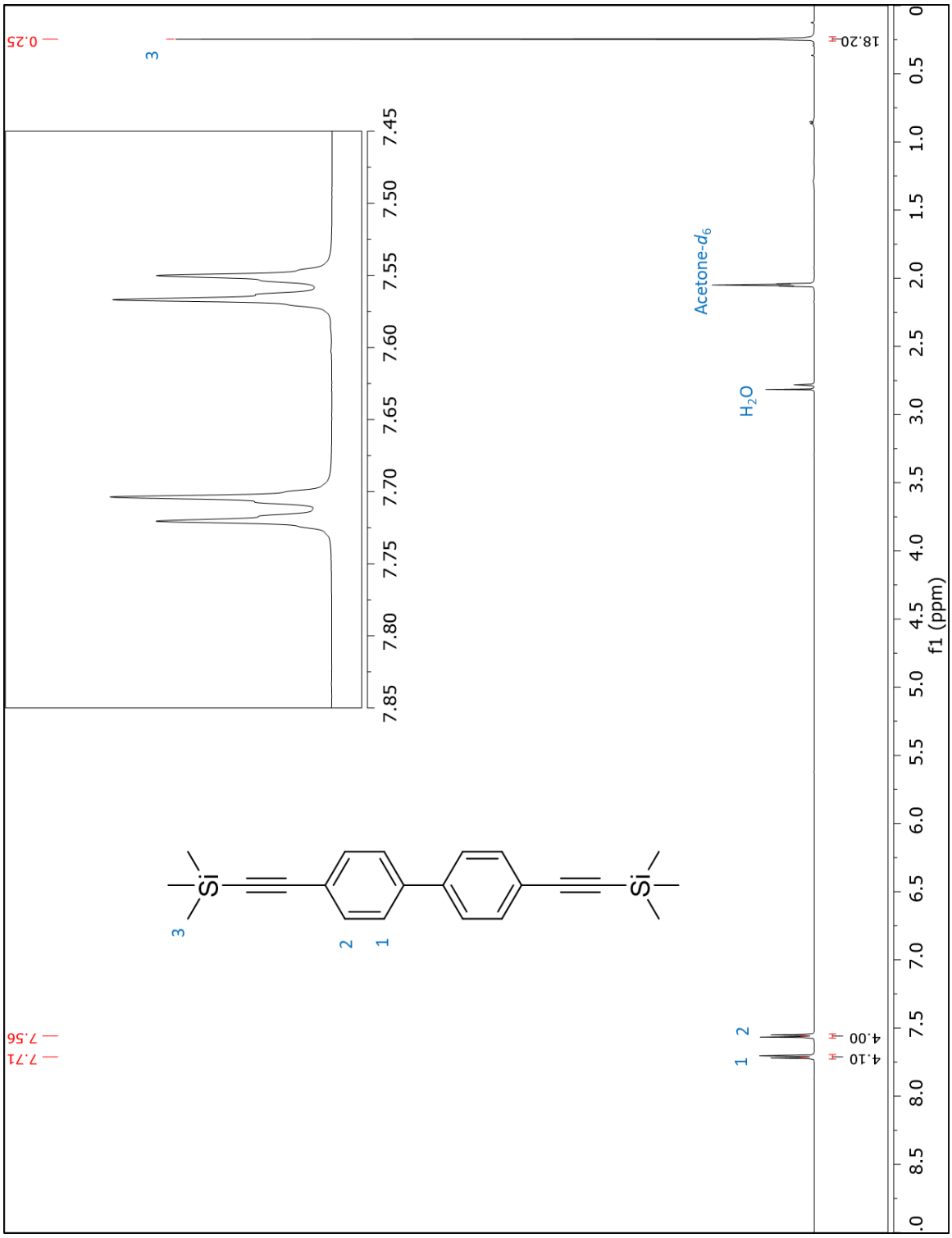

Figure A 3: *^{1}H NMR spectrum of 4,4'-bis-Trimethylsilylethynyl-1,1'-biphenyl.*

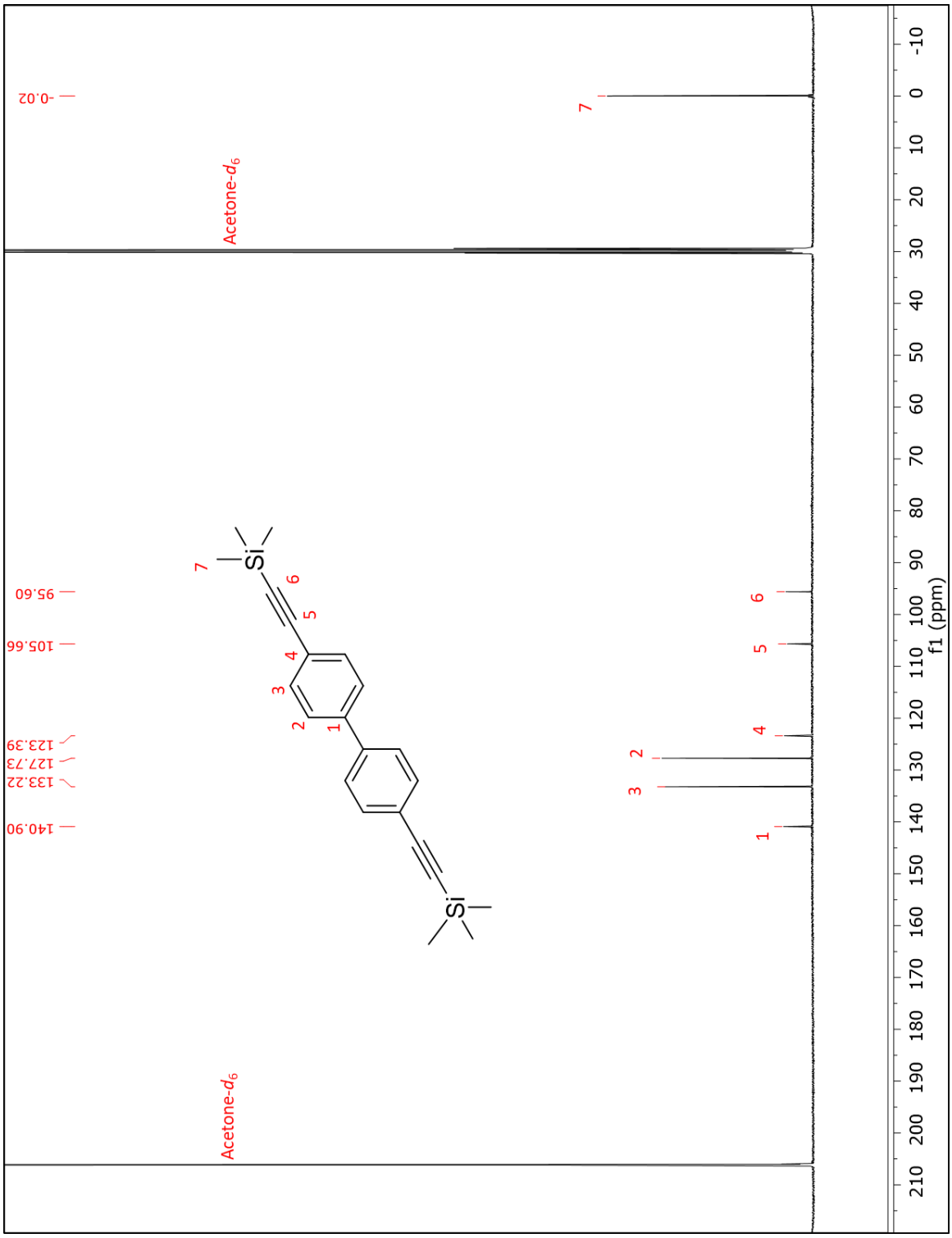

Figure A 4: *^{13}C NMR spectrum of 4,4'-bis-trimethylsilylethynyl-1,1'-biphenyl.*

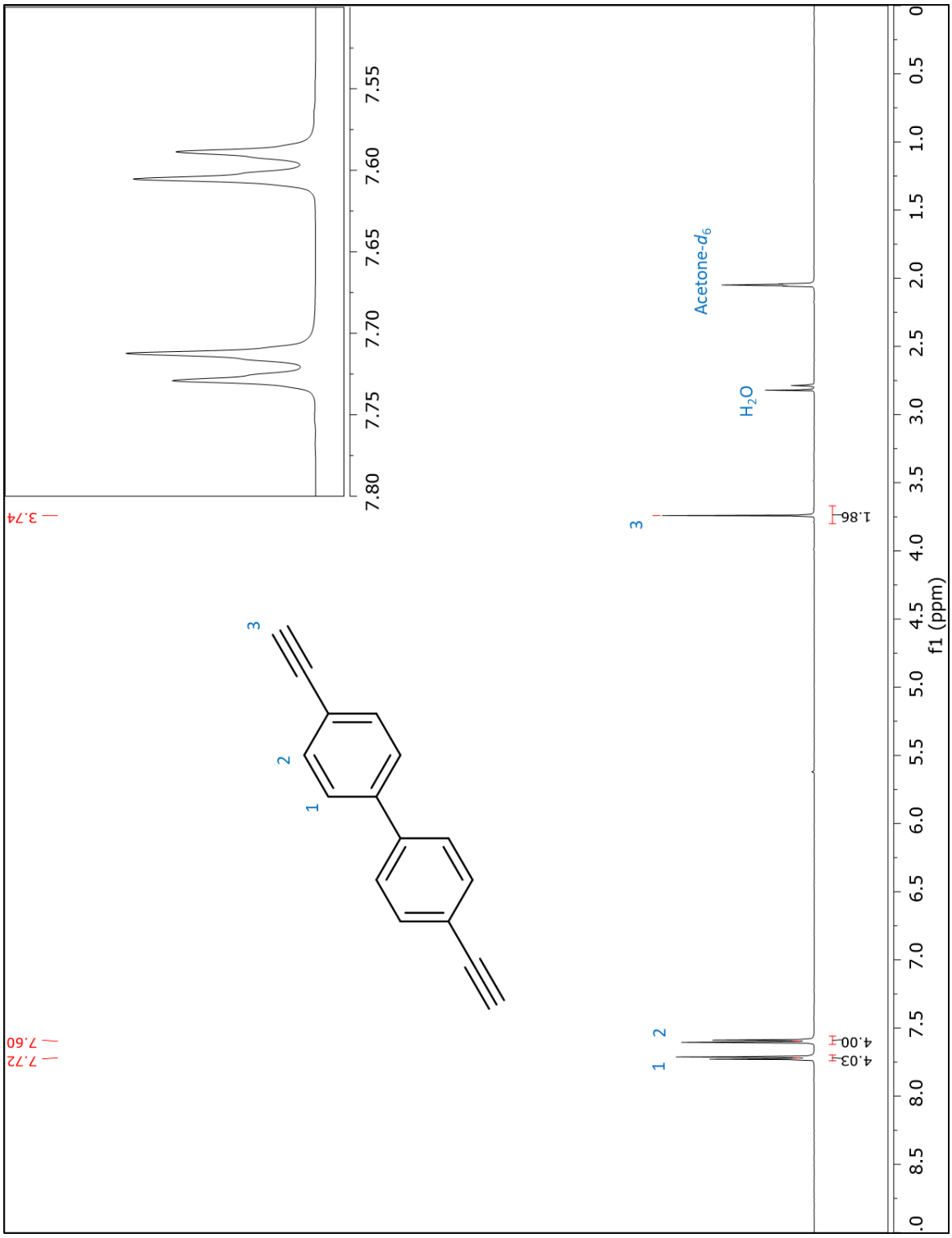

Figure A 5: *^{1}H NMR spectrum of 4,4'-diethynyl-1,1'-biphenyl (p-BPL).*

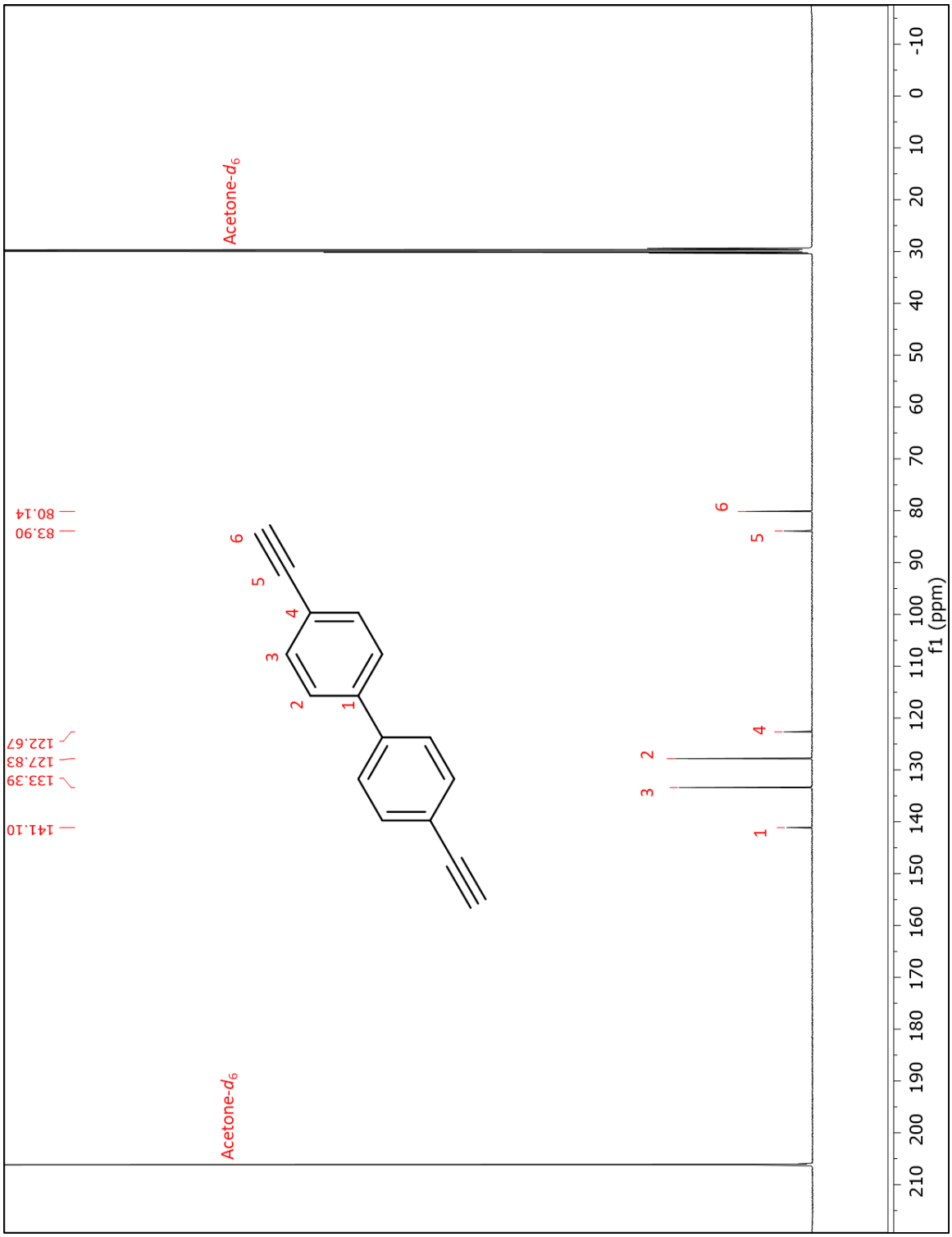

Figure A 6: *^{13}C NMR spectrum of 4,4'-diethynyl-1,1'-biphenyl (p-BPL).*

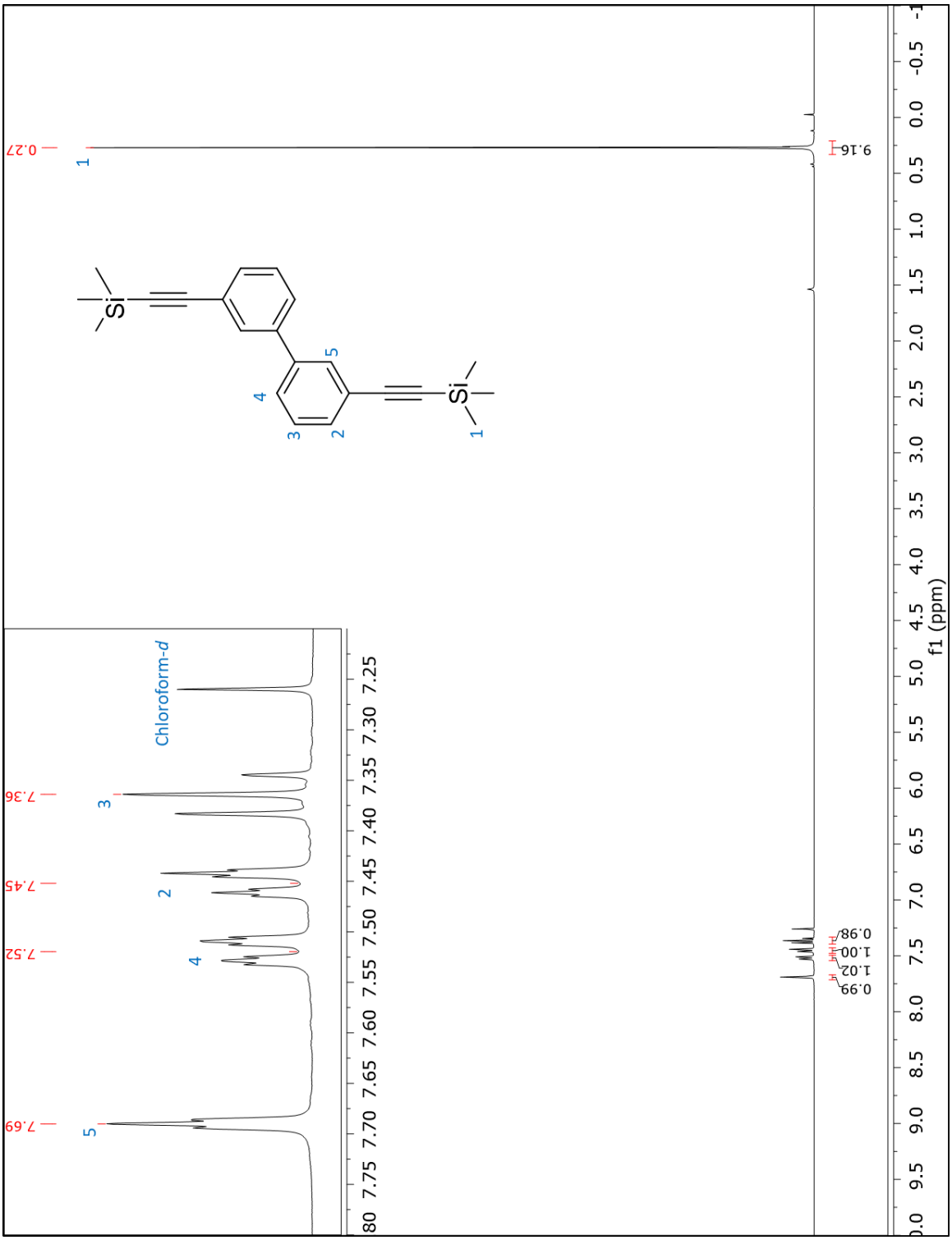

Figure A 7: *^{1}H NMR spectrum of 3,3'-bis-trimethylsilylethynyl-1,1'-biphenyl.*

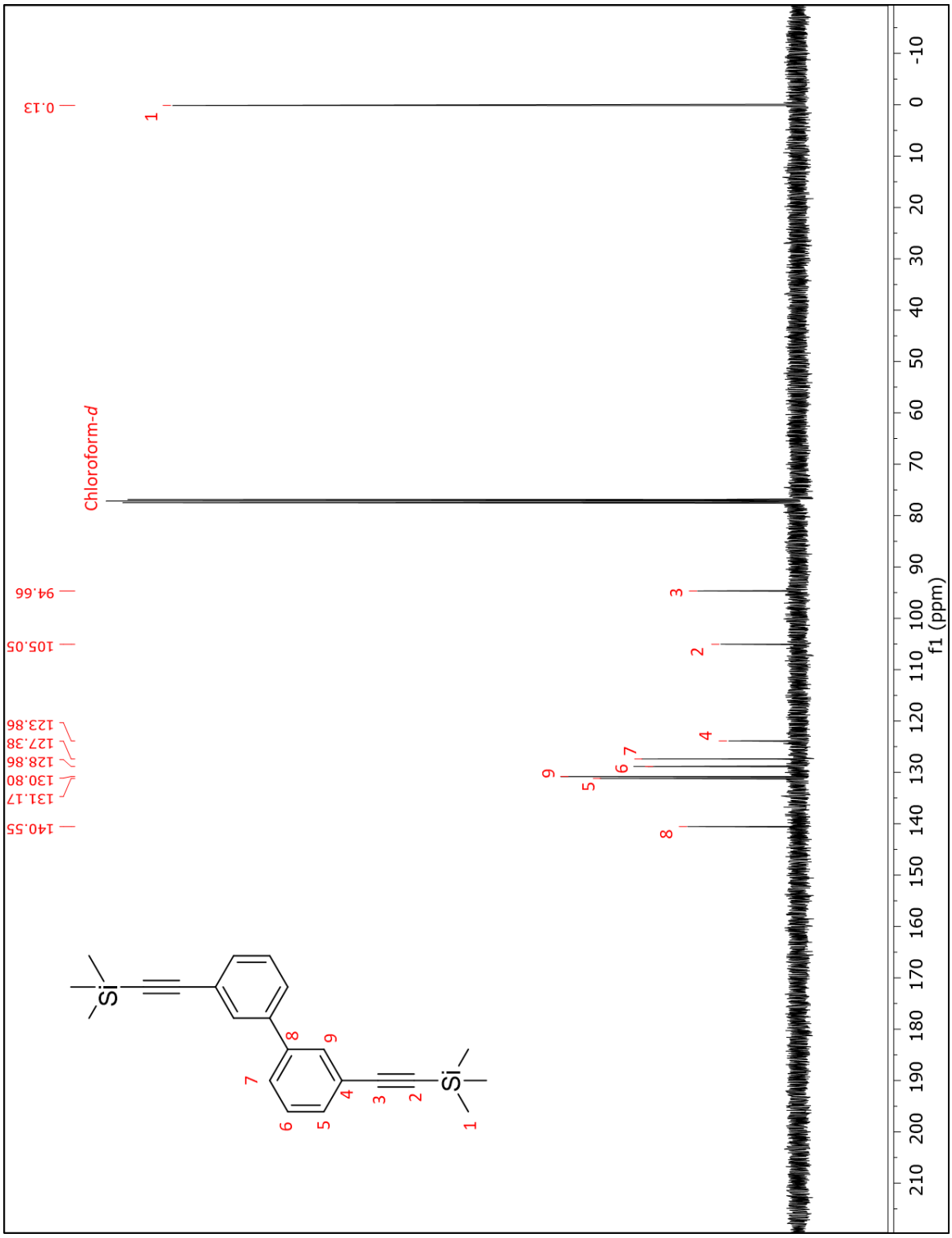

Figure A 8: *^{13}C NMR spectrum of 3,3'-bis-Trimethylsilylethynyl)-1,1'-biphenyl.*

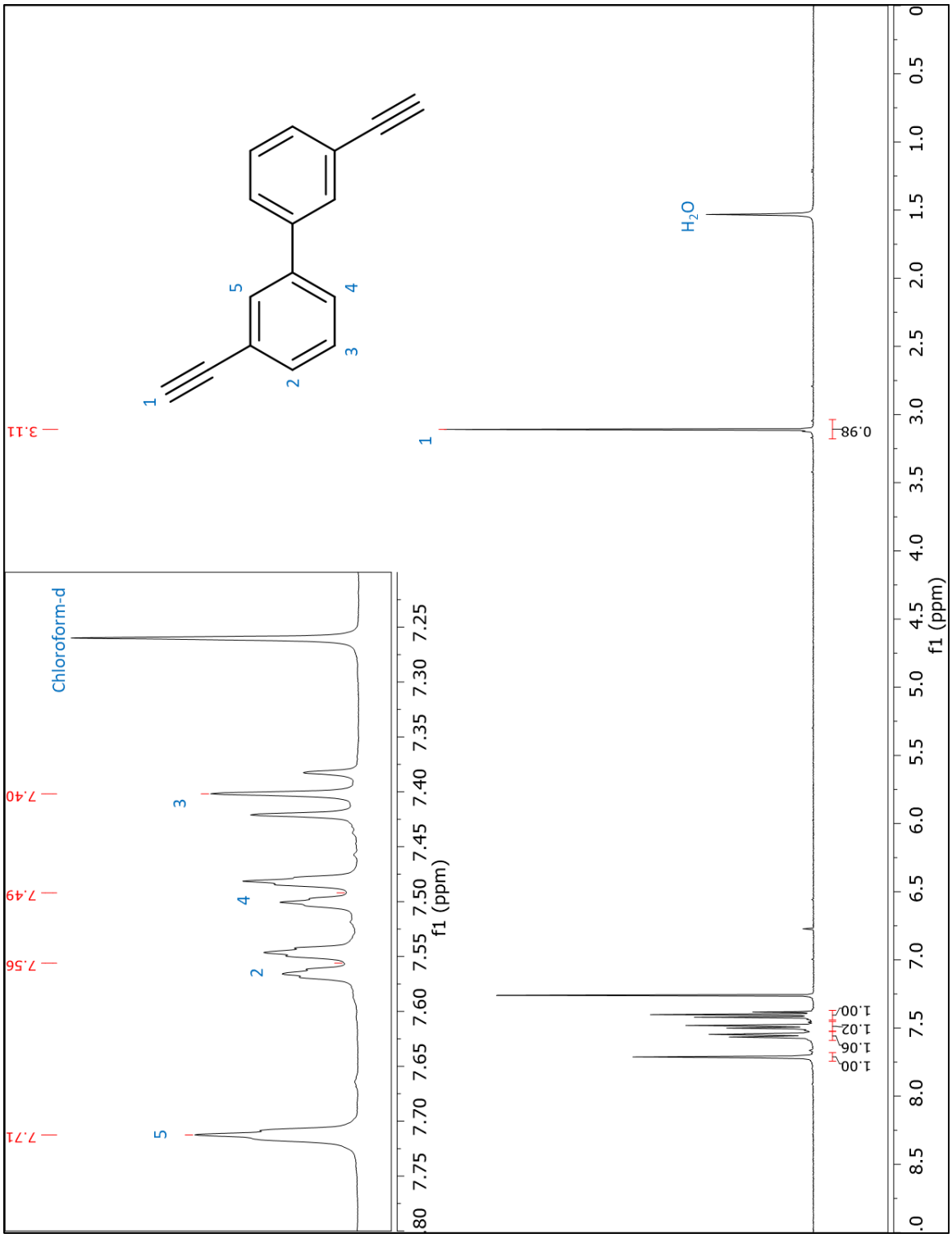

Figure A 9: *^{1}H NMR spectrum of 3,3'-diethynyl-1,1'-biphenyl (m-BPL).*

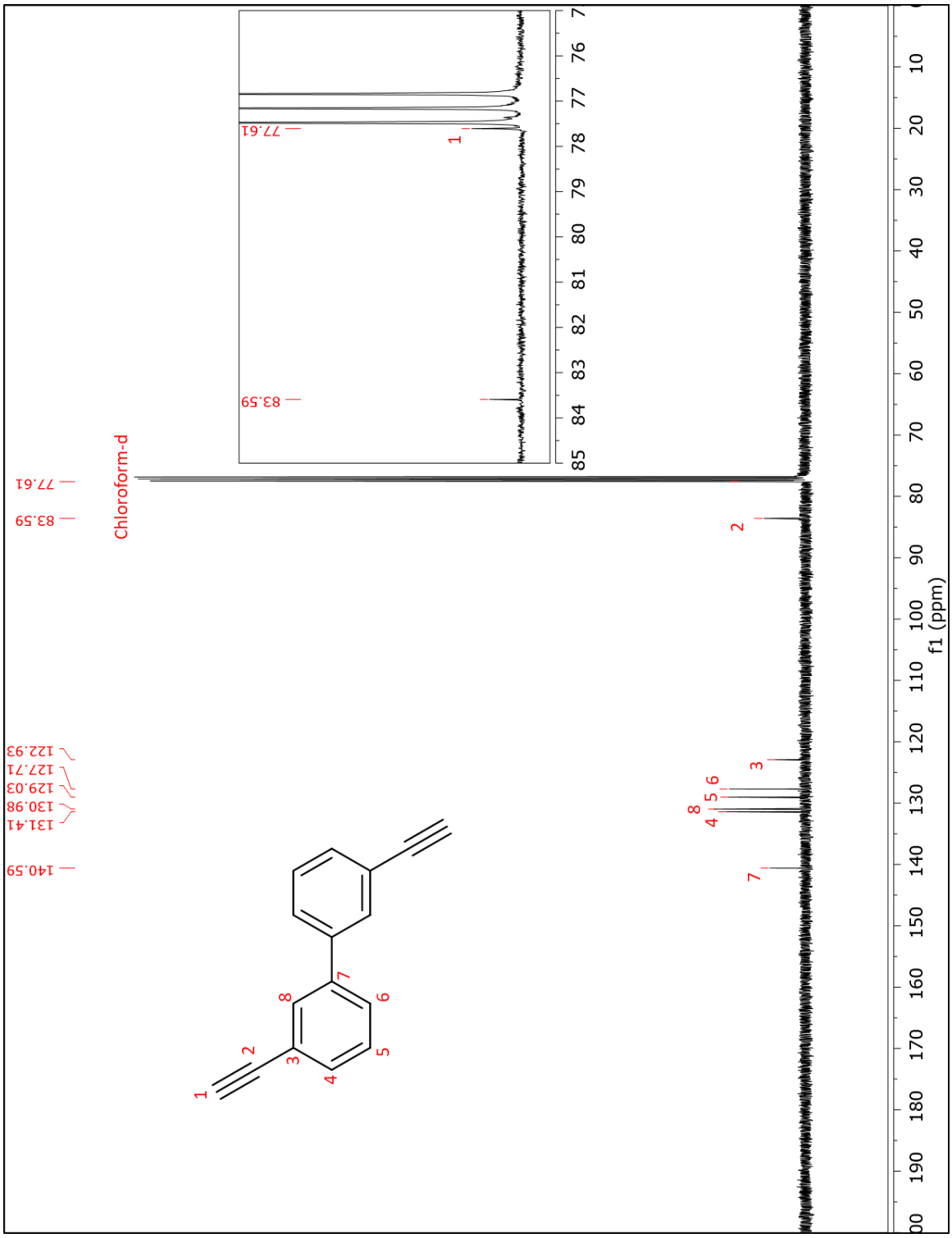

Figure A 10: *^{13}C NMR spectrum of 3,3'-diethynyl-1,1'-biphenyl (m-BPL).*

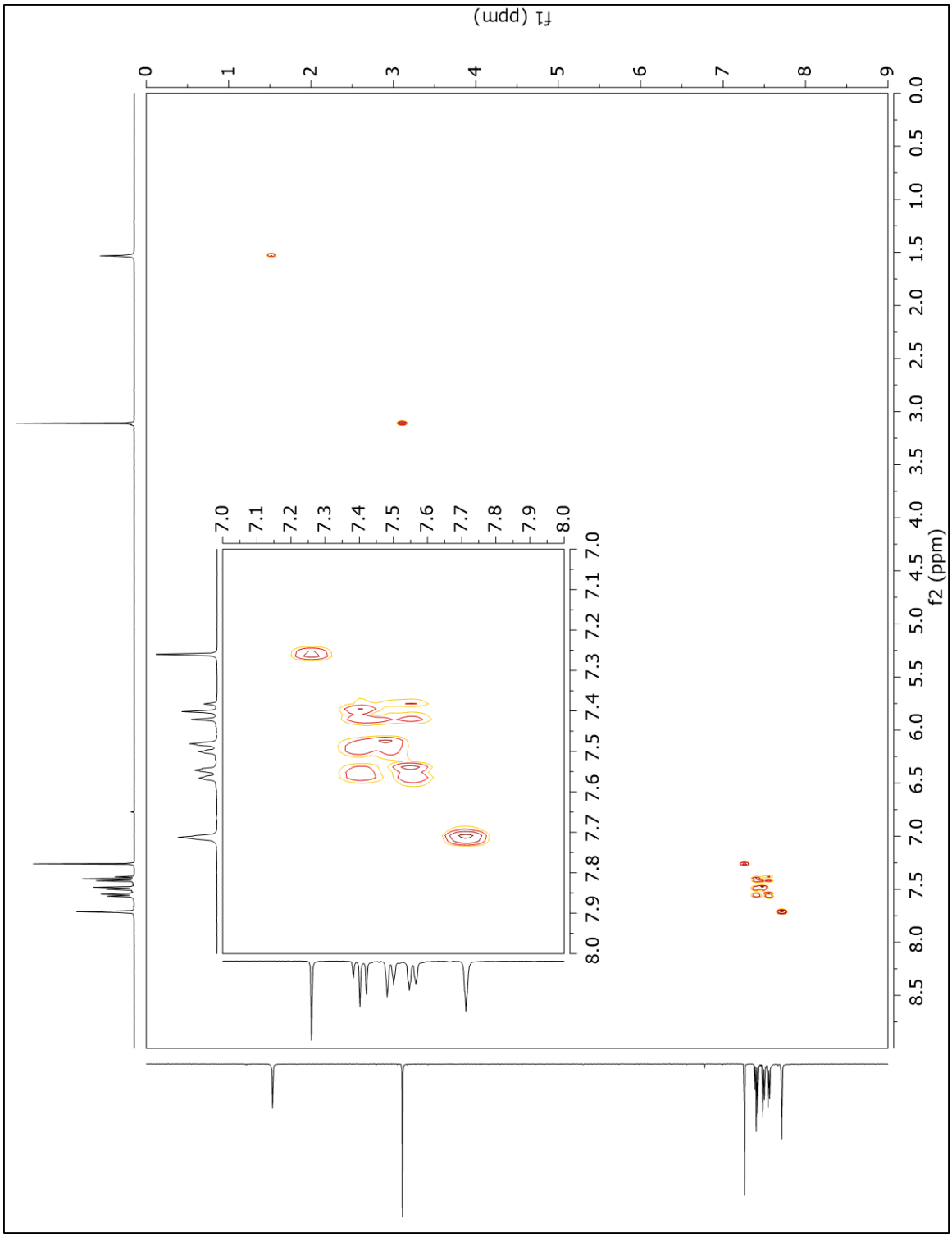

Figure A 11: *2D COSY NMR spectrum of 3,3'-diethynyl-1,1'-biphenyl (m-BPL).*

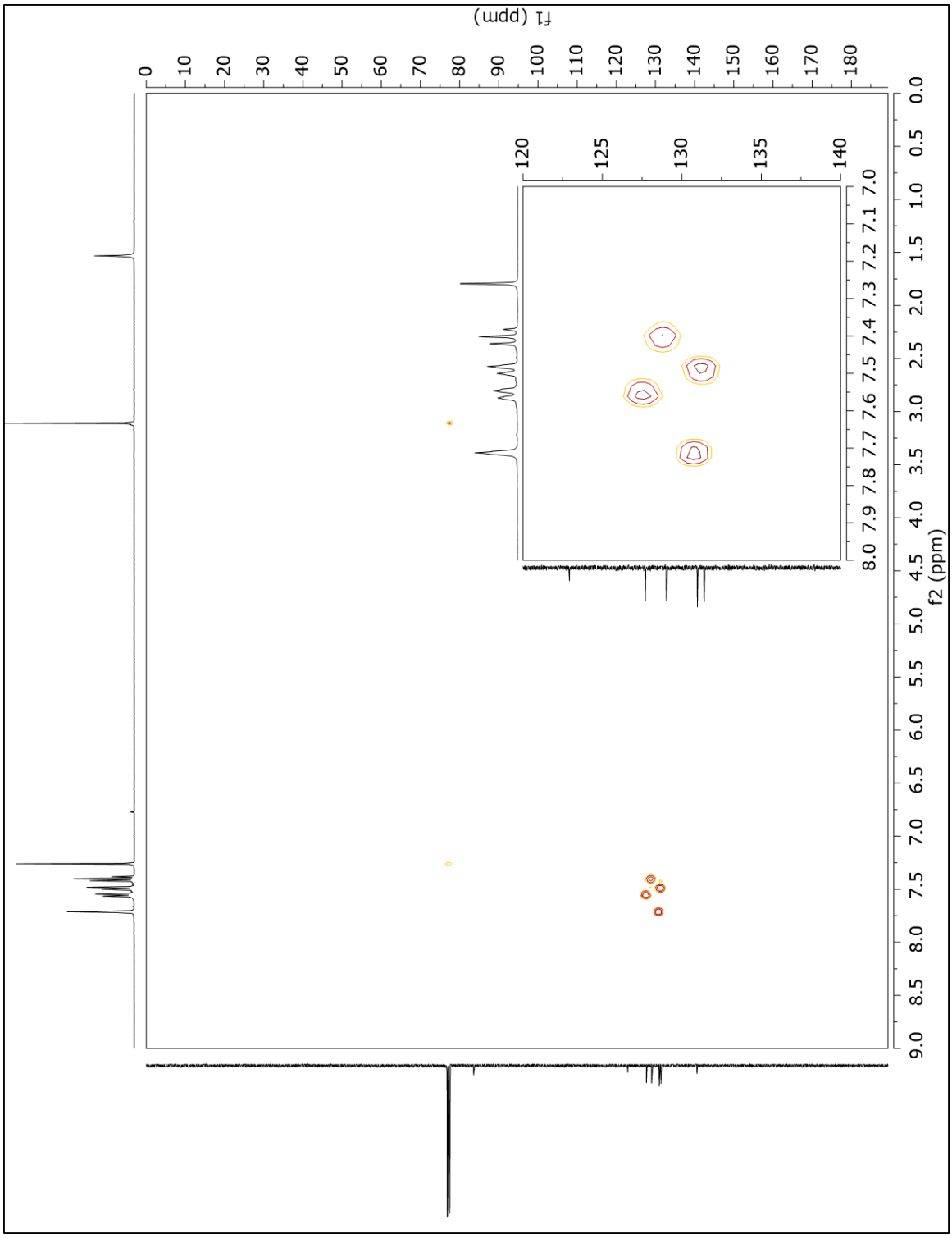

Figure A 12: *2D HSQC NMR spectrum of 3,3'-diethynyl-1,1'-biphenyl (m-BPL).*

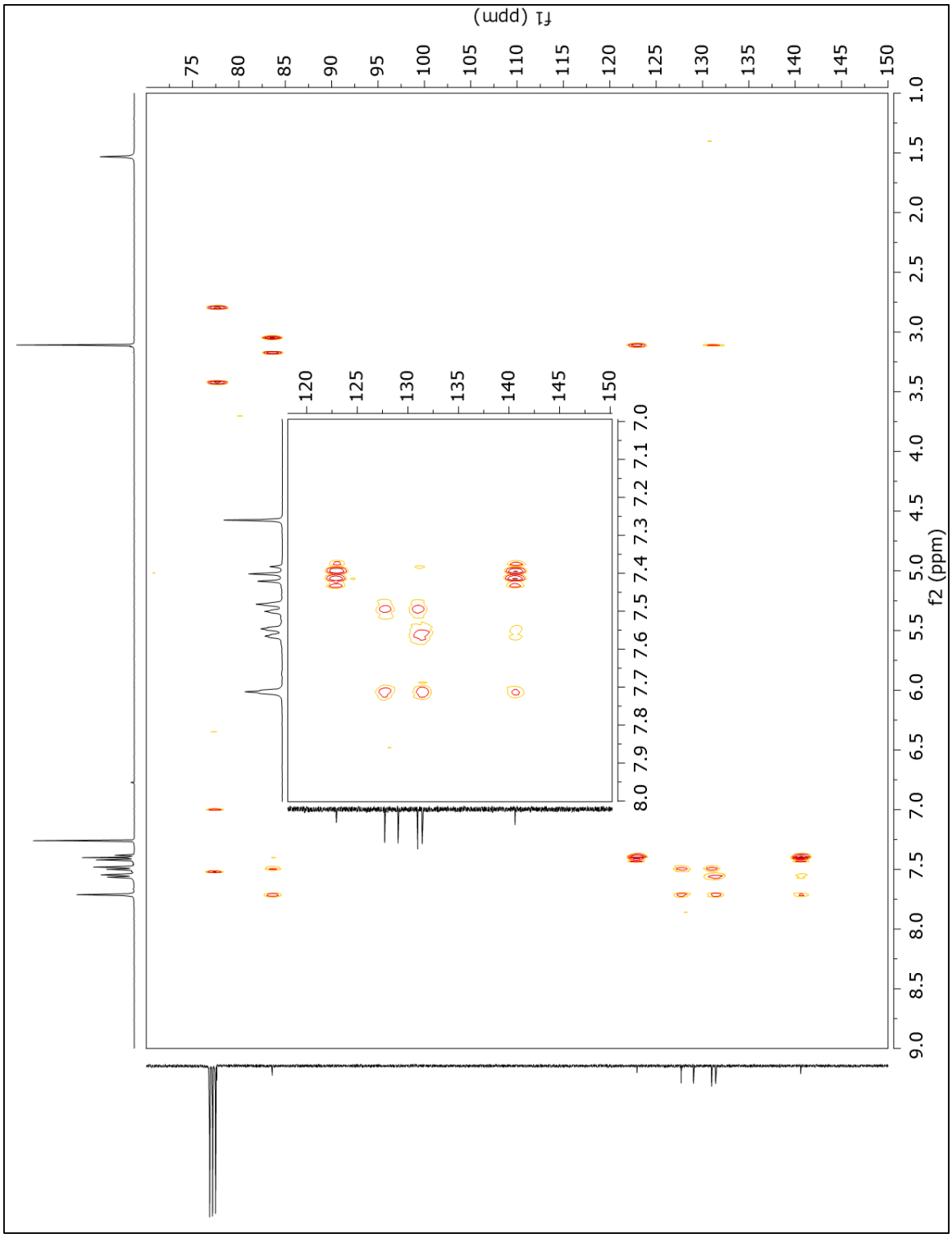

Figure A 13: *2D HMBC NMR spectrum of 3,3'-diethynyl-1,1'-biphenyl (m-BPL).*

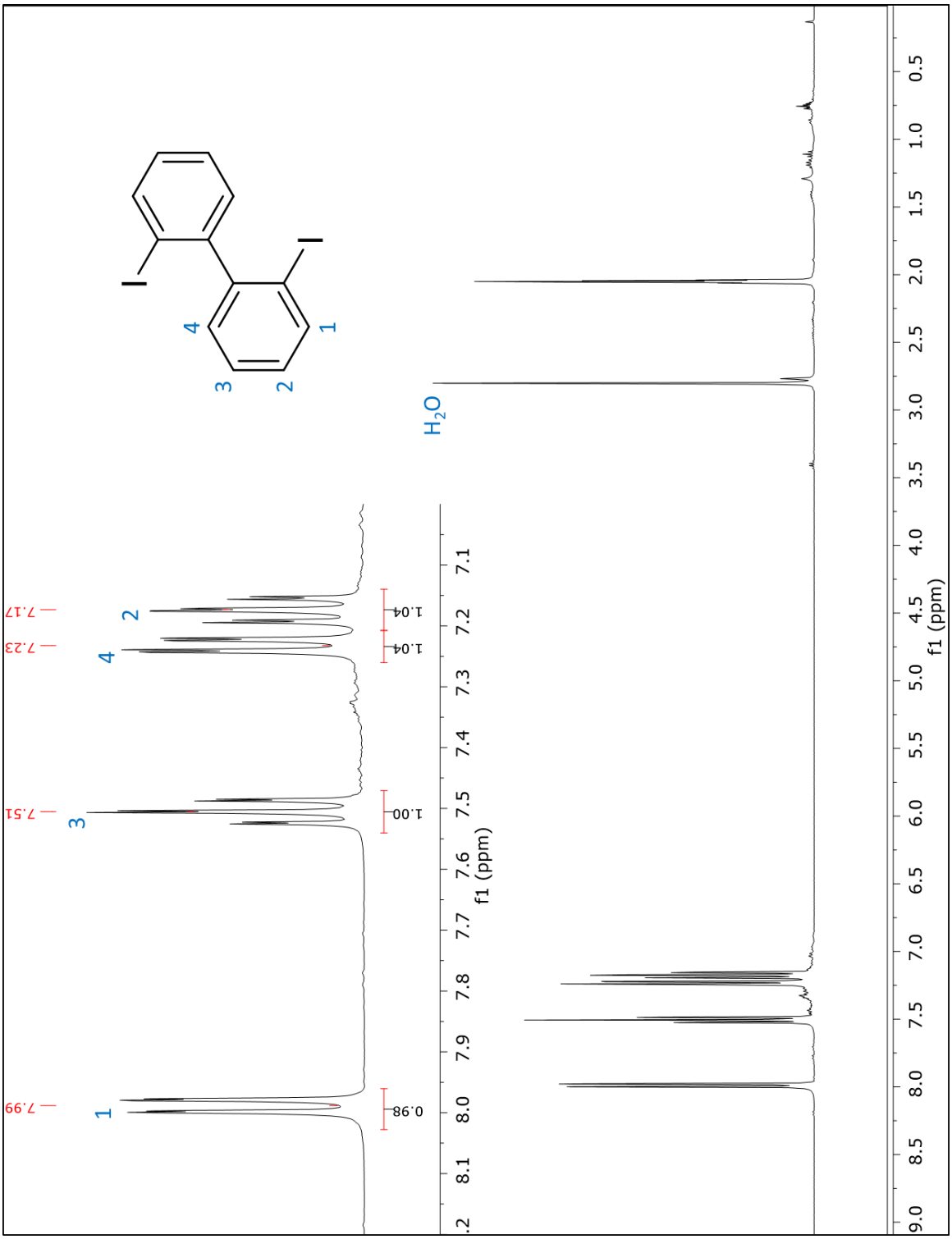

Figure A 14: *^{1}H NMR spectrum of 2,2'-diiodobiphenyl.*

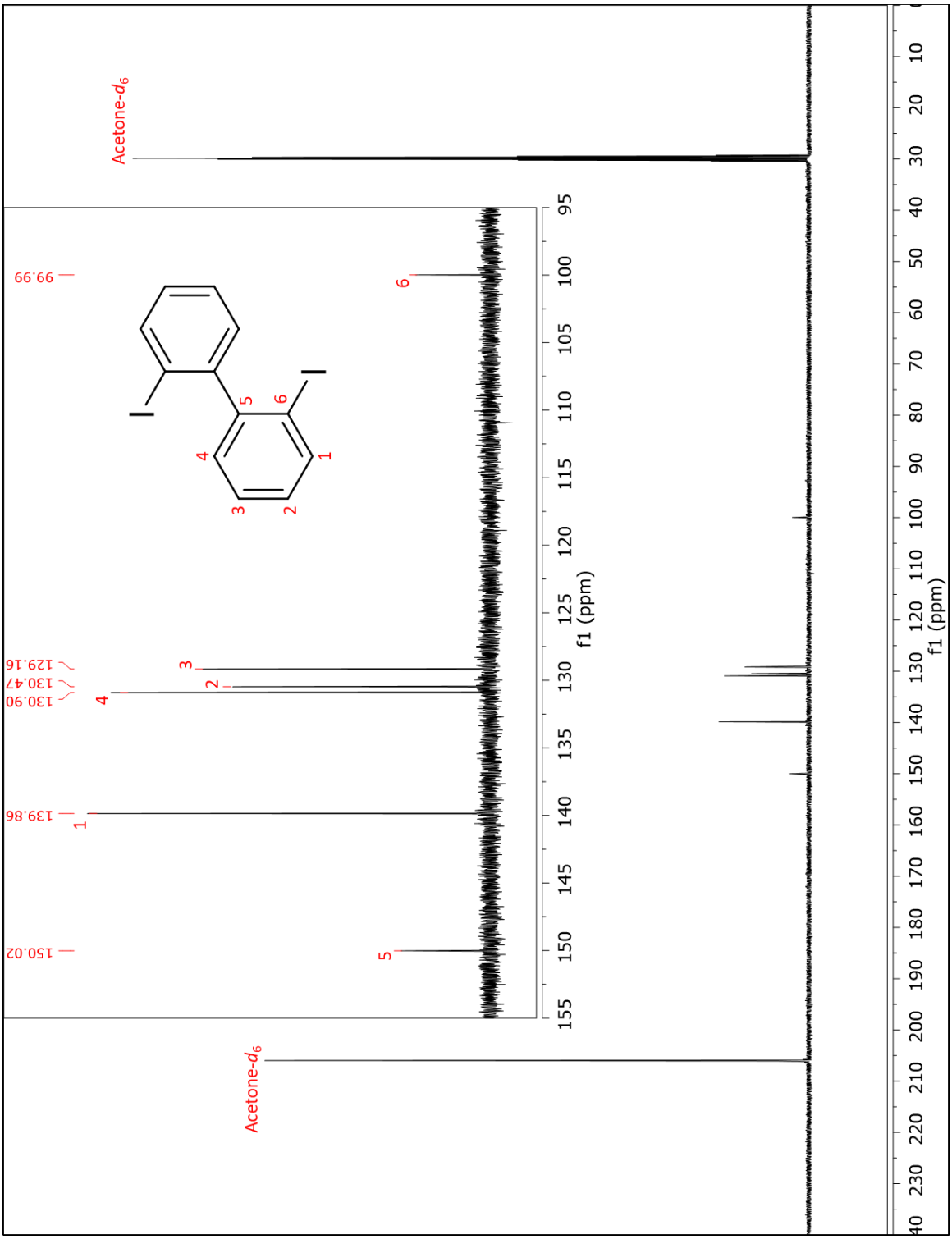

Figure A 15: *^{13}C NMR spectrum of 2,2'-diiodobiphenyl.*

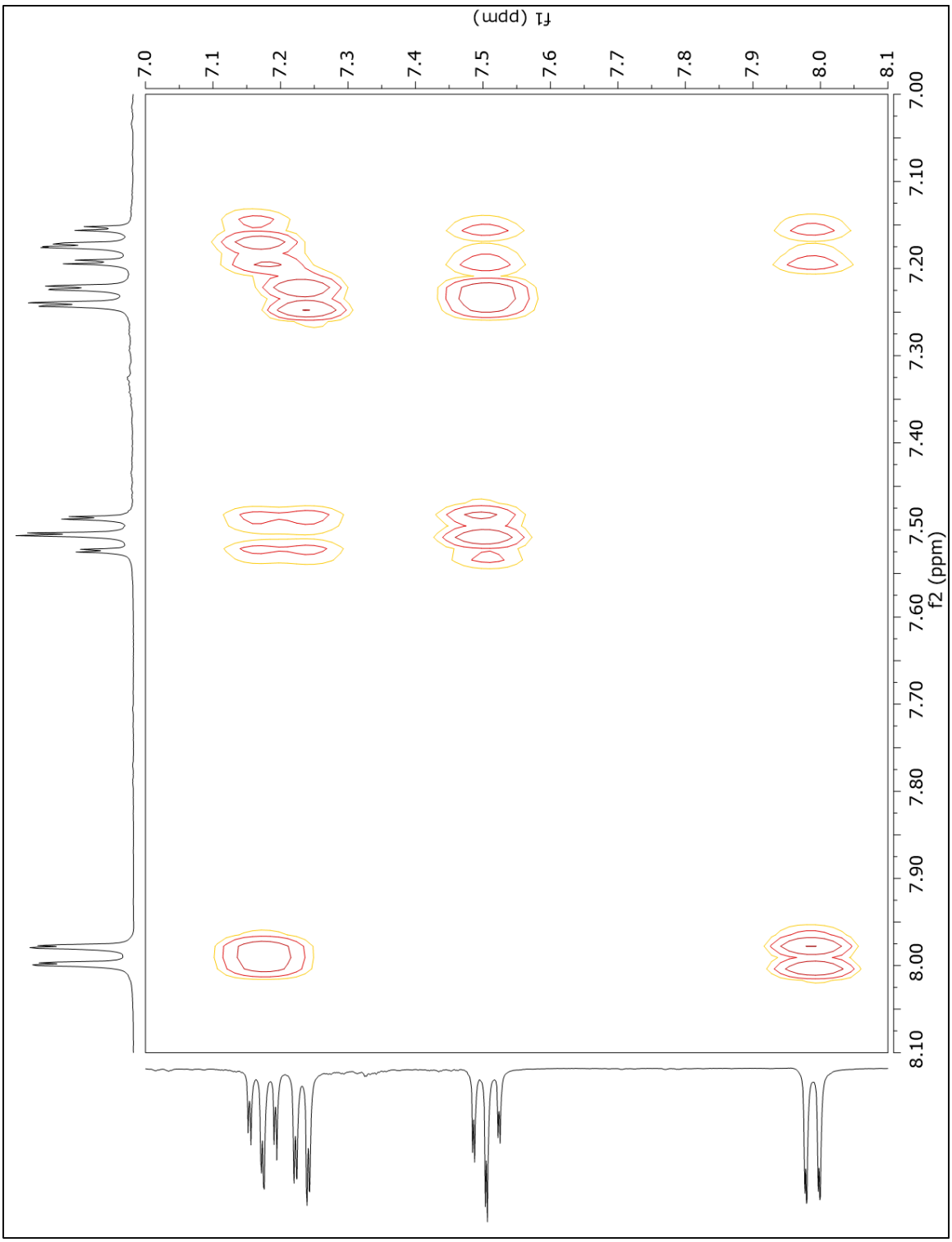

Figure A 16: *2D COSY NMR spectrum of 2,2'-diiodobiphenyl.*

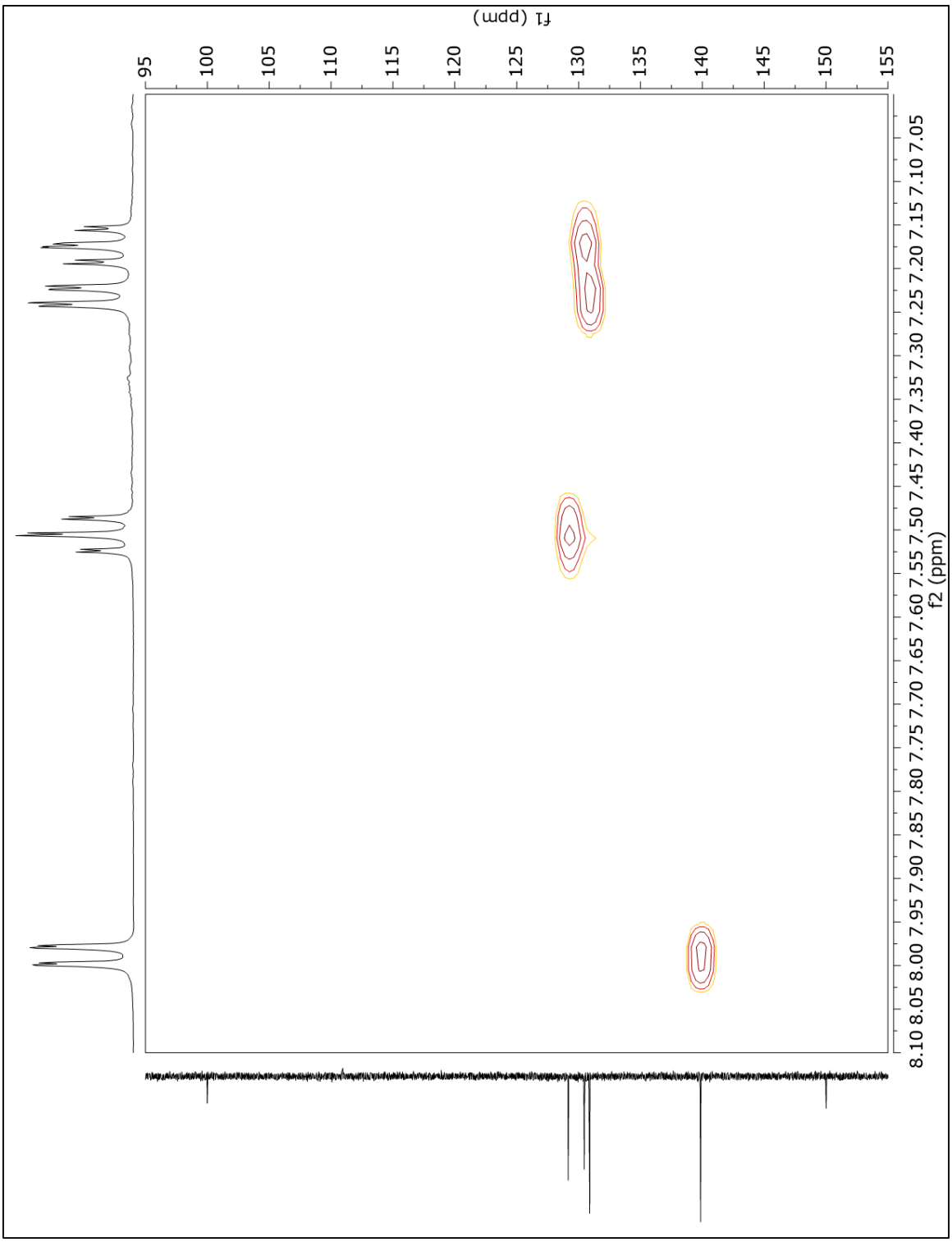

Figure A 17: *2D HSQC NMR spectrum of 2,2'-diiodobiphenyl.*

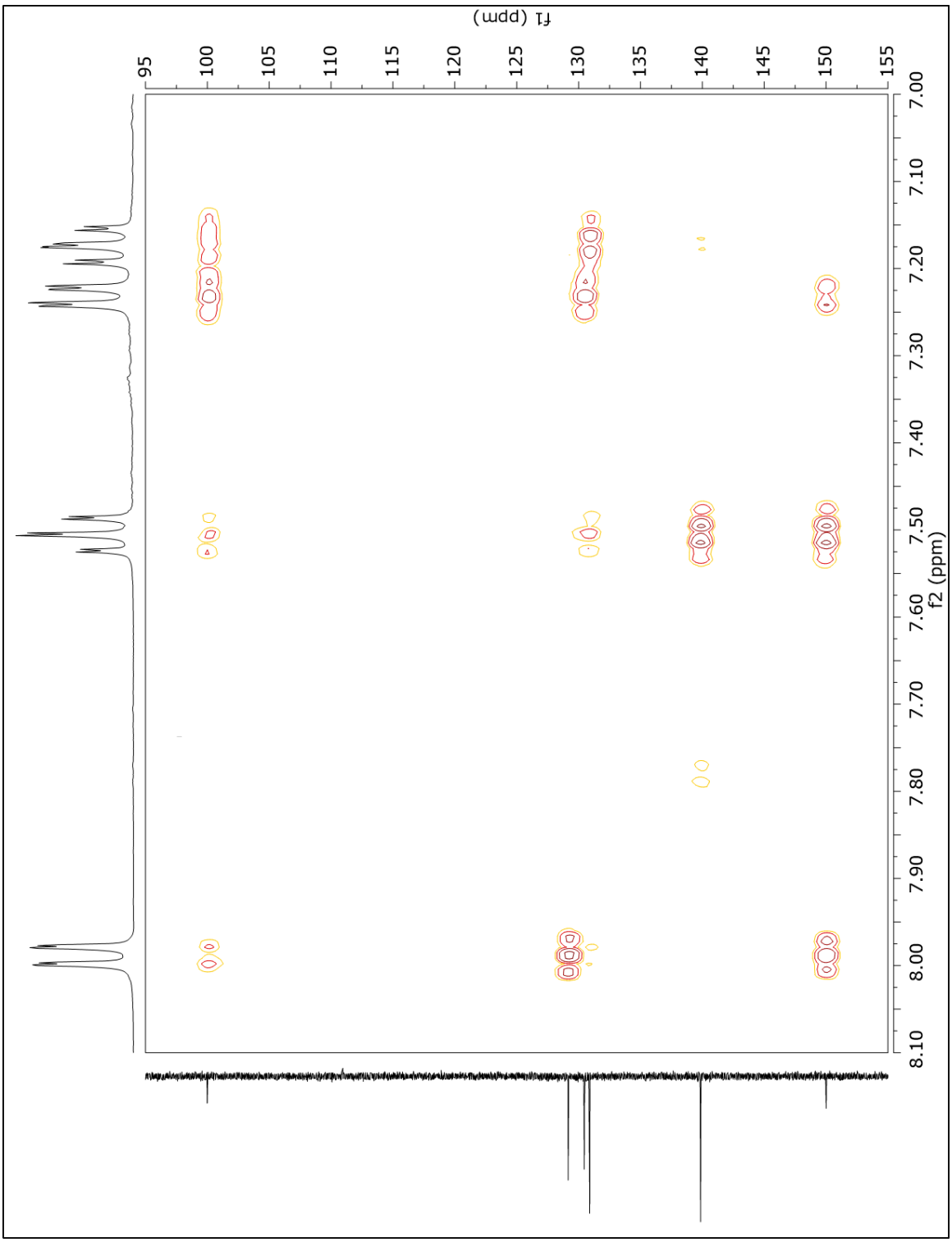

Figure A 18: *2D HMBC NMR spectrum of 2,2'-diiodobiphenyl.*

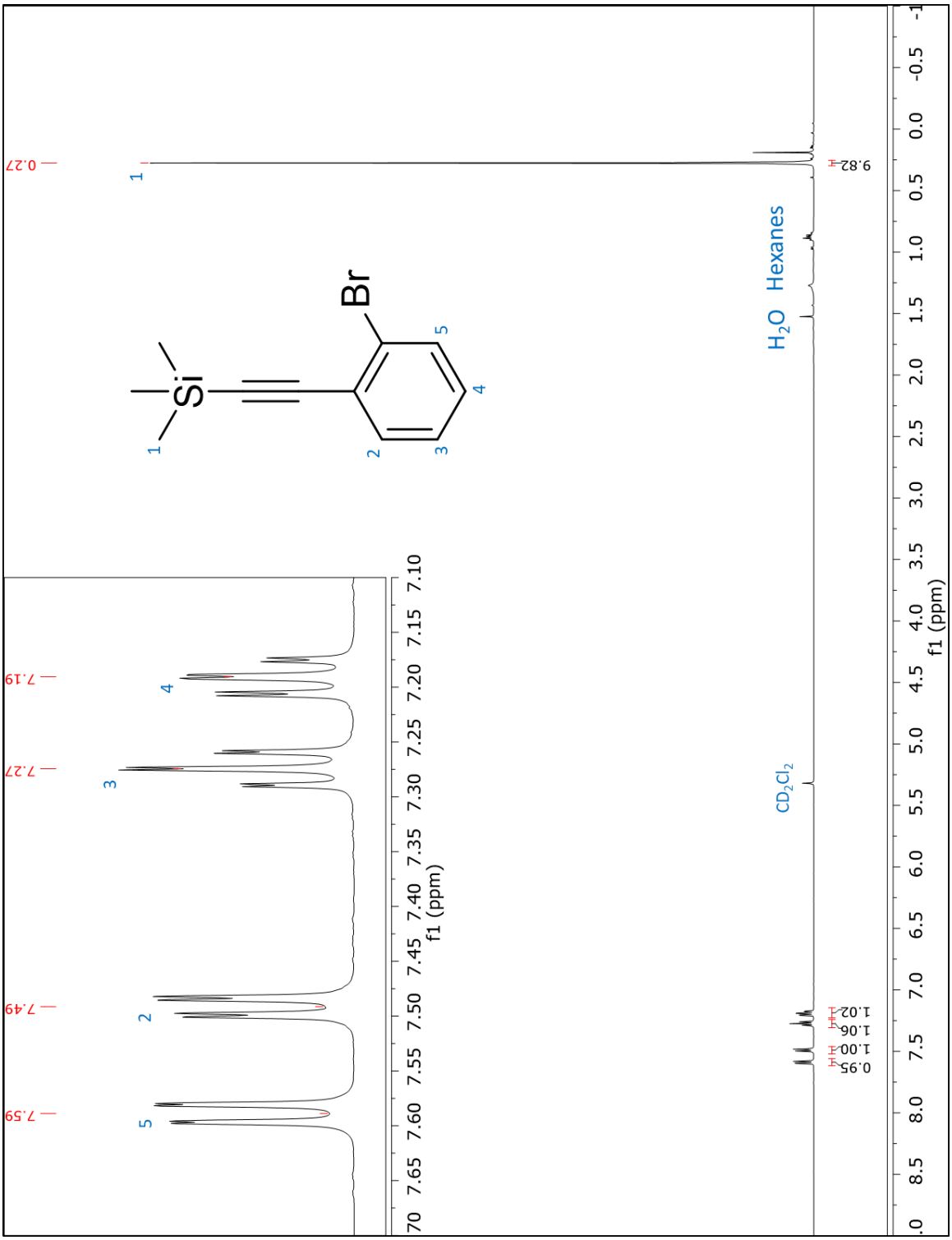

Figure A 19: *[1]H NMR spectrum of ((2-bromophenyl)ethynyl)trimethylsilane.*

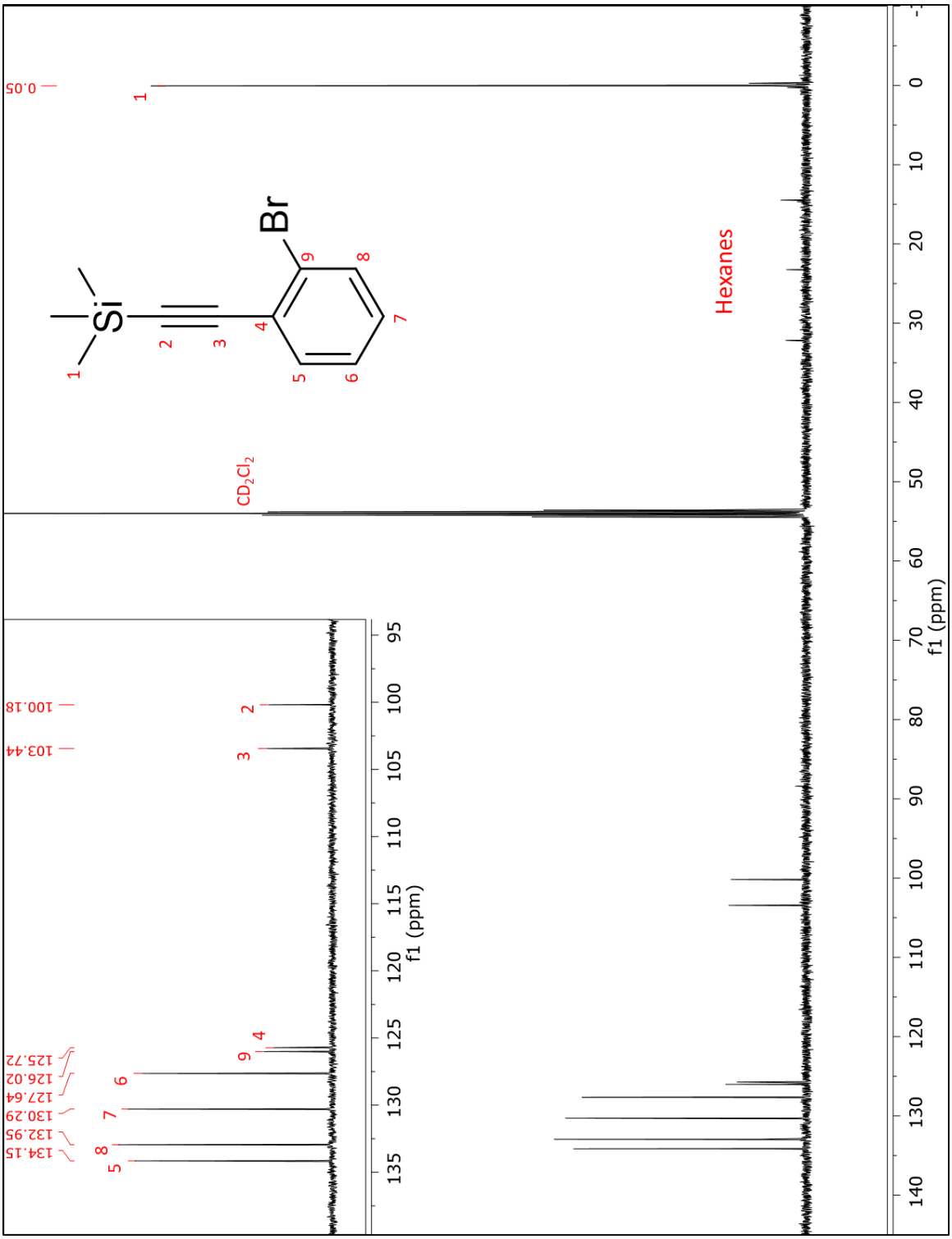

Figure A 20: *^{13}C NMR spectrum of ((2-bromophenyl)ethynyl)trimethylsilane.*

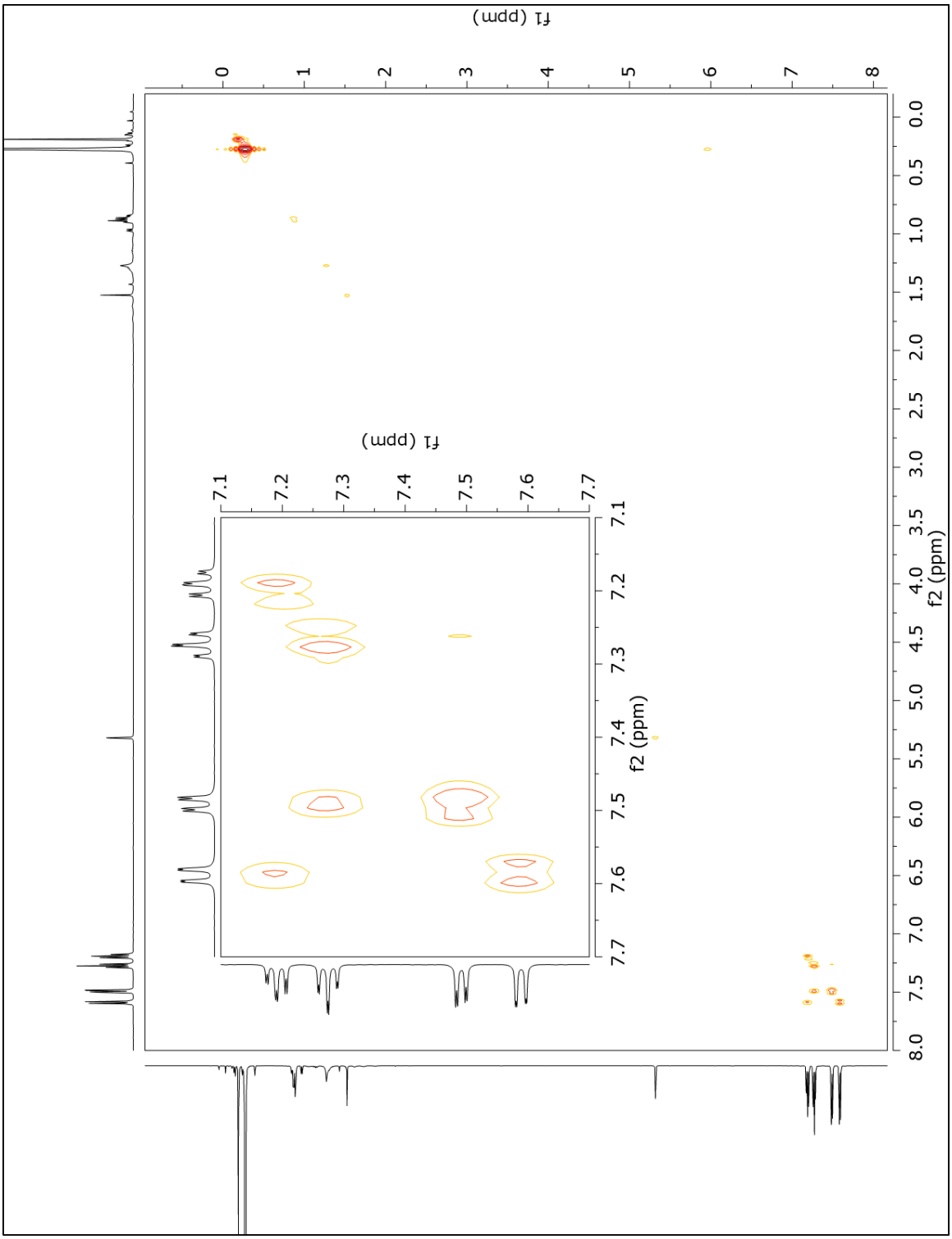

Figure A 21: *2D COSY NMR spectrum of ((2-bromophenyl)ethynyl)trimethylsilane.*

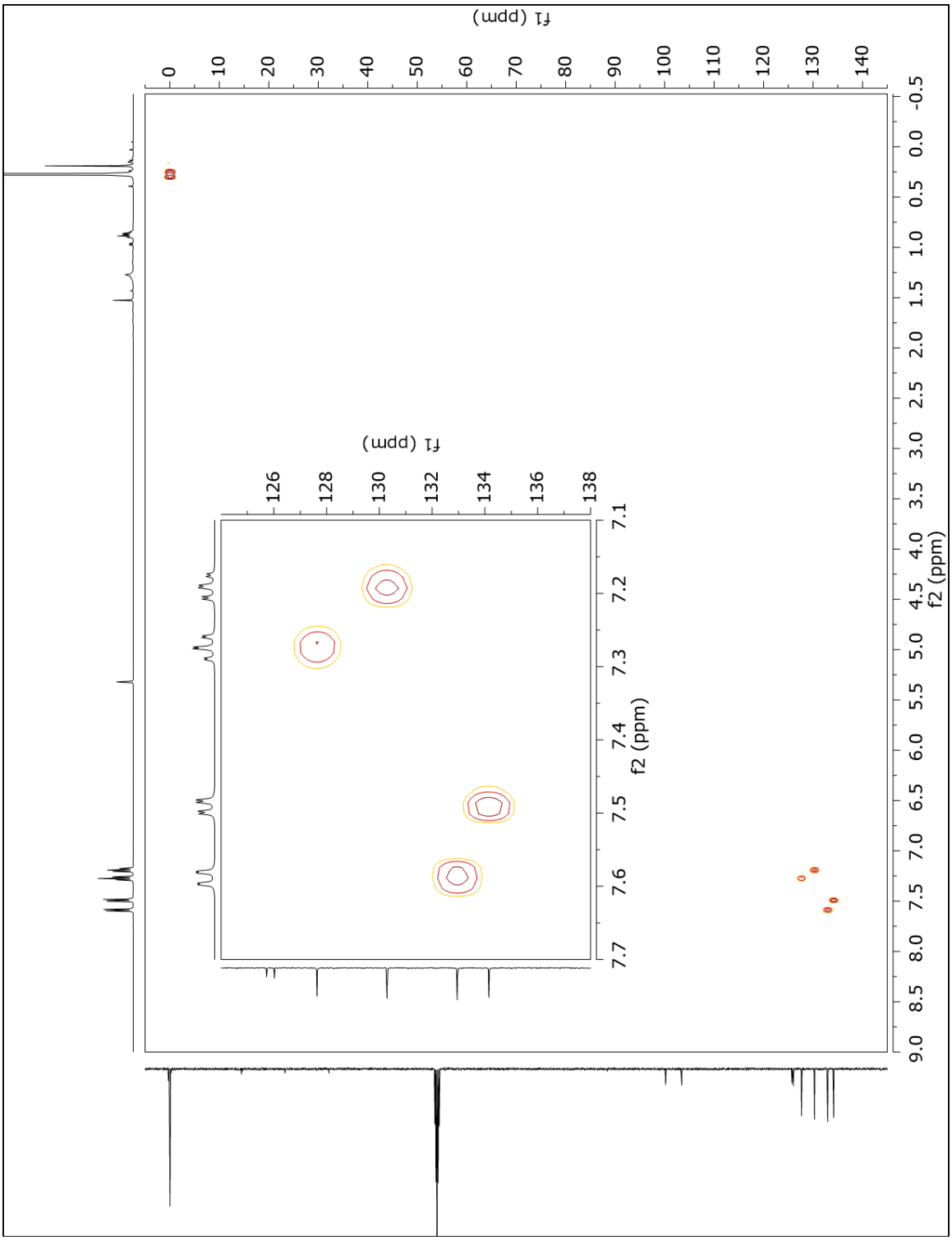

Figure A 22: *2D HSQC NMR spectrum of ((2-bromophenyl)ethynyl)trimethylsilane.*

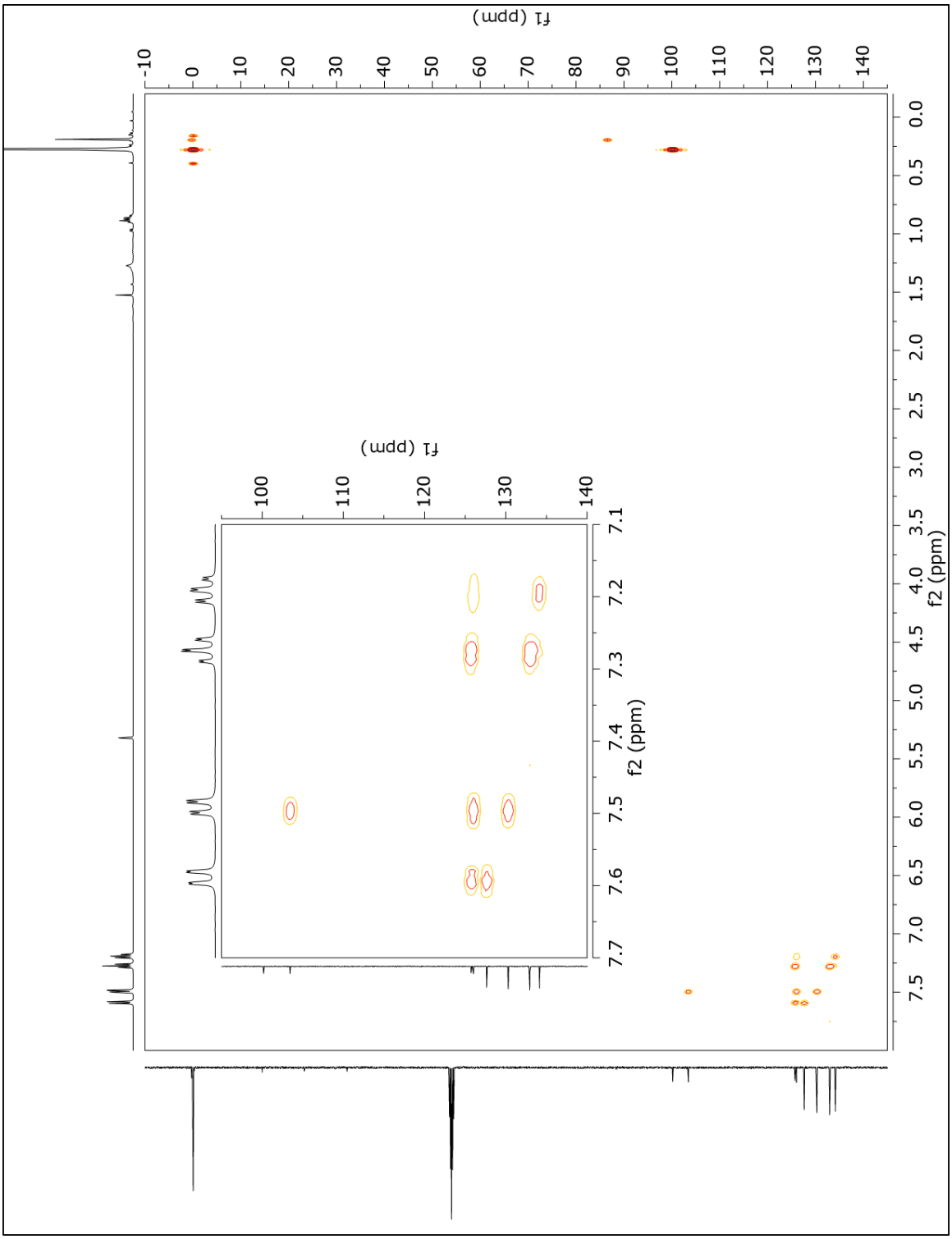

Figure A 23: *2D HMBC NMR spectrum of ((2-bromophenyl)ethynyl)trimethylsilane.*

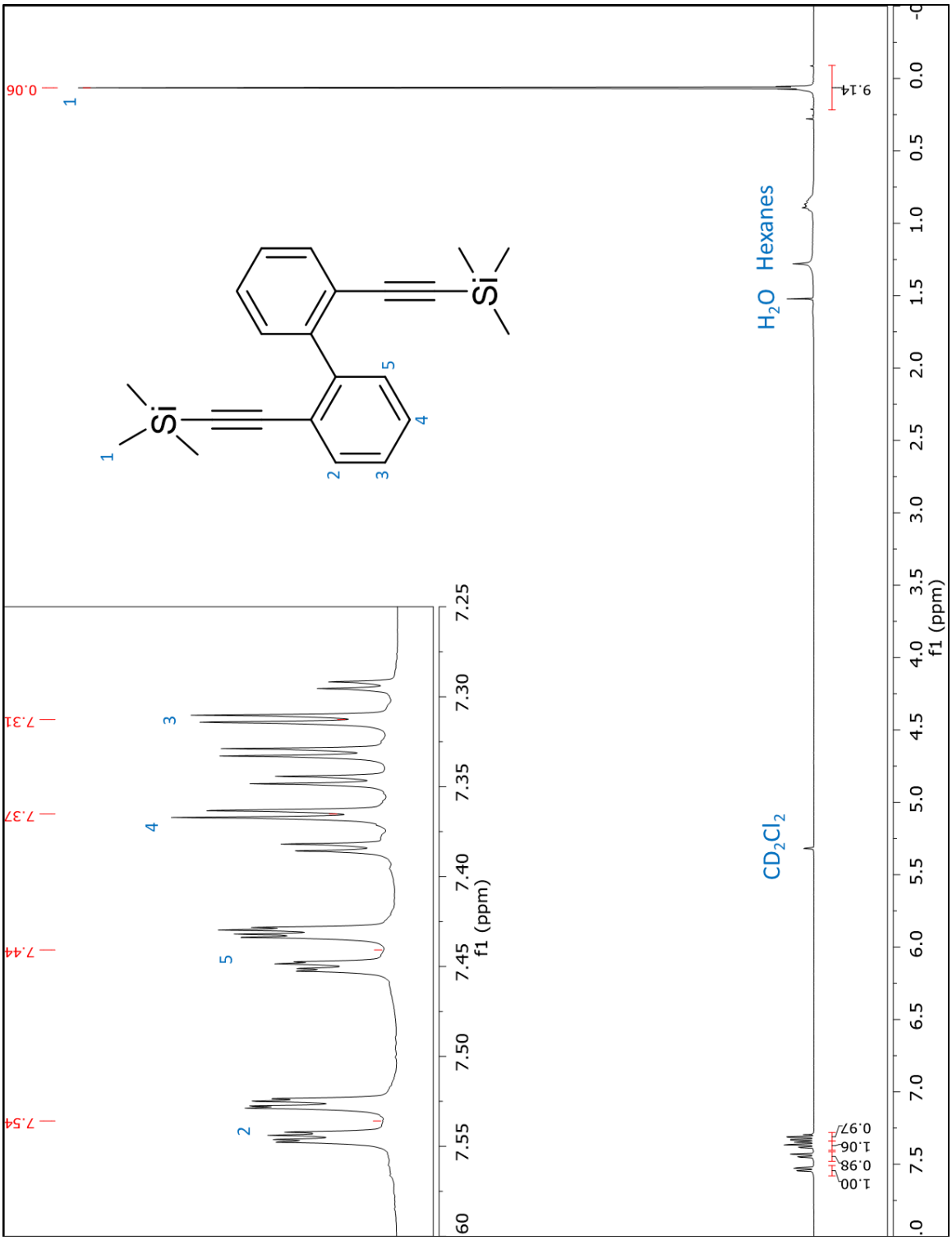

Figure A 24: *[1]H NMR spectrum of 2,2'-bis-trimethylsilylethynyl-1,1'-biphenyl.*

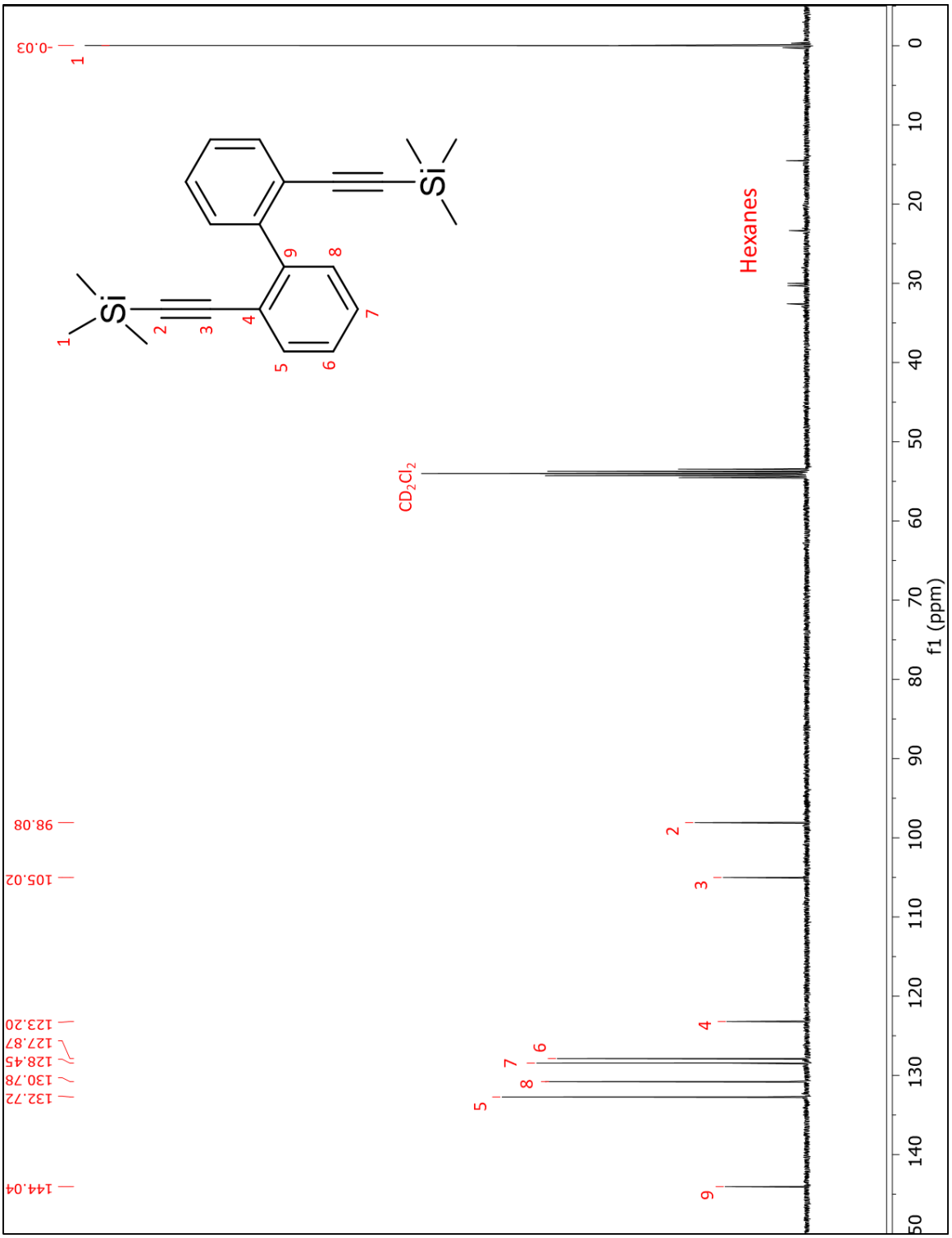

Figure A 25: *^{13}C NMR spectrum of 2,2'-bis-trimethylsilylethynyl-1,1'-biphenyl.*

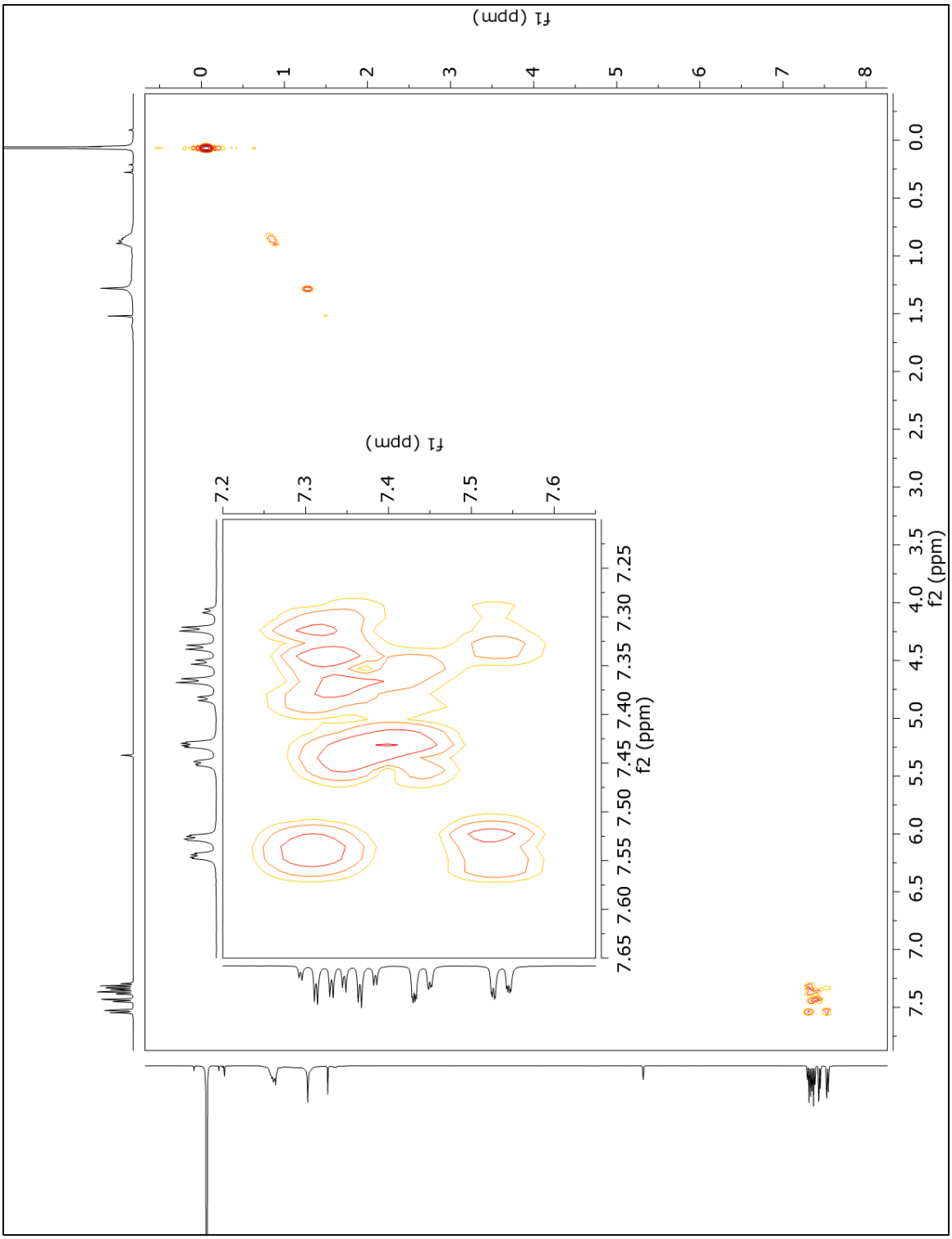

Figure A 26: *2D COSY NMR spectrum of 2,2'-bis-trimethylsilylethynyl-1,1'-biphenyl.*

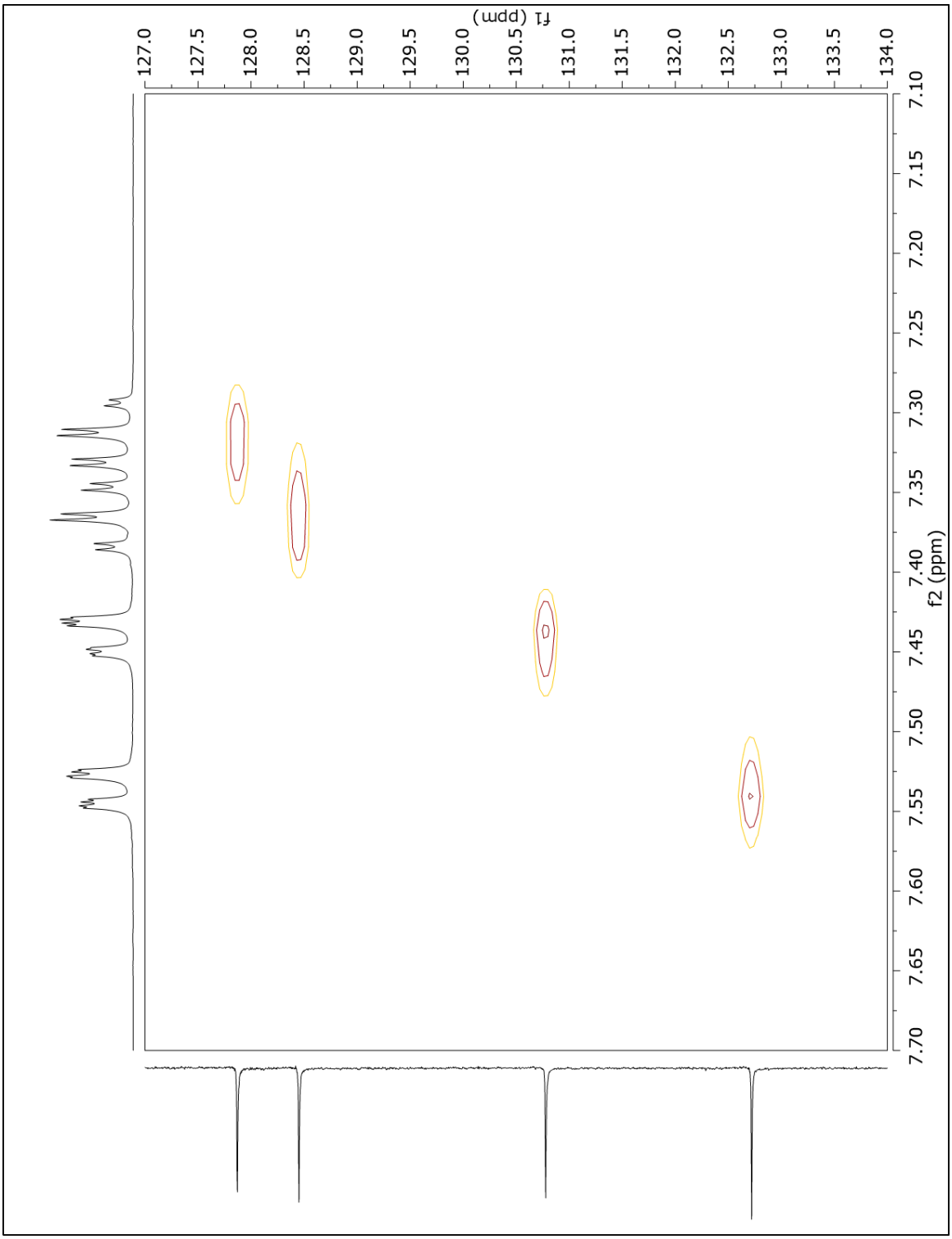

Figure A 27: *2D HSQC NMR spectrum of 2,2'-bis-trimethylsilylethynyl-1,1'-biphenyl.*

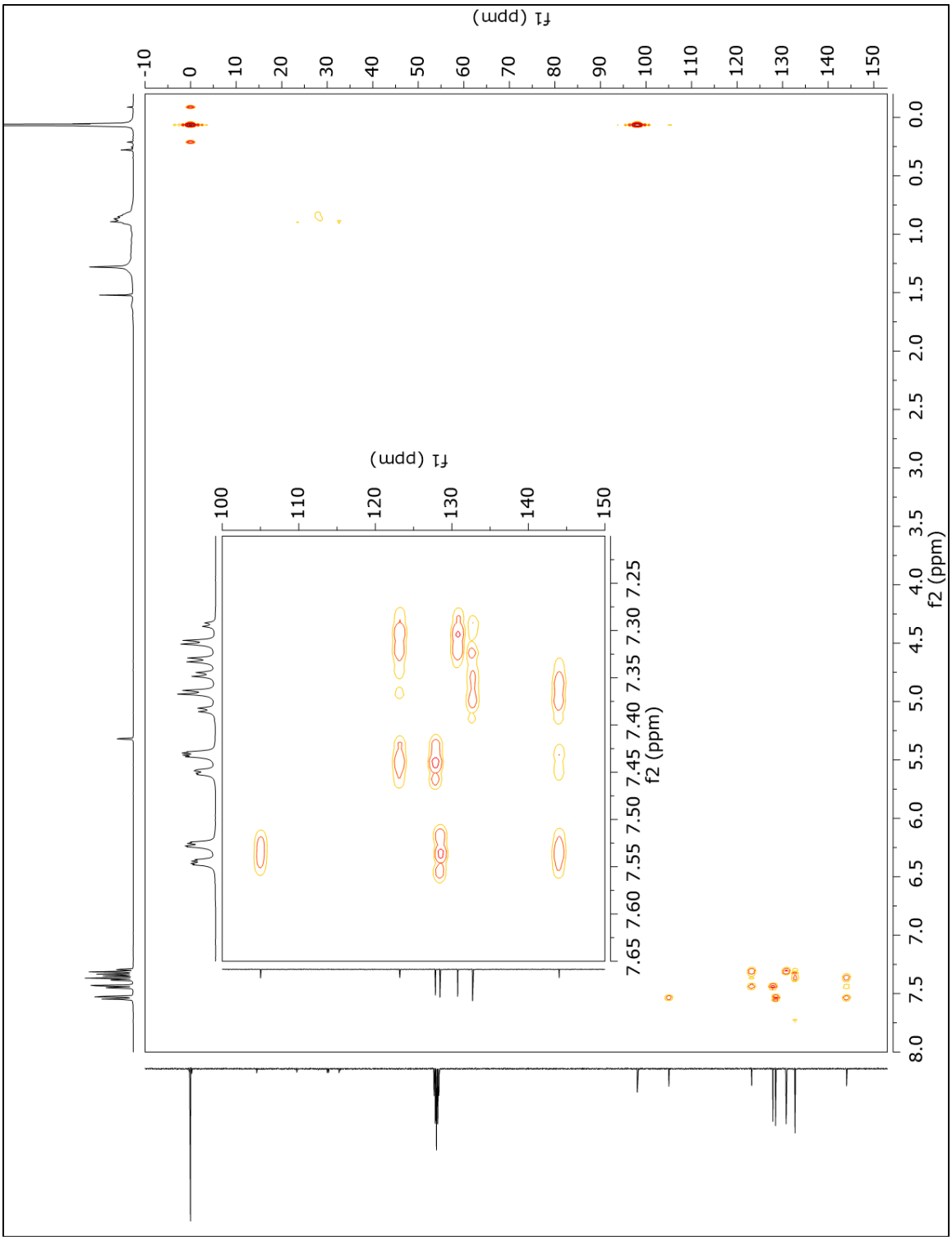

Figure A 28: *2D HMBC NMR spectrum of 2,2'-bis-trimethylsilylethynyl-1,1'-biphenyl.*

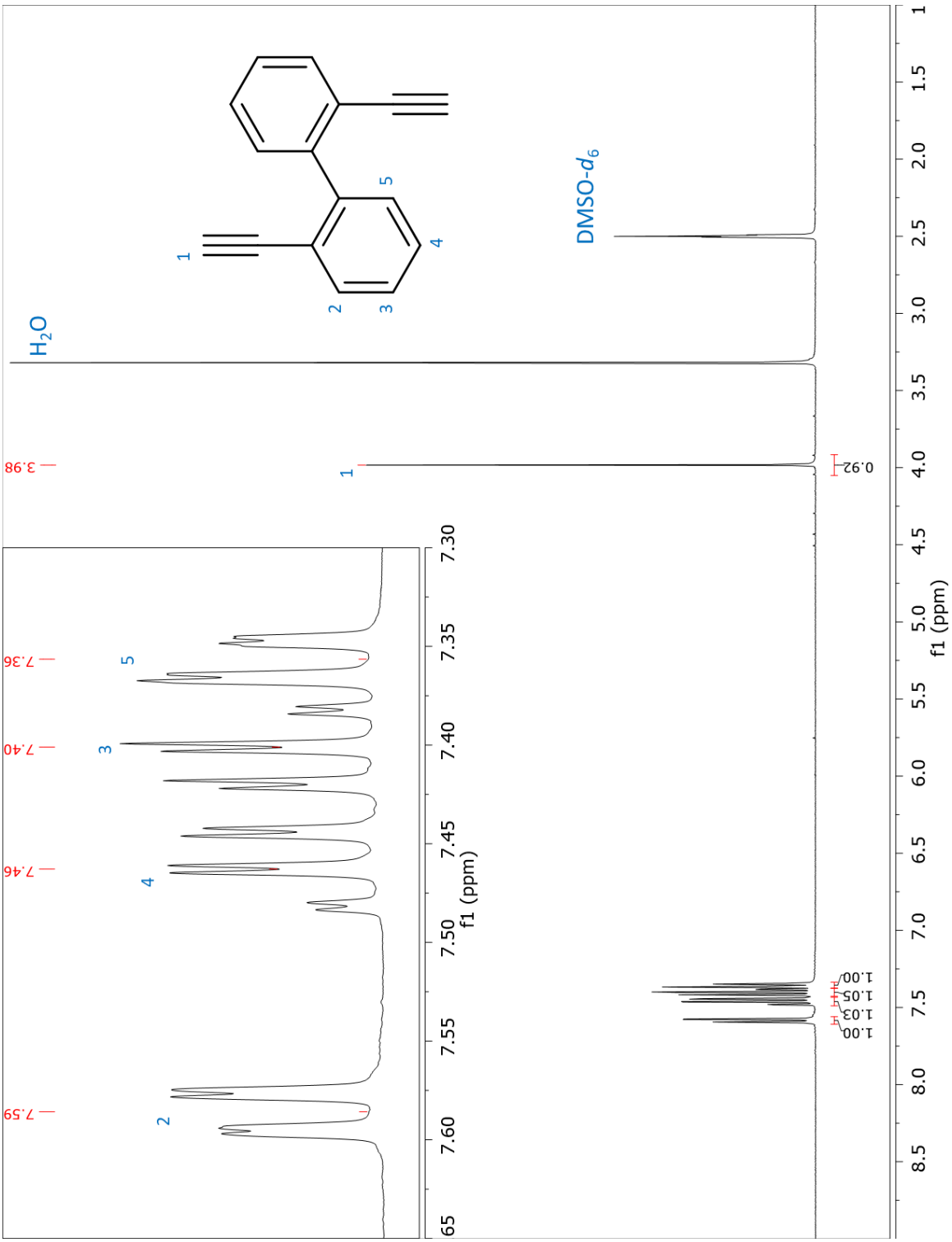

Figure A 29: *^{1}H NMR spectrum of 2,2'-diethynyl-1,1'-biphenyl (o-BPL).*

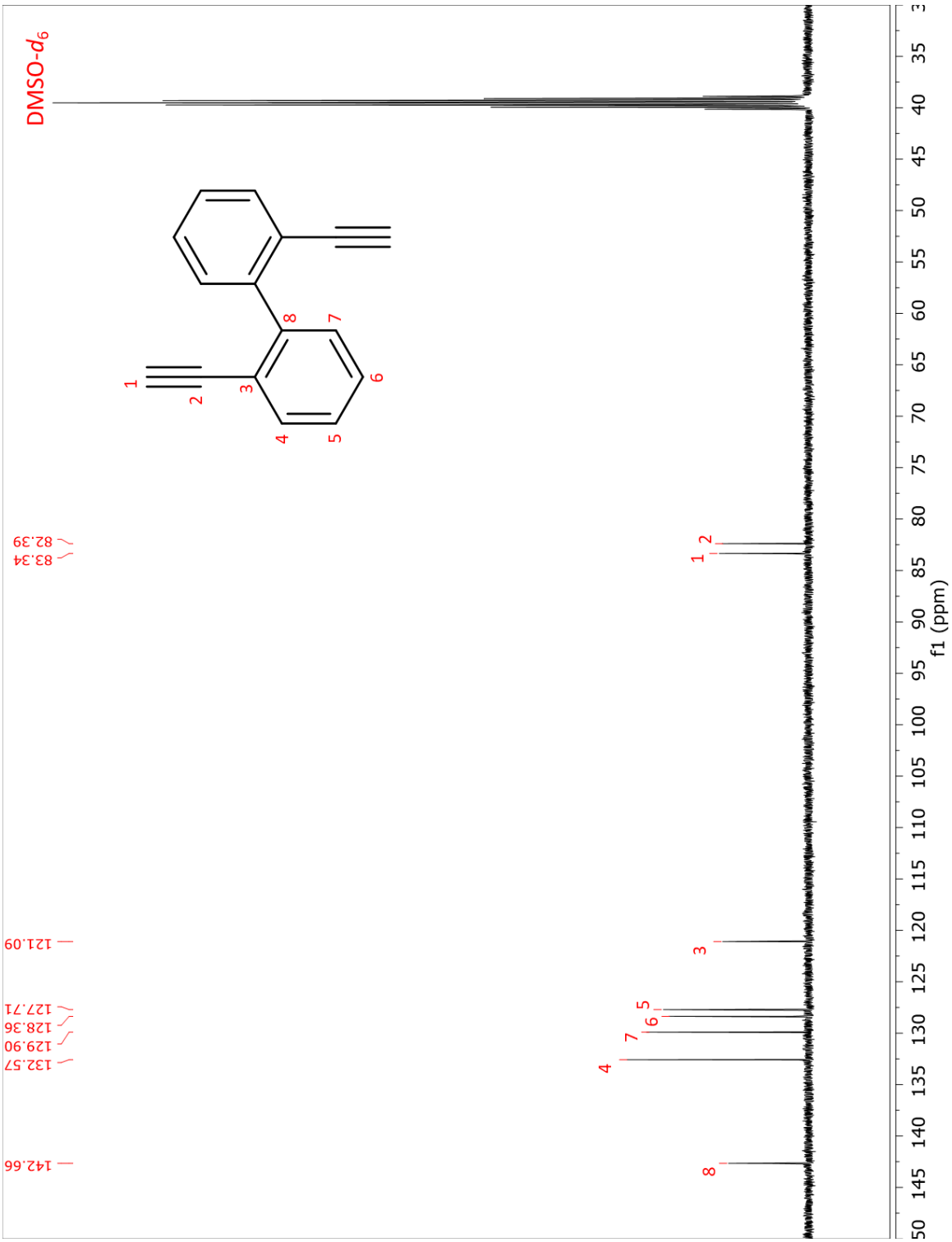

Figure A 30: *^{13}C NMR spectrum of 2,2'-diethynyl-1,1'-biphenyl (o-BPL).*

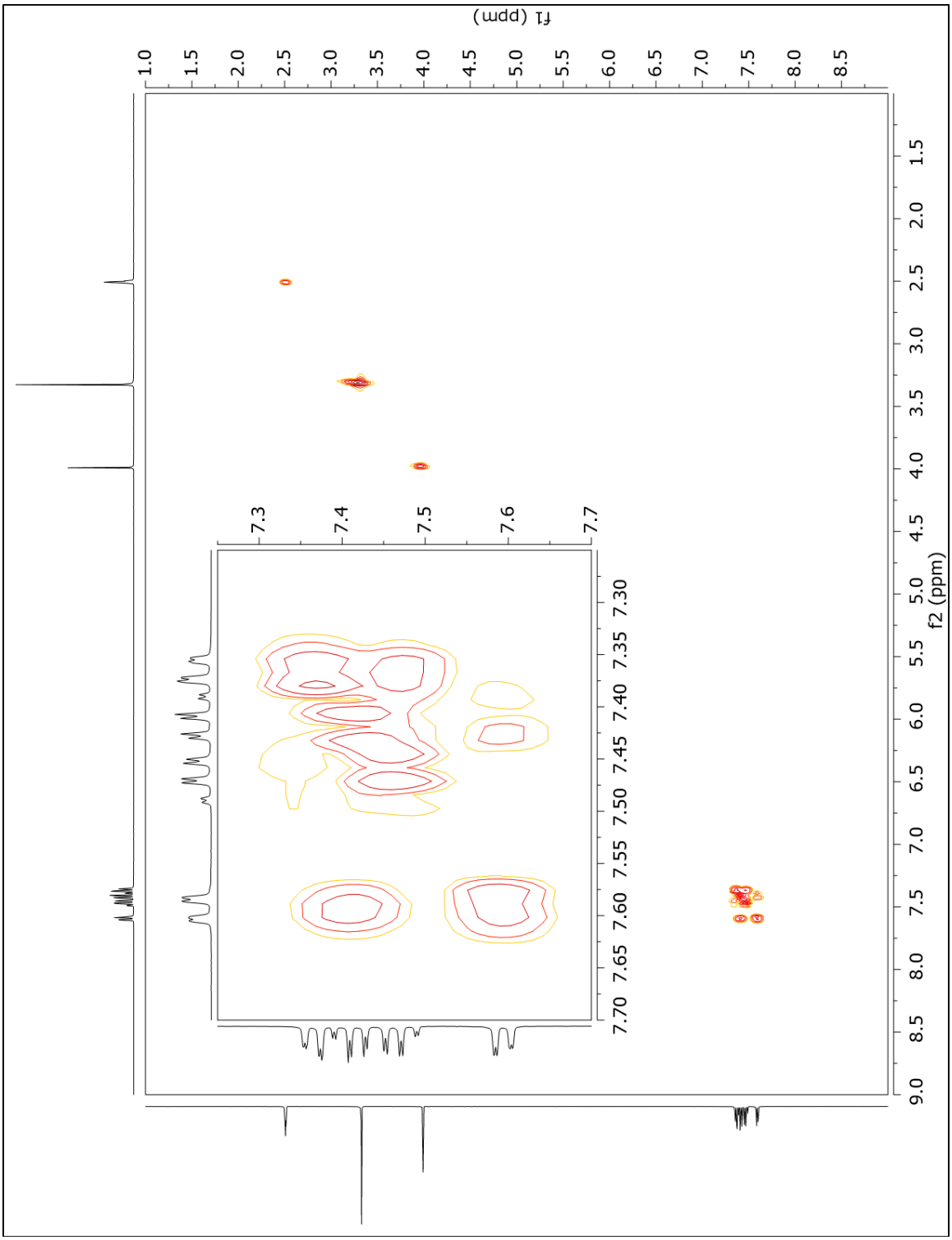

Figure A 31: *2D COSY NMR spectrum of 2,2'-diethynyl-1,1'-biphenyl (o-BPL).*

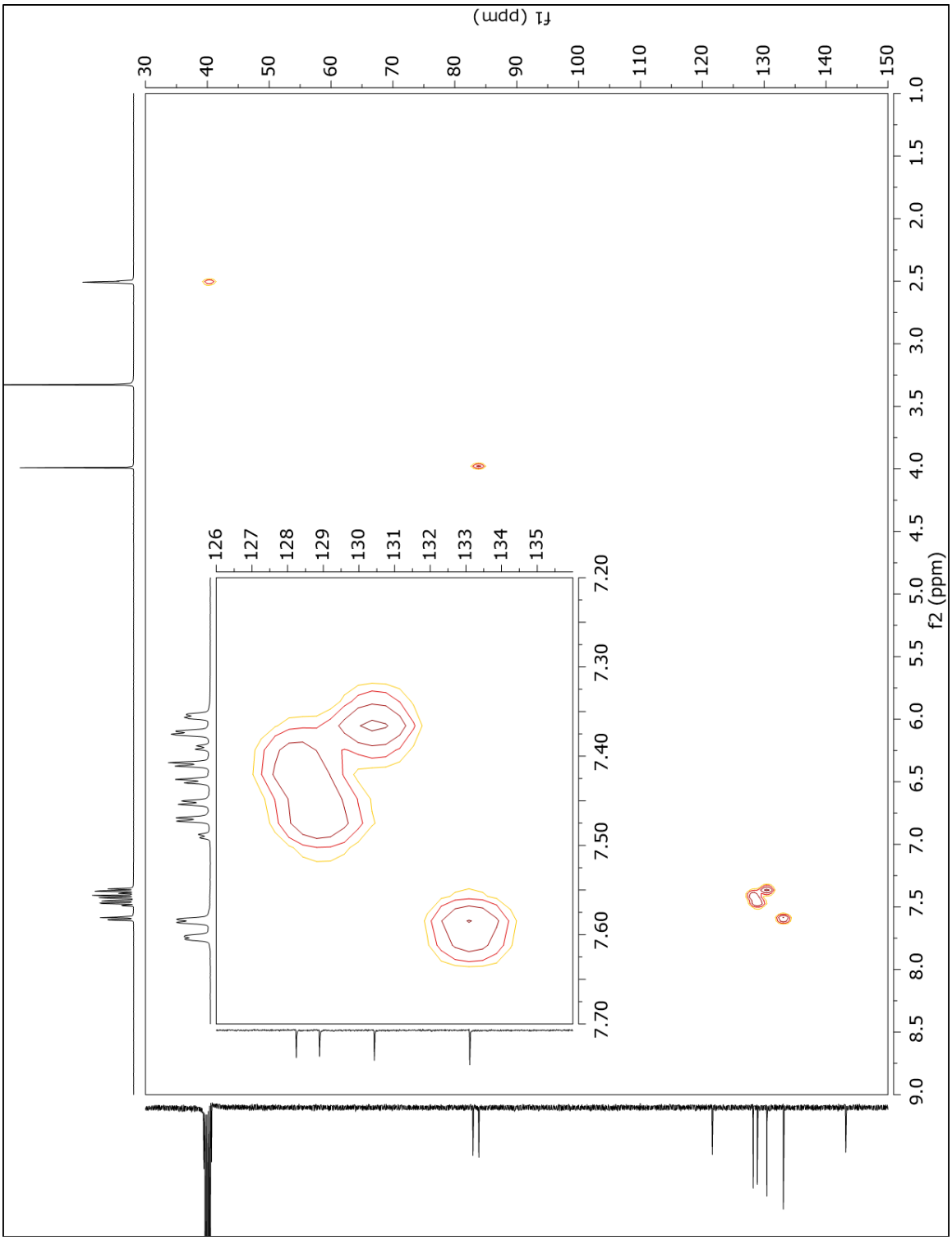

Figure A 32: *2D HSQC NMR spectrum of 2,2'-diethynyl-1,1'-biphenyl (o-BPL).*

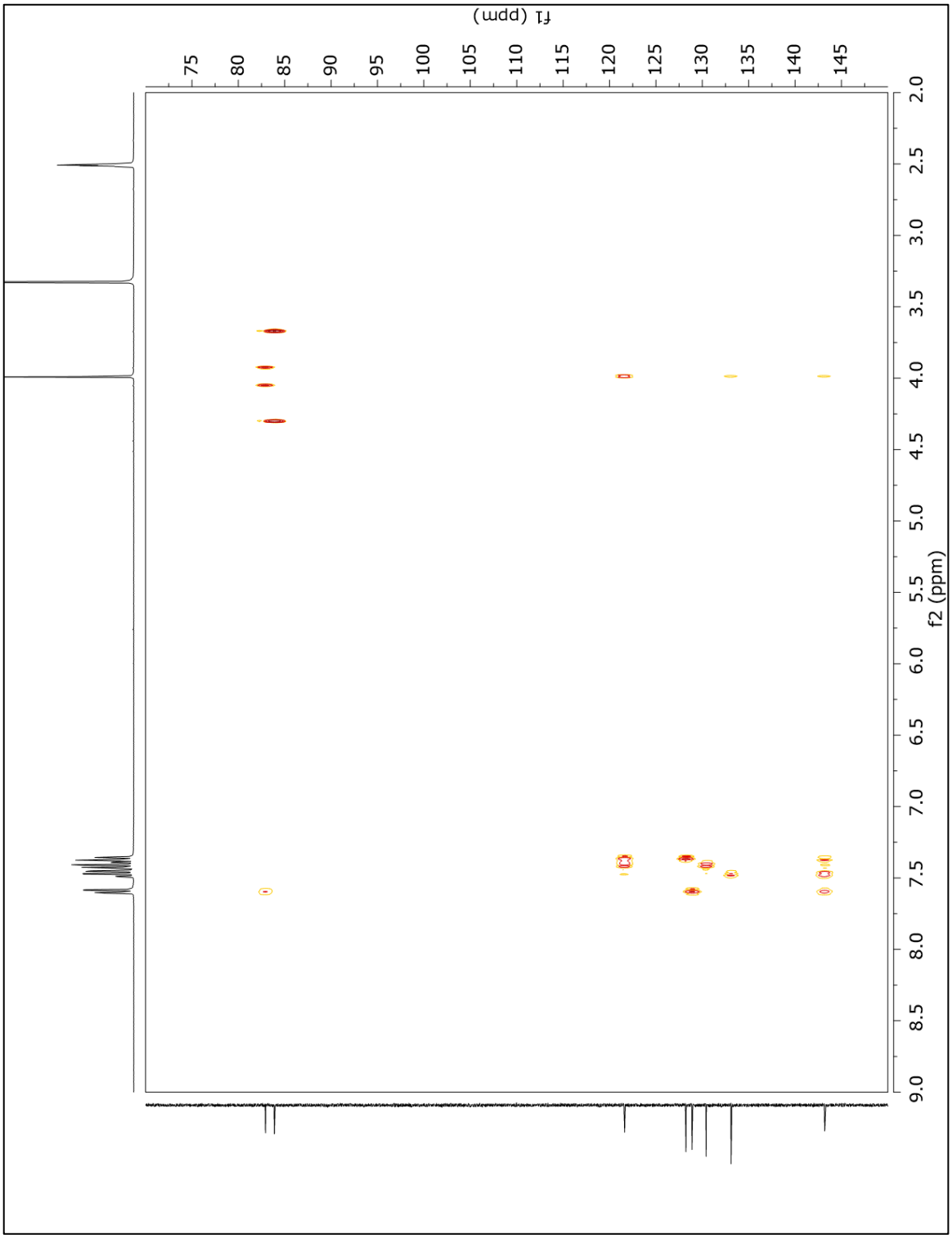

Figure A 33: *2D HMBC NMR spectrum of 2,2'-diethynyl-1,1'-biphenyl (o-BPL).*

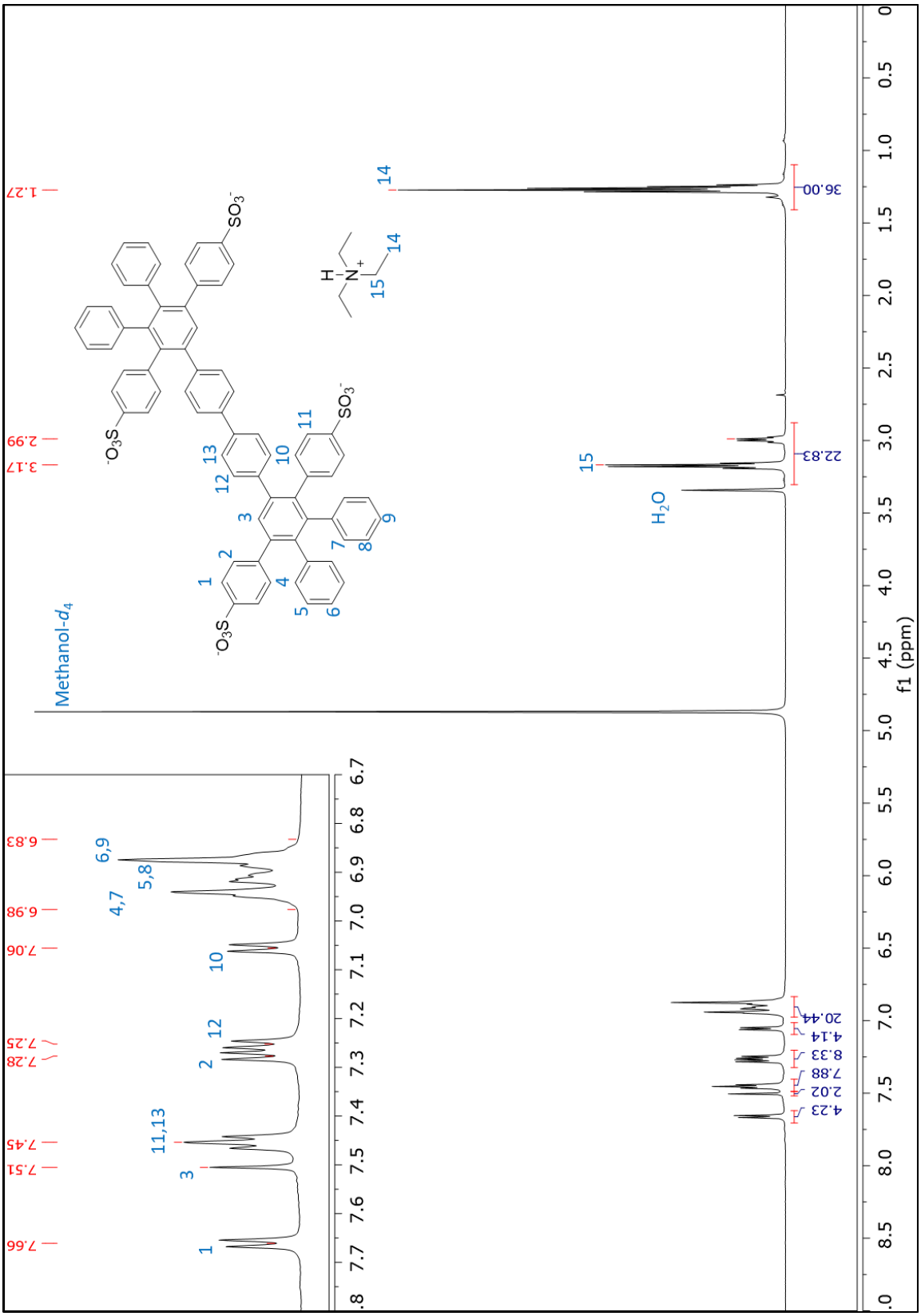

Figure A 34: *^{1}H NMR spectrum of 4,4'-biphenyl model compound (MC-Bp).*

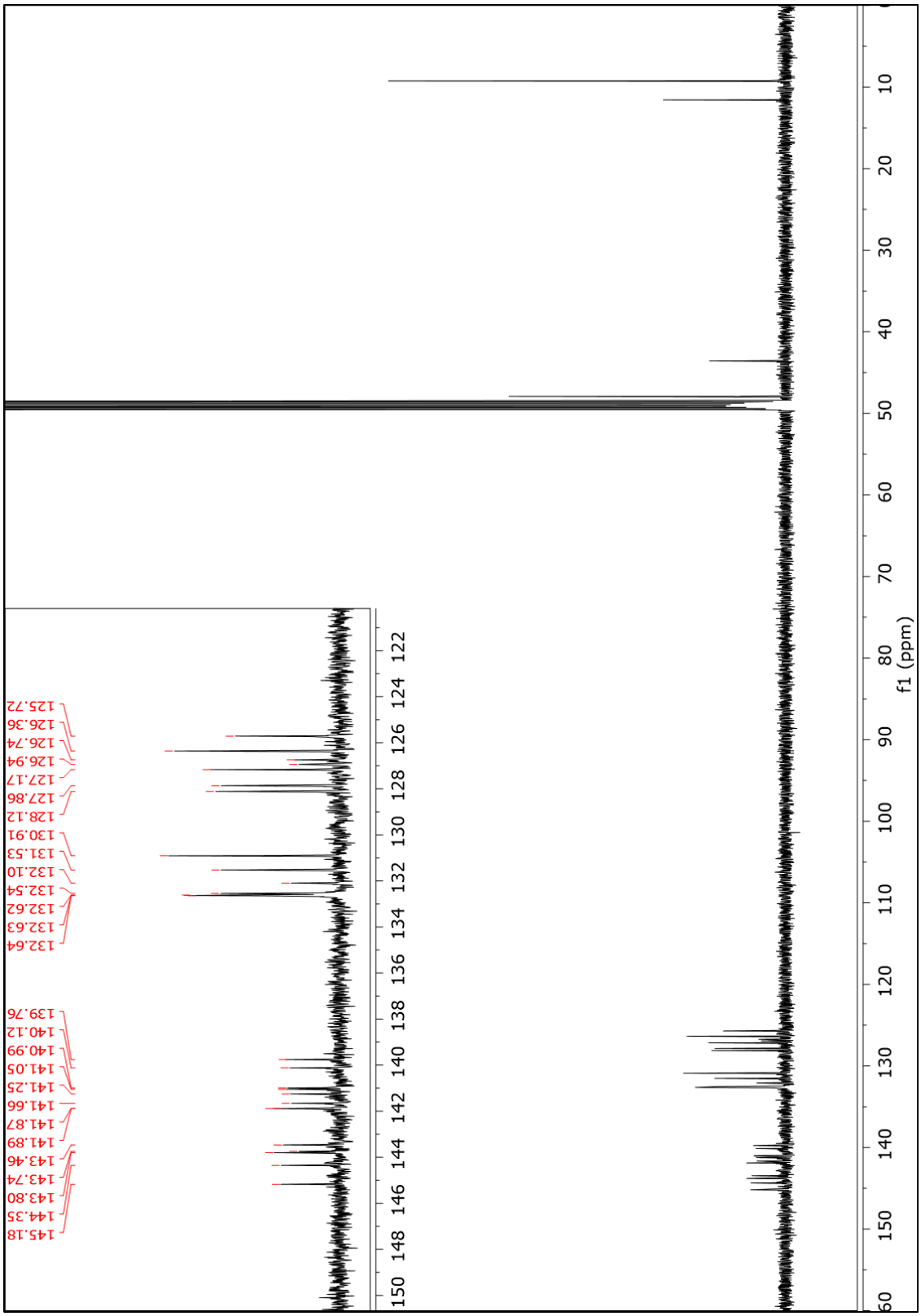

Figure A 35: *^{13}C NMR spectrum of 4,4'-biphenyl model compound (MC-Bp).*

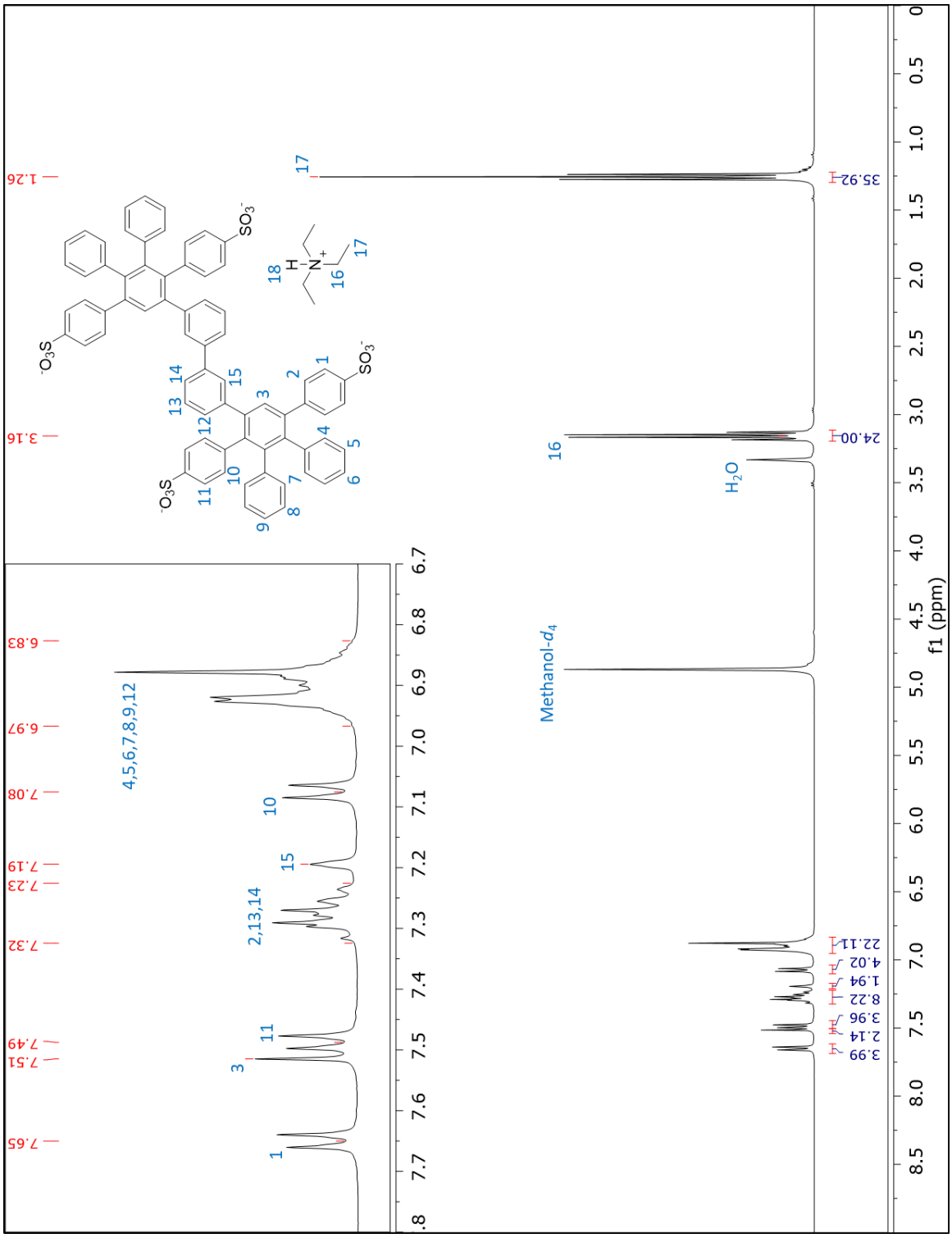

Figure A 36: *^{1}H NMR spectrum of 3,3'-biphenyl model compound (MC-Bm).*

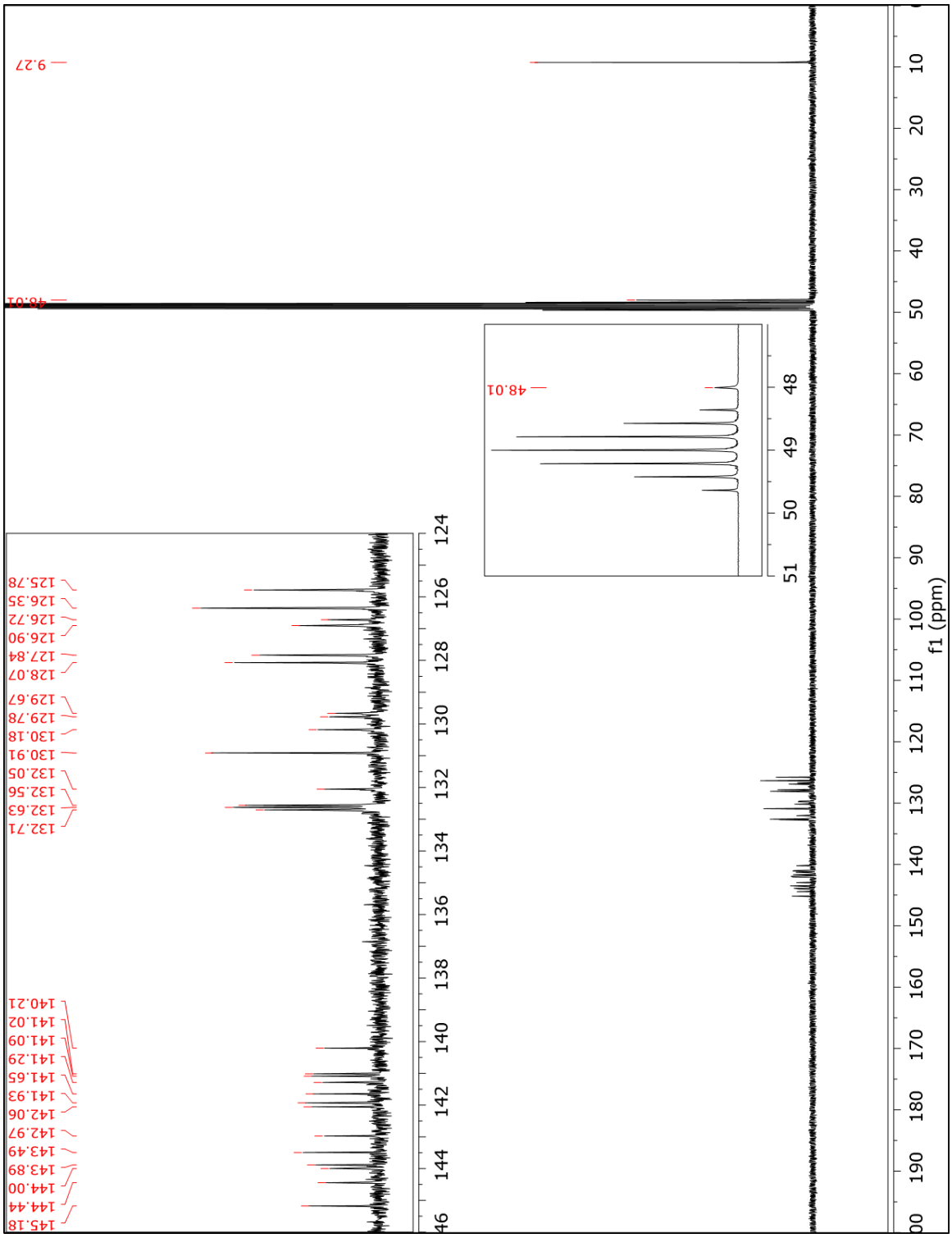

Figure A 37: *^{13}C NMR spectrum of 3,3'-biphenyl model compound (MC-Bm).*

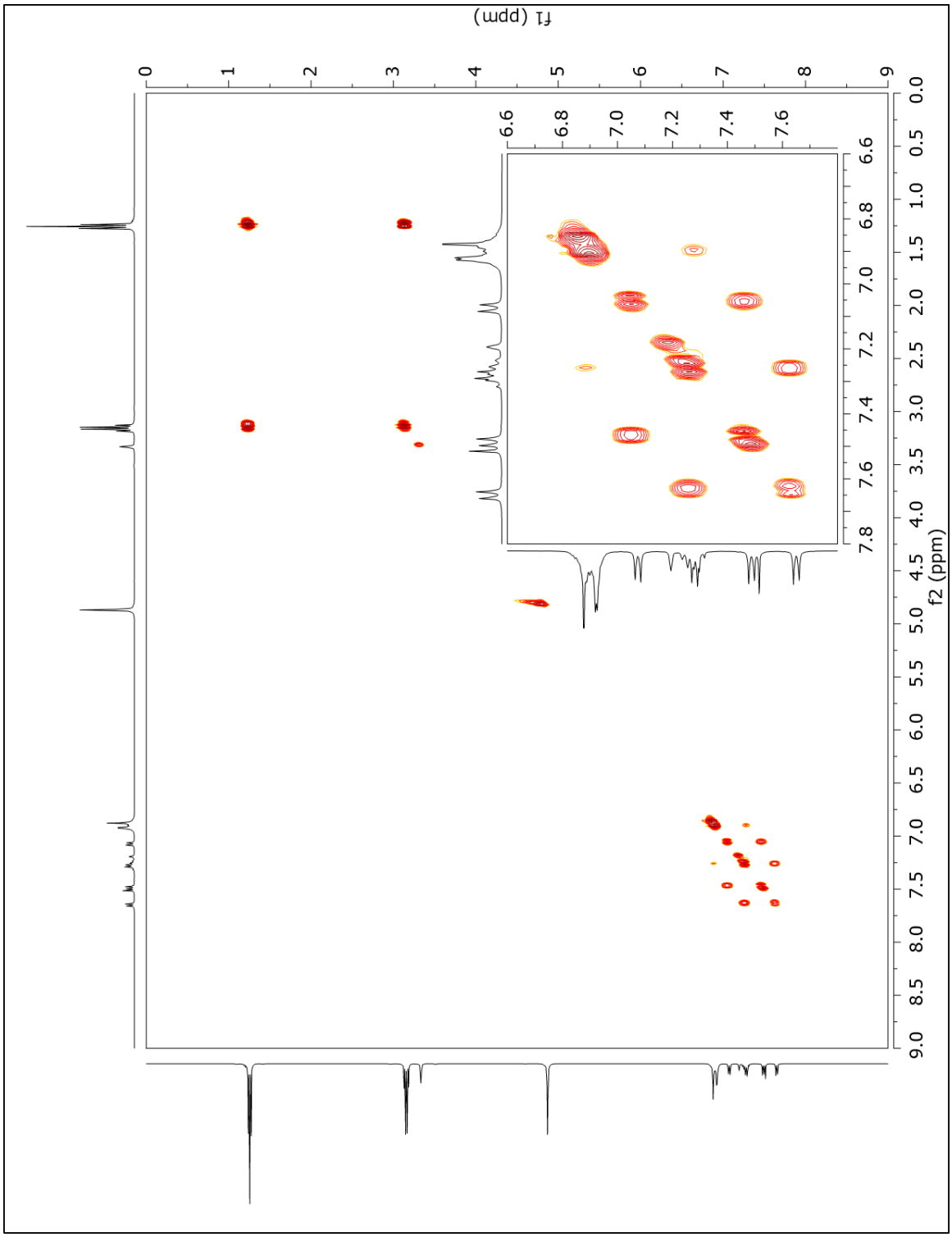

Figure A 38: *2D COSY NMR spectrum of 3,3'-biphenyl model compound (MC-Bm).*

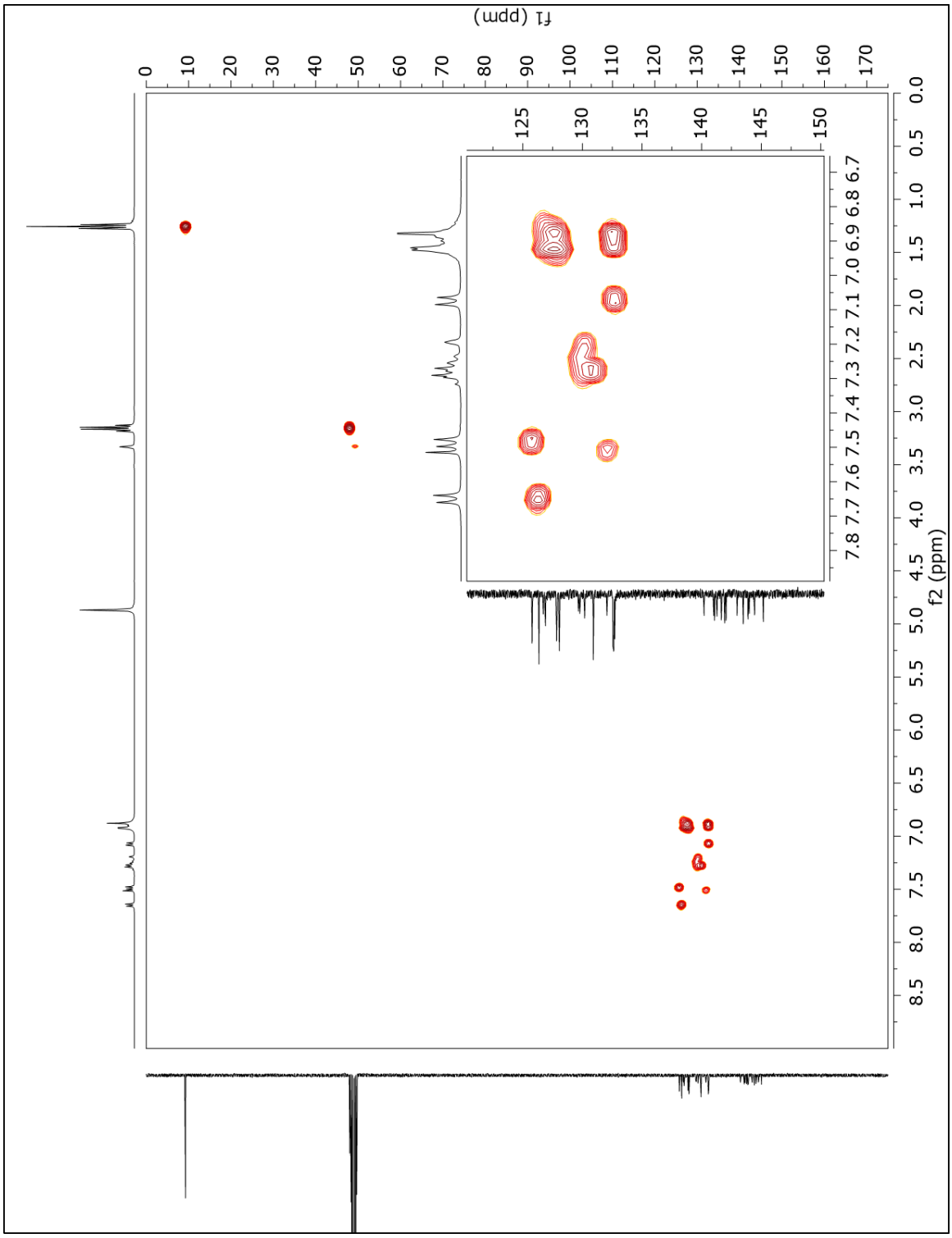

Figure A 39: *2D HSQC NMR spectrum of 3,3'-biphenyl model compound (MC-Bm).*

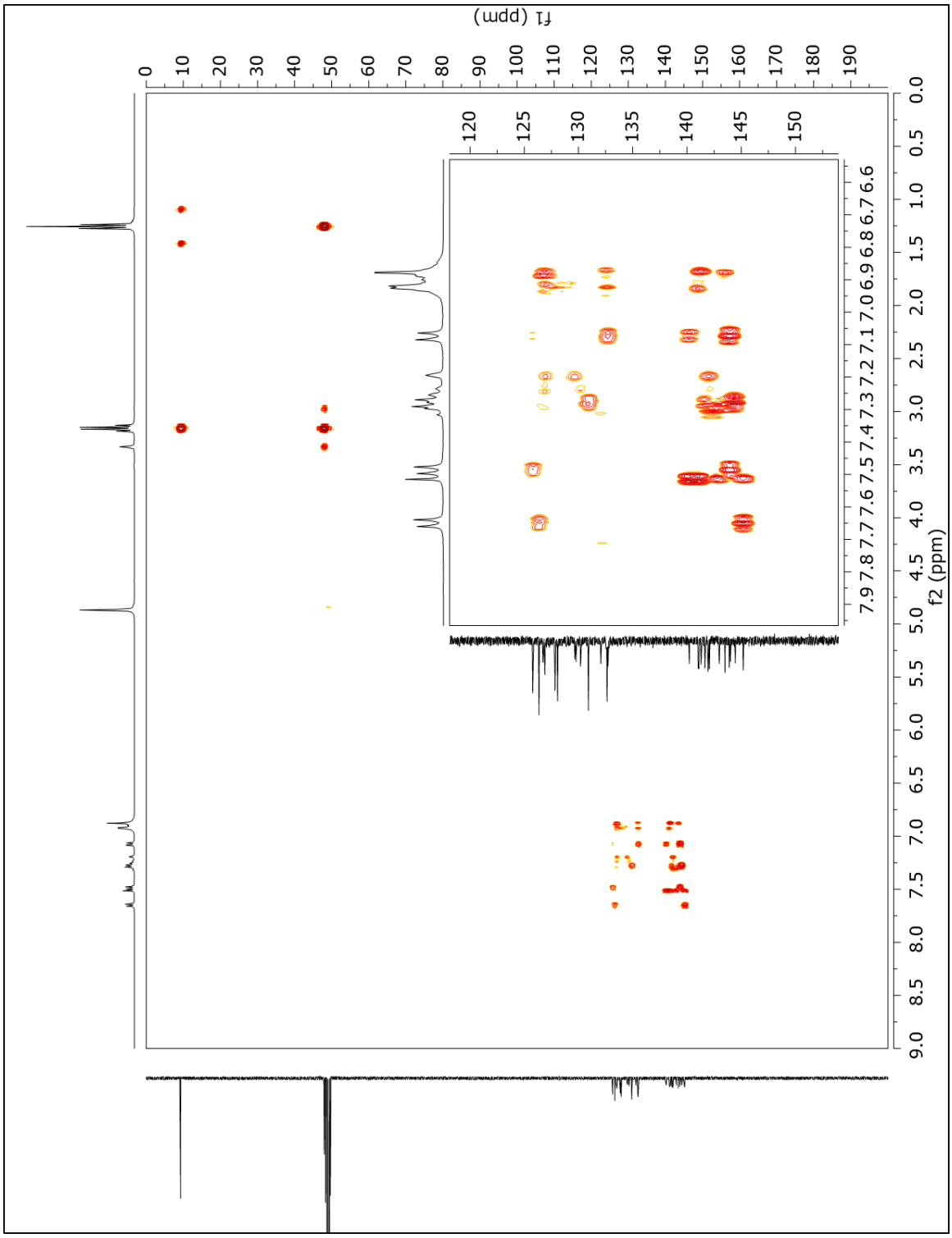

Figure A 40: *2D HMBC NMR spectrum of 3,3'-biphenyl model compound (MC-Bm).*

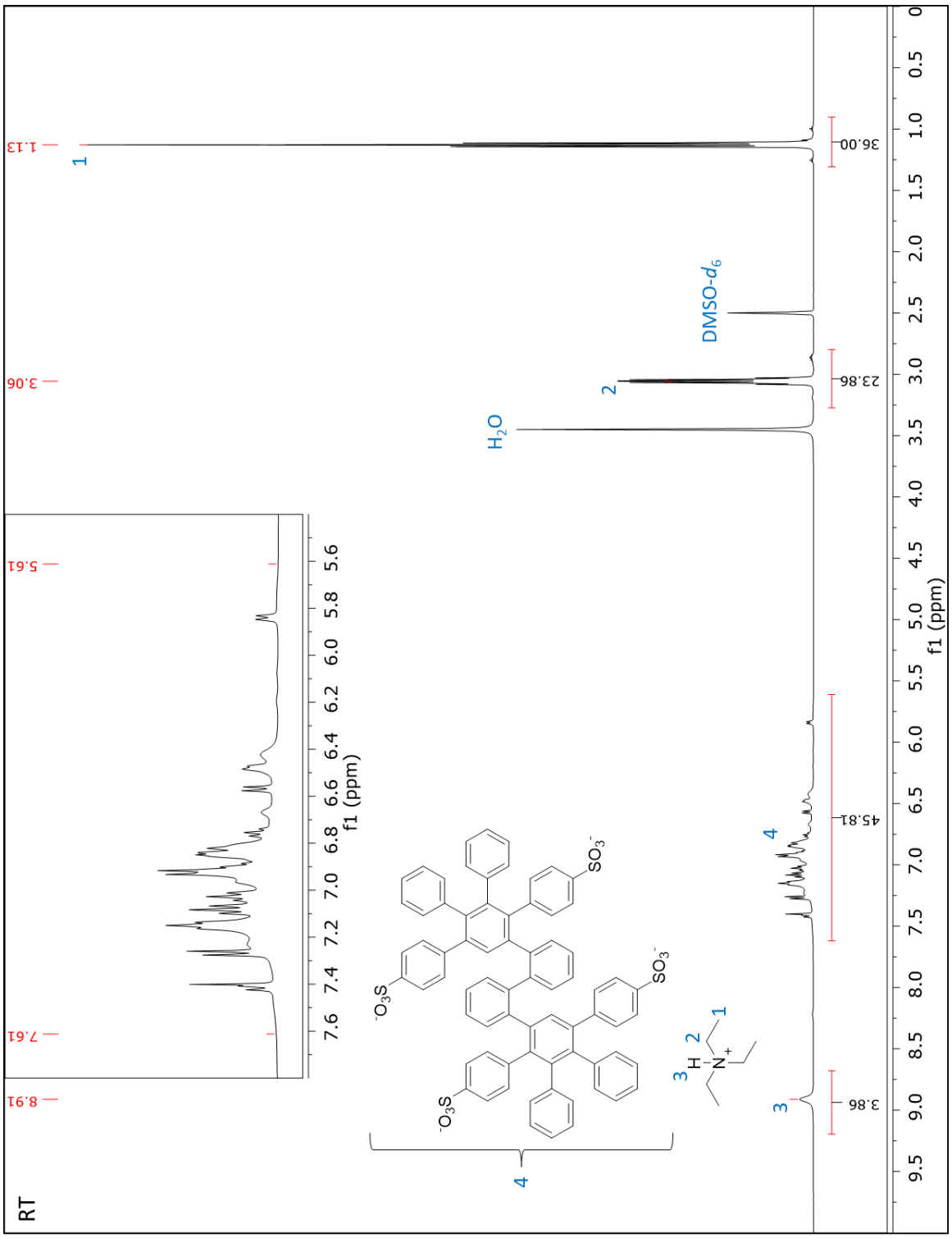

Figure A 41: *Room temperature ^{1}H NMR spectrum of 2,2'-biphenyl model compound (MC-Bo) in DMSO-d_6.*

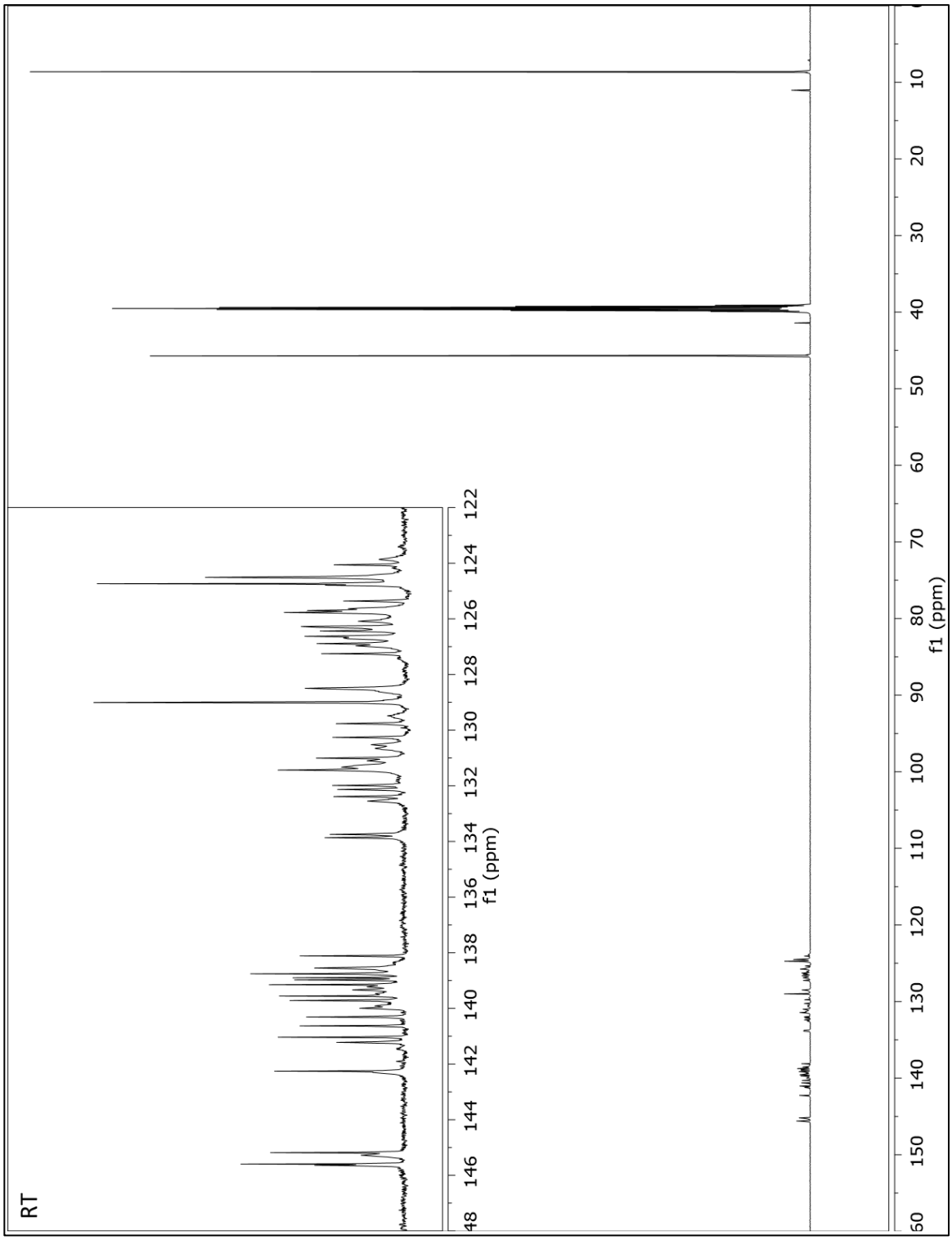

Figure A 42: *Room temperature ^{13}C NMR spectrum of 2,2'-biphenyl model compound (MC-Bo) in DMSO-d_6.*

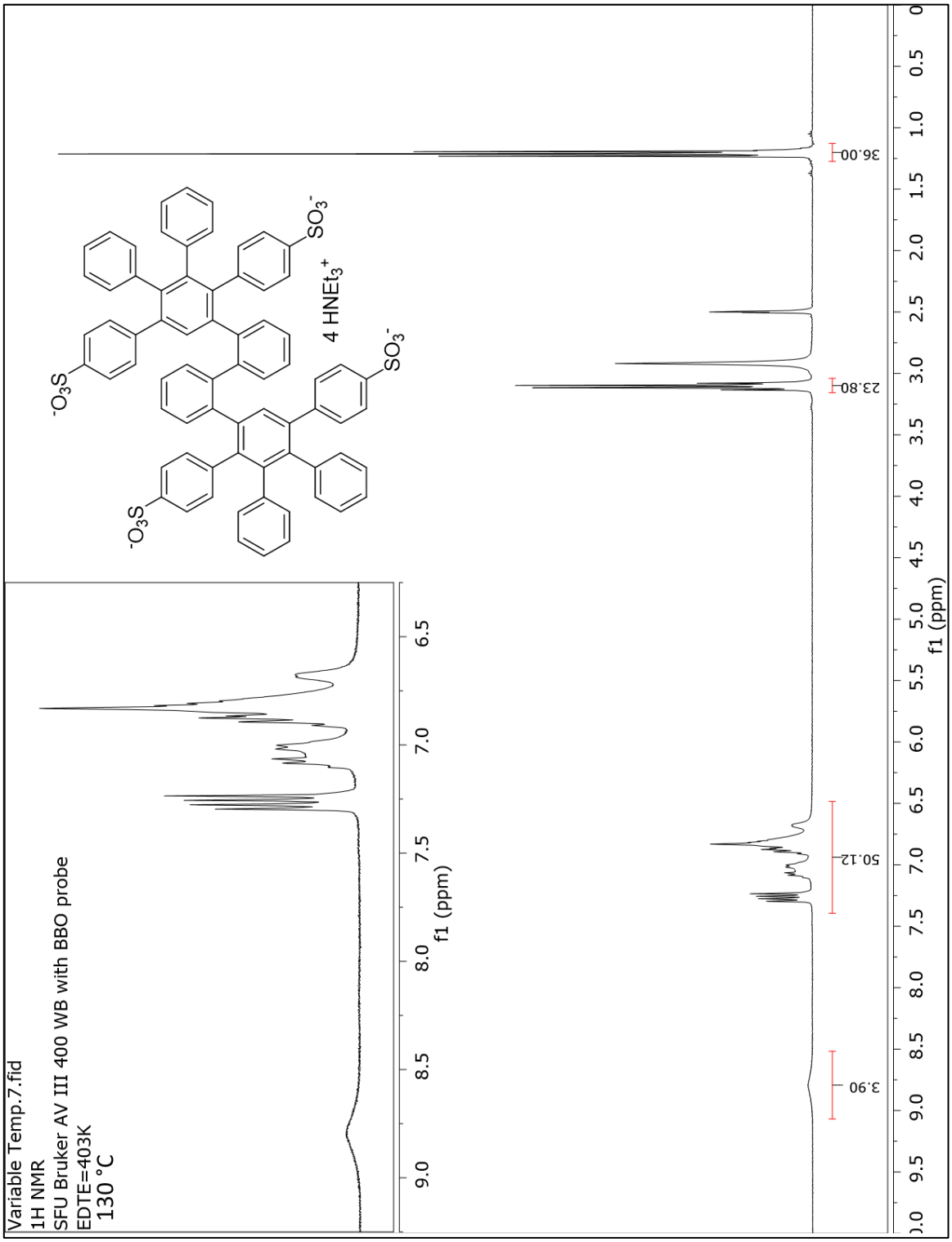

Figure A 43: *130 °C ^{1}H NMR spectrum of 2,2'-biphenyl model compound (MC-Bo) in DMSO-d_6.*

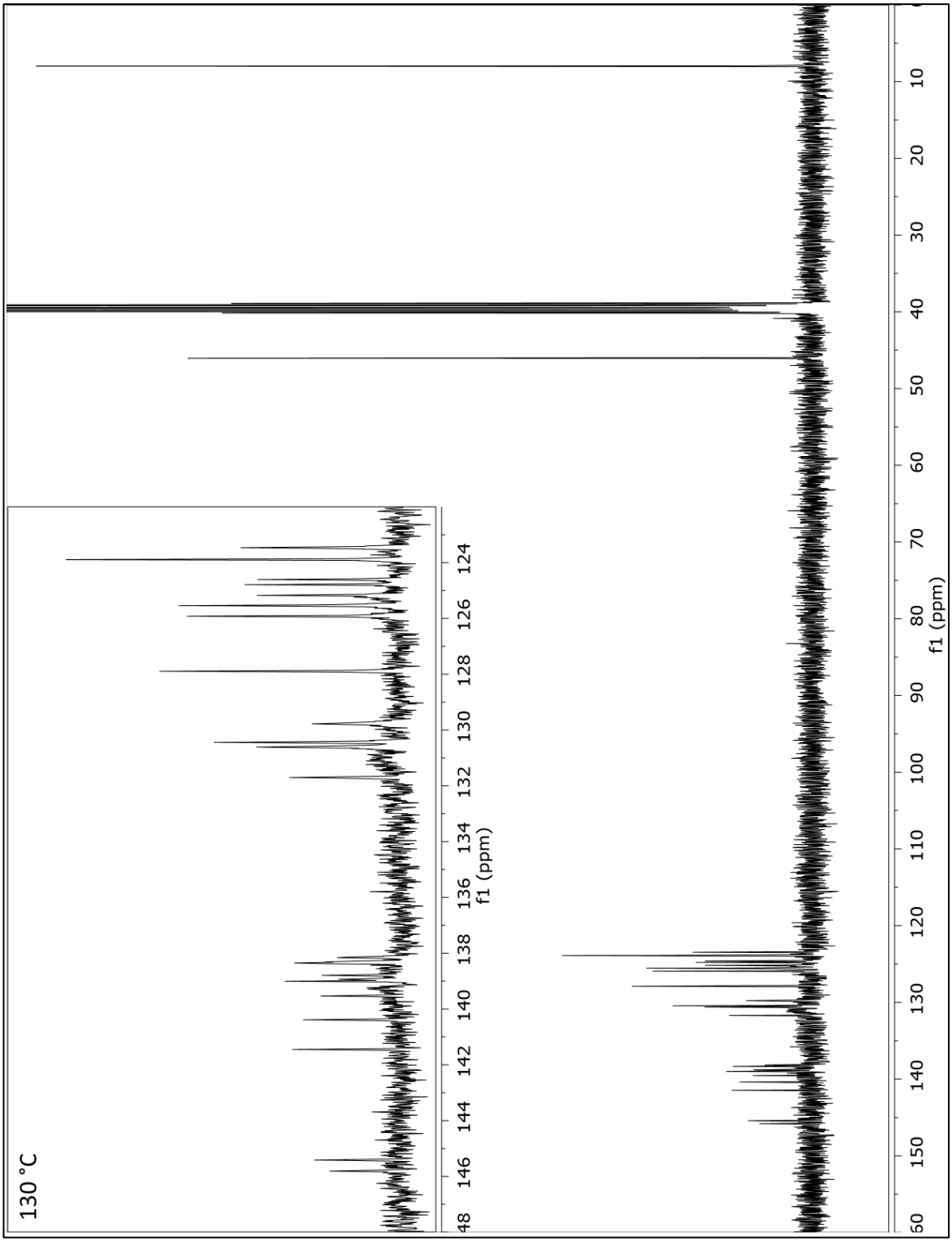

Figure A 44: *130 °C ^{13}C NMR spectrum of 2,2'-biphenyl model compound (MC-Bo) in DMSO-d_6.*

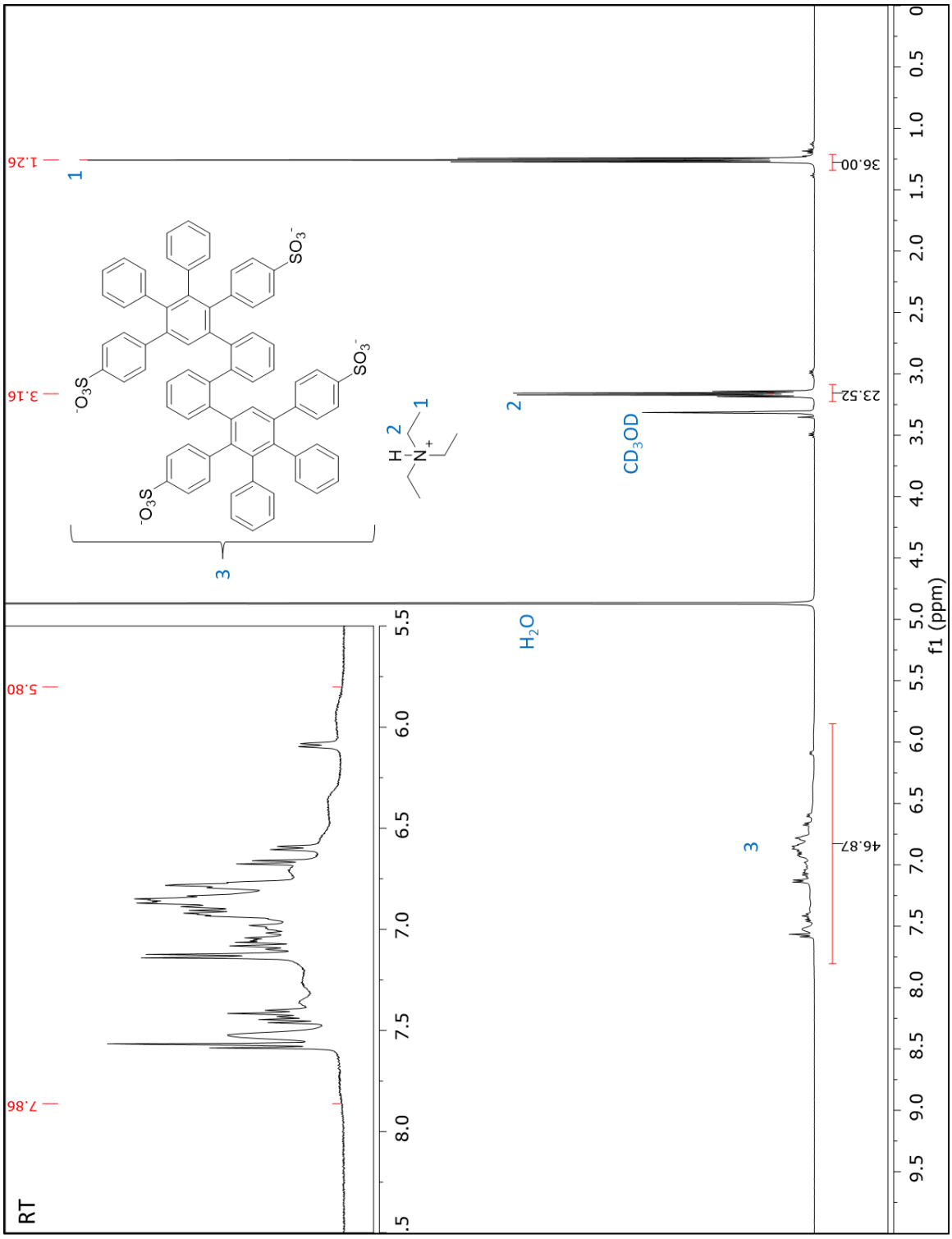

Figure A 45: *Room temperature ^{1}H NMR spectrum of 2,2'-biphenyl model compound (MC-Bo) in CD_3OD.*

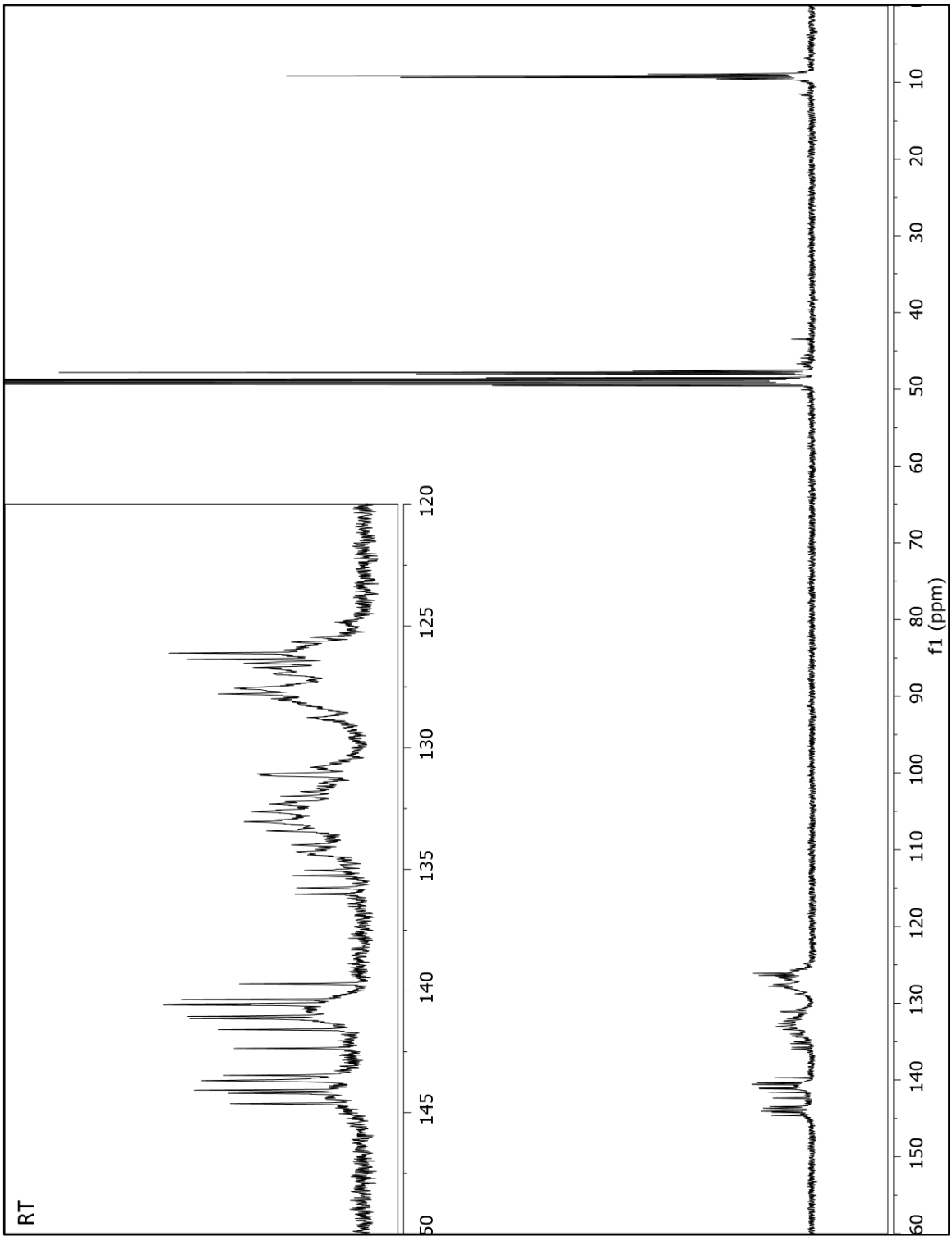

Figure A 46: *Room temperature ^{13}C NMR spectrum of 2,2'-biphenyl model compound (MC-Bo) in CD_3OD.*

Appendix B.

Supporting Information for Chapter 4

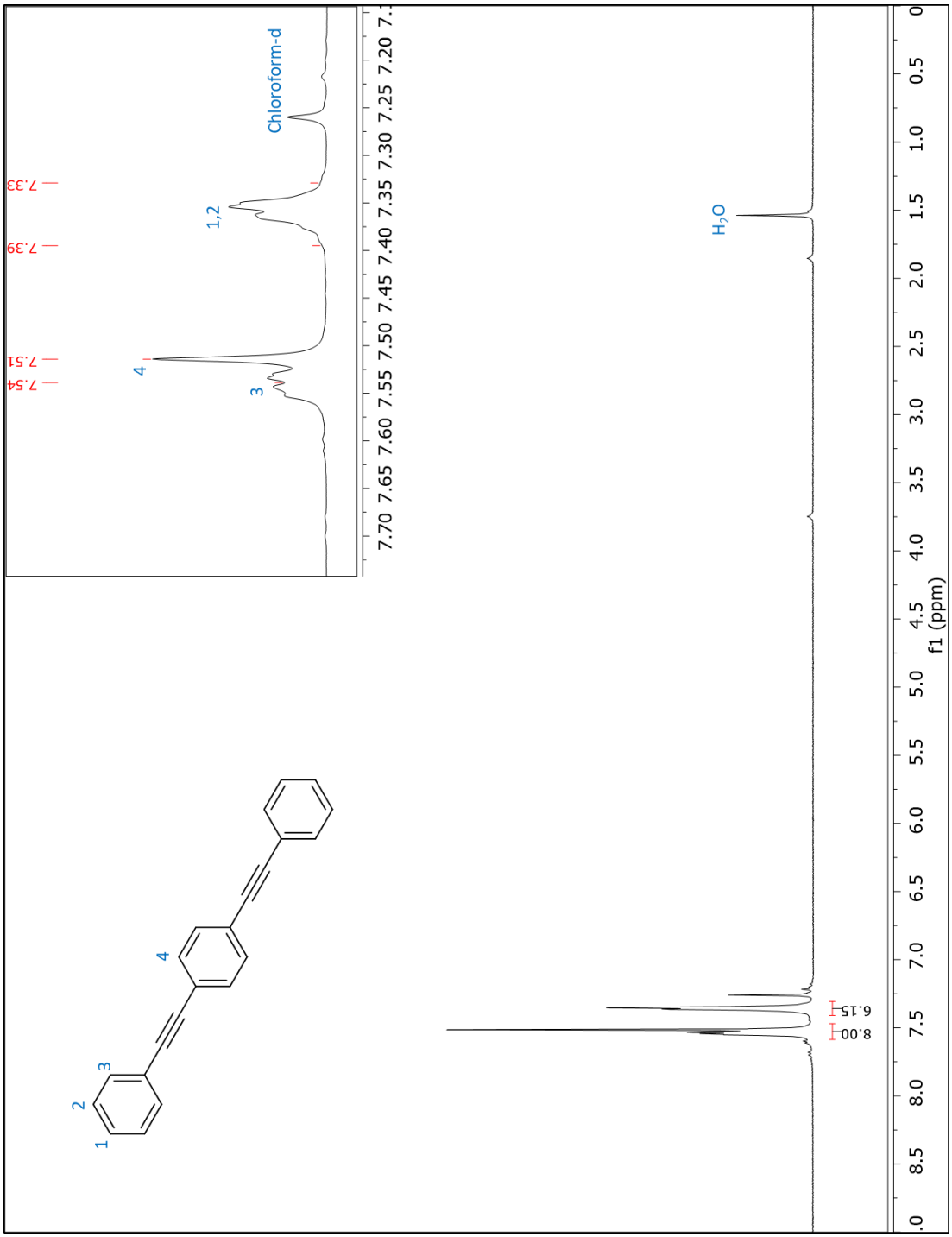

Figure B 1: *^{1}H NMR spectrum of 1,4-bis-phenylethynylbenzene.*

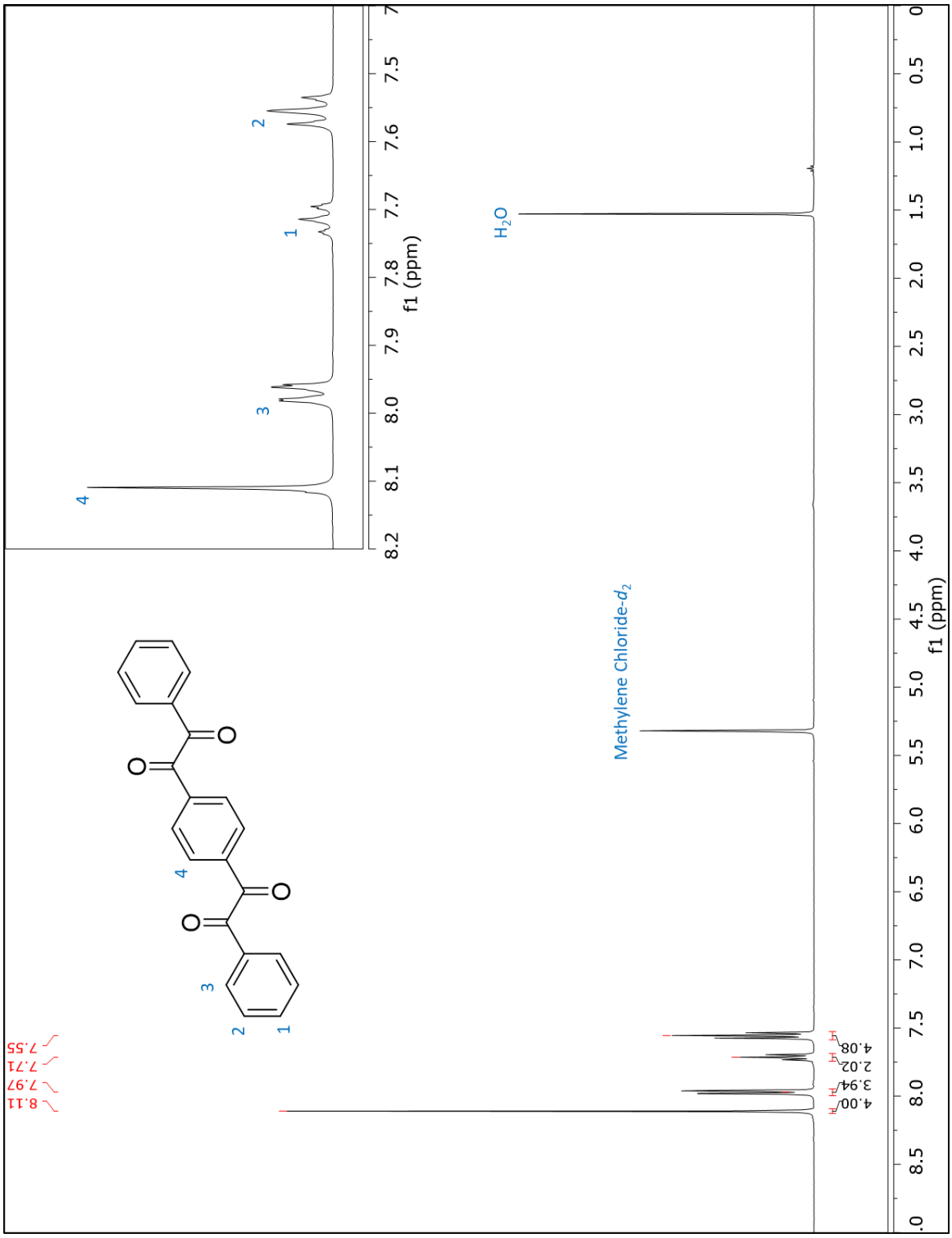

Figure B 2: *^{1}H NMR spectrum of 2,2'-(1,4-phenylene)-bis-1-phenylethane-1,2-dione.*

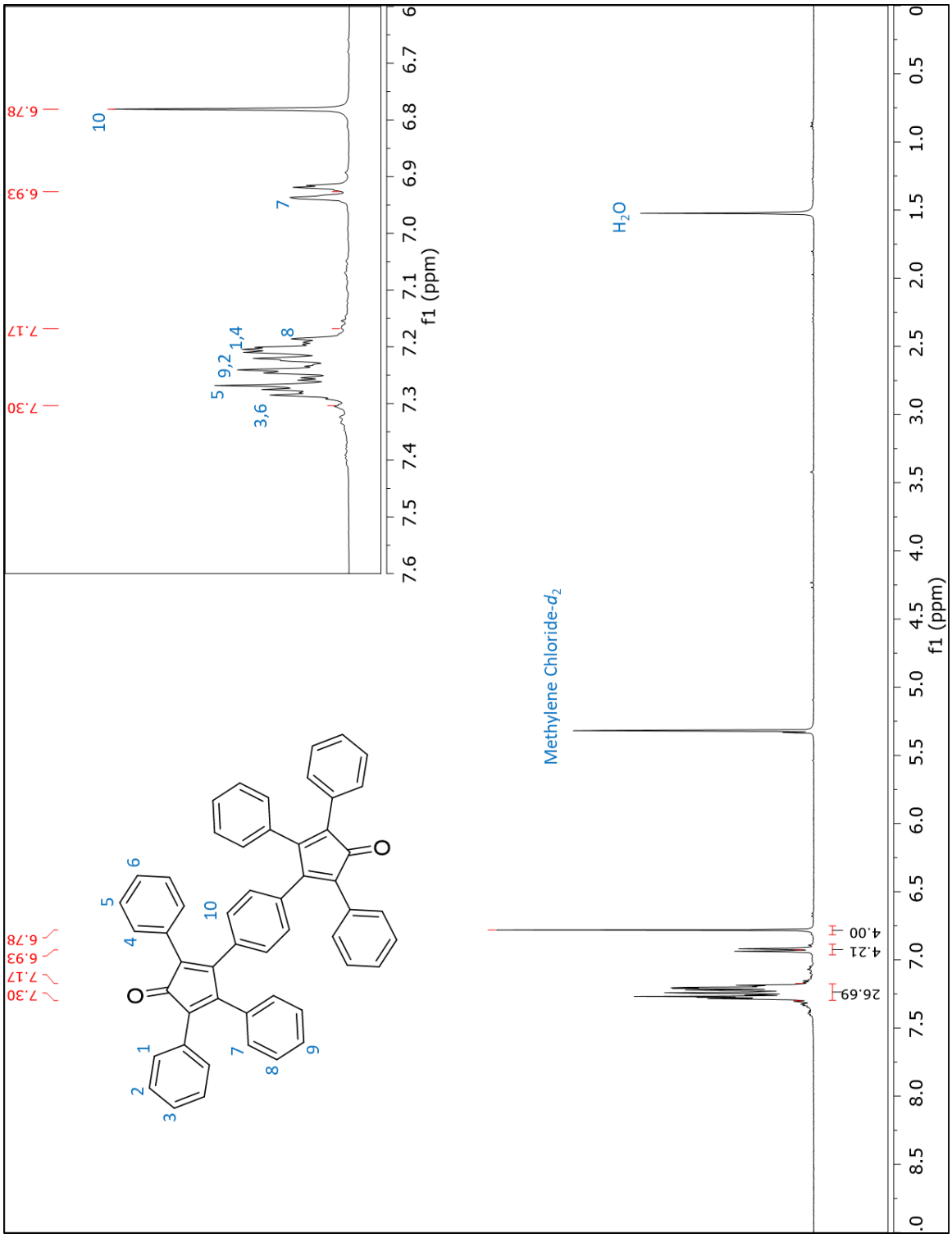

Figure B 3: *^{1}H NMR spectrum of 4,4'-(1,4-phenylene)-bis-2,3,5-triphenylcyclopenta-2,4-dien-1-one (bistetracyclone).*

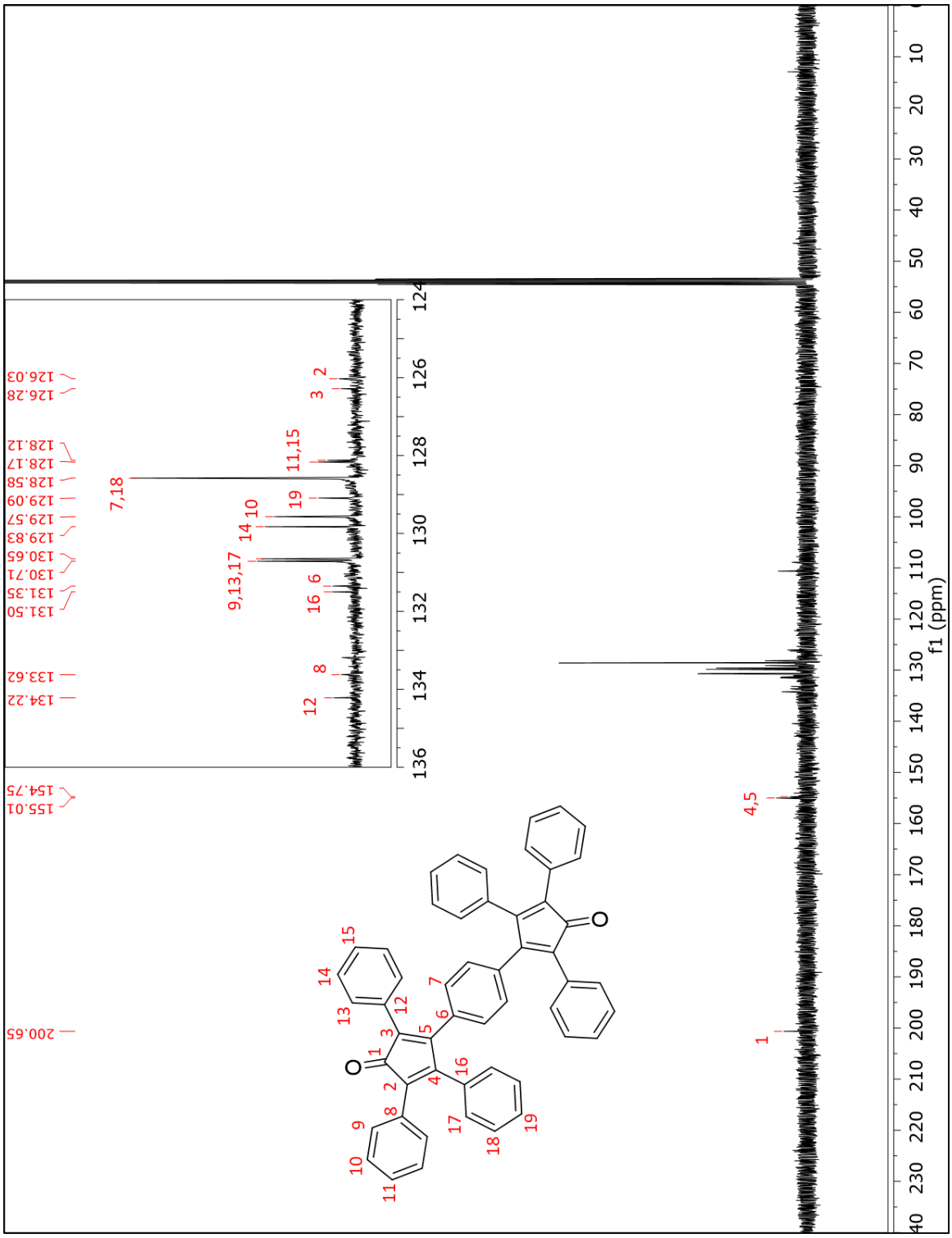

Figure B 4: *^{13}C NMR spectrum of 4,4'-(1,4-phenylene)-bis-2,3,5-triphenylcyclopenta-2,4-dien-1-one (bistetracyclone).*

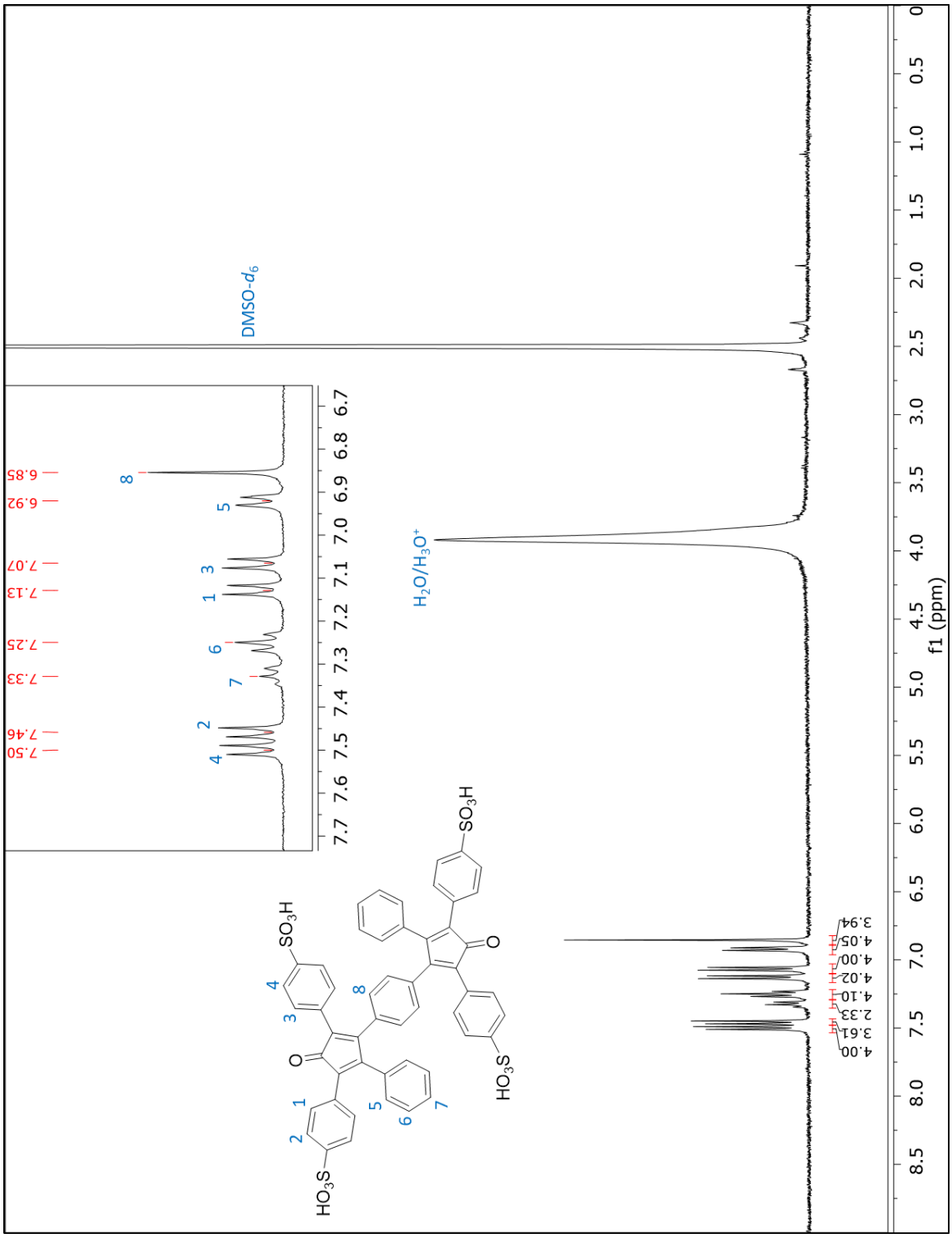

Figure B 5: *^{1}H NMR spectrum of tetra(para-sulfonated) bistetracyclone (sBTC).*

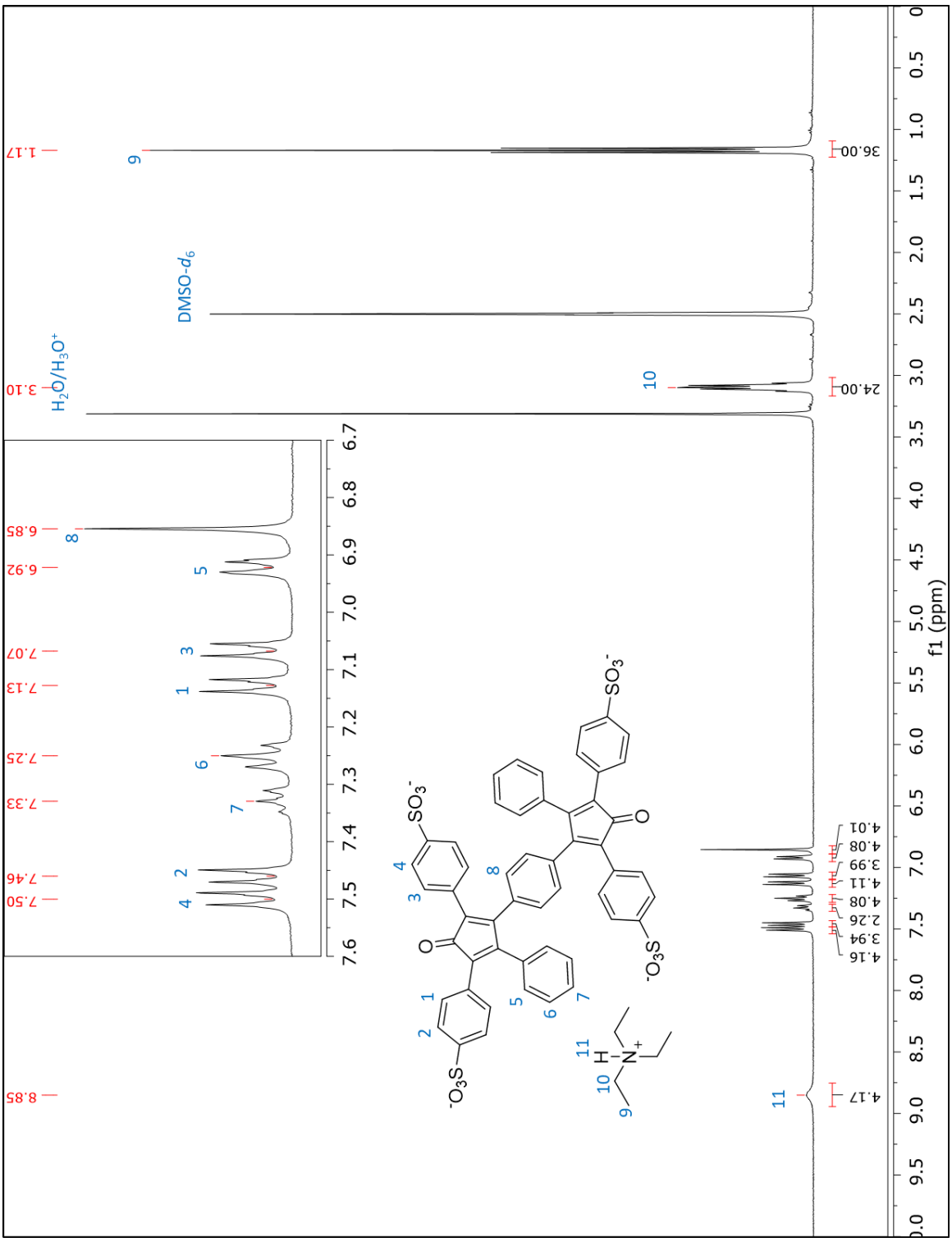

Figure B 6: *^{1}H NMR spectrum of tetra(para-sulfonated) bistetracyclone triethylammonium salt (TEAsBTC).*

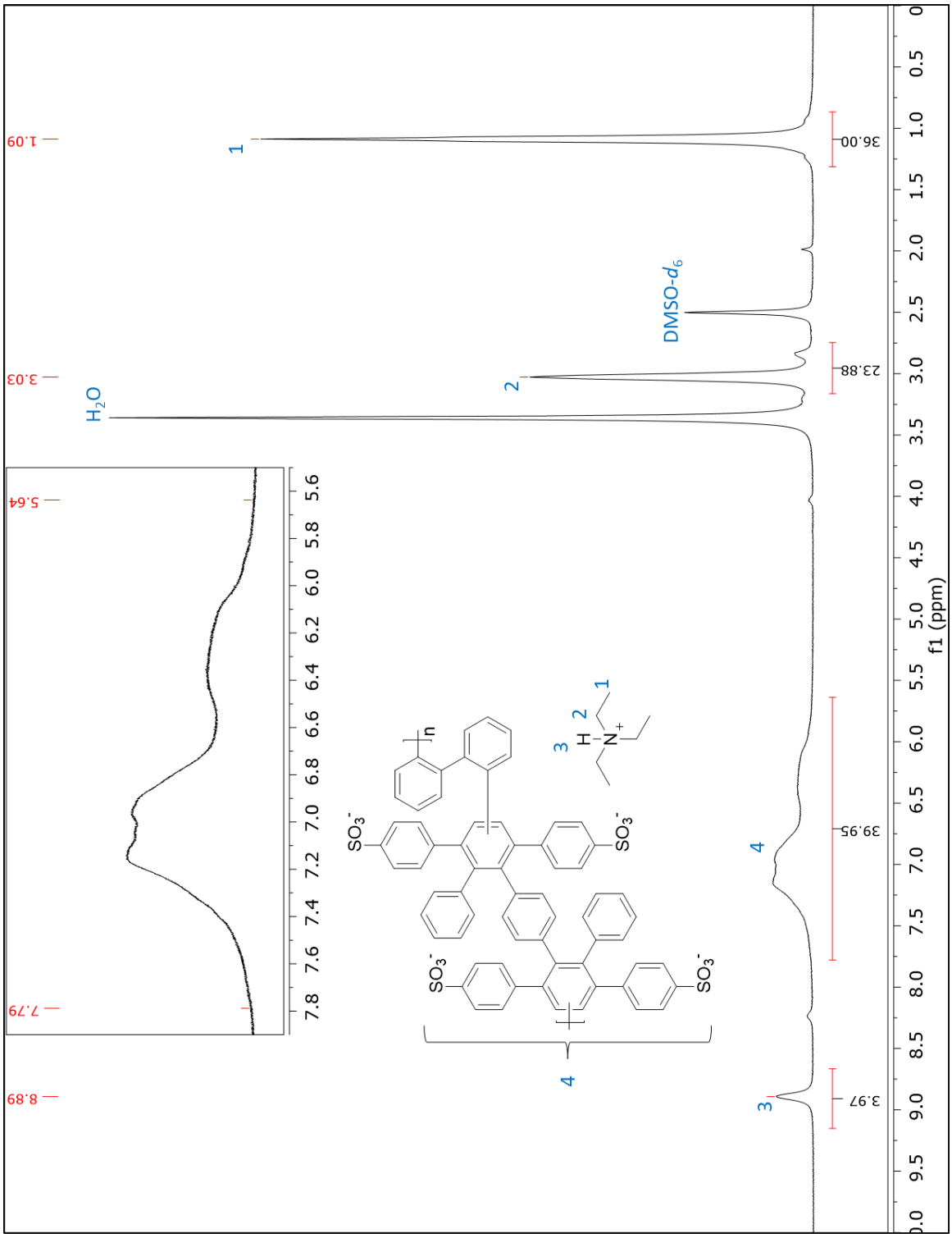

Figure B 7: *^{1}H NMR spectrum of sulfonated polyphenylene ortho-biphenyl triethylammonium salt (sPPBo-HNEt3^{+}).*

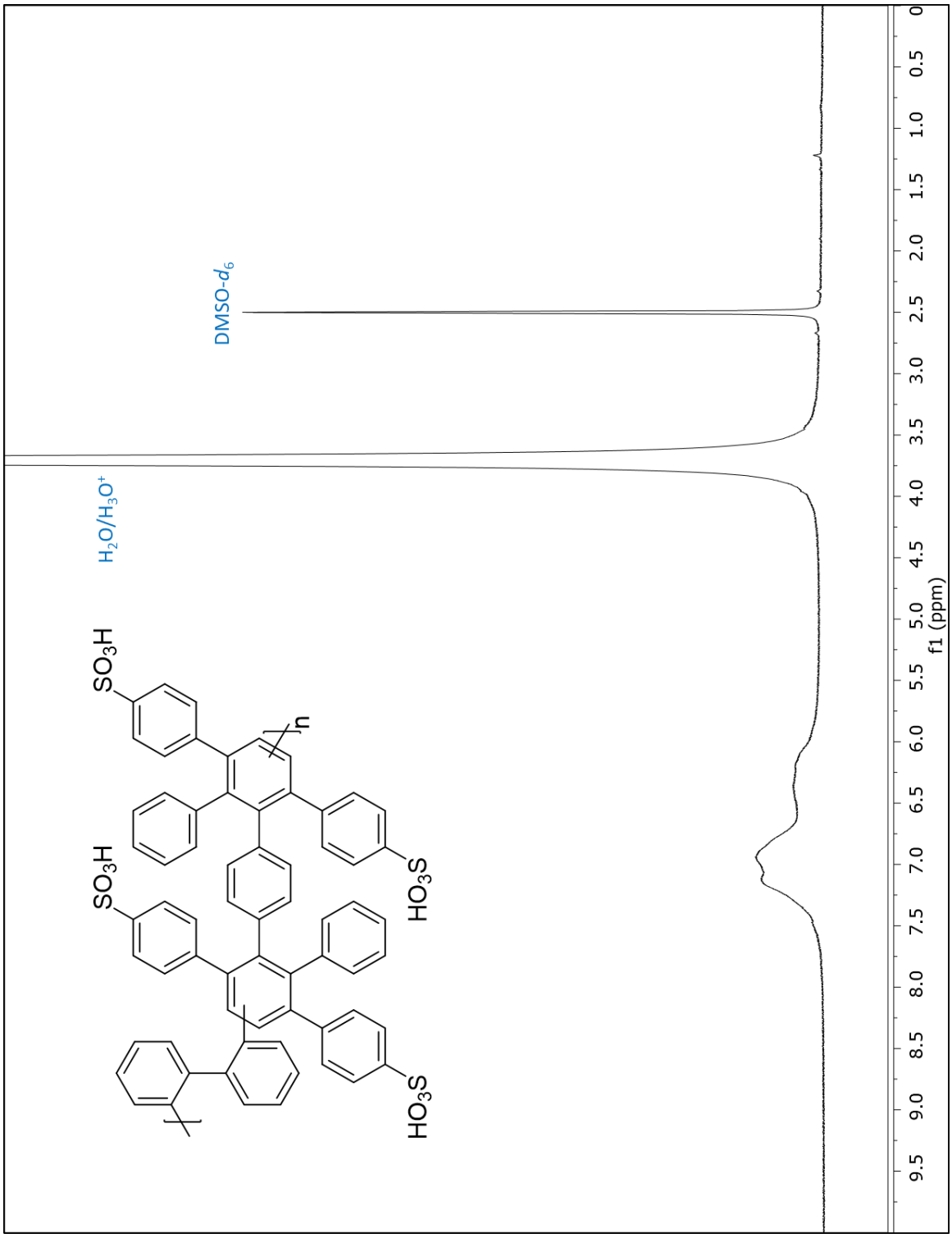

Figure B 8: *^{1}H NMR spectrum of sulfonated polyphenylene ortho-biphenyl (sPPBo-H$^+$).*

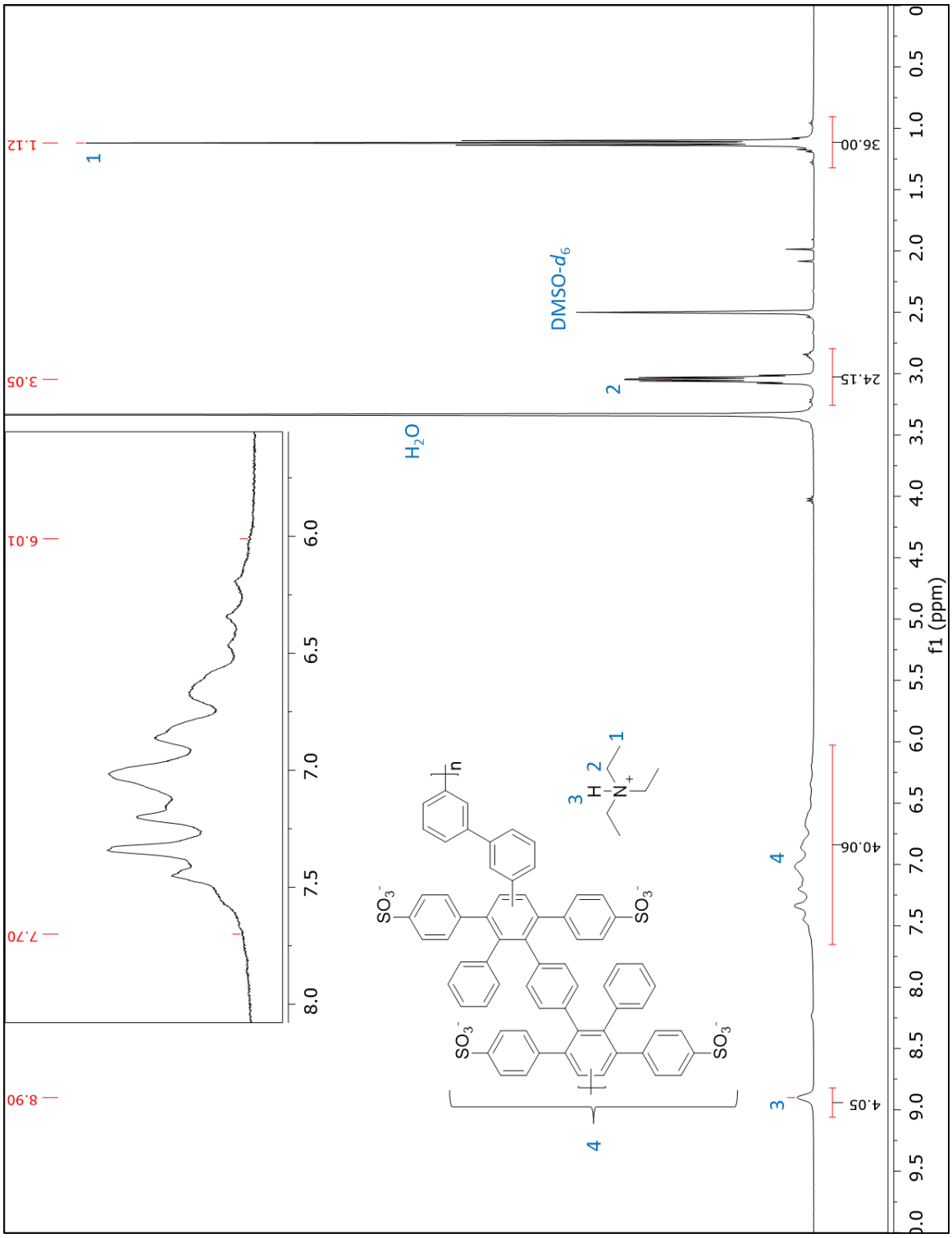

Figure B 9: *^{1}H NMR spectrum of sulfonated polyphenylene meta-biphenyl triethylammonium salt (sPPBm-HNEt3$^+$).*

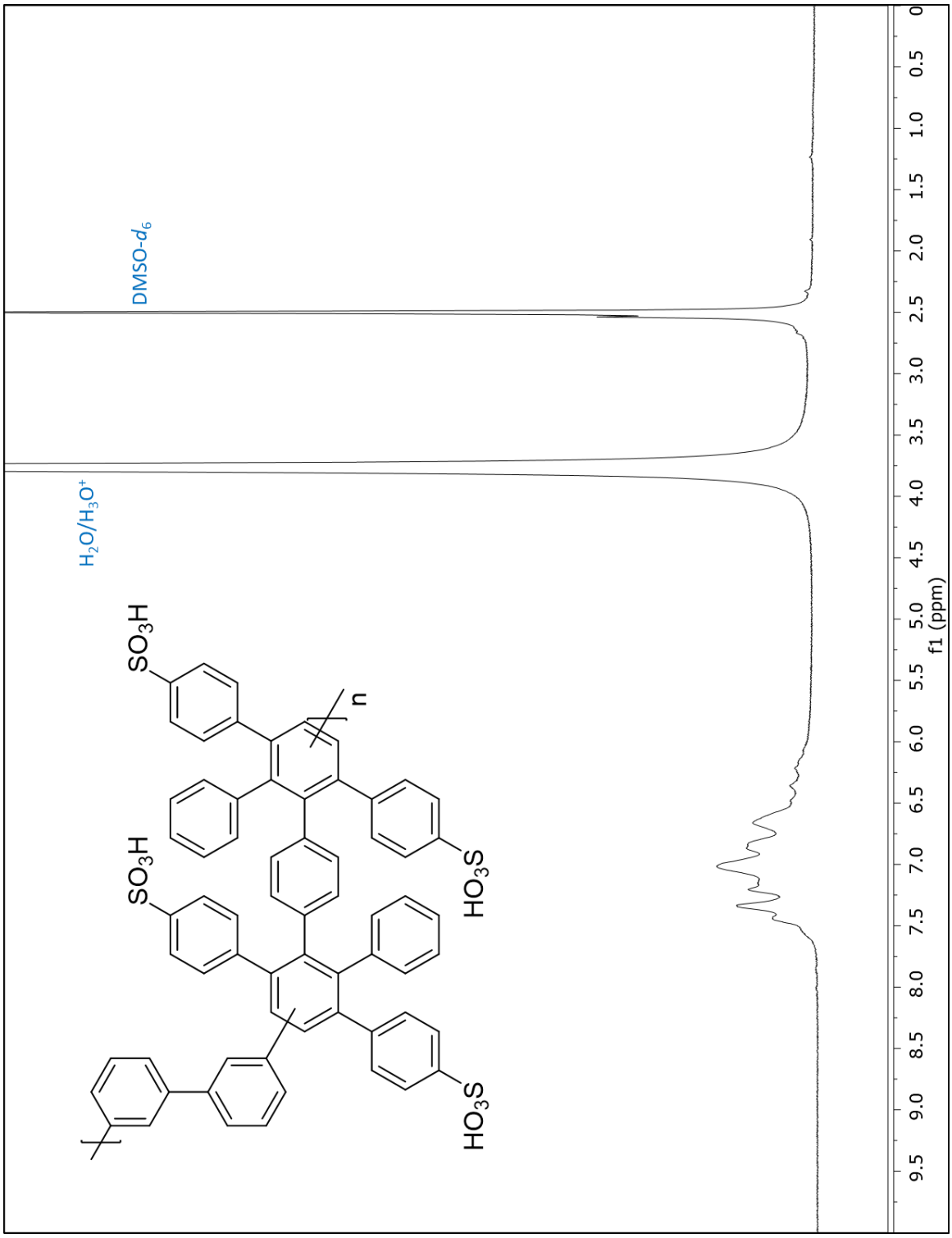

Figure B 10: *^{1}H NMR spectrum of sulfonated polyphenylene meta-biphenyl (sPPBm-H^+).*

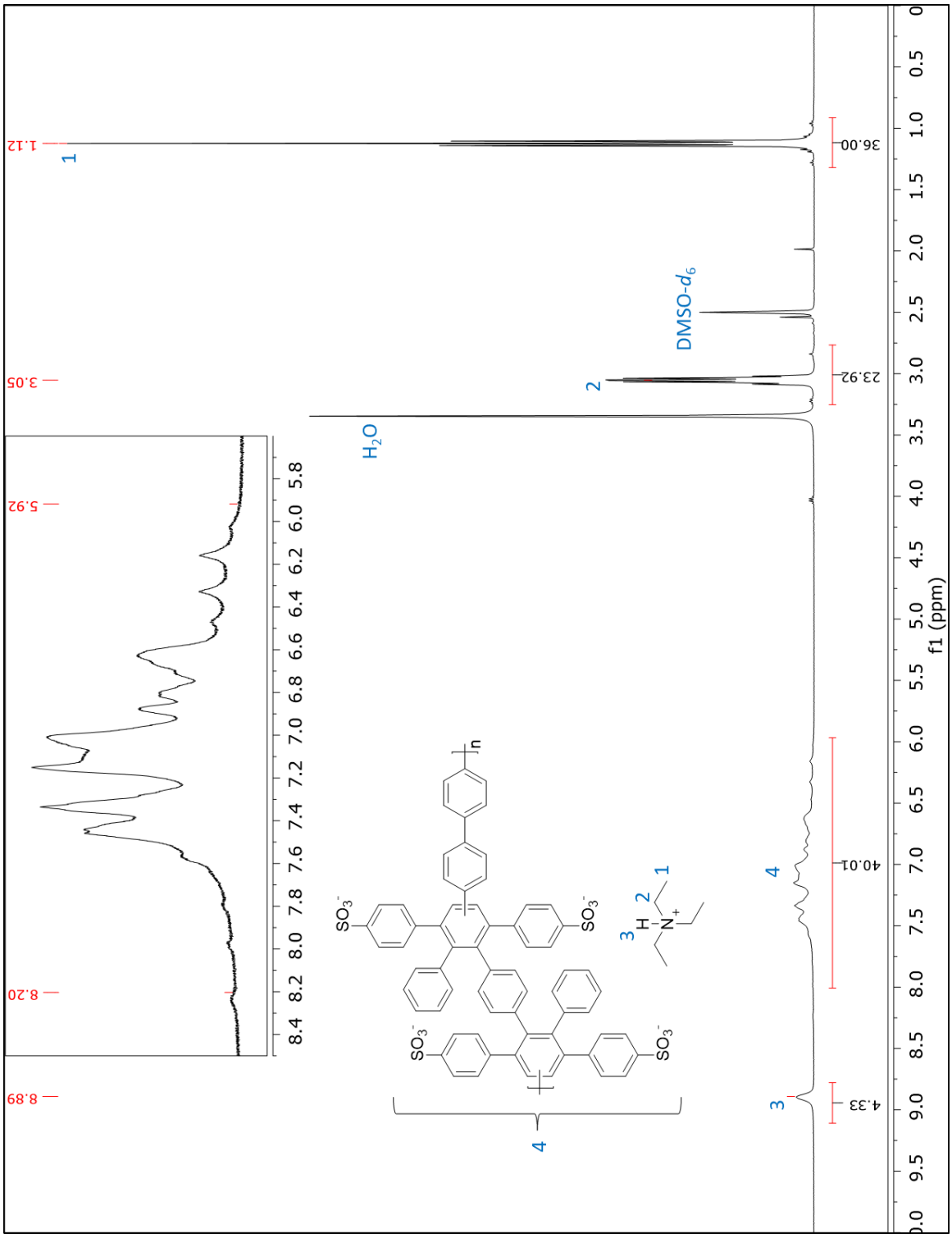

Figure B 11: *^{1}H NMR spectrum of sulfonated polyphenylene para-biphenyl triethylammonium salt (sPPBp-HNEt3$^+$).*

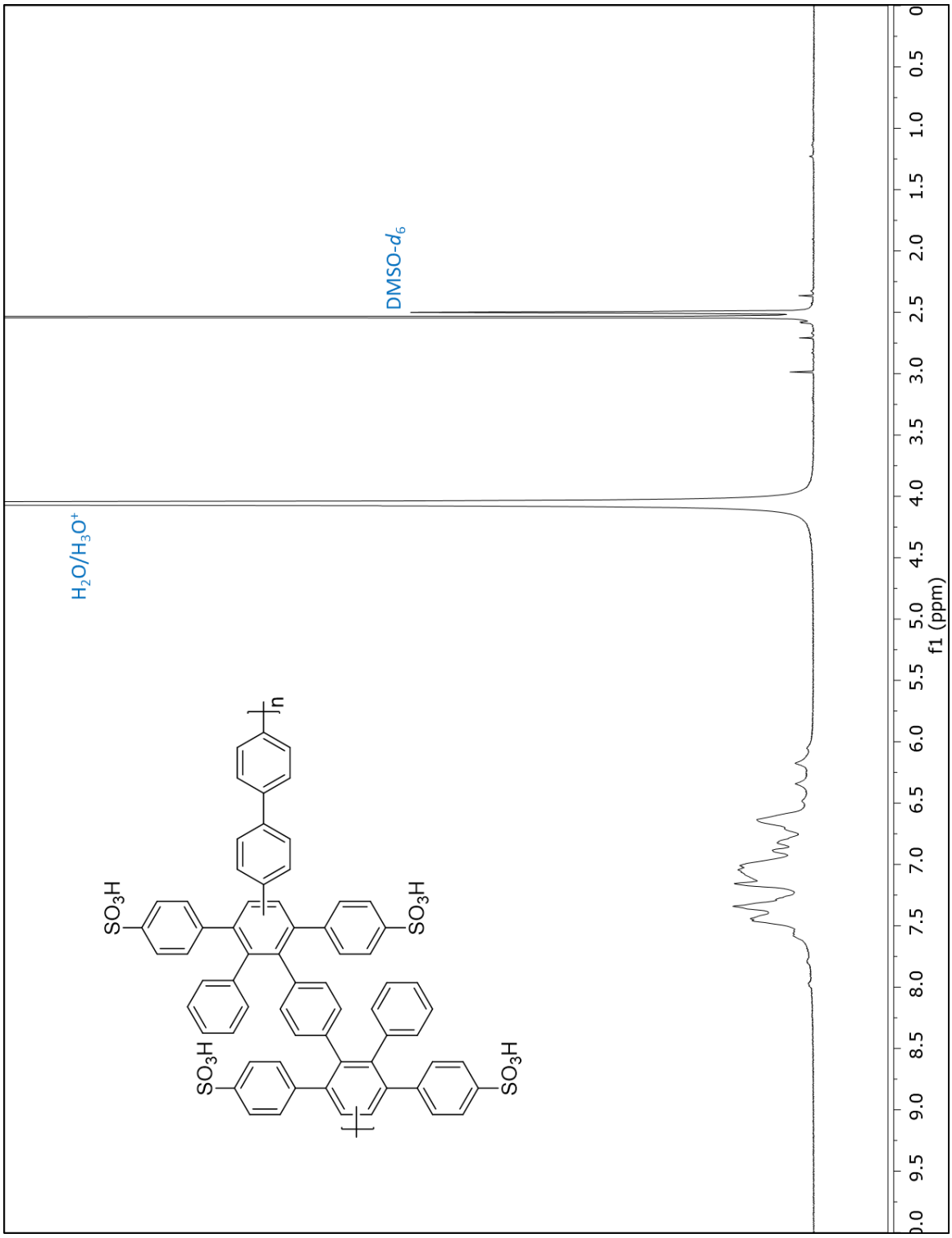

Figure B 12: *^{1}H NMR spectrum of sulfonated polyphenylene para-biphenyl (sPPBp-H$^+$).*

Appendix C.

Supporting Information for Chapter 5

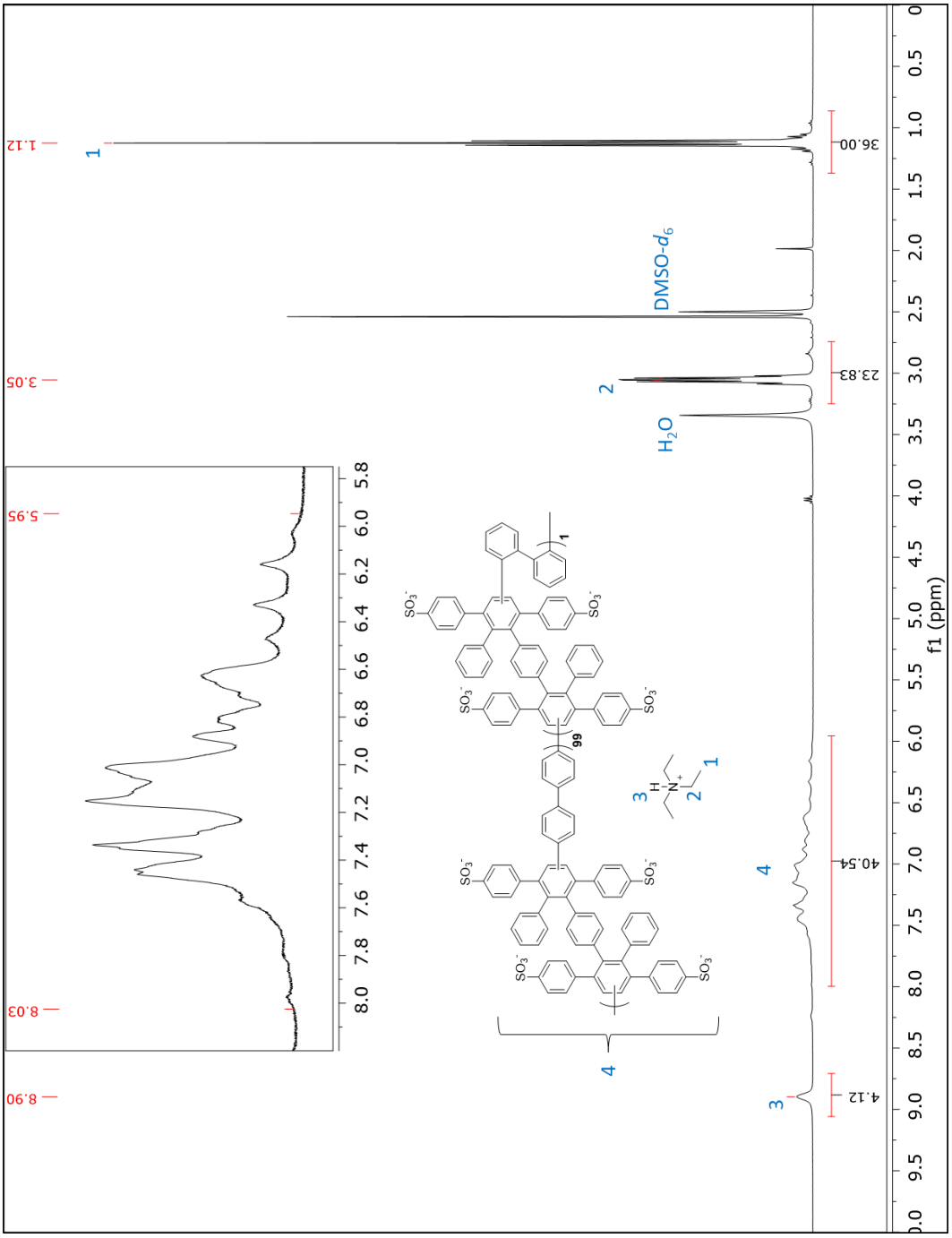

Figure C 1: *^{1}H NMR spectrum of sulfonated poly(phenylene) para-ortho-1%-biphenyl triethylammonium salt (sPPBpoHNEt$_3^+$-1%).*

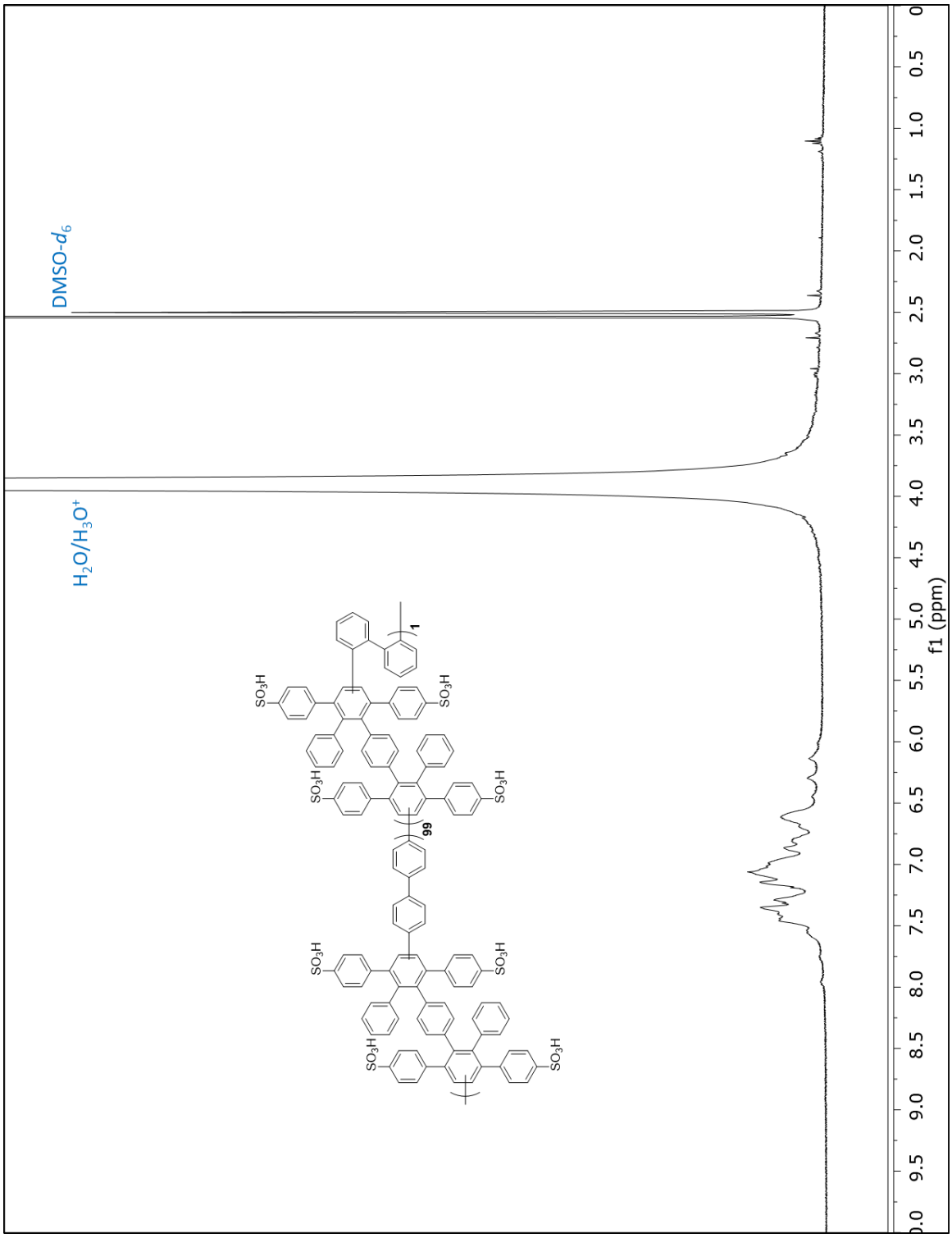

Figure C 2: *^{1}H NMR spectrum of sulfonated poly(phenylene) para-ortho-1%-biphenyl (sPPBpoH$^+$-1%).*

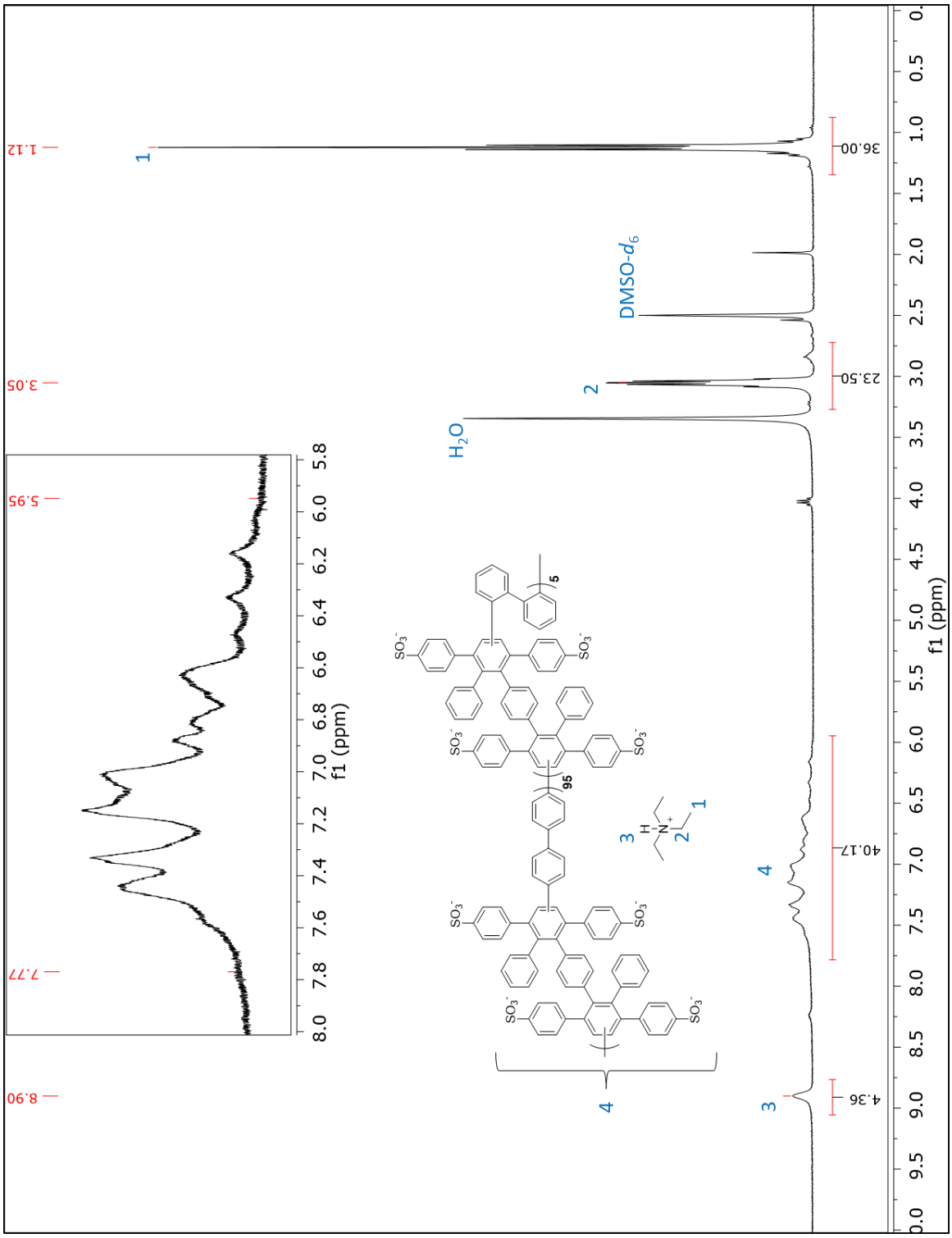

Figure C 3: *^{1}H NMR spectrum of sulfonated poly(phenylene) para-ortho-5%-biphenyl triethylammonium salt (sPPBpoHNEt$_3^+$-5%).*

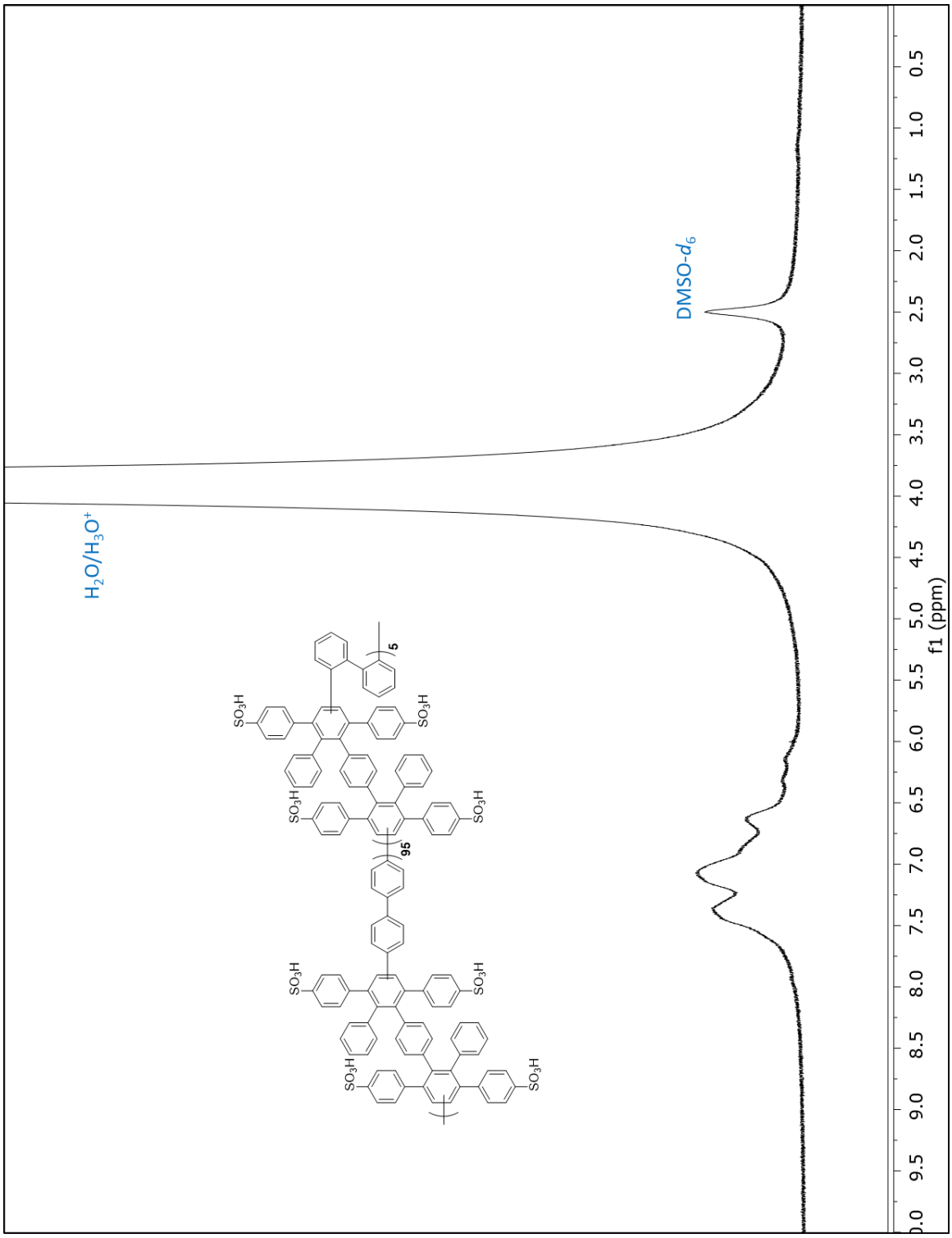

Figure C 4: *^{1}H NMR spectrum of sulfonated poly(phenylene) para-ortho-5%-biphenyl (sPPBpoH^{+}-5%).*

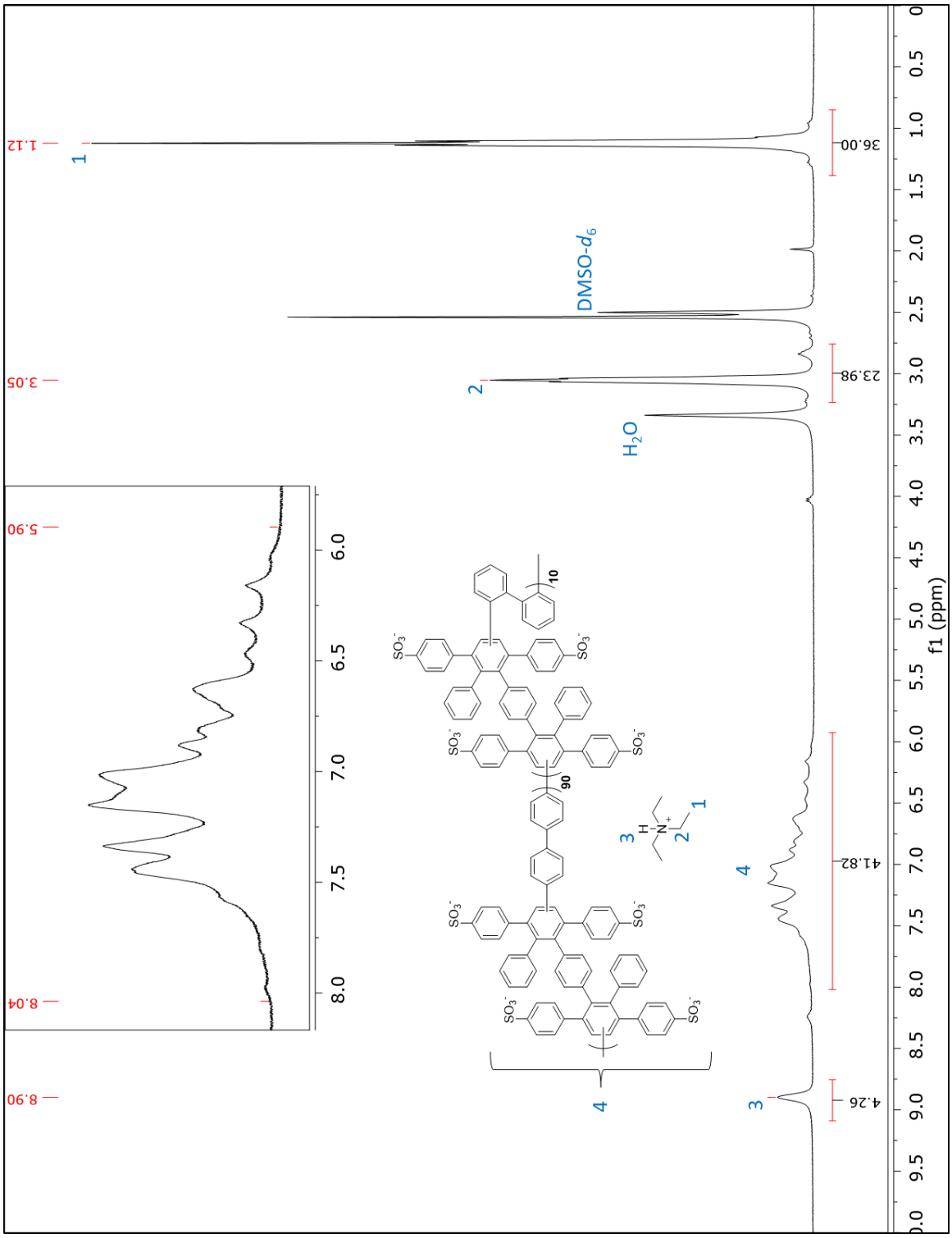

Figure C 5: *^{1}H NMR spectrum of sulfonated poly(phenylene) para-ortho-10%-biphenyl triethylammonium salt (sPPBpoHNEt$_3^+$-10%).*

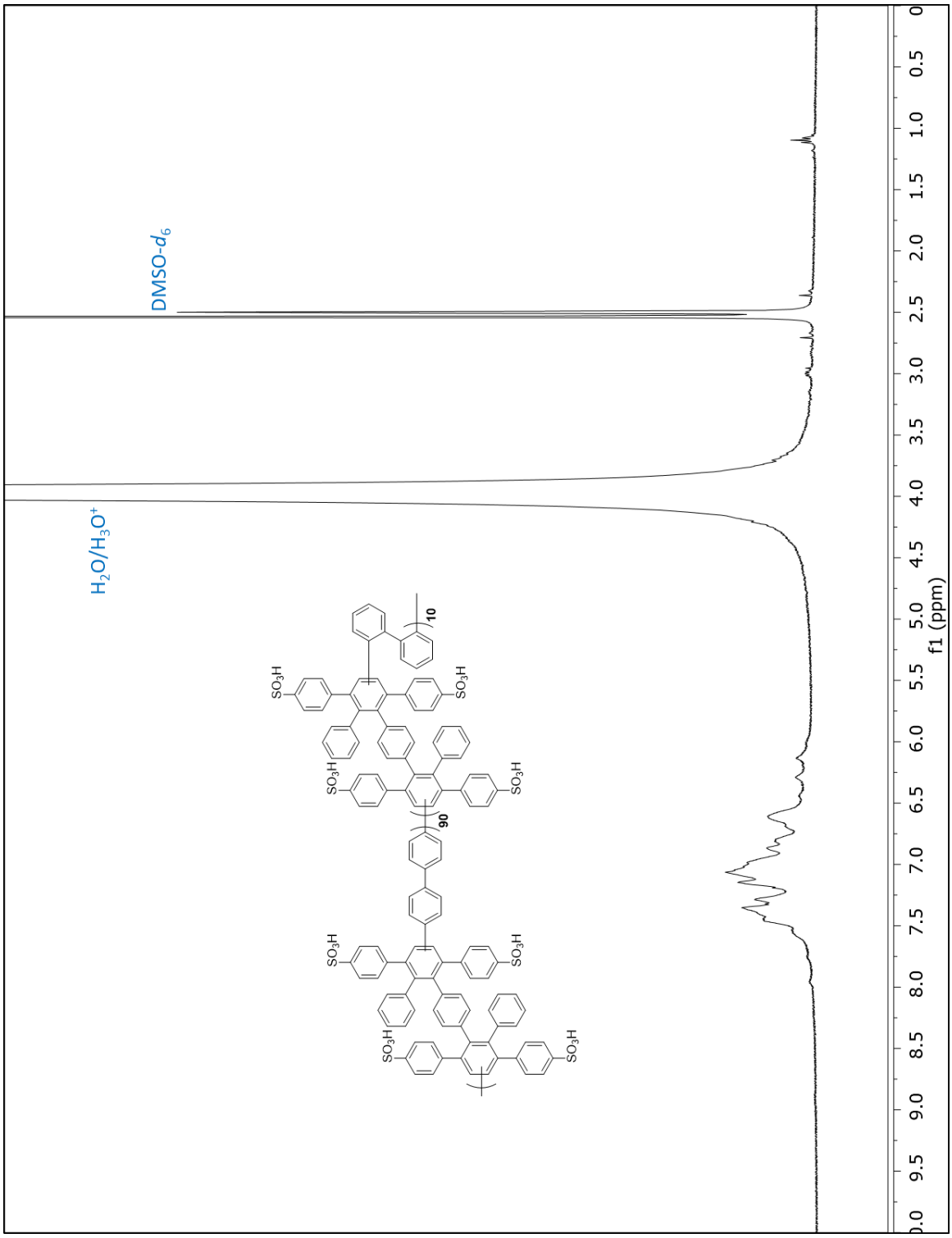

Figure C 6: *^{1}H NMR spectrum of sulfonated poly(phenylene) para-ortho-10%-biphenyl (sPPBpoH$^+$-10%).*

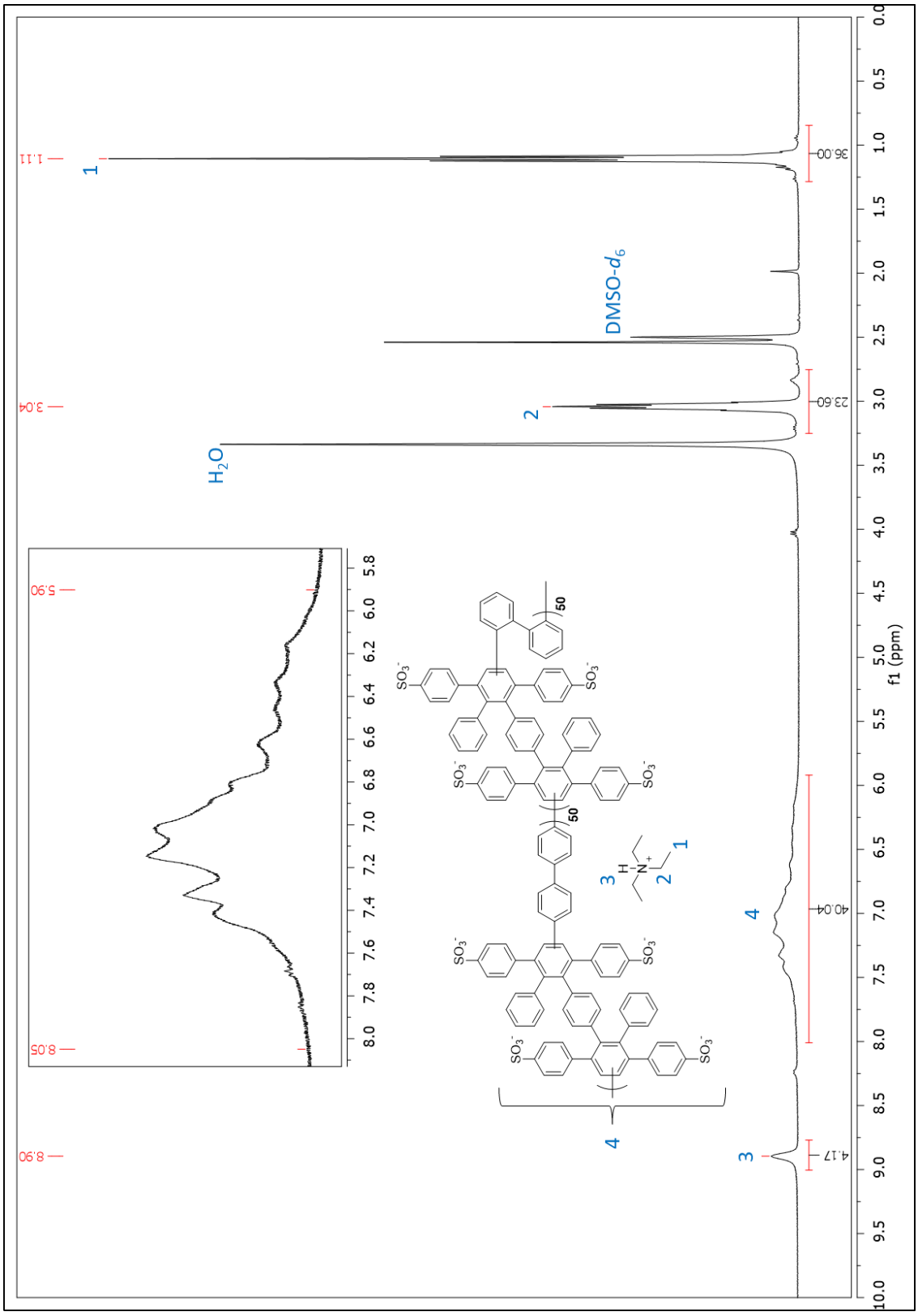

Figure C 7: *^{1}H NMR spectrum of sulfonated poly(phenylene) para-ortho-50%-biphenyl triethylammonium salt (sPPBpoHNEt$_3^+$-50%).*

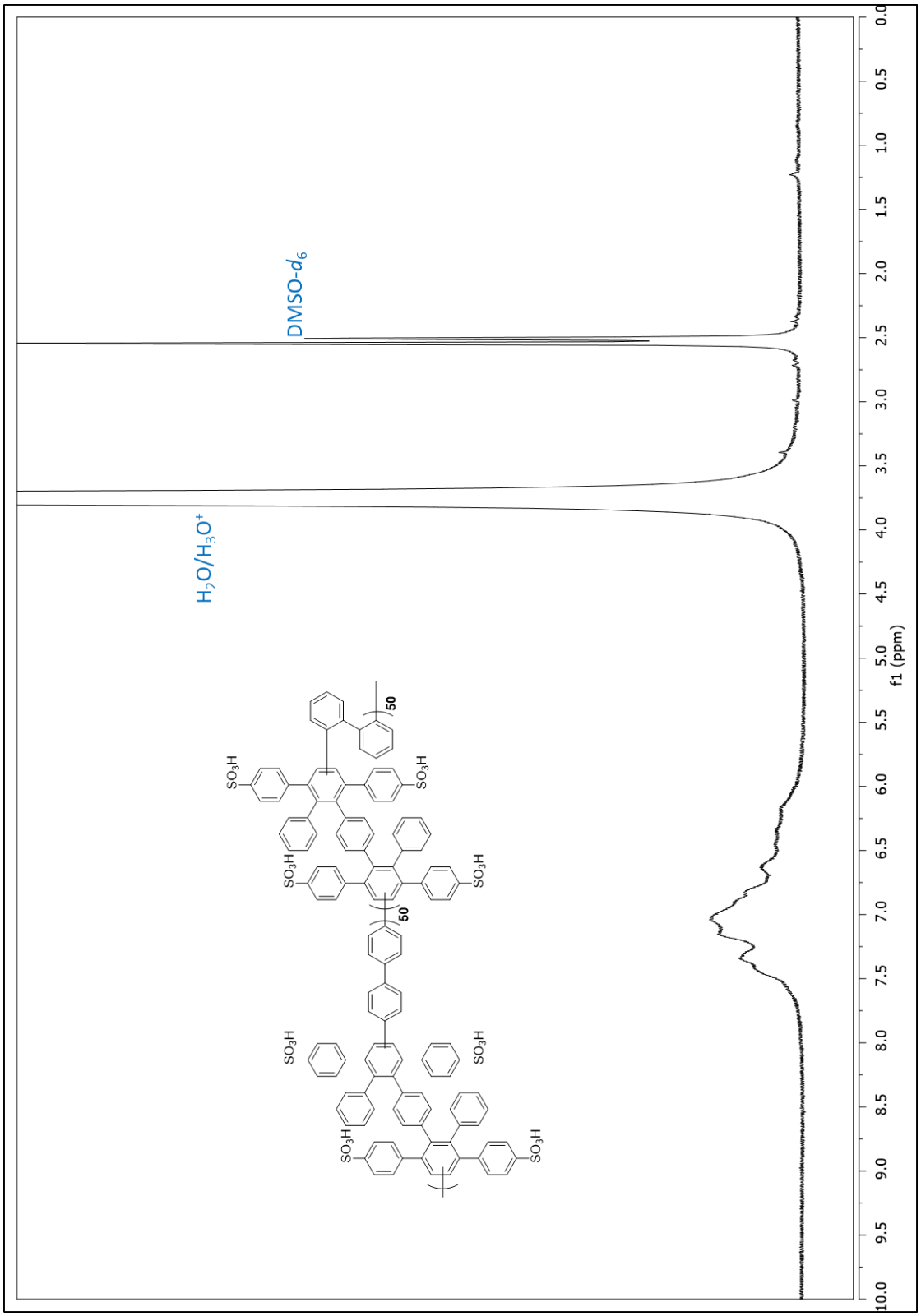

Figure C 8: *^{1}H NMR spectrum of sulfonated poly(phenylene) para-ortho-50%-biphenyl (sPPBpoH$^+$-50%).*

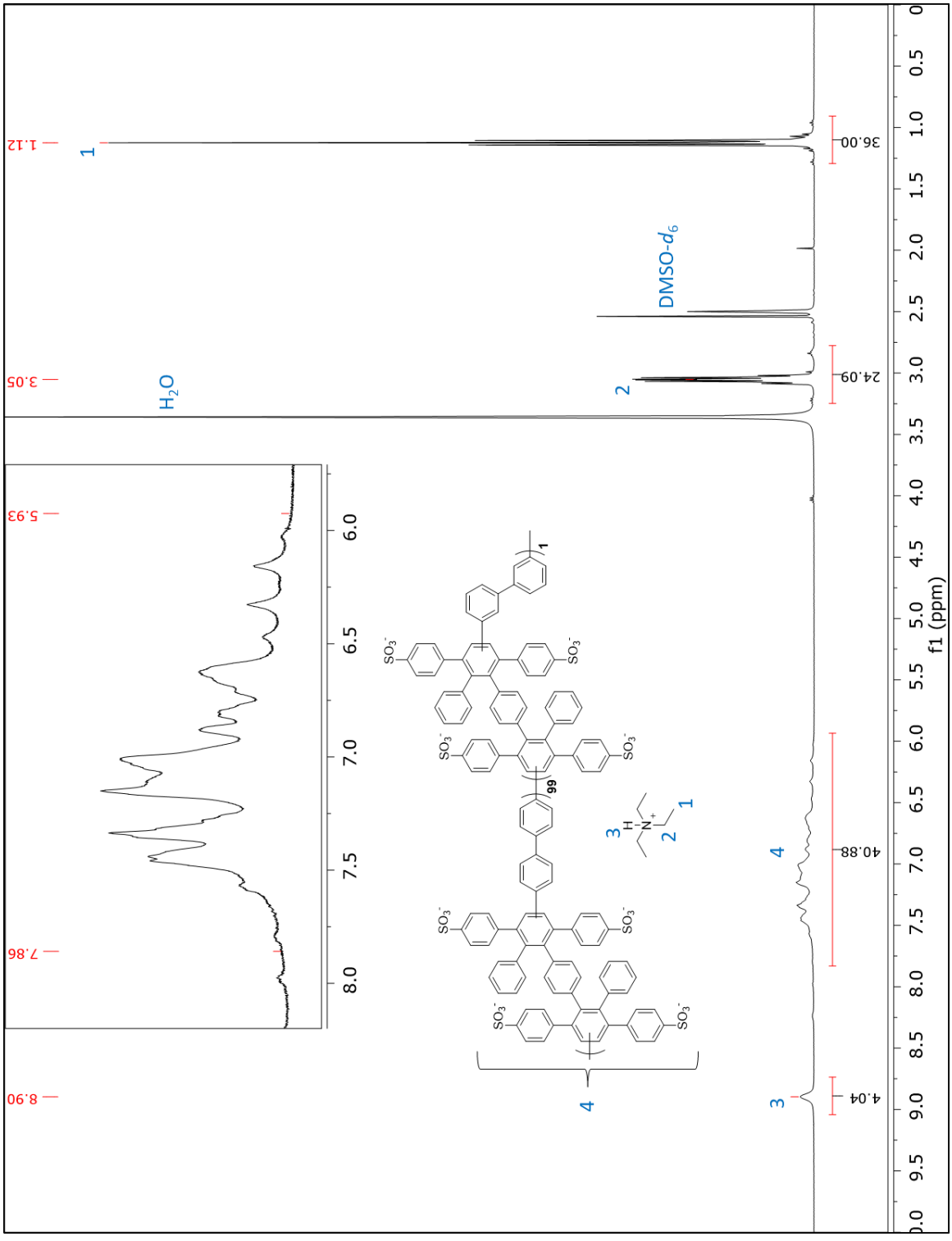

Figure C 9: *^{1}H NMR spectrum of sulfonated poly(phenylene) para-meta-1%-biphenyl triethylammonium salt (sPPBpmHNEt$_3^+$-1%).*

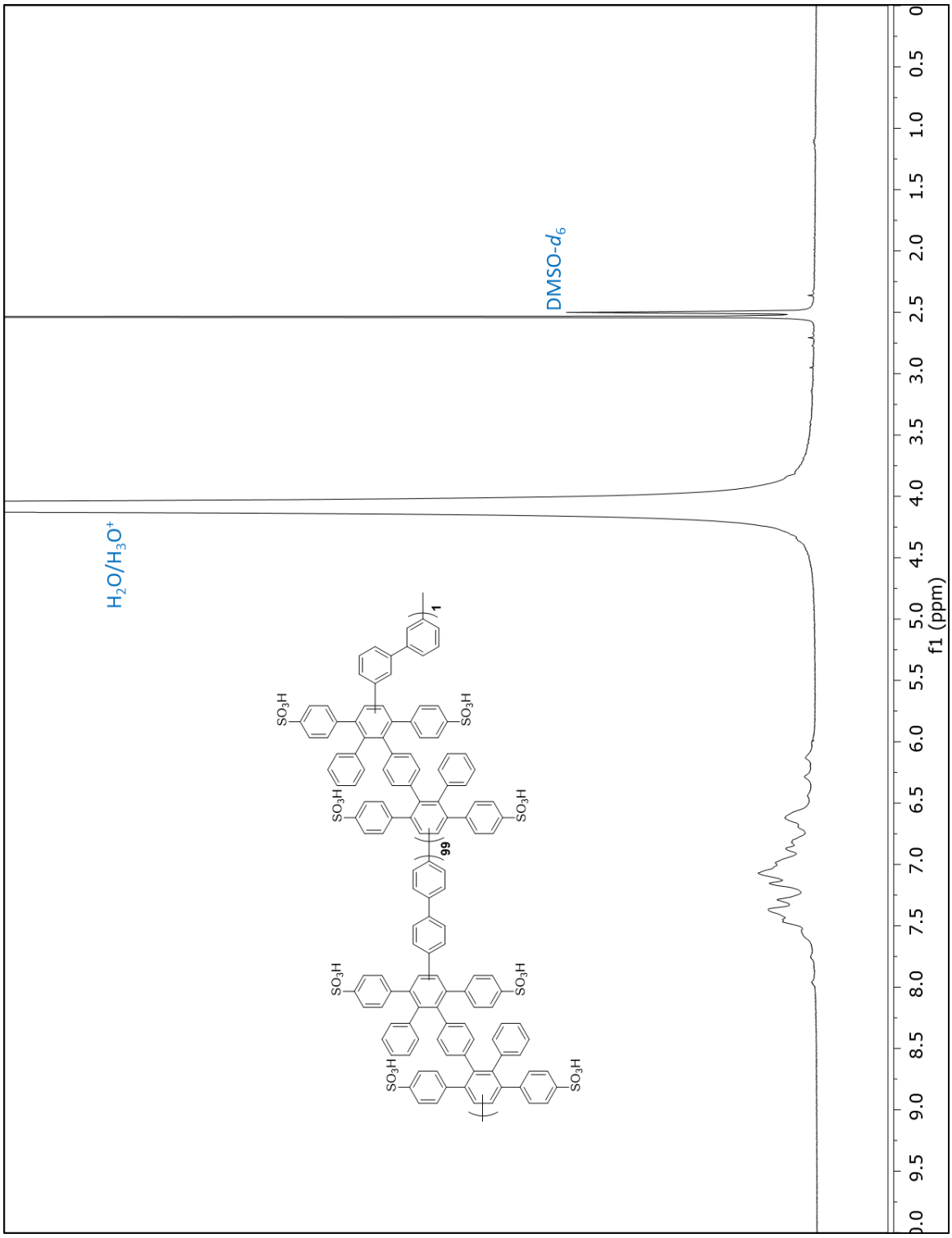

Figure C 10: *^{1}H NMR spectrum of sulfonated poly(phenylene) para-meta-1%-biphenyl (sPPBpmH$^+$-1%).*

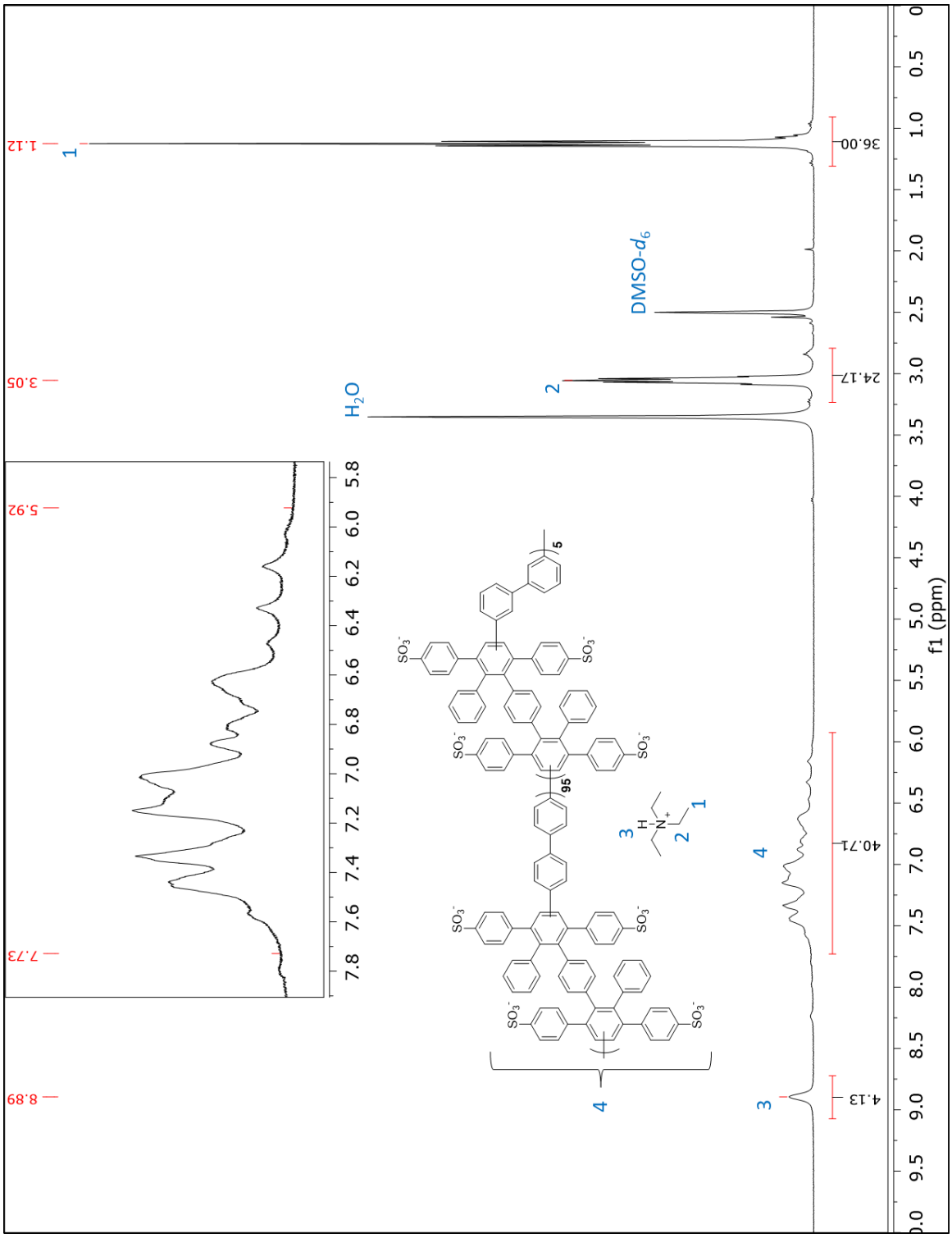

Figure C 11: *^{1}H NMR spectrum of sulfonated poly(phenylene) para-meta-5%-biphenyl triethylammonium salt (sPPBpmHNEt$_3^+$-5%).*

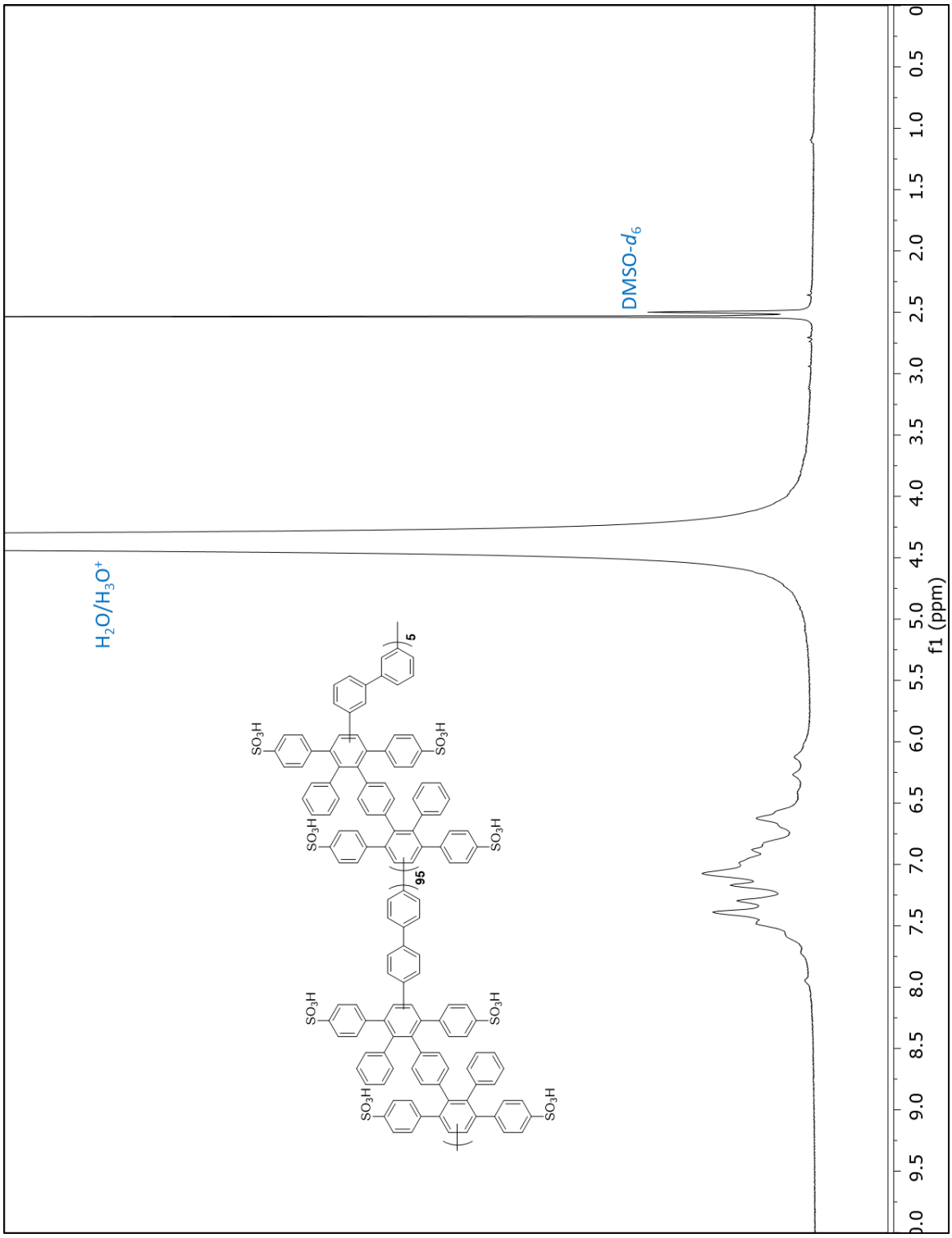

Figure C 12: *^{1}H NMR spectrum of sulfonated poly(phenylene) para-meta-5%-biphenyl (sPPBpmH$^+$-5%).*

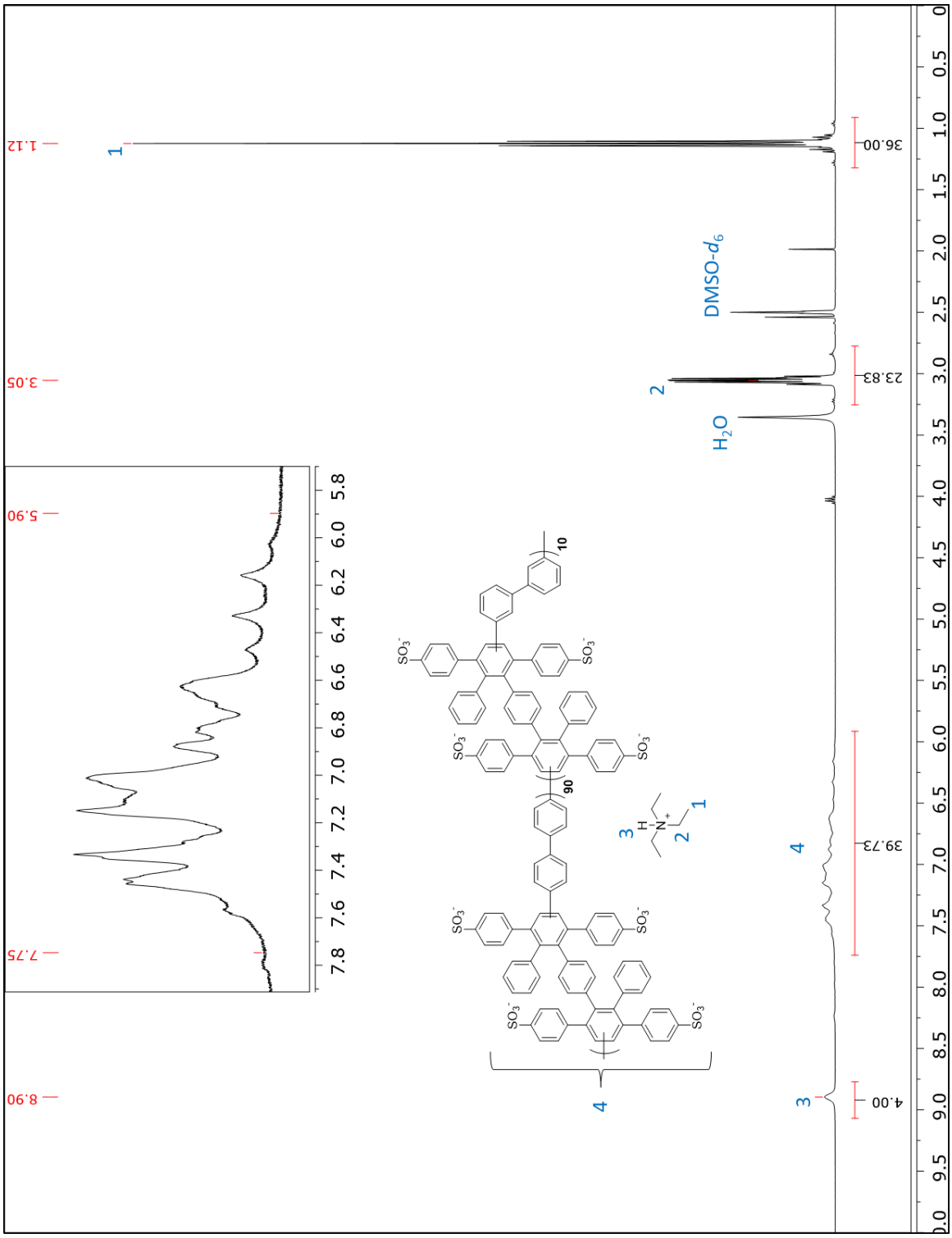

Figure C 13: *^{1}H NMR spectrum of sulfonated poly(phenylene) para-meta-10%-biphenyl triethylammonium salt (sPPBpmHNEt$_3^+$-10%).*

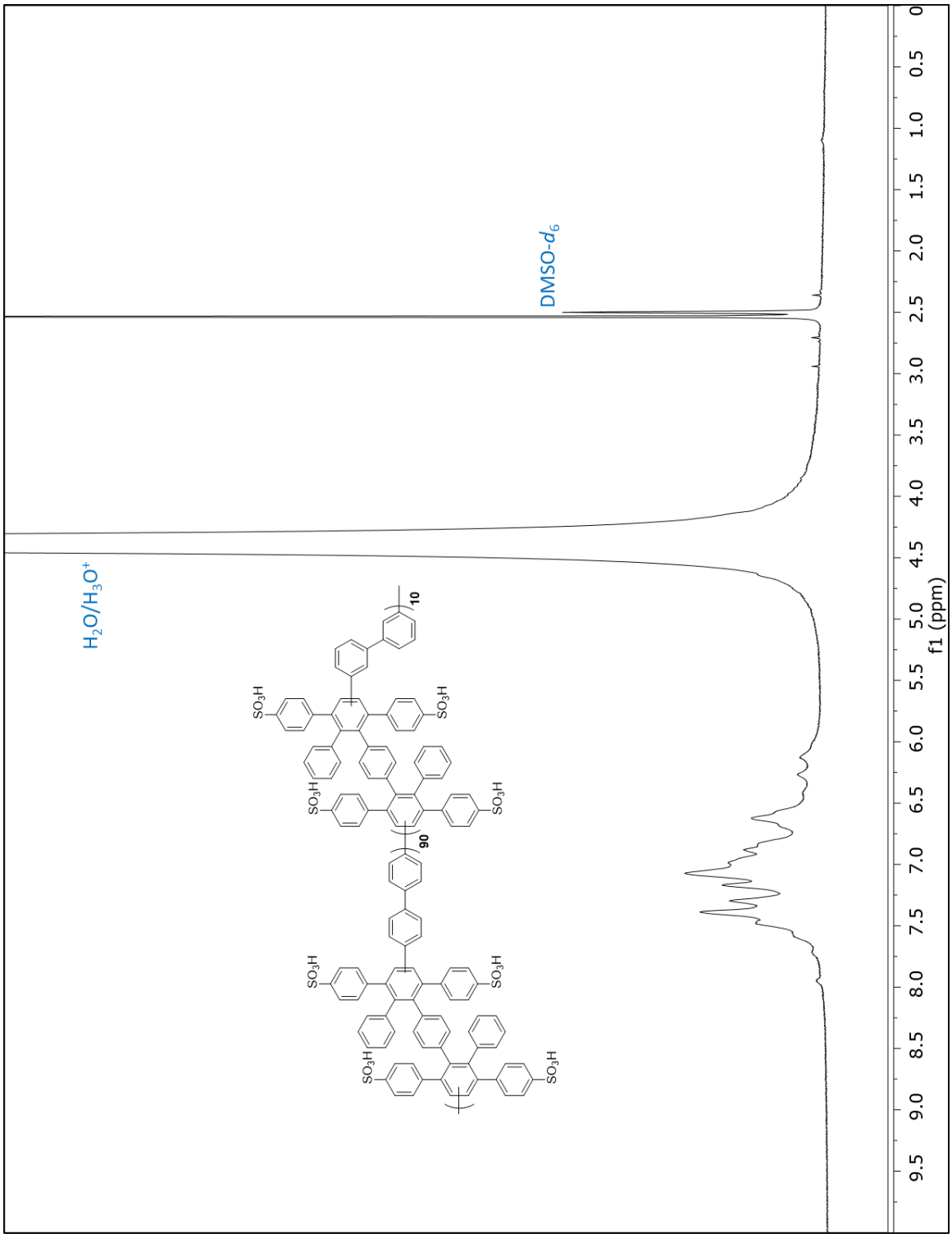

Figure C 14: *^{1}H NMR spectrum of sulfonated poly(phenylene) para-meta-10%-biphenyl (sPPBpmH$^+$-10%).*